AD NUMBER

AD357954

CLASSIFICATION CHANGES

TO: unclassified

FROM: confidential

LIMITATION CHANGES

TO:

Approved for public release, distribution unlimited

FROM:

Notice: Release only to Department of Defense Agencies is authorized. Other certified requesters shall obtain release approval from Director, Defense Nuclear Agency, Attn: STTI. Washington, DC 20305. Release or announcement to foreign governments or their nationals is not

AUTHORITY

DTRA ltr, 2 Mar 2001; Same.

CONFIDENTIAL

WT-1628

This document consists of 198 pages.

No. [redacted] of 175 copies, Series A

Operation

HARDTACK

April - October 1958

Project 3.4

LOADING AND RESPONSE OF SURFACE-SHIP HULL STRUCTURES FROM UNDERWATER BURSTS (U)

Issuance Date: December 11, 1961

HEADQUARTERS FIELD COMMAND
DEFENSE ATOMIC SUPPORT AGENCY
SANDIA BASE, ALBUQUERQUE, NEW MEXICO

FORMERLY RESTRICTED DATA

Handle as Restricted Data in foreign dissemination. Section 144b, Atomic Energy Act of 1954.

This material contains information affecting the national defense of the United States within the meaning of the espionage laws Title 18, U. S. C., Secs. 793 and 794, the transmission or revelation of which in any manner to an unauthorized person is prohibited by law.

CONFIDENTIAL

Inquiries relative to this report may be made to

Chief, Defense Atomic Support Agency
Washington 25, D. C.

When no longer required, this document may be destroyed in accordance with applicable security regulations.

DO NOT RETURN THIS DOCUMENT

USAEC Division of Technical Information Extension, Oak Ridge, Tennessee

WT-1628

OPERATION HARDTACK — PROJECT 3.4

LOADING AND RESPONSE OF SURFACE-SHIP HULL STRUCTURES FROM UNDERWATER BURSTS (U)

W. W. Murray, Project Officer

Underwater Explosions Research Division
Norfolk Naval Shipyard
Portsmouth, Virginia

CONFIDENTIAL

WT-1628

OPERATION HARDTACK—PROJECT 3.4

LOADING AND RESPONSE OF SURFACE-SHIP HULL STRUCTURES FROM UNDERWATER BURSTS (U)

W. W. Murray, Project Officer

Underwater Explosions Research Division,
Norfolk Naval Shipyard,
Portsmouth, Virginia

ABSTRACT

The objectives were to: (1) determine safe delivery ranges for surface ships from the standpoint of hull deflections; (2) determine the lethal ranges for merchant ships from the standpoint of hull deflections; and (3) obtain basic information on hull response to provide check points for model tests and for high-explosive tapered-charge tests.

The project participated in two underwater nuclear tests: Shots Wahoo and Umbrella.

Gages and recording centers were installed in the DD-474, DD-592, DD-593, EC-2, and (for Shot Wahoo only) a barge (YC) to document the basic hull response of these surface ships. The gage choice and layout on the target ships were governed by a determination to measure velocities, displacements, deflections, pressures, strains, rolling, and pitching. The total number of gages employed on all ships was about 170. The system used for recording the gage readings placed primary reliance on magnetic-tape recordings with a frequency-response flat up to 10 kc.

Measurements were obtained on the EC-2 and DD-593 during Shot Wahoo and on the EC-2 and all three DD's during Shot Umbrella. Failures of the command-timing signal system led to a complete loss of data on DD-474 and DD-592 during Shot Wahoo. A hull-damage survey of the EC-2 and the DD's was conducted after each shot. The test results secured both from the instrumentation effort and the hull-damage survey are presented.

The basic hull loading and response, together with their relation to free-water pressures, are described for each of the target ships. The hull damage measured in the EC-2 after each test was nearly identical. Hull damage was slight; the only significant hull deformation was found in the attacked side where side-frame deformation amounted to about 1 inch, and hull plating deformation to about 1 inch. No hull damage definitely attributable to the tests was observed on the DD's.

The following conclusions refer to underwater nuclear bursts and are specifically concerned with Wahoo and Umbrella conditions. The terms "Wahoo conditions" and "Umbrella conditions" include yield, shot geometries, bottom reflections, thermal-gradient characteristics, and target ship types.

From the standpoint of hull damage, the following safe delivery ranges for destroyers have been demonstrated: 2,900 feet under Wahoo conditions and 1,900 feet under Umbrella conditions. Minimum safe delivery ranges, from the standpoint of hull damage alone, are controlled by the direct shock wave alone under Wahoo and Umbrella conditions and are estimated to be 2,400 feet under Wahoo conditions and 1,700 feet under Umbrella conditions. For these estimates, hull deformation comparable in its operational significance to that sustained by the EC-2 is considered to be the maximum amount that can be called safe.

The lethal ranges for the EC-2 from the standpoint of hull damage are controlled by the direct shock wave under Wahoo and Umbrella conditions and may be estimated by use of the energy-density rule. The assumption that a 1.5-foot deformation of the attacked side frames represents lethal damage leads to the estimate that under both Wahoo and Umbrella conditions a horizontal range of 1,100 to 1,200 feet, or less, is lethal.

Checkpoints for small-scale Underwater Explosions Research Division (UERD) model experiments were obtained from both Shots Wahoo and Umbrella. However, no direct correlation with the UERD full-scale high-explosive tapered-charge tests (Project 3.1, Operation Hardtack) is possible because of the loss of data on the DD-592 during Shot Wahoo.

Basic information of hull response as related to free-field pressures and loading measurements was obtained, which is expected to prove valuable in extrapolating the results of Wahoo and Umbrella to other conditions.

FOREWORD

This report presents the final results of one of the projects participating in the military-effect programs of Operation Hardtack. Overall information about this and the other military-effect projects can be obtained from ITR-1660, the "Summary Report of the Commander, Task Unit 3." This technical summary includes: (1) tables listing each detonation with its yield, type, environment, meteorological conditions, etc.; (2) maps showing shot locations; (3) discussions of results by programs; (4) summaries of objectives, procedures, results, etc., for all projects; and (5) a listing of project reports for the military-effect programs.

PREFACE

The Underwater Explosions Research Division (UERD), Norfolk Naval Shipyard, assisted in the planning phases of Shots Wahoo and Umbrella. While the planning of such a large undertaking involved many individuals from many organizations, it is particularly pleasant to acknowledge the valuable contributions made to overall Wahoo planning by Dr. A. H. Keil, who at the time was Chief Scientist of UERD.

Project 3.4 could hardly have been carried out without the assistance of an enthusiastic team formed from personnel of the UERD. In the preparations for participation in Operation Hardtack, Mr. J. F. Shepherd and Mr. R. R. Walker made outstanding contributions to the success of the undertaking. After completion of the tests, the data reduction was expedited considerably by the interest of Mr. R. R. Walker who designed ingenious electronic devices to take advantage of the magnetic-tape recording system.

During the analysis phase of the project, several UERD personnel outside the immediate project team participated. The author is particularly appreciative of the valuable services rendered by Mr. R.M. Santamaria.

Special appreciation is expressed to the Naval Ordnance Laboratory Project 1.1 team; the Project 1.1 results were made available to UERD in advance of publication, and this facilitated immeasurably the task of analyzing Project 3.4 data.

CONTENTS

FIGURES

Chapter 1

INTRODUCTION

1.1 OBJECTIVES

The general tactical needs of the Navy underlying the underwater nuclear test phase of Operation Hardtack are to know the safe delivery range for surface-ship delivery of an underwater nuclear weapon, and to know the lethal range for merchant ships attacked by an underwater nuclear weapon. Operation Hardtack, in itself, was expected to satisfy these needs under two specific conditions. To be in a position to extrapolate the results obtained from Hardtack to any given tactical situation, it was necessary that the many complex phenomena occurring during the underwater tests be thoroughly documented. The measurements constituting this documentation are essential to an understanding of the events, which is a prerequisite to good weapon-effect predictions.

From the point of view of Program 3, whose primary interest is in the structural mechanical effects of nuclear bursts, the guiding aims in planning the tests were to: (1) document the free-field pressures, the loading histories (at the hulls), the target response histories, the equipment response histories, and the final hull and equipment damage; (2) provide checkpoints for model tests; and (3) provide checkpoints for tapered-charge full-scale tests. The second aim envisions the application of a relatively inexpensive experimental tool, i. e., model tests, to the prediction of basic response histories and gross hull damage. The third aim opens the door to the application of the tapered-charge technique in deriving statistical rules relating target response histories to equipment damage.

The special interest of Project 3.4 was primarily in the hull deformation and the basic target response of the surface ships. The specific objectives were to: (1) determine the safe range for surface ship delivery of an underwater nuclear weapon, from the standpoint of hull deflection; (2) determine the lethal range for merchant ships attacked by an underwater nuclear weapon, from the standpoint of hull deflection; and (3) obtain basic information on hull response as related to free-field pressures and loading measurements, so as to provide checkpoints for model experiments and for full-scale tests using high-explosive (HE) tapered charges.

1.2 BACKGROUND

To make weapon-effect predictions for surface ships under general conditions, it is necessary to understand the entire range of transition from the production of free-field pressures in the water through to the final hull and equipment damage within the ship. This range can be broken into the following phases: (1) the generation of free-field pressures; (2) the relation between the free-field pressures and both the loading at the hull and the initial hull response (the interaction problem);

(3) the transmission of the initial hull motions to the remainder of the ship (the shock pattern throughout the ship); (4) the relation between the initial hull motion (hull response) and the type and amount of damage produced in the ship's hull (hull damage); and (5) the relation between the magnitude of shock level that is observed in the shock pattern throughout the ship and the resulting equipment damage (shock damage).

Generally speaking, Phases 1, 2, and 3 are basic investigations relating the response to the loading and the free-field pressures, while Phases 4 and 5 concern the mechanical damage to the ship and the equipment and aim at establishing scales, or rules, relating the initial hull response to degrees of damage to the ship and the equipment aboard as well as degrees of inoperability. It is therefore obvious that, with respect to the general Navy objectives, the hull-response study (Project 3.4) cannot basically be separated from either the free-field pressure study (Projects 1.1 and 1.5) or from the equipment-shock study (Projects 3.3 and 3.8).

Little or no theoretical knowledge is at hand that will enable reliable predictions to be made of the effect of underwater nuclear bursts on surface ships, nor are the phenomena well enough understood to allow specific test results to be extrapolated with confidence to the general tactical situation. It is true that some theoretical knowledge (References 1 and 2) is available for the prediction of pressure histories at a point near the water surface in the case of the direct shock wave from an underwater explosion in deep water. It is also true that there remain situations for which this is not easy (Reference 3).

Moreover, even though the direct shock wave throughout much of the range of practical interest may be reasonably well predicted in deep water, the formation and subsequent closure of a cavitated surface layer (Reference 4) is at present not well understood. The pressure loading resulting from this closure cannot definitely be ruled out as of secondary importance in controlling the safe delivery range for surface ships under all conditions. Then, too, in many practical operational situations where the water depth is likely to range between, say, 500 to 5,000 feet (that is, the water depth is likely to be neither shallow nor deep) it would appear to be quite possible that the bottom reflections cause a shock response in the ship as severe or more severe than the shock response arising from the direct wave (Reference 5). Methods of predicting the characteristics of bottom-reflected waves have not been adequately formulated. In addition, a complicated interplay between the cavitation caused near the water surface by the direct shock wave and the bottom reflection will exist; it may even be that the bulk cavitation will, under certain conditions, screen out the bottom-reflected wave. Entirely aside from this, there is also a good likelihood that the bottom-reflected wave will itself give rise to bulk cavitation near the water surface. The difficulties in predicting pressures near the water surface when the burst occurs in deep water are compounded when the burst takes place in shallow water.

In any event, even if the pressures in the water about the ship are known, no reliable theoretical means exist by which the loading pressures at the hull or the initial velocity motions in the hull of the ship may be predicted. Attempts to do this on the basis of studying the theoretical response of a thin-plane, infinite and flexible plate to an acoustic pressure wave (the Taylor theory) are meaningful for a narrow range of special conditions, for a very short time, but are hardly reliable for the general situation of a nuclear explosion (Reference 6) of practical interest. Finally, even if the initial motions of the ship's hull were known, it is hardly possible on theoretical grounds alone, to predict (for nuclear explosion) either the shock pattern throughout the ship or the final significance of these shock motions for hull damage and equipment damage.

The lack of firm theoretical concepts concerning the generation of damage in surface ships by nuclear underwater bursts makes it imperative that basic information be obtained on hull response as related to free-field pressures and loading measurements. This

requires an extensive instrumentation of the target ships as well as measurements of the free-water pressures.

Relatively little experimental data is at present available on the hull and equipment shock-damage effects of underwater nuclear weapons against surface ships. Only two underwater nuclear tests involving surface ships had been conducted by this country; Operation Crossroads (Shot Baker) and Operation Wigwam. Neither of these tests produced data that can be reliably generalized to answer the general tactical problem. Shot Baker involved very special conditions, and neither the underwater phenomena nor the ship responses were extensively recorded. During Operation Wigwam, surface-ship targets were limited to support barges, and the shock motions recorded on these barges cannot be reliably interpreted in terms of damage to larger ships with Navy installed equipment.

Another source of information is provided by tests on small-scale models. The most extensive series of instrumented-model tests were carried out during the period, 1955 to 1957, at Underwater Explosions Research Division (UERD) employing rather realistically scaled models of a C-2 merchant ship (Reference 6) and a cruiser (Reference 7), the former on $^1/_{35}$ scale and the latter on $^1/_{22}$ scale. These models were, for the most part, tested at full draft under side-attack. However, a few tests were conducted with C-2 models at full draft attacked end-on, and at half-draft attacked side-on (Reference 8). The model tests carried out at UERD covered a great variety of charge weights and attack geometries and are, thus, expected to provide an extremely valuable means of extrapolating the results of full-scale tests, e. g., Hardtack, to other tactical situations. Moreover, since the model tests yielded a direct comparison of the response of two quite different types of ships (C-2 and cruiser), they are expected to provide valuable clues in extrapolating the results of Operation Hardtack to other types of surface ships.

An experimental tool (developed by UERD) is available to investigate the effects of the direct pressure wave resulting from a side-on nuclear attack against a full-scale surface ship without the actual use of a nuclear explosion. This is the tapered-charge technique investigated by Hardtack Project 3.1, which offers a method of establishing statistical rules relating the initial hull motions to the final equipment damage. The validity of this technique for certain phases of the response has already been suggested by model tests (Reference 9). It was expected that Project 3.1 would yield a full-scale demonstration of the application of the tapered-charge tool to a destroyer.

The Navy underwater nuclear-test phase of Operation Hardtack consisted of two shots designed to meet the objectives under two specific and distinct conditions: Shot Umbrella was to be in shallow (coastal) water, whereas Wahoo was to be in relatively deep water. In both tests it was understood that a nuclear device of 10 kt (± 20 percent) yield would be fired. Wahoo was to be fired at a depth of 500 feet (± 10 percent) in water about 3,000 feet deep, above a sloping bottom at a site southwest of the Eniwetok Atoll (Figure 1.1). Umbrella was to be fired at a depth of approximately 150 feet (± 10 percent) with the device on the water bottom (a reasonably level one) at a site in the southwest portion of the Eniwetok Lagoon (Figure 1.1).

Surface ships were to be present in both tests. The major surface ship targets were three destroyers drawn from reserve status (DD-474, DD-592, and DD-593) and one merchant ship (SS Michael Moran, an EC-2-S-Class design). The placement of the target ships was planned with the test conditions in mind. The ships of direct interest to Project 3.4 in the Wahoo and Umbrella arrays are indicated in Table 1.1 : this list includes one of the barges (YC-1) used in the Wahoo array. All planned target standoffs are given in Table 1.1 with reference to the midpoints of the ships. Indicated also in Table 1.1 are recommended tolerances in target standoff and orientation that it was hoped would be met in the final target placement.

The Wahoo and Umbrella test plans were made to help achieve the general Navy needs. The primary role of the destroyers was, of course, to help in satisfying the tactical need to know the safe-delivery range for destroyers delivering an underwater nuclear weapon. The DD's were therefore placed in positions where it was expected they would sustain light to moderate shock damage.

The EC-2 was to be used, in conjunction with the UERD model tests, to assist in satisfying the need to know the lethal range for merchant ships attacked by an underwater nuclear weapon. It was, therefore, to be placed side-on in a position to sustain moderate hull damage. The role of the YC-1, aside from the mooring requirements, was to yield further information on the effects of bulk cavitation.

One special feature of the array plans deserves emphasis. It was planned to attack DD-592 side-on. This same destroyer was previously attacked side-on with tapered charges during Project 3.1 under conditions of similar shock level. Thus, the completion of Operation Hardtack was expected to yield a final demonstration of the validity of the tapered-charge technique. A direct comparison was to be possible between the response of a full-scale ship to side-on nuclear attack and that of the same ship to side-on HE tapered-charge attack.

1.3 SCOPE OF REPORT

The instrumentation results obtained by Project 3.4 from participation in Wahoo and Umbrella are presented. The test results are analyzed and discussed, particularly insofar as they pertain to Phases 2, 3, and 4 of the overall range of phenomena discussed in Section 1.2. Attention is confined to the two underwater nuclear tests of Operation Hardtack.

TABLE 1.1 PLANNED PLACEMENT OF TARGET SHIPS INSTRUMENTED BY PROJECT 3.4

Shot	Target	Horizontal Distance from Surface Zero	Orientation	Direction (Relative) Prevailing Wind *
		feet		
Wahoo	DD-474	3,000 + 300 − 100	Stern end-on (± 15°)	down
	DD-592	5,000 + 400	Stbd side-on (± 15°)	down
	DD-593	9,000 ± 500	Stern end-on (± 15°)	down
	EC-2	2,300 + 200 − 100	Stbd side-on (± 15°)	up (approximate)
	YC-1	3,500 + 500 − 300	Immaterial	up (approximate)
Umbrella	DD-474	2,000 + 200 − 100	Stern end-on (± 15°)	down
	DD-592	3,000 ± 300	Stbd side-on (± 15°)	down
	DD-593	8,000 ± 500	Stern end-on (± 15°)	down
	EC-2	1,600 + 200 − 100	Port side-on (± 15°)	cross

* From surface zero.

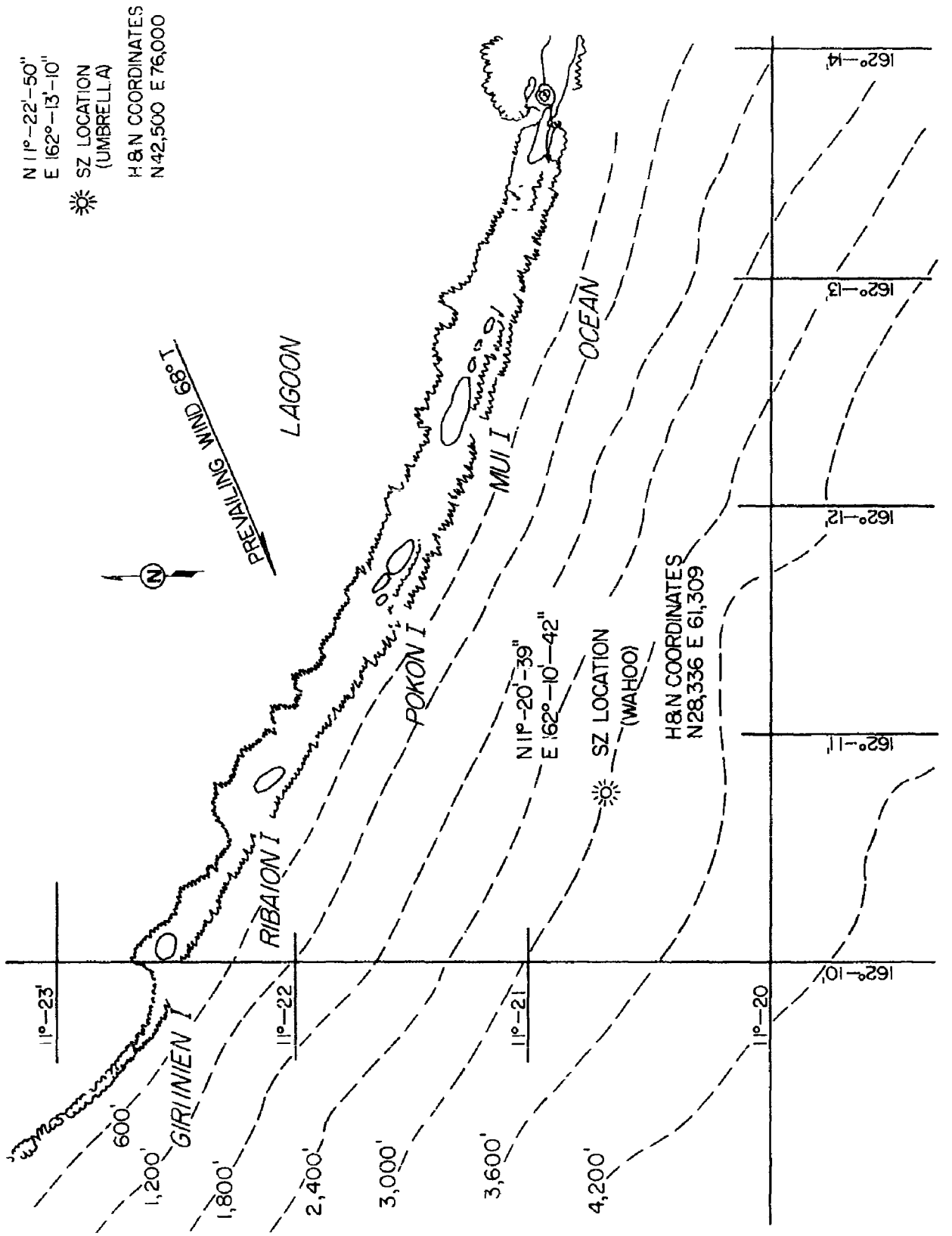

Figure 1.1 Test sites at Eniwetok Atoll for Shots Wahoo and Umbrella.

Chapter 2

PROCEDURE

2.1 OPERATIONS

General test preparations of interest to UERD were made at Long Beach Naval Shipyard (LBNS) and Pearl Harbor Naval Shipyard (PHNS). An inspection of the major target ships (including audigage measurements of the shell plating) indicated that their hulls were in good condition. The major target ships—three DD's and one EC-2 (Section 1.2)—were instrumented at LBNS, while the YC 1 (Hull YC-1413) was readied at PHNS. Following a UERD proposal, a special ballasting arrangement for the EC-2 had been planned under BUSHIPS auspices; the purpose of this arrangement was to help insure that the EC-2 remained afloat after sustaining hull damage from Shot Wahoo. This ballasting plan was implemented at LBNS in accordance with the scheme indicated in Figure 2.1.

Most of the special preparations for the tests required by Project 3.4 were completed before departure of the target ships for the Eniwetok Proving Ground (EPG). Five 60 kva diesel-engine generators were installed at LBNS on the major target ships in order to supply power for UERD equipment: one each in the three DD's (captain's stateroom) and two in the EC-2 (in a main deck space just to the port of the Project 3.4 instrument room recording center). The diesel generators were installed on wooden planks to protect the generators from damage due to the shock motions arising in the tests.

Air conditioning and humidity control equipment were installed at LBNS in the instrumentation spaces on the DD's and EC-2. This equipment was capable of maintaining the temperature at not over 90°, and relative humidity at about 50 percent. Cameras, with special mounts, were provided by Edgerton, Germeshausen, and Grier, Inc. (EG&G) and installed in the EC-2 at LBNS. The gage foundations and recording equipment, together with the connecting instrumentation cables, were installed in the DD's and EC-2 at LBNS. The recording equipment was installed on a specially designed shock-mounted platform within the instrument recording centers on the DD's and on the EC-2.

Preparations for a careful hull-damage survey of the EC-2 were also carried out at LBNS; punch marks and other reference points were made with the help of a surveyor's transit. The special preparations for the YC-1 were made at PHNS; storage batteries, motor generators, gage foundations, etc., were installed. Laboratory facilities were provided in a UERD trailer that was shipped to EPG.

Certain special tasks remained to be performed at EPG. Gages interior to the ships were installed; the final hookup of the gages and recording equipment was completed. The pressure gages and their cables were secured to the outer hull surfaces of the three DD's and the EC-2. The instrument recording facilities on YC-1, within the interior compartment just forward of the centerline, were completed. The laboratory trailer was set up on Parry Island. Checkouts of the equipment were accomplished on the target ships (both in the lagoon and at the Wahoo array) by project personnel. At the time of evacuation of the target ships, just before Shot Wahoo, the generators were left running, the air conditioners left on, all relays energized from batteries, and equipment was left ready to accept the timing signals from EG&G.

The activity between tests involved the following steps. The EC-2 was towed to the lagoon after Shot Wahoo. Because of the susceptibility of photographic film to damage from radiation, the films in the EG&G motion-picture cameras were removed from the EC-2 at the earliest practical time. In addition, the project records were removed as soon as reentry to the target ships was permitted. As soon after Shot Wahoo as possible, the project carried out detailed damage measurements on the hull of the EC-2 ; these were made with a surveyor's transit in sufficient detail to yield actual damage contours of the ship's hull. As soon as the target ships were reasonably free from radiological contamination, instrumentation engineers boarded the target ships, conducted a detailed inspection, and prepared a damage report on the instrumentation installations. Technical photographs of gages, instruments, and hull damage aboard the target ships were made as required. Data obtained on magnetic tape was played back within the UERD laboratory trailer, and data reduction was carried out to an extent sufficient to carry out a preliminary analysis. Equipment aboard the YC-1 was salvaged. Repairs to damaged equipment were effected and preparations made for participation in Shot Umbrella.

The windup phase of the operation took place after completion of Shot Umbrella. Data was secured after the test in a manner similar to that after Shot Wahoo. Playback again took place in the UERD laboratory trailer, and a preliminary analysis of the Umbrella test results was made. Arrangements were made for shipment of all shore-based equipment back to UERD. All equipment aboard the DD-474, DD-592, and DD-593 was left installed until these ships returned to the United States. Arrangements were made with LBNS for removal of this equipment and subsequent shipment to UERD, Norfolk Naval Shipyard (NNSY). Equipment aboard the EC-2 was salvaged at EPG and shipped back to UERD. Data reduction and analysis were completed after return to UERD.

2.2 INSTRUMENTATION

2.2.1 Preliminary Remarks. The YC-1 was instrumented in a sufficiently simple manner as to warrant only a cursory discussion. The basic idea was to install on YC-1, in the interior compartment just forward of the centerline, a few (6) velocity meters and to measure the vertical bodily motion of the YC-1 by recording directly (i.e., without amplification) on a visicorder (utilizing radiation-insensitive paper). The exact location of the meters, as well as other detailed information, has no significance inasmuch as no results were secured on the YC-1.

On the three destroyers, instrumentation was essentially similar though not identical. The largest difference was on DD-593, where gages had been installed in a similar fashion to that on the other DD's but were not actually all recorded: this was done to allow for the possibility that the relative positions of the DD's would be changed in the Umbrella array —an eventuality that did not arise. There was no great difference in the instrumentation of the target ships in Shots Wahoo or Umbrella.

Previous experience had shown the value of measuring as much of the pertinent phenomenology of the test event as was feasible, without imposing artificial limitations based on prevailing theories or on current notions of what had practical significance and what did not. In particular, it was deemed desirable to measure the target-ship response throughout its complete history, to measure this response with high-fidelity equipment, and to measure the individual phases of the response at all representative locations on the ships. At the same time, every attempt was made to increase the safety margin to insure that results would actually be obtained under field conditions; therefore, different types of gages and recordings were used to duplicate the most vital measurements.

It was planned to measure: loading pressures and velocities at the hulls, bodily velocities and displacements (both horizontal and vertical) of the ship as a whole, hull deflections

and strains (in the case of the EC-2), and flexural strains (in the case of the DD's). A photographic effort was to be made (contracted to EG&G) to record with high-speed motion-picture cameras the hull and bulkhead deflections within the EC-2 and to record with motion picture cameras stationed on shore, the bodily motion of the EC-2. In addition, a few free-water pressure measurements were made at shallow depths in order to supplement Project 1.1 measurements.

2.2.2 Gages Employed. The gages were basically of the same types that have previously been successfully employed by UERD in the field (Reference 10). In some cases modifications have been made which will be briefly indicated.

The pressure gage was of the piezoelectric (PE) type, wherein an electrical charge is produced on the faces of a crystal proportional to the applied pressure. The particular gages used had tourmaline as the sensitive element and had a gage factor of about 25 micro micro coulombs per pound per square inch ($\mu\mu$ c/ psi). Since the diameter of the gage was about $\frac{7}{8}$ inch, the transit time of an acoustic signal across the gage was less than 20 μsec. The time constant of the input circuit was on the order of 100 msec.

Each velocity meter (VM) consisted of a bar magnet seismically mounted within a coil of wire wrapped about a plastic core. Whenever the core was moved relative to the magnet the voltage induced in the coil would be proportional to the relative velocity of the motion, within a certain relative displacement range, called the linear range of the meter. In view of the seismic suspension, the VM could be conveniently used to measure absolute velocities.

Two types of VM were used to measure vertical velocities. These differed primarily in their mechanical characteristics. One was a small meter with a core length of 13.5 inches, a coil length of 5 inches, and a core diameter of $\frac{7}{8}$ inch. It had a linear range of about 2 inches and a suspension system natural period of about 200 msec. Stops were incorporated to prevent the magnet's exceeding the linear range of the meter. The high-frequency response of this velocity meter was primarily limited by its mechanical characteristics; it is estimated that this meter was capable of following changes in velocity having a duration as small as, say, 0.5 msec. The other type of velocity meter was larger, with a core length of 17 inches, a coil length of 15 inches, and a core diameter of $2\frac{3}{4}$ inches. It had a linear range of about 6 inches and a suspension system with a natural period of about $\frac{1}{3}$ second. This meter was not provided with stops. It was estimated to be capable of recording changes in velocity occurring over about 1.0 msec.

The velocity meter used to record horizontal velocities was essentially identical to the small vertical velocity meter except that its core diameter was $2\frac{3}{4}$ inches. The suspension system attachment for the magnet was, of course, designed somewhat differently; however, the resulting natural frequency was similar to that of the small vertical meter.

The natural frequencies of the velocity meter suspension systems were measured for nearly every gage. The results are listed in Table 2.1. The natural vibrations of the magnet mass and coil spring system are so slightly damped that this feature has no practicle significance for velocity meters.

The mechanical deflection (MD) gage consisted essentially of resistance wire wound on a rod and a sliding contact on the wire. Whenever the rod was moved with respect to the contact, the change in resistance to one end of the wire would be directly proportional to the deflection. Ordinarily, the sliding contact was rigidly attached to some structure.

Displacement gages, or seismic deflection (SD) gages were essentially deflection gages with the sliding contact attached to a seismically suspended mass. The natural frequency of the suspension was less than 2 cps. Whereas the deflection gage measured relative deflections, the displacement gage measured absolute displacements.

The natural vibration characteristics of the displacement gage suspension systems were measured for individual gages, and the results are listed in Table 2.2. The damping refers to an equivalent viscous damping defined by, $2 f \log A_1/A_2$, where f is the natural frequency and A_1 and A_2 are successive amplitudes spaced one period apart.

The strain gages (ST) were standard, commercial, resistance-wire strain gages (SR-4) and changes in length were measured by changes in resistance. These gages were bonded directly to the surface under test and had an active gage length of 6 inches.

The roll (R) and pitch (P) indicators are identical, differing only in orientation. The indicator consisted of a rigidly mounted potentiometer with a pendulum attached to its shaft. Changes in angle were registered as changes in resistance. The gage natural frequency was on the order of 1 cps.

The cameras employed to record hull damage development within Hold 3 of the EC-2 were Fairchild HS-100 movie cameras (13-mm lens, 16-mm film). They were shock mounted (for protection against shock damage), shielded by lead (for protection of the film against radiation), and enclosed in a waterproof case (for protection against flooding of the hold). Lighting was provided by photoflood lamps, powered by batteries.

2.2.3 Gage Locations. The locations of UERD gages on the destroyers are shown schematically in Figure 2.2 and in cross-sectional views in Figures 2.3 through 2.8. In parentheses after some of the gages shown in these figures is indicated the particular DD for which the location was applicable; an unmarked gage indicates that the location was applicable to all three DD's. With two exceptions, these locations were identical for Shots Wahoo and Umbrella. These exceptions are also indicated in parentheses after the gages shown in the figures. Not all gages shown in these figures were actually recorded on all DD's. More detailed information is given in Tables 2.3 through 2.5: this information is limited to gages that were actually recorded.

The locations of the UERD gages on the EC-2 are shown schematically in Figure 2.9, in a plan view in Figure 2.10, and in cross-sectional views of Figures 2.11 and 2.12. The symbols in parentheses have the same meaning as for the destroyers. Further detailed information is given in Table 2.6.

The high-speed motion-picture cameras installed by EG&G in Hold 3 of the EC-2 were located as shown in Figure 2.13. Also indicated roughly are the fields of view of these cameras.

Photographs of typical gage installations are given in Figures 2.14 through 2.20.

2.2.4 Recording Concepts and Equipment. The primary recording medium was magnetic tape. This choice was made in order to provide protection for the records against radiation. A limited number of string-oscillograph channels were recorded by means of photographic paper on each ship; the paper used was rather radiation insensitive. The cameras on the EC-2, of course, employed photographic film.

Two types of tape-recording equipment were used: Ampex FR-114 and S-3041. Eight recorders of each type were employed for recording use on the target ships.

The FR-114 equipment recorded 14 channels on tape 1 inch wide. The principles of frequency modulation were used to attain a low-frequency response to direct current. With a tape speed of 60 in/sec, a frequency response flat (within $\frac{1}{2}$ decibel) up to 10 kc was obtained. The equipment required a signal input of about 1.4 volts to achieve 40-percent deviation of the 54-kc carrier frequency.

The S-3041 equipment recorded seven independent data tracks on tape $\frac{1}{2}$ inch wide. The only tape speed available on this equipment was 30 in/sec. Two slightly different concepts were used for recording the data on S-3041 equipment. Some of the tracks on each recorder employed the same wide-bank FM recording techniques previously described, with only one

gage being recorded by each track. However, because the slower tape speed, the carrier frequency used was 27 kc, and the maximum frequency response expected was about 3 kc. Other tracks on each recorder were multiplexed to the extent that each track served to record data from two sources having more limited requirements as to frequency response. The method for multiplexing these signals was that commonly used in telemetering systems. Each signal source frequency modulated an individual oscillator. Two (or more) of the oscillator outputs could then be mixed and recorded on the same tape track, provided that the carrier and side bands from each oscillator were frequencies that would not interfere with those of the other oscillators. By playing the recorded data back through appropriate filters and discriminators, the original information could be separated and recovered.

Multiplexing use was minimized, because this technique has several disadvantages. The frequency response of each multiplexed channel was less than that of the wide-band channels, since the available frequency spectrum, in this case, had to contain two or more data channels without overlap or interference. For the same reason, the maximum deviation of each carrier was only $7\frac{1}{2}$ percent (or 15 percent, depending on the specific carrier frequency involved); therefore, the noise due to flutter was more significant. Intermodulation between oscillators made an additional contribution to the overall noise of the system. The combination of these factors resulted in the signal-to-noise ratio of the multiplexed channels being considerably poorer than that of the wide-band channels.

The string oscillographs were 906 visicorders, manufactured by Minneapolis-Honeywell Corporation. This equipment was capable of recording six channels of data on specially sensitized paper 6 inches wide. The maximum paper speed was 50 in/sec. The strings provided a frequency response flat to about 1,000 cps.

The recordings obtained on the visicorders installed on the major target ships were, in many cases, duplicates of those tape-recording channels that were selected as the most significant measurements. This multiple recording provided greater insurance for success in the event of equipment failure and also provided data quickly for the preliminary evaluation of the test results.

The recording medium of the cameras in Hold 3 of the EC-2 was 16-mm plus X photographic film (black and white). The film was run through the cameras at approximately 500 frames/sec.

2.2.5 Protection and Distribution of the Recording Equipment. The UERD recording center in each of the major ships was located as shown in Figures 2.2 and 2.9. The recording center for YC-1 was the interior compartment just forward of the centerline. Since no measurements were secured on YC-1, this barge will not be discussed.

All equipment on the major target ships was mounted on a specially designed shock-mounted table. This shock mount essentially consisted of a paired (top and bottom) system of air-ride springs stablized horizontally by steel springs. The system used on the DD's is shown in Figure 2.21; that for the EC-2 shown in Figure 2.22.

The vertical system used on the DD's consisted of eight air-ride (Firestone AY-28) springs supporting a total weight of about 5,500 pounds (platform plus equipment). The air overpressure in the lower springs was 29 psi while that in the upper springs was 11 psi; under these conditions, the springs supported the weight at their midpositions and were capable of undergoing a displacement of ± 4.5 inches. The natural frequency of small vertical vibrations was approximately 3 cps.

The horizontal system used on the DD's consisted of eight steel coil springs (4.8-inch-diameter coils of 1.19-inch-diameter wire) each with a spring constant of 4,200 lb/in.; four of these formed an athwartships system and four a longitudinal system. These springs were prestretched 1.25 inches and had a natural frequency of about 5.5 cps in each direction.

The system used on the EC-2 was similar. However, the total weight was nearly twice as great, and expected displacements were greater. The number of air-ride springs were doubled in series to allow for greater displacement. For Shot Wahoo, the air overpressure in the upper springs was 37 psi while that in the lower springs was 60 psi; for Shot Umbrella the corresponding pressures were about 52 and 75 psi. The allowable vertical displacement was about ± 9 inches while the natural frequency was about 3 cps for Shot Wahoo and slightly higher for Shot Umbrella. The steel springs were doubled in parallel, and the transverse (or longitudinal) natural frequency was about 5.5 cps.

The rooms on the major target ships that housed the recording centers were air conditioned and dehumidified in order to protect the equipment.

The recording equipment in the DD-474 consisted of two FR-114 recorders, two S-3041 recorders, and one 906 visicorder. Without including the visicorder, this arrangement provided 32 gage recording channels. The actual distribution of the gages among the recording channels for Shot Umbrella is given in Table 2.7. (The distribution for Shot Wahoo is not given, because no records were obtained in this test.)

The DD-592 had the same equipment as the DD-474, with the exception that it contained only one S-3041 tape recorder. The distribution of the gages among the recording channels in DD-592 is given in Table 2.8 for Shot Umbrella. (The distribution for Shot Wahoo is not given, because records were not obtained.)

The DD-593 had the same equipment as the DD-592. The distribution of the gages among the recording channels is given in Table 2.9; the small differences between Shots Wahoo and Umbrella are noted.

The recording equipment in the EC-2 consisted of two FR-114 recorders, four S-3041 recorders, and one 906 visicorder. An overall view of the recording equipment on EC-2 (fairly typical of the arrangement on all ships) is shown in Figure 2.23. Without including the visicorder, this arrangement provided about 48 data channels. The distribution of the gages among the recording channels is given in Table 2.10: the differences between Shots Wahoo and Umbrella are noted.

2.2.6 Calibration of Equipment. All equipment was calibrated immediately prior to the test by automatic insertion of a standard signal into each recording channel at the point where the gage connects to the recording equipment. Thus, the entire circuit, except the gage itself, was calibrated. The gages themselves were calibrated at UERD prior to the test.

In the case of strain gages, deflection gages, and roll and pitch indicators, where a change of resistance was measured, the standard signal supplied was determined by a known resistance. Where a voltage was being measured, as in the velocity meters, a standard voltage was supplied from mercury cells. The only other circuits requiring calibration were the pressure-recording channels, where an electrical charge was measured; these circuits were calibrated with the use of a standard capacitor.

2.2.7 Timing and Fiducial Signals. Timing signals were generated by crystal-controlled oscillators with an output frequency of 1 kc. This signal was fed to one channel of each recorder unit and used as a time standard. One out of every 10 timing pips was increased in amplitude to facilitate the record evaluation; one out of every 100 pips was further increased in amplitude.

Fiducial signals (provided by EG&G) indicated zero time. These signals were imposed on the timing channel in such a manner as to superimpose a pulse on the timing signals.

2.2.8 Sequence of Operations. All equipment, except the diesel-engine generators, was energized and operated by command signals received from EG&G. On each target ship,

EG&G provided a central receiving station with a hard wire running to relays within the Project 3.4 recording center.

Primary power was applied to all equipment on the major ships upon receipt of the signal at −30 minutes. In the event that this signal was not received, power was applied by the signal at −15 minutes. The tape transports started at −1 minute. The calibration signals were supplied to pressure recording channels from −15 seconds to −5 seconds. At −5 seconds, the film drive on the string oscillograph started, and calibration signals were applied to all channels not previously calibrated. At −1 second, all equipment returned to the operate condition and was then in a position to record the zero time signal and the data from the gages. Five minutes after zero time, all equipment was secured. The point of no return, of course, was at −1 minute, because the tape was then moving.

If the signal at −1 minute was not received, the signal at −15 seconds started the tape transports and the film drive on the string oscillographs. Alternate signals were automatically supplied by UERD equipment for all commands after the starting of the tape transports, in the event that any of these were not received from EG&G equipment.

2.3 DESCRIPTION OF DATA HANDLING

After Shots Wahoo and Umbrella, the raw data was, for the most part, on magnetic tapes, on photographic (radiation-insensitive) paper, and on photographic film. Of these, the last item pertains only to the motion-picture film obtained by EG&G during Shot Wahoo; the processing of this film (though not the analysis) was a responsibility of EG&G and will not be discussed here. Additional information, obtained by damage measurements of the EC-2 hull (made with a surveyor's transit), are sufficiently simple in concept as to need no discussion here.

The raw data (the first two items) was secured from the UERD recording centers on the target ships and was transferred to the UERD laboratory trailer for an initial processing. In the main, this processing simply consisted of developing the photographic paper and playing back selected magnetic tapes, primarily with the use of a visicorder. One FR-114 unit and one S-3042 playback unit were available for this purpose within the trailer. The handling of the photographic paper was a routine matter and warrants no further discussion. The magnetic tape playback is described below.

When a magnetic tape was played back, the output of the playback machine was a voltage reproduction of the original signal applied to the recorder. If the tape was played back at a speed slower than that at which it was recorded, an effect of time magnification was produced. Therefore, all of the frequencies involved in the recording process were reduced by the ratio of the speed change. FR-114 recorders were run at a tape speed of 60 in/sec while recording; on playback the FR-114 reproduce machine was run at 1.875 in/sec which gave a speed reduction of 32 to 1. Thus, for a frequency response of 0 to 10 kc during the recording phase, a band width of only 312.5 cps was required for the unit into which the signal was played back. The 3042 reproducer operates only at 30 in/sec, the same speed as the 3042 recorder. Therefore, a band width of 3 kc in the unit into which the signal was played back was required if no loss in fidelity was desired.

All tapes were played back into a visicorder, which had various paper speeds ranging from 0.2 to 50 in/sec. These speeds allowed the reproduction of signals recorded on the FR-114 machines to have time scales ranging from 6.4 to 1,600 in/sec, with no loss in fidelity. In the case of the 3042 reproducer, however, the maximum time scale obtained was 50 in/sec, and the frequency response of the reproduced record was somewhat poorer than that on the tapes.

Final processing of the magnetic tape data took place at UERD, following the return of project personnel from the field. A more elaborate treatment was then applied to the data

obtained by use of FR-114 equipment; data recorded by the 3042 unit was deemphasized, since it was not so readily amenable to automatic data reduction techniques. The purpose of this treatment was to extract as much physically meaningful information from the raw data as possible; the major data reduction techniques are described below.

During the shots, the recorders were, in several cases, subjected to noticeable shock loadings, even though they were mounted on shock mitigating platforms. Since the signal actually recorded on the tape was a carrier signal, frequency modulated by the gage signal, any variation of tape speed showed up as a spurious signal superimposed on the gage record when this was played back. To counteract these effects of shock, one channel on each recorder was used as a reference channel; no signal except the carrier frequency was recorded on it. When played back, the only output from a reference channel represented the spurious signal caused by tape speed variations. The first data reduction step was, therefore, to subtract electronically the reference channel signal from the gage channel signal. An example of the benefit achieved by this technique is shown in Figure 2.24.

In many cases it was desired to integrate the raw records, both for its own sake and as an intermediate step for further treatment. Two methods were successfully employed: an electronic device operating on signals from the tapes themselves and a high-speed digital computer (IBM 650) operating on cards read from playbacks of the raw record. The electronic integrating device is shown schematically in Figure 2.25: a Kintel 111-A amplifier was used after severance of its internal feedback loop.

Both velocity and displacement records were seismically corrected in accordance with the basic equation outlined below:

$$V_{corrected} = V_{meter} + \frac{a}{\omega} \int^t V_{meter}\, dt + \omega^2 \int^t dt \int^t V_{meter}\, dt$$

Where:

V = velocity, either as read by the meter or corrected

ω = natural undamped angular frequency

a = damping constant as used in Table 2.2

An example of a seismic correction is shown in Figure 2.26. Again, seismic corrections were carried out by two methods: an electronic device operating directly from the tapes and a digital computer operating from cards punched while reading the playbacks. The electronic method consisted of a suitable combination of electronic multipliers, integraters, and summers. Its basic element was the integrating circuit described above.

Velocity records were further corrected to compensate for the jumps introduced into the record when the meter magnet hit the stops. This jump correction was in every case carried out after the seismic correction procedure was applied and simply consisted of shifting the baseline up or down in such a fashion as to smoothly connect the records before and after the jumps. An example is shown in Figure 2.27.

The correction procedure for both seismic motions and stops was considered to yield physically meaningful measurements of ships motions in most cases for about 200 msec after arrival of the first shock wave. However, for later times, inevitable errors, due mainly to errors in establishing the baseline and in securing accurate values for gage natural frequencies, led to a slowly varying baseline upon which the true motion resulting from a later loading was superimposed. This naturally gave rise to additional difficulties in extracting information on the response to such later phenomena as the sea-bottom-reflected wave. The problem was solved rather straightforwardly simply by extrapolating the slowly varying trace found prior to such a later signal arrival and using this extrapolated

curve as a corrected baseline from which to read the record. An example of this procedure is given in Figure 2.28. To be sure, the resulting measurements of the response to a later loading could not be considered reliable for quite as long a time as was the case for the response to the first shock wave.

In certain special cases, fully corrected velocity measurements were utilized to deduce the shock spectrum at a corresponding location. This was done on a high-speed digital computer (IBM 650) in accordance with the well-known governing equations for the response of a single-degree-of-freedom system:

$$\frac{\omega^2 |y|}{g} = \frac{\omega^2}{g} \int_0^t V(t') \cos\omega (t - t') \, dt'$$

Where:

V = the velocity applied to the base of the system

t = the time

ω = the natural angular frequency of the single-degree-of-freedom system

g = 32 ft/sec^2

$|y|$ = the maximum absolute displacement

The term on the left-hand side is ordinarily designated the maximum absolute acceleration in g's and represents the quantity used in later plots.

TABLE 2.1 NATURAL FREQUENCIES OF VELOCITY METERS

Gage	Natural Frequency			
	DD-474	DD-592	DD-593	EC-2
	cps	cps	cps	cps
VM-1	5.85	5.60	5.56	5.00
VM-2	5.56	5.26	5.44	5.95
VM-3	5.19	5.47	5.46	5.40
VM-4	5.05	5.26	5.18	2.83
VM-5	5.45	5.19	5.25	5.06
VM-5a	*	*	*	2.82
VM-6	4.97	5.38	5.46	2.63
VM-7	5.35	5.03	4.80	4.63
VM-7a	*	*	*	5.44
VM-8	5.02	5.46	5.26	5.89
VM-9	5.47	5.33	5.54	5.71
VM-9a	*	*	*	5.13
VM-10	5.11	5.64	5.30	4.75
VM-11	5.01	5.15	5.92	4.78
VM-12	*	4.90	*	5.30
VM-13	*	*	*	2.79
VM-14	5.05	5.64	5.27	2.67
VM-15	4.85	*	5.38	4.96
VM-16	5.11	5.30	5.01	5.19
VM-16a	*	*	*	5.46
VM-17	5.56	5.11	5.00	4.46
VM-18	5.21	*	5.18	*

* Indicates no gage or gages not recorded.

TABLE 2.2 NATURAL VIBRATION CHARACTERISTICS OF SEISMIC DEFLECTION GAGES

Gage	Natural Frequency			Damping Constant *		
	EC-2	DD-474	DD-592	EC-2	DD-474	DD-592
	cps	cps	cps	1/sec	1/sec	1/sec
SD-1	X	1.60	1.75	X	0.63	1.42
SD-2	1.58	1.67	1.75	1.36	0.77	0.68
SD-3	1.35	1.65	1.72	0.35	0.81	0.52
SD-4	1.52	1.90	1.64	0.79	0.66	1.15
SD-5	1.33	1.70	1.67	1.73	0.86	0.57
SD-6	–	1.67	1.72	–	0.54	0.77

* $2f \log A_1/A_2$, where f is the natural frequency and A_1 and A_2 are successive amplitudes spaced one period apart.

TABLE 2.3 GAGE LOCATIONS ON DD-474, SHOT UMBRELLA

Gage	Orientation	Frame Number	Cross Section Location	Specific Location
VM-1	Vertical	18	Centerline	On keel 9 inches aft of bulkhead at Frame 18
VM-2	Vertical	72	Centerline	On keel 2 inches aft of bulkhead at Frame 72, 2 inches to starboard
VM-3	Radial	72	Starboard	On shell longitudinal No. 6 at bulkhead, $2\frac{1}{2}$ inches aft of frame
VM-4	Vertical	72	Centerline	On central bulkhead stiffener, 41 inches above keel, 2 inches aft of Frame 72
VM-5	Vertical	72	Port near centerline	On main deck over longitudinal No. 2, $2\frac{3}{4}$ inches forward of Frame 72
VM-6	Vertical	72	Centerline	On deck of sea cabin over bulkhead
VM-7	Vertical	$70\frac{1}{2}$	$44\frac{3}{8}$ inches stbd of CL	On deck of sea cabin near center of deck panel
VM-8	Vertical	$82\frac{1}{2}$	Centerline	On junction of keel and transverse stiffener
VM-9	Vertical	81	Starboard near centerline	On shell longitudinal No. 1 between transverse stiffeners
VM-10	Radial	$82\frac{1}{2}$	Port	On shell longitudinal No. 6, $4\frac{1}{4}$ inches forward of transverse stiffener
VM-11	Radial	$82\frac{1}{2}$	Starboard	On shell longitudinal No.6, $4\frac{1}{4}$ inches forward of transverse stiffener
VM-14	Vertical	$120\frac{1}{2}$	Centerline	On keel 4 inches aft of transverse stiffener
VM-15	Vertical	119	Starboard near centerline	On shell longitudinal No.1 between transverse stiffeners
VM-16	Vertical	148	Centerline	On keel, 2 inches stbd of centerline, $3\frac{3}{8}$ inches forward of Frame 148 bulkhead
VM-17	Vertical	148	Centerline	On main deck, $2\frac{1}{4}$ inches forward of bulkhead, $2\frac{1}{2}$ inches port of centerline
VM-18	Vertical	$146\frac{1}{2}$	Port near centerline	On main deck panel between deck longitudinal No. 1 and 2
SD-1	Vertical	18	Centerline	On second platform, 20 inches aft of Frame 18
SD-2	Vertical	70	Port	On main deck over longitudinal No.2, 3 inches fwd of Frame 70
SD-3	Vertical	$70\frac{1}{2}$	$12\frac{1}{2}$ inches stbd of CL	On deck of sea cabin near center of deck panel
SD-4	Vertical	110	Starboard near centerline	On main deck over longitudinal No. 2, 36 inches fwd of Frame 110
SD-5	Vertical	146	Port near centerline	On main deck panel between deck longitudinal No. 1 and 2
SD-6	Vertical	157	Centerline	On first platform 34 inches aft of Frame 157 at bulkhead
ST-1	Longitudinal	97	Port near centerline	On main deck directly over deck longitudinal No. 2 (extends from 2 inches fwd of Frame 97 to $30\frac{3}{4}$ inches aft of Frame 97)
ST-2	Longitudinal	146	Port near centerline	On main deck directly over deck longitudinal No. 2 (extends from Frame 147 to 31 inches fwd of Frame 147)
PE-1		18	Centerline	Under keel at bulkhead
PE-2		72	Centerline	Under keel at bulkhead
PE-3		$82\frac{1}{2}$	Centerline	Under junction of keel and transverse stiffener
PE-4		$82\frac{1}{2}$	Port	Under junction of shell longitudinal No. 6 and transverse stiffener
PE-5		$82\frac{1}{2}$	Starboard	Under junction of shell longitudinal No. 6 and transverse stiffener
PE-6		$120\frac{1}{2}$	Centerline	Under junction of keel and transverse stiffener
P-1	Longitudinal	71	Centerline	At 01 deck level, $23\frac{1}{2}$ inches port of centerline

TABLE 2.4 GAGE LOCATIONS ON DD-592, SHOT UMBRELLA

Gage	Orientation	Frame Number	Cross Section Location	Specific Location
VM-1	Vertical	18	Centerline	On keel 10 1/8 inches aft bulkhead at Frame 18
VM-2	Vertical	72	Centerline	On keel 2 3/4 inches aft bulkhead at Frame 72
VM-3	Radial	72	Starboard	On shell longitudinal No. 6 at bulkhead, 4 1/2 inches aft of frame
VM-4	Vertical	72	Centerline	On central bulkhead stiffener 37 1/4 inches above keel, 2 3/8 inches aft of Frame 72
VM-5	Vertical	72	29 inches port of CL	On main deck 2 3/4 inches fwd of Frame 72
VM-6	Vertical	72	Centerline	On deck of sea cabin over bulkhead
VM-7	Vertical	70 1/2	44 inches stbd of CL	On deck of sea cabin near center of deck panel
VM-8	Vertical	82 1/2	Centerline	On junction of keel and transverse stiffener
VM-9	Vertical	81	Starboard near centerline	On shell longitudinal No. 1 between transverse stiffeners
VM-10	Radial	82 1/2	Port	On shell longitudinal No. 6 just aft of transverse stiffener
VM-11	Radial	82 1/2	Starboard	On shell longitudinal No. 6, 4 1/4 inches aft of transverse stiffener
VM-12	Transverse	72	Centerline	At the center of gravity (14 feet 9 inches above bottom of keel)
VM-14	Vertical	120 1/2	Centerline	On keel 6 1/2 inches fwd of transverse stiffener
VM-16	Vertical	148	Centerline	29 inches above keel, 2 1/4 inches fwd of Frame 148 bulkhead
VM-17	Vertical	148	Centerline	On main deck, 2 inches fwd of bulkhead
SD-1	Vertical	18	Centerline	On second platform, 20 1/8 inches aft of Frame 18
SD-2	Vertical	54	5 ft 5 inches port of CL	On first deck 20 3/4 inches fwd of Frame 54 bulkhead
SD-3	Vertical	70 1/2	13 1/2 inches stbd of CL	On deck of sea cabin near center of deck panel
SD-4	Vertical	92 1/2	Centerline	On main deck over bulkhead
SD-5	Vertical	146	Port near centerline	On main deck panel between deck longitudinal No. 1 and 2
SD-6	Vertical	157	Centerline	On first platform 33 3/4 inches aft of Frame 157 bulkhead
PE-1		99	8 1/2 feet off stbd side	Free-water PE, 27 feet under water surface
PE-2		99	8 1/2 feet off stbd side	Free-water PE, 18 feet under water surface
PE-3		82 1/2	Centerline	Under junction of keel and transverse stiffener
PE-4		82 1/2	Port	Under junction of shell longitudinal No. 6 and transverse stiffener
PE-5		82 1/2	Starboard	Under junction of shell longitudinal No. 6 and transverse stiffener
PE-6		120 1/2	Centerline	Under junction of keel and transverse stiffener
R-1	Transverse	66	Centerline	At 01 deck level

TABLE 2.5 TABULATION OF GAGE LOCATIONS ON DD-593, SHOTS WAHOO AND UMBRELLA

Gage	Orientation	Frame Number	Cross Section Location	Specific Location
VM-1	Vertical	18	Centerline	On keel 10 1/4 inches aft of bulkhead at Frame 18
VM-2	Vertical	72	Centerline	On keel 3 inches aft of bulkhead at Frame 72, 2 inches starboard of centerline
VM-3	Radial	72	Starboard	On shell longitudinal No. 6 at bulkhead, 2 1/2 inches aft of frame
VM-4	Vertical	72	Centerline	On central bulkhead stiffener, 40 inches above keel, 2 1/2 inches aft of Frame 72
VM-5	Vertical	72	1 1/2 inches stbd of CL	On main deck, 6 1/2 inches fwd of Frame 72
VM-6	Vertical	72	Centerline	On deck of sea cabin over bulkhead
VM-7	Vertical	70 1/2	45 inches stbd of CL	On deck of sea cabin near center of deck panel
VM-8	Vertical	82 1/2	Centerline	On junction of keel and transverse stiffener, 5 inches fwd of Frame 82 1/2
VM-9	Vertical	81	Starboard near centerline	On shell longitudinal No. 1 between transverse stiffeners, 1 inch fwd of frame
VM-10	Radial	82 1/2	Port	On shell longitudinal No. 6, 1 1/2 inches down from center of longitudinal just aft of transverse stiffener
VM-11	Radial	82 1/2	Starboard	On shell longitudinal No.6, 2 inches up from center of longitudinal just aft of transverse stiffener
VM-14	Vertical	120 1/2	Centerline	On keel at transverse stiffener
VM-15	Vertical	119	Starboard near centerline	On shell longitudinal No. 1 between transverse stiffeners
VM-16	Vertical	148	Centerline	29 inches above keel, 2 1/2 inches fwd of Frame 148 bulkhead
VM-17	Vertical	148	2 inches stbd of CL	On main deck, 2 inches fwd of bulkhead
VM-18	Vertical	147	13 inches port of CL	On main deck panel between deck longitudinal No. 1 and 2, 6 inches fwd of Frame 147
PE-1		18	Centerline	Under keel at bulkhead
PE-2		72	Centerline	Under keel at bulkhead
PE-3		82 1/2	Centerline	Under junction of keel and transverse stiffener
PE-4		82 1/2	Port	Under junction of shell longitudinal No. 6 and transverse stiffener
PE-5		82 1/2	Starboard	Under junction of shell longitudinal No. 6 and transverse stiffener
PE-6		120 1/2	Centerline	Under junction of keel and transverse stiffener

TABLE 2.6 GAGE LOCATIONS ON EC-2, SHOTS WAHOO AND UMBRELLA

Gage	Orientation	Frame Number	Cross Section Location	Specific Location
VM-1	Vertical	88	2½ inches stbd of CL	On inner bottom 2¾ inches fwd of Frame 88
VM-2	Vertical	88	Port	On inner bottom 2½ inches fwd of Frame 88, 4 inches from port shell
VM-3	Vertical	88	Starboard	On inner bottom 2½ inches fwd of Frame 88, 3½ inches from stbd shell
VM-4 *	Vertical	88	Centerline	On bulkhead, center 37½ inches above second deck, 7 inches aft of Frame 88
VM-5	Vertical	89	Centerline	On bulkhead, base 26¼ inches above bridge level, 2½ inches fwd of Frame 89
VM-5A *	Vertical	89	7 inches stbd of CL	On bulkhead, center 27 inches above bridge level, 4¾ inches fwd of Frame 89
VM-6 *	Vertical	85	7¼ inches stbd of CL	Center 22⅝ inches above bridge level, 17¾ inches fwd of Frame 85
VM-7	Vertical	98	Centerline	On inner bottom 3 inches aft of Frame 98
VM-7A	Vertical	98	Centerline	On inner bottom 3 inches fwd of Frame 98
VM-8	Vertical	98	Port	On inner bottom 2¾ inches aft of Frame 98, 3½ inches from port shell
VM-9	Vertical	98	Starboard	On inner bottom 2½ inches aft of Frame 98, 4 inches from stbd shell
VM-9A	Vertical	98	Starboard	On inner bottom 2½ inches aft of Frame 98, 7¾ inches from stbd shell
VM-10	Transverse	98	Port	On shell stiffener 8 feet 9 inches above inner bottom
VM-11	Transverse	98	Starboard	On shell stiffener 8 feet 9 inches above inner bottom,
VM-12	Vertical	108	Centerline	On bulkhead, base 11 feet 10 inches above inner bottom, 2¾ inches fwd of Frame 108
VM-13 *	Vertical	108	Centerline	On bulkhead, center 46 inches below second deck, 7 inches fwd of Frame 108
VM-14 *	Vertical	92½	9¾ inches stbd of CL	Center 23¾ inches above inner bottom, 16½ inches fwd of Frame 93
VM-15	Transverse	88	Centerline	13 feet 11 inches above inner bottom, 20¼ inches fwd of Frame 88
VM-16	Vertical	88	2½ inches stbd of CL	Base 48½ inches above inner bottom, 2¾ inches fwd of Frame 88
VM-16A	Vertical	88	2½ inches port of CL	Base 48½ inches above inner bottom, 2½ inches fwd of Frame 88
VM-17	Transverse	88	Centerline	On overhead above bridge level
SD-1	Vertical	87	Centerline	On inner bottom 28 inches fwd of Frame 88
SD-2	Vertical	88½	37 inches stbd of CL	On second deck 15 inches aft of Frame 88
SD-3	Vertical	86½	Centerline	On bridge level 41¼ inches fwd of Frame 88
SD-4	Vertical	105	11 feet 2 inches stbd of CL	On inner bottom 5 inches fwd of Frame 105
SD-5	Vertical	94	9¾ inches stbd of CL	On inner bottom 22 inches fwd of Frame 95
PE-1		98	Centerline	Under keel
PE-2		98	Port	At intersection off shell and inner bottom
PE-3(W)		98	Just off stbd side	Free-water PE, 22 feet under water surface
PE-3(U)		148	23 feet off stbd side	Free-water PE, 10 feet under water surface
PE-4		98	Port	On shell 8 feet 9 inches above inner bottom
PE-5(W)		98	Just off stbd side	Free-water PE, 22 feet under water surface
PE-5(U)		148	23 feet off stbd side	Free-water PE, 27 feet under water surface
PE-6(W)		88	Just off port side	Free-water PE, 47 feet under water surface
PE-6(U)		148	23 feet off stbd side	Free-water PE, 44 feet under water surface
MD-1	Transverse	78	Starboard	On shell stiffener, 8 feet 9 inches above inner bottom
MD-2(W)	Transverse	82	Starboard	On shell stiffener, 8 feet 9 inches above inner bottom
MD-2(U)	Transverse	82	Port	On shell stiffener, 8 feet 9 inches above inner bottom
MD-3	Transverse	78	Port	On shell stiffener, 8 feet 9 inches above inner bottom
MD-4(W)	Transverse	87	Starboard	Between shell stiffener and bulkhead stiffener, 8 feet 9 inches above inner bottom
MD-4(U)	Transverse	87	Port	Between shell stiffener and bulkhead stiffener, 8 feet 9 inches above inner bottom
MD-5	Vertical	86½	Centerline	On inner bottom 12 inches aft of Frame 86
MD-6(W)	Vertical	86½	12 feet 8 inches stbd of CL	On inner bottom 12 inches aft of Frame 86
MD-6(U)	Vertical	86½	12 feet 8 inches port of CL	On inner bottom 12 inches aft of Frame 86
ST-1	Longitudinal	97½	Starboard	On shell plating 8 feet 9 inches above inner bottom midway between shell stiffeners
ST-2	Longitudinal	98½	Starboard	On shell plating 8 feet 9 inches above inner bottom midway between shell stiffeners
R-1	Transverse	88	Centerline	On overhead above main deck level
P-1	Longitudinal	88	Centerline	On overhead above main deck level

Notes: * Large velocity meter. (W) indicates gage position used only in Wahoo. (U) indicates gage position used only in Umbrella. A indicates a gage at an essentially duplicate position.

TABLE 2.7 GAGE DISTRIBUTION AMONG RECORDING CHANNELS IN DD-474, SHOT UMBRELLA

FR-114 Tape Recorder	FR-114 Tape Recorder	S-3041 Tape Recorder	S-3041 Tape Recorder	906 Visicorder
PE-1 PE-3	PE-2 PE-4	VM-3	VM-7	Timing and Fiducial
PE-5 VM-1	PE-6 VM-2	VM-18	SD-2	VM-6
P-1 ST-1	VM-4 VM-5	SD-6	VM-15	VM-8
Timing and Fiducial VM-9	Timing and Fiducial VM-6	Timing and Fiducial	Timing and Fiducial	VM-4
VM-10 SD-3	ST-2 VM-11	R.S. *	R.S. *	VM-11
VM-16 VM-17	SD-1 VM-14	R.S. * R.S. *	R.S. * R.S. *	SD-2
SD-4 R.S. *	SD-5 R.S. *	VM-8 ST-2	VM-17 P-1	ST-1

*R. S. = Reference signal.

TABLE 2.8 GAGE DISTRIBUTION AMONG RECORDING CHANNELS IN DD-592, SHOT UMBRELLA

FR-114 Tape Recorder	FR-114 Tape Recorder	S-3041 Tape Recorder	906 Visicorder
PE-1 PE-3	PE-2 PE-4	SD-3	Timing and Fiducial
PE-5 VM-1	PE-6 VM-2	SD-4	VM-4
VM-3 VM-8	VM-4 VM-5	Reference	VM-6
Timing and Fiducial VM-9	Timing and Fiducial VM-6	Timing and Fiducial	VM-8
VM-10 VM-12	VM-7 VM-11	SD-6	VM-11
VM-16 VM-17	R-1 VM-14	SD-5 R-1	SD-2
SD-1 R.S. *	SD-2 R. S. *	R.S.* R.S. *	SD-5

* R.S. = Reference signal.

TABLE 2.9 GAGE DISTRIBUTION AMONG RECORDING CHANNELS IN DD-593, SHOTS WAHOO AND UMBRELLA

FR-114 Tape Recorder	FR-114 Tape Recorder	906 Visicorder
PE-1 PE-3	PE-2 PE-4	Timing and Fiducial
PE-5 VM-1	PE-6 VM-2	VM-4
VM-3 VM-8	VM-4 VM-5	VM-6(W) and VM-14(U)
Timing and Fiducial	Timing and Fiducial	VM-8
VM-9 VM-10 –	VM-6 VM-7 VM-11	VM-11
VM-16 VM-17	– VM-14	VM-1
VM-18 Reference	VM-15 Reference	VM-16

Notes: (W) Indicates recording position used in Wahoo.
(U) Indicates recording position used in Umbrella.

TABLE 2.7 GAGE DISTRIBUTION AMONG RECORDING CHANNELS IN DD-474, SHOT UMBRELLA

FR-114 Tape Recorder	FR-114 Tape Recorder	S-3041 Tape Recorder	S-3041 Tape Recorder	906 Visicorder
PE-1 PE-3	PE-2 PE-4	VM-3	VM-7	Timing and Fiducial
PE-5 VM-1	PE-6 VM-2	VM-18	SD-2	VM-6
P-1 ST-1	VM-4 VM-5	SD-6	VM-15	VM-8
Timing and Fiducial VM-9	Timing and Fiducial VM-6	Timing and Fiducial	Timing and Fiducial	VM-4
VM-10 SD-3	ST-2 VM-11	R.S. *	R.S. *	VM-11
VM-16 VM-17	SD-1 VM-14	R.S. * R.S. *	R.S. * R.S. *	SD-2
SD-4 R.S. *	SD-5 R.S. *	VM-8 ST-2	VM-17 P-1	ST-1

*R.S. = Reference signal.

TABLE 2.8 GAGE DISTRIBUTION AMONG RECORDING CHANNELS IN DD-592, SHOT UMBRELLA

FR-114 Tape Recorder	FR-114 Tape Recorder	S-3041 Tape Recorder	906 Visicorder
PE-1 PE-3	PE-2 PE-4	SD-3	Timing and Fiducial
PE-5 VM-1	PE-6 VM-2	SD-4	VM-4
VM-3 VM-8	VM-4 VM-5	Reference	VM-6
Timing and Fiducial VM-9	Timing and Fiducial VM-6	Timing and Fiducial	VM-8
VM-10 VM-12	VM-7 VM-11	SD-6	VM-11
VM-16 VM-17	R-1 VM-14	SD-5 R-1	SD-2
SD-1 R.S. *	SD-2 R.S. *	R.S. * R.S. *	SD-6

* R.S. = Reference signal.

TABLE 2.9 GAGE DISTRIBUTION AMONG RECORDING CHANNELS IN DD-593, SHOTS WAHOO AND UMBRELLA

FR-114 Tape Recorder	FR-114 Tape Recorder	906 Visicorder
PE-1 PE-3	PE-2 PE-4	Timing and Fiducial
PE-5 VM-1	PE-6 VM-2	VM-4
VM-3 VM-8	VM-4 VM-5	VM-6(W) and VM-14(U)
Timing and Fiducial	Timing and Fiducial	VM-8
VM-9 VM-10 --	VM-6 VM-7 VM-11	VM-11
VM-16 VM-17	-- VM-14	VM-1
VM-18 Reference	VM-15 Reference	VM-16

Notes: (W) indicates recording position used in Wahoo.
(U) indicates recording position used in Umbrella.

TABLE 2.10 GAGE DISTRIBUTION AMONG RECORDING CHANNELS IN EC-2, SHOTS WAHOO AND UMBRELLA

Frame 114	Frame 114	S-3041	S-3041	S-3041	S-3041		906 Visicorder
PE-1 PE-2	PE-3 PE-4	VM-6	VM-17	PE-1(W) VM-11(U)	—	—	Timing
PE-5 VM-5	PE-6 VM-1	ST-1(W), Ref (U)	ST-2(W), Ref (U)	VM-11(W), Ref (U)	VM-6(W)	SD-1(W)	VM-5A(W), VM-3(U)
VM-7(W), R-1(U), VM-8	VM-2 VM-3(W), VM-14(U)	MD-1(W), MD-4(U)	MD-3(W), MD-2(U)	VM-14	MD-2(W)	R-1(W)	VM-7A
Timing VM-9(W), SD-3(U)	Timing VM-4	Timing	Timing	Timing	Timing		VM-9(W), VM-16(U)
VM-11 VM-12(W), SD-2(U)	VM-5A VM-7A	MD-5	MD-4(W), MD-1(U)	MD-6	SD-2(W)	Reference Signal (W)	VM-16(W), SD-5(U)
VM-13 VM-15 VM-16	VM-9A VM-10 VM-16A(W), MD-3(U)	SD-4	SD-5(W) P-1(U)	SD-1	SD-3(W)	P-1(W)	SD-4(W), MD-5(U)
Reference Signal	Reference Signal	Reference Signal	Reference Signal	Reference Signal	VM-1(W)	SD-4(W)	

(W) indicates gage position used only in Wahoo. (U) indicates gage position used only in Umbrella. A indicates a gage at an essentially duplicate position.

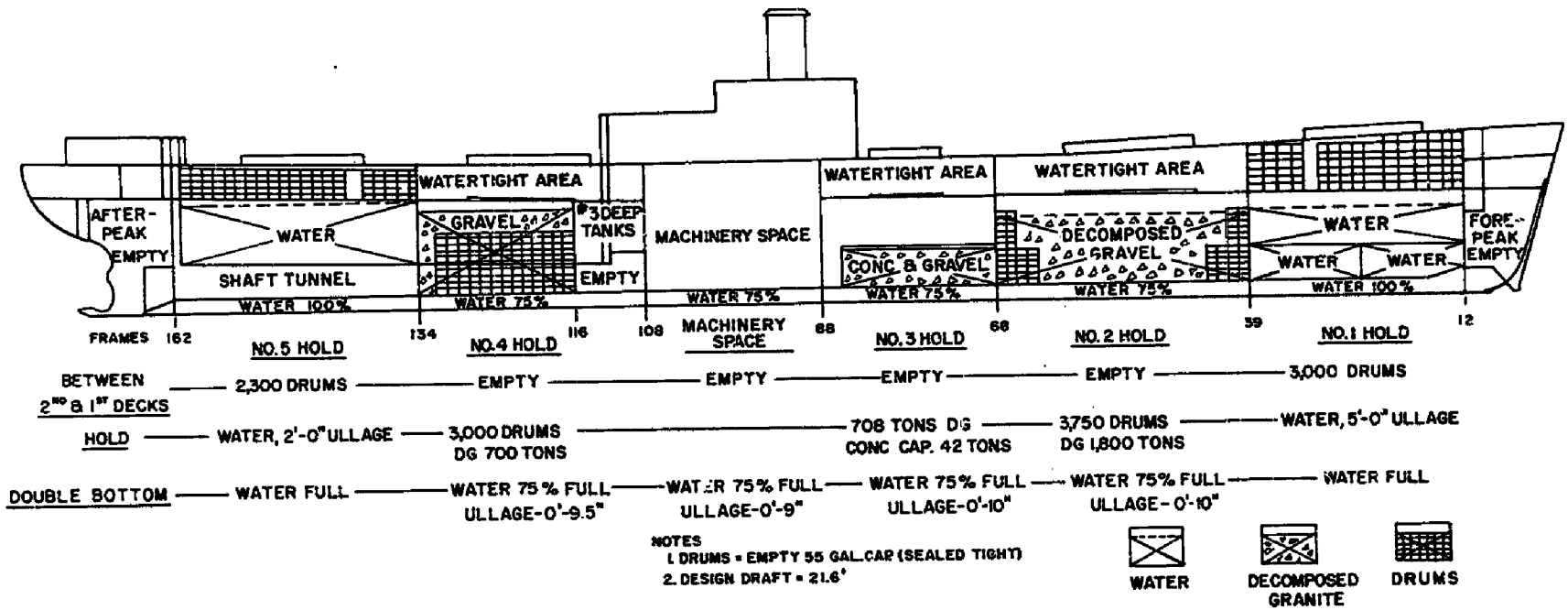

Figure 2.1 EC-2 ballast plan.

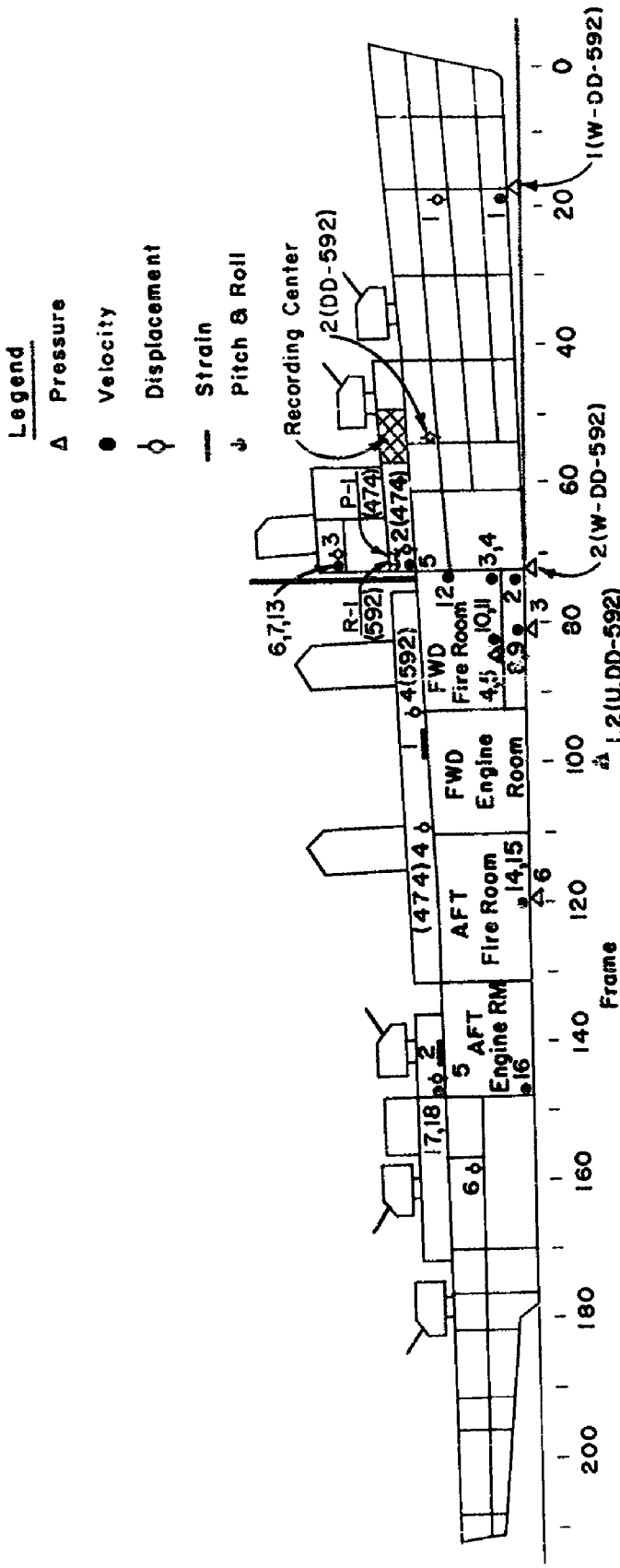

Figure 2.2 DD gage locations, overall schematic.

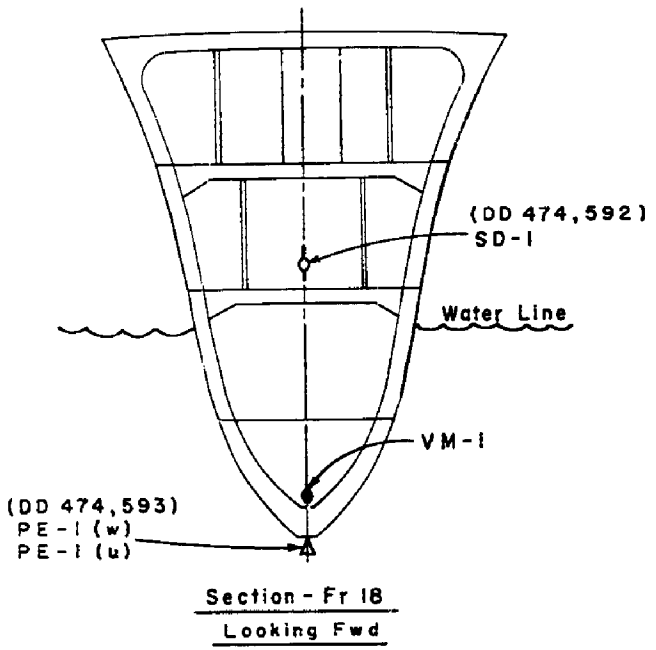

Figure 2.3 Destroyer gage locations.

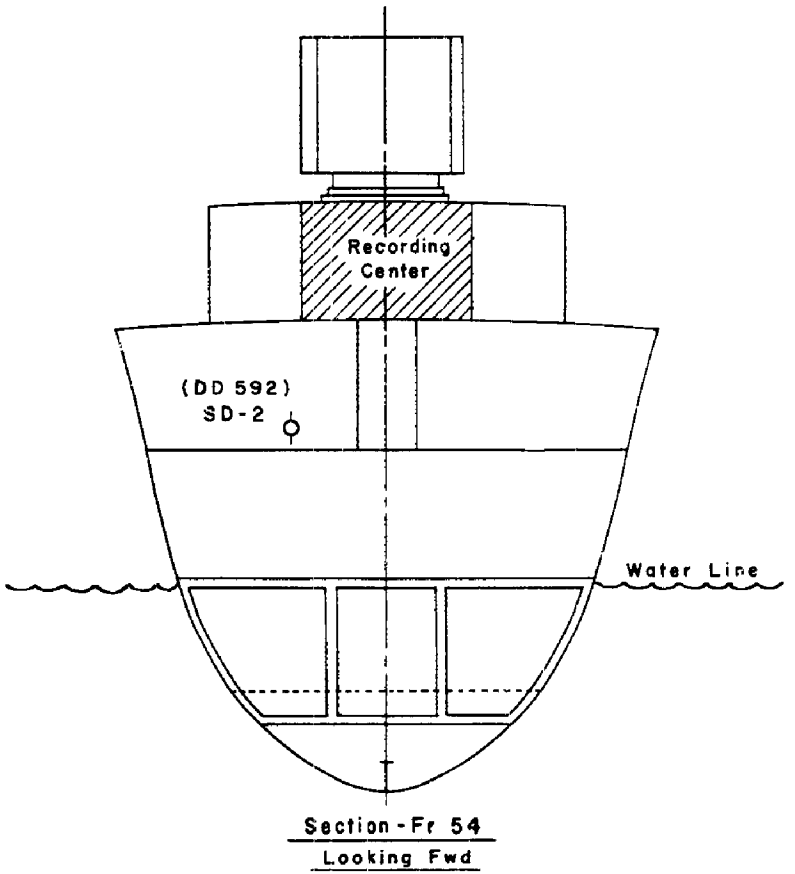

Figure 2.4 Destroyer gage locations.

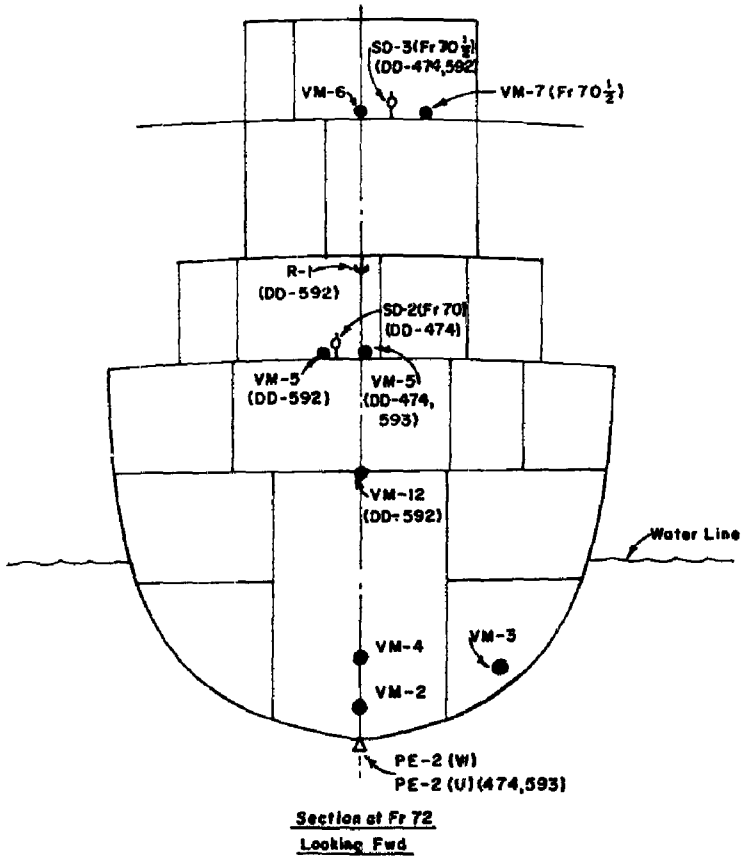

Figure 2.5 Destroyer gage locations.

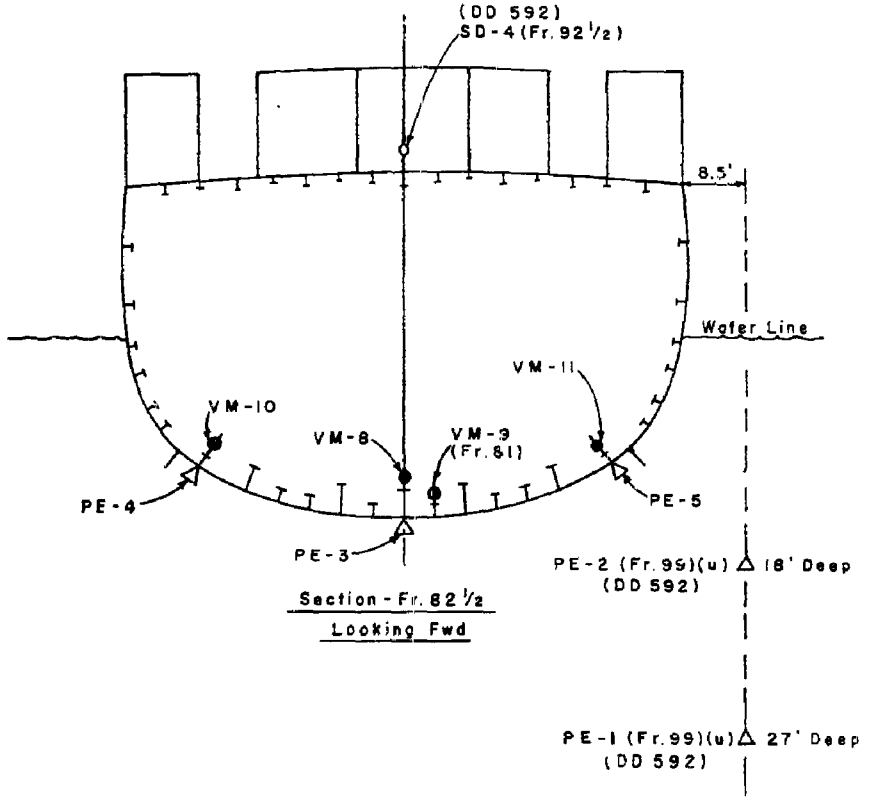

Figure 2.6 Destroyer gage locations.

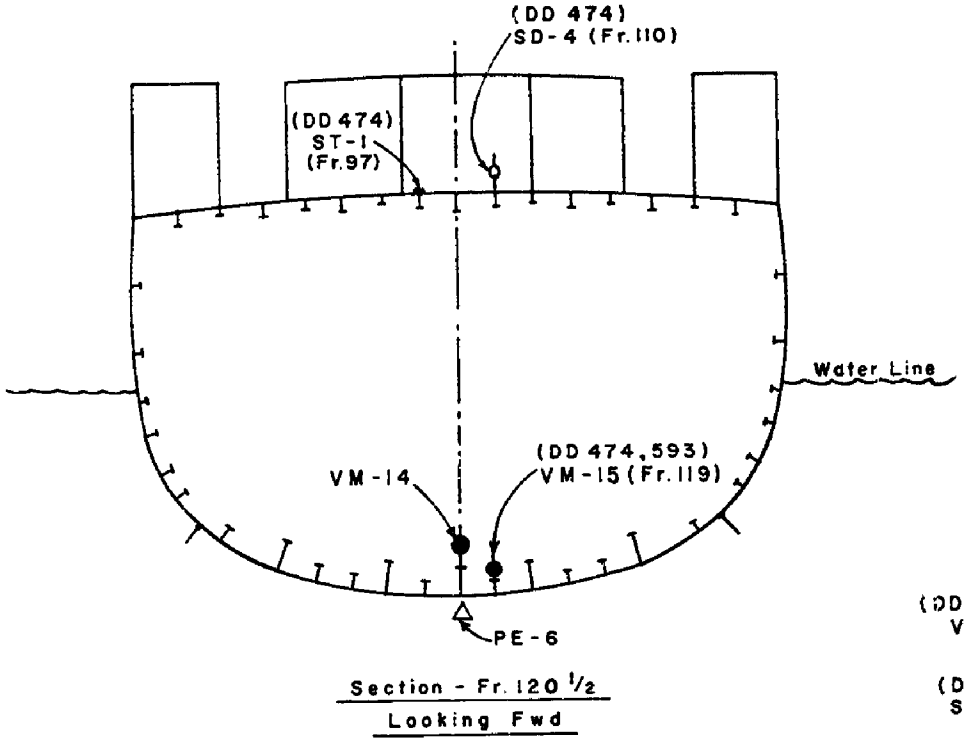

Figure 2.7 Destroyer gage locations.

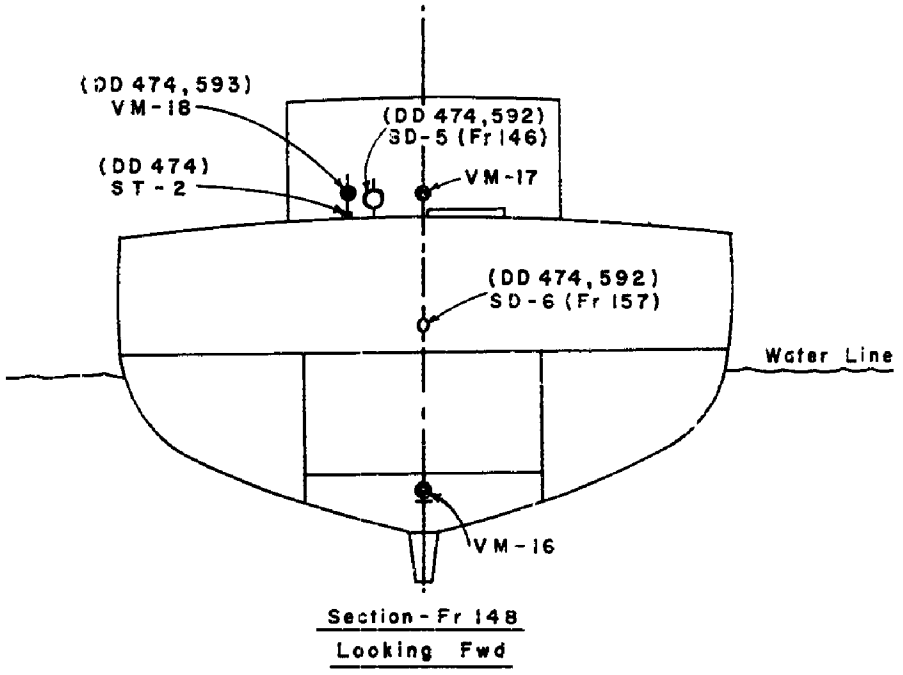

Figure 2.8 Destroyer gage locations.

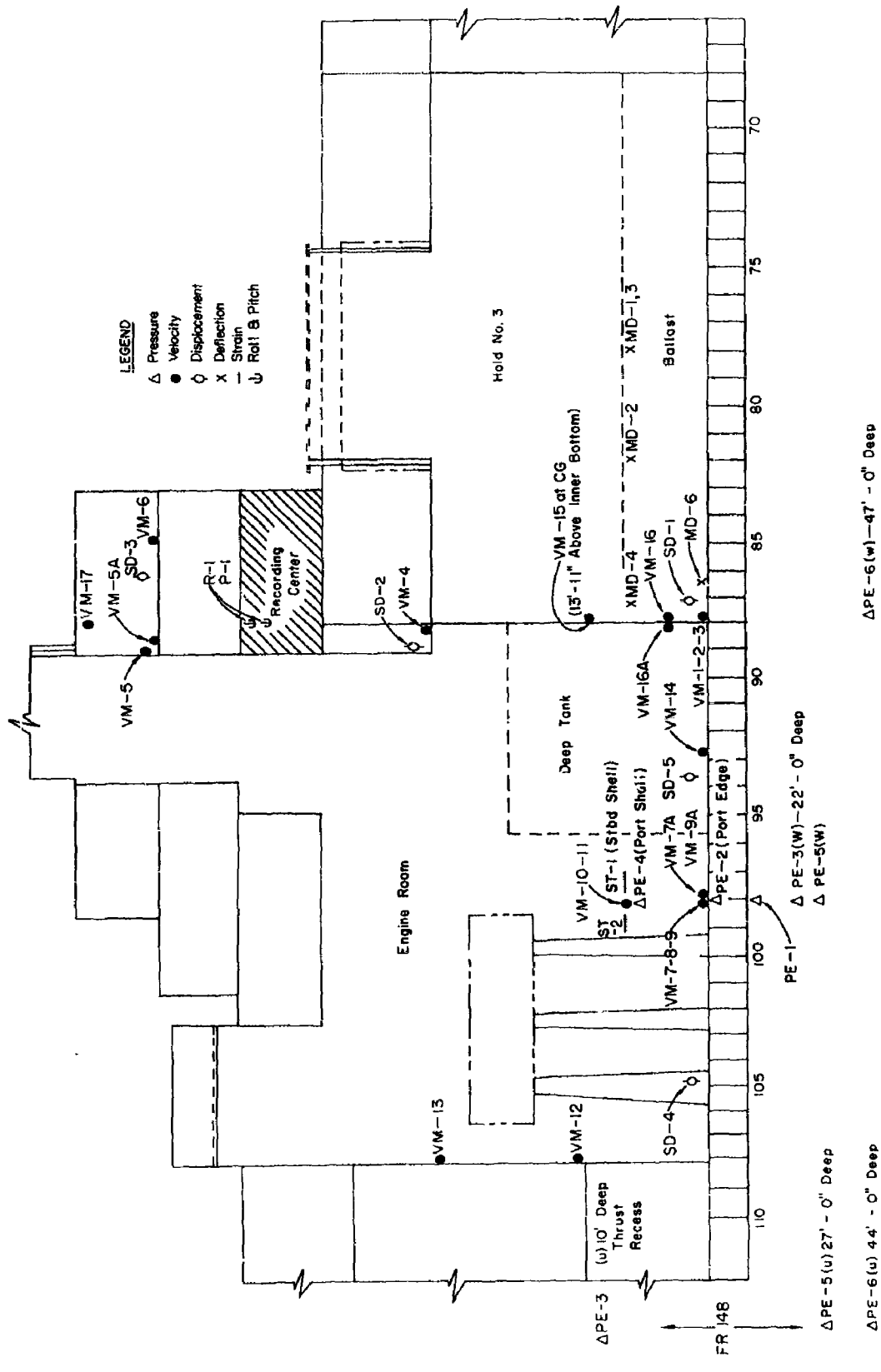

Figure 2.9 EC-2 gage locations.

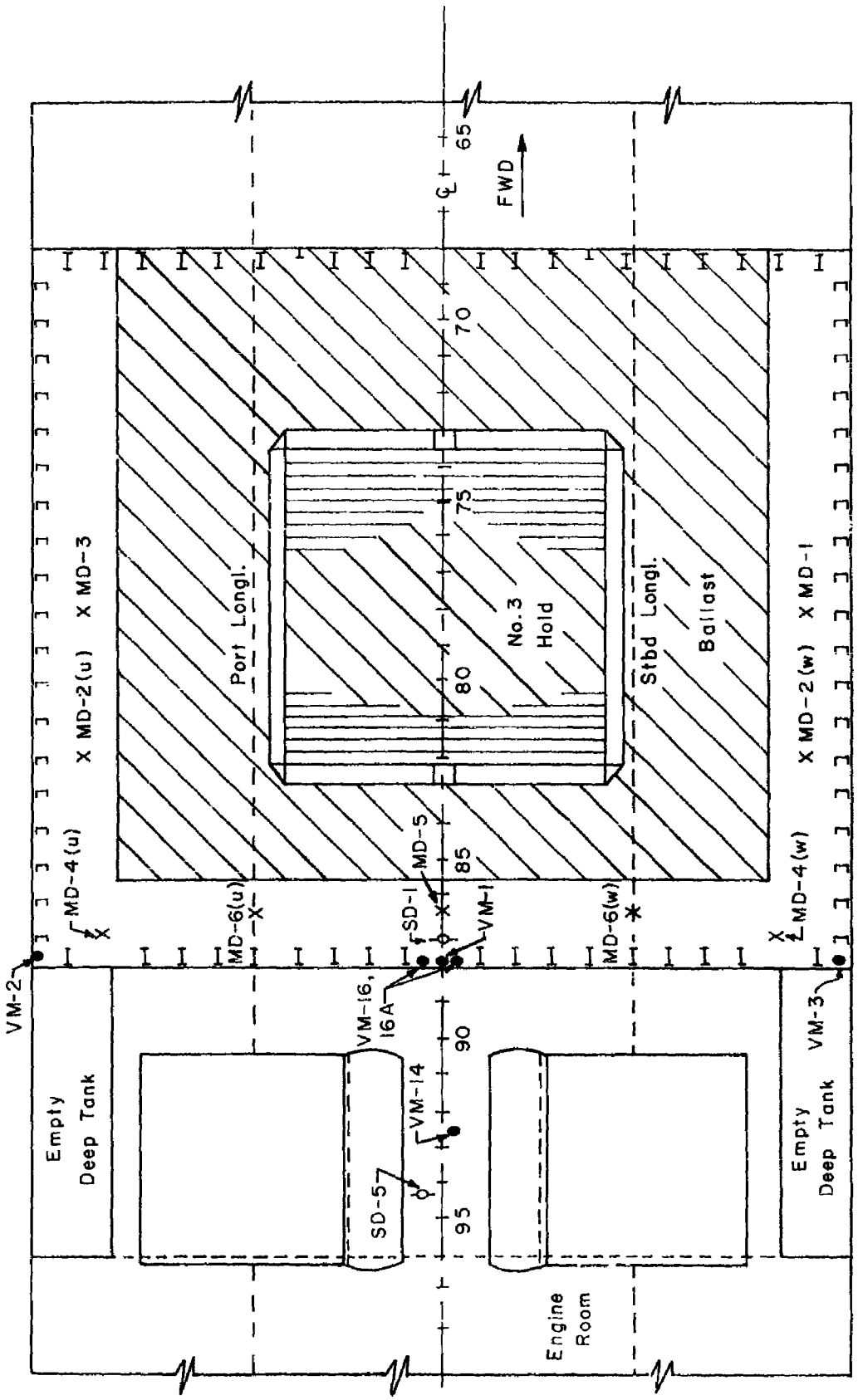

Figure 2.10 EC-2 gage locations.

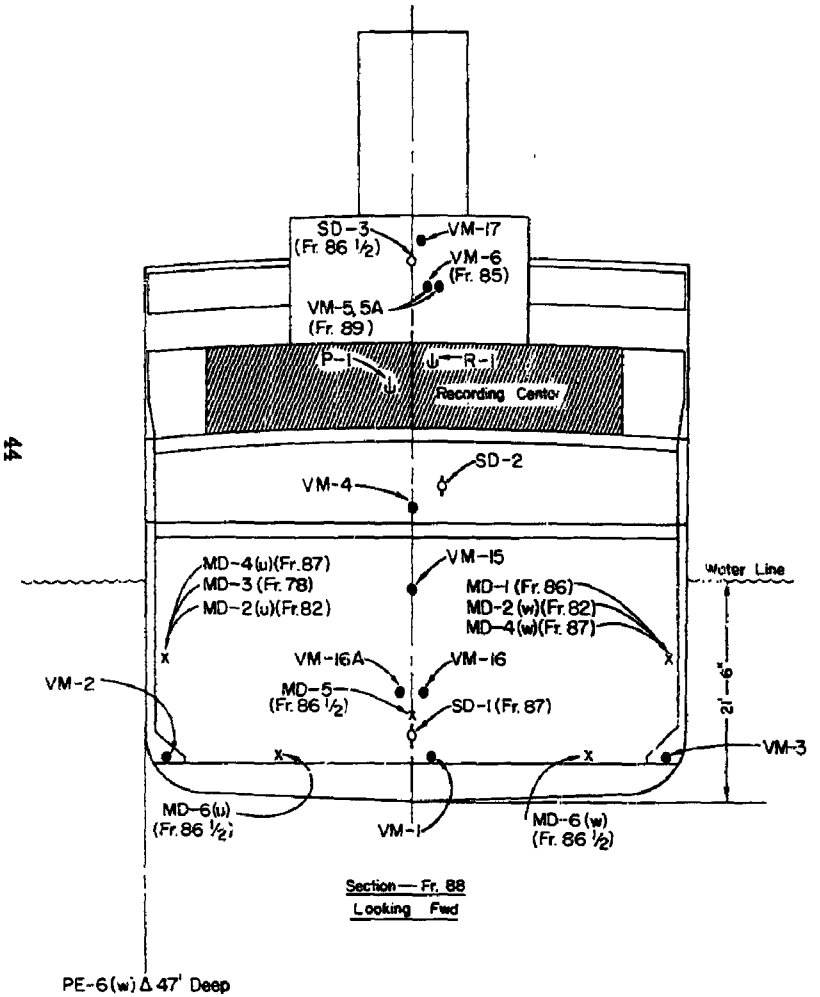

Section — Fr. 88
Looking Fwd

Figure 2.11 EC-2 gage locations, Frames 78 to 89.

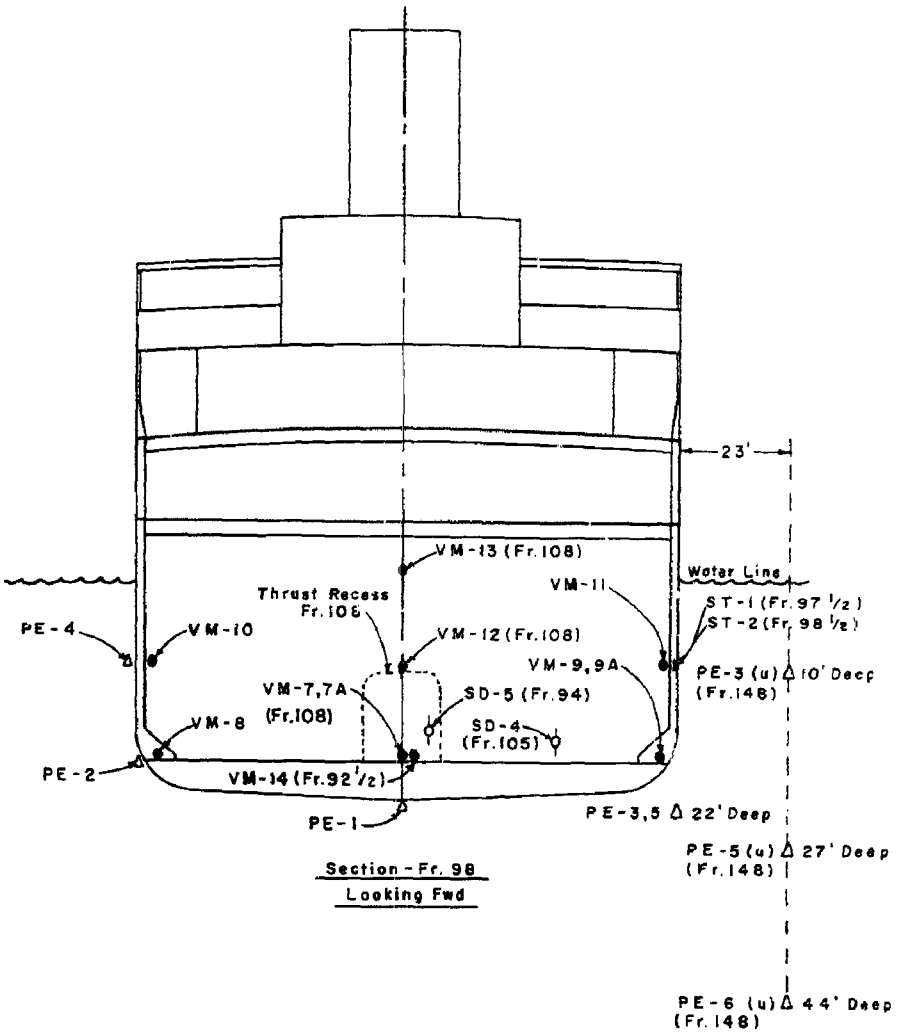

Section - Fr. 98
Looking Fwd

Figure 2.12 EC-2 gage locations, Frames 92 1/2 to 108.

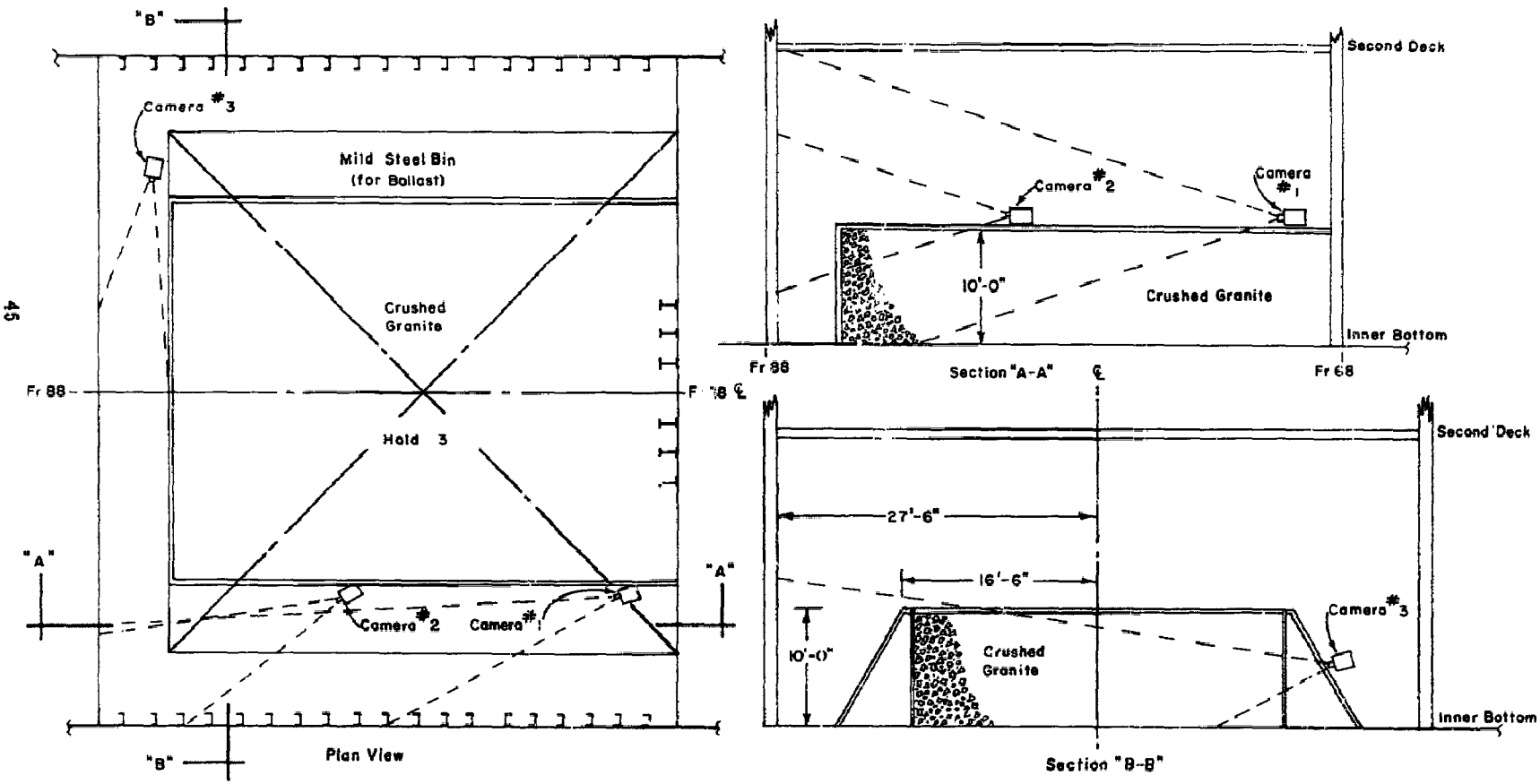

Figure 2.13 Camera locations, EC-2 (Hold 3).

Figure 2.14 Typical small velocity meter installation.

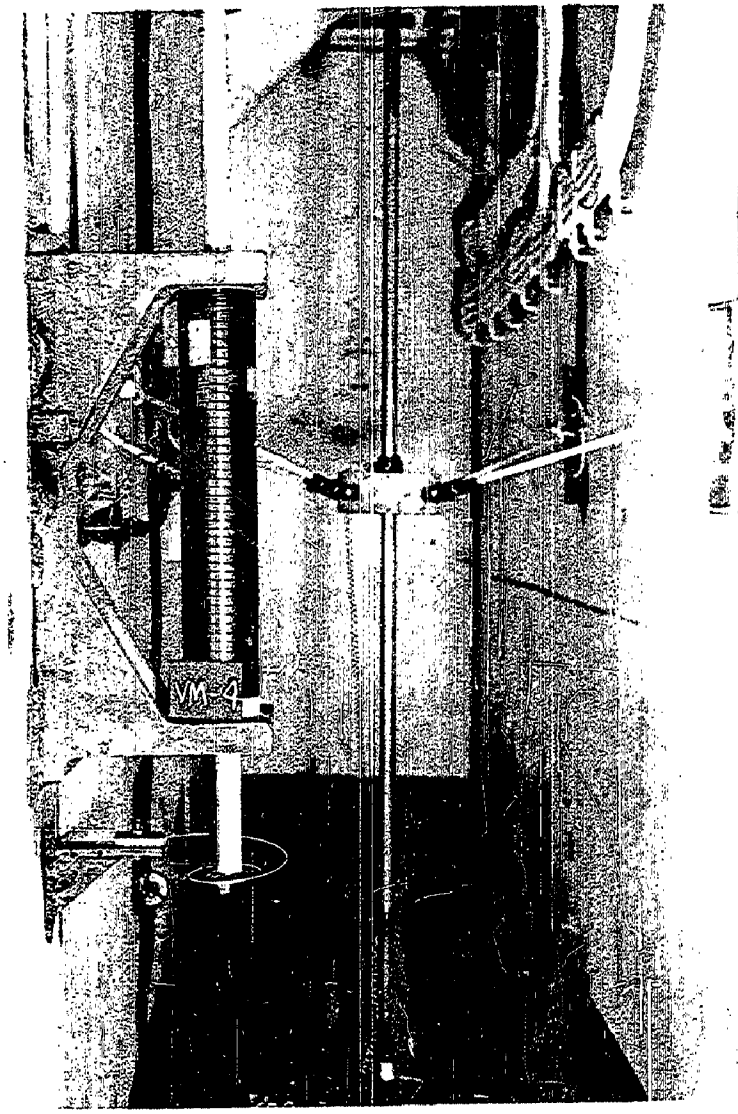

Figure 2.15 Typical large velocity meter installation (seismic deflection gage in background).

Figure 2.16 Typical horizontal velocity meter installation.

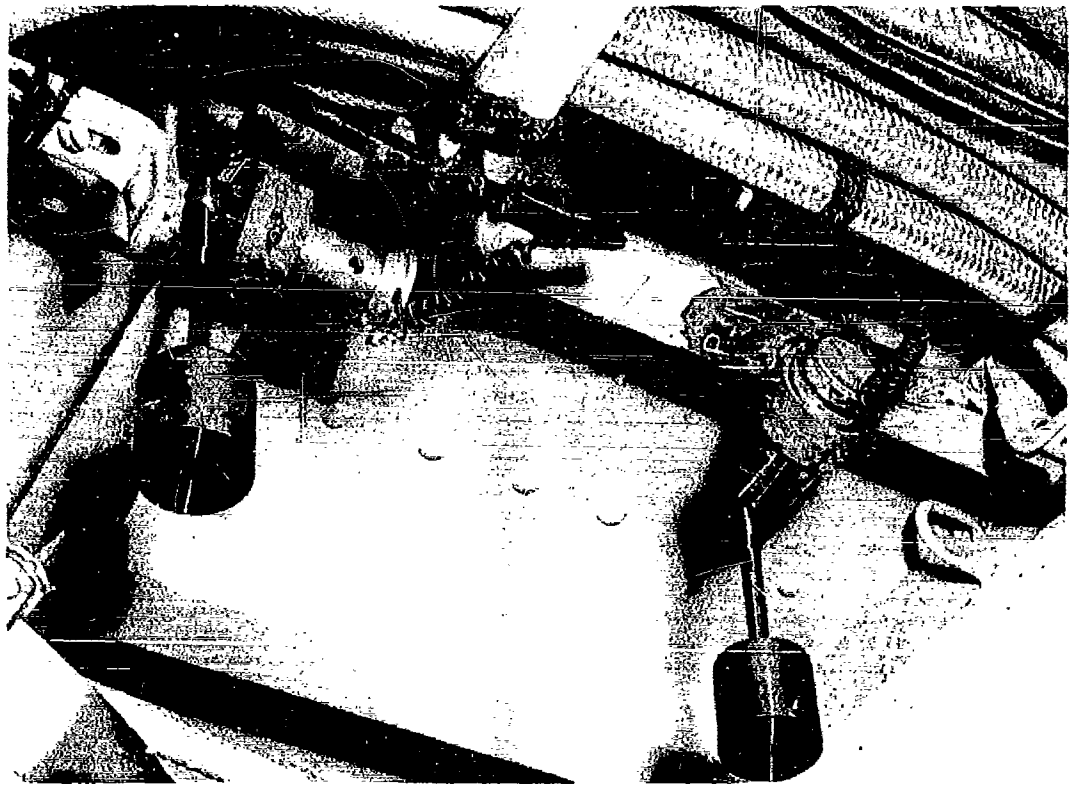

Figure 2.17 Roll and pitch gage installation.

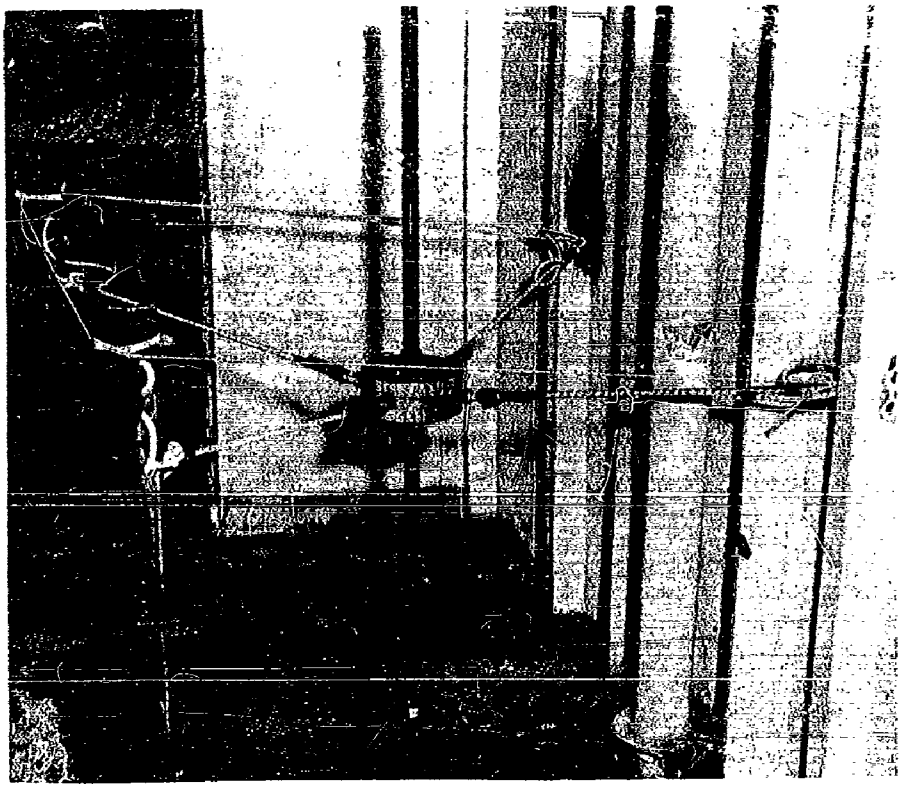

Figure 2.18 Typical displacement gage installation.

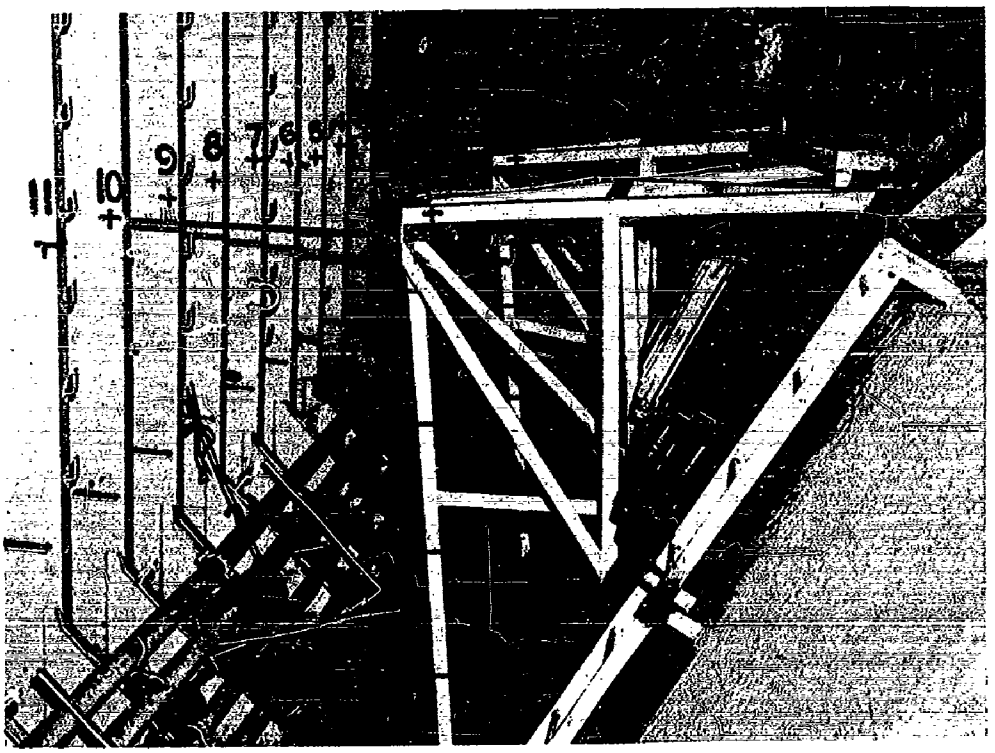

Figure 2.19 Deflection gage installation on EC-2 (Hold 3).

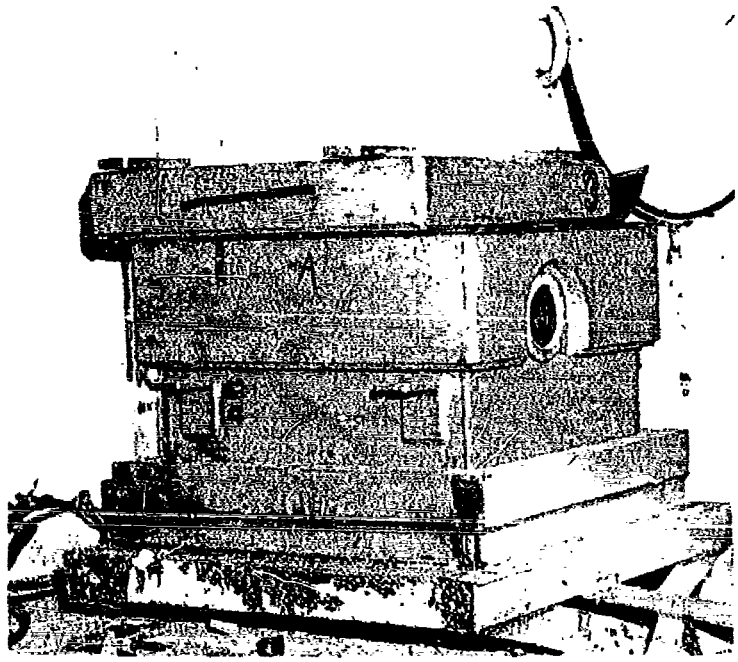

Figure 2.20 Camera mount on EC-2.

Figure 2.21 DD instrument platform shock mounting system.

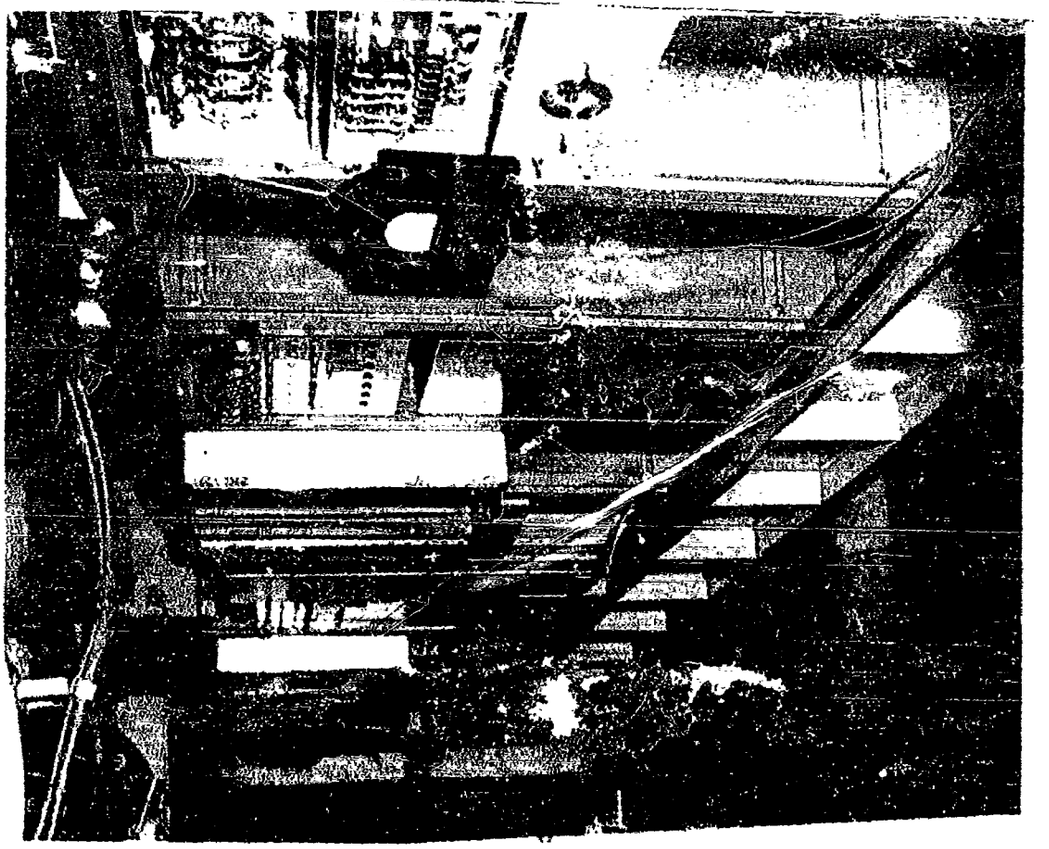

Figure 2.23 Recording equipment on EC-2 instrument platform.

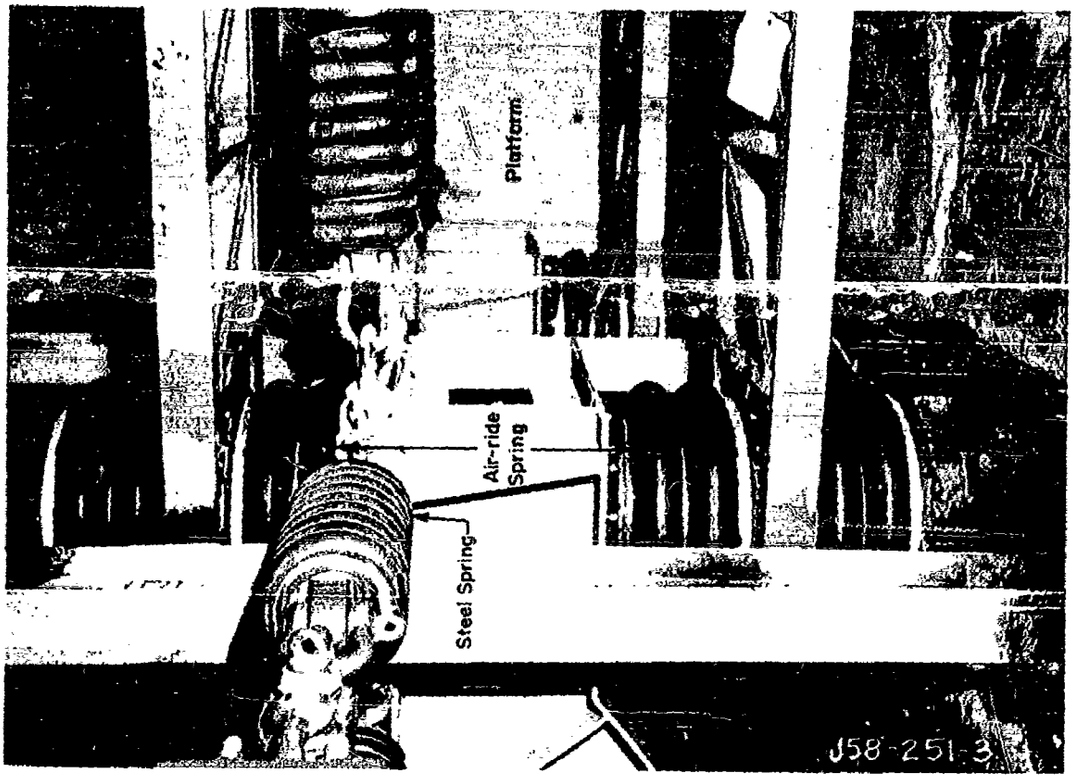

Figure 2.22 EC-2 instrument platform shock mounting system.

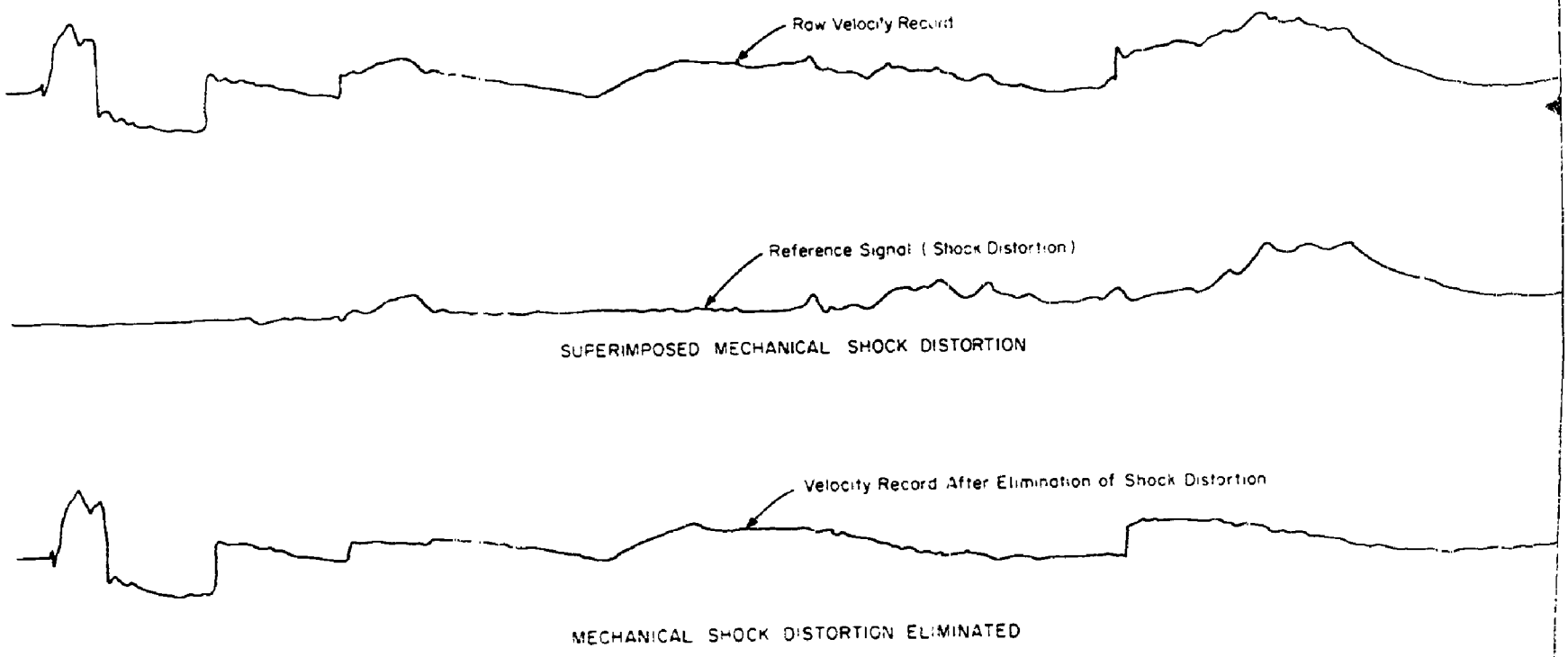

Figure 2.24 Example of the elimination of mechanical shock distortion.

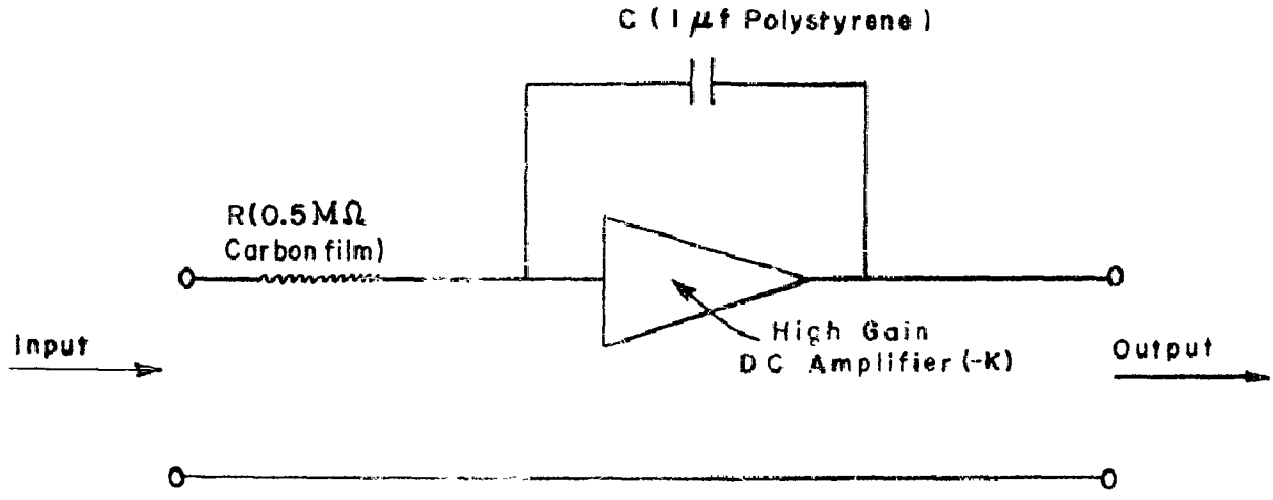

Figure 2.25 Basic electronic integrating device schematic.

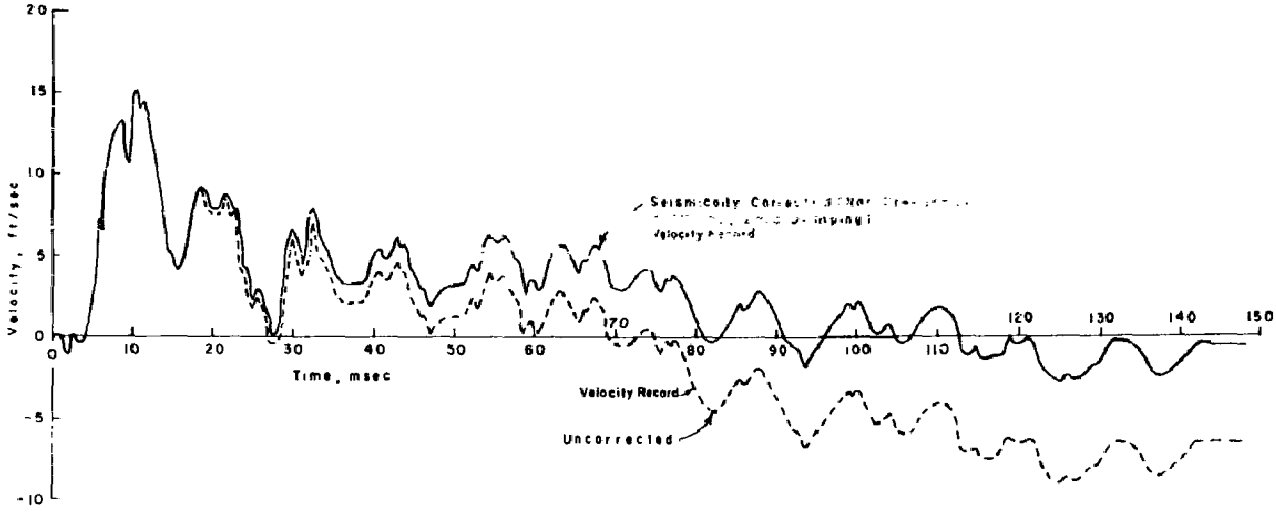

Figure 2.26 Example of seismically corrected record.

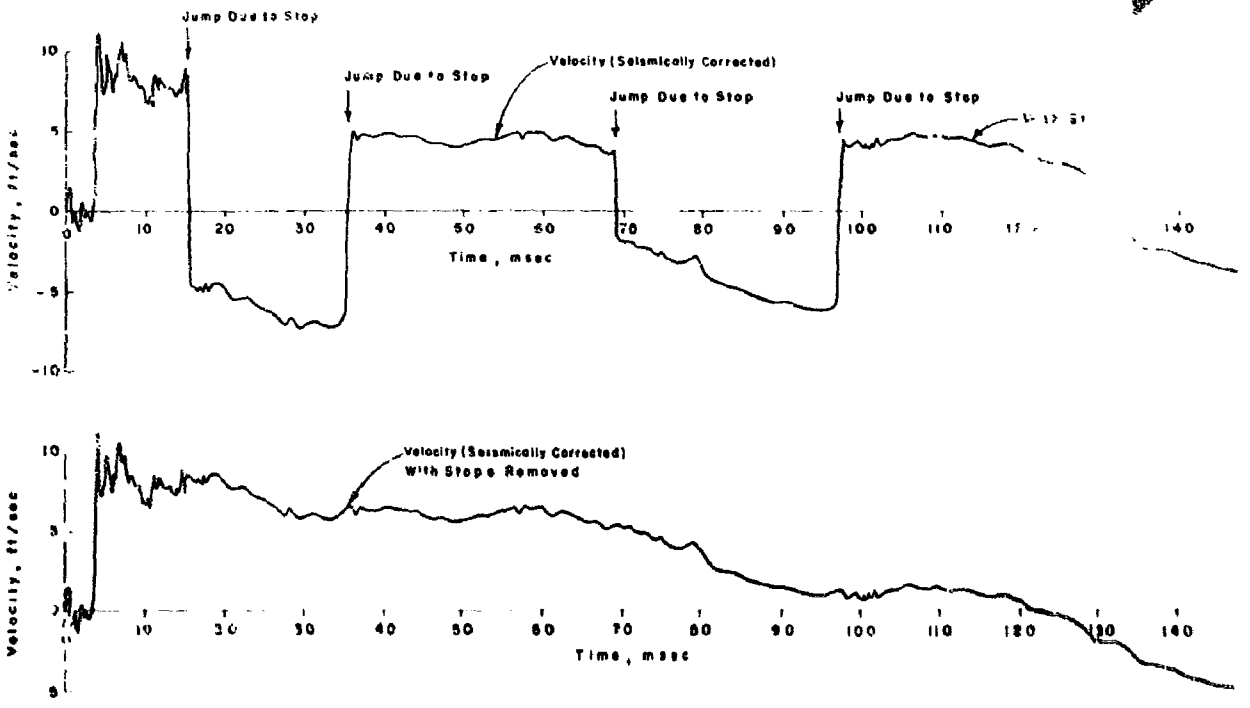

Figure 2.27 Example of correcting a velocity record for steps.

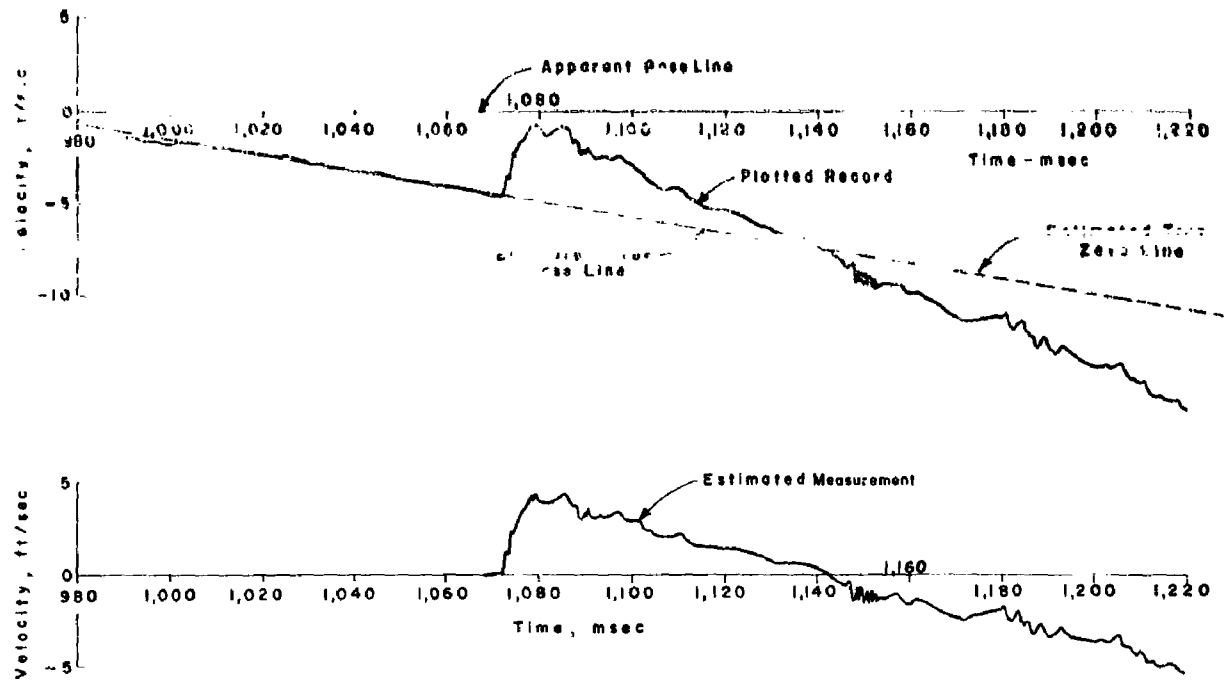

Figure 2.28 Procedure for reading reflected wave response.

Chapter 3

RESULTS AND ANALYSIS

3.1 PRELIMINARY REMARKS

During Shot 1, all measurements were obtained only on the EC-2 and DD-593. The immediate causes of malfunction on the other target ships included: (1) on the DD-592, a leakage of washdown water into the ship's interior and onto a switchboard caused a short circuit that tripped the circuit breaker through which the ship's emergency power was provided; (2) on the DD-474, a faulty power switch disconnected the EG&G timing signal equipment from the ship's emergency 100-kw diesel generator, and (3) on the YC-1, an unknown circumstance. Inasmuch as the EG&G timing-signal receivers on the DD's were powered by the ship's emergency generators but had no backup power system and were not monitored, these malfunctions led to a complete lack of Project 3.4 data on the DD-474 and DD-592.

The measurements obtained on the DD-593 were rather uniformly of good quality. Most of the measurements obtained by the FR-114 recorders on the EC-2 were also of good quality, except that some distortion was noticeable in the records because of mechanical shock motions introduced into the recording equipment, especially when the recording platform bumped the superstructure deck above (Figure 3.1). The severity of the shock may be judged by the damage to the recording gear (Figure 3.2) and, also, by the damage to the generators (Figure 3.3). However, the distortion of key records introduced by the shock could be eliminated electronically over the time periods of chief interest (Section 2.3), and the vital information was obtained.

Measurements obtained by the S-3041 recorders on the EC-2 were of relatively poor quality. The most important consequence of this was a loss of most of the seismic displacement data. A damage survey of the EC-2 hull was successfully completed, and an examination of the DD-474 hull was also made. High-speed motion pictures of the hull deformation in Hold 3 of the EC-2 were obtained by EG&G.

Representative examples of the measurements are discussed in the remaining sections of this chapter. All results presented have been fully corrected, in accordance with the procedures outlined in Section 2.3, and represent physical measurements, rather than raw records.

3.2 OVERALL RANGE OF EFFECT OF UNDERWATER PHENOMENA

The effects of the overall phenomena are shown in Figures 3.4 and 3.5. The main phases of the loading and response are marked on the figures: direct shock wave, cavitation reloading subsequent to the direct wave, sea-bottom-reflected shock wave, and cavitation reloading subsequent to the reflected wave (directly observed only at DD-593). In addition, two typical precursor waves are indicated: hull precursor and sea-bottom precursor (DD-593 only).

Examination of the one FR-114 recorder on the EC-2, which continued to function at very late times, provided some evidence of the occurrence of further phenomena. However,

this evidence consisted largely of times at which something happened; response measurements were not obtained.

3.3 HULL LOADING AND HULL RESPONSE

The early hull loading and hull response of the EC-2 are illustrated by the solid curves shown in Figure 3.6. Notice that both the direct and reflected pressure wave phases are shown. As a matter of general interest one of the free-water pressure measurements is added (see dashed curve) for comparison. A similar examination of the hull loading and response of the DD-593 is made in Figure 3.7.

3.4 CROSS-SECTION DISTRIBUTION OF HULL RESPONSE

The velocities measured over the cross section of the EC-2 hull are shown in Figure 3.8. Again, only short intervals of time are shown both for the direct and reflected waves.

A similar comparison for the DD-593 is not considered of sufficient interest to include, inasmuch as the attack, in this case, was end-on.

3.5 LONGITUDINAL DISTRIBUTION OF LOADING AND HULL RESPONSE

The EC-2 was attacked side-on and instrumented by Project 3.4 only in the engine room and Hold 3; thus, there is no information leading to a comparison of the response of the EC-2 along the entire length of the ship. However, it is interesting to observe the effect on bottom velocities of the location of the velocity meter in relation to heavy masses along the bottom of the ship (Figure 3.9). VM-7A was located close to large machinery masses, that VM-14 was located in an open area of the bottom (relatively far away from large weights), and that VM-1 was near a bulkhead and only a few feet from the large ballast mass in Hold 3.

The longitudinal distribution of the loading and response along the length of the DD-593 is illustrated in Figure 3.10. Of chief interest is the response due to the reflected wave. Note that the sea-bottom seismic precursor pressure wave gave rise to a response prior to that due to the regularly (specular) reflected wave and that the latter response is superimposed on the former.

3.6 RESPONSE DISTRIBUTION UPWARD THROUGH SHIP

The distribution of the early response upward through the EC-2 is illustrated in Figure 3.11 by a few velocity records obtained at various positions along the forward engine-room bulkhead.

A similar study of the response distribution in a DD-593 bulkhead is presented in Figure 3.12. In this case the response to the regularly reflected wave is superimposed on the response to a sea-bottom precursor pressure wave.

3.7 BODILY RESPONSE OF TARGET SHIPS

Some insight into the bodily motion of the target ships may be gained by comparing the responses measured at representative locations. It should, of course, be realized that it is impossible to measure directly such bodily motions as the vertical motion of the center of gravity of a ship, the pitching motion, and the like. However, in many cases a straightforward examination of measurements at a variety of locations suffices for a determination of the characteristics of the bodily motions.

The vertical velocities measured at various representative locations on the EC-2, after the direct shock wave, are reproduced over a long time interval in Figure 3.13. The few valid vertical displacement histories measured on the EC-2 at various locations are shown in Figure 3.14. In addition, a typical velocity record (VM-7 from Figure 3.13) was integrated and is also shown in Figure 3.14 to demonstrate the degree of consistency between Figures 3.13 and 3.14.

No similar treatment of the DD-593 measurements is meaningful in terms of establishing the vertical bodily motion of the DD-593 following the direct shock wave.

Vertical velocities measured at various representative locations on the EC-2 indicate the vertical bodily motion following the reflected wave (Figure 3.15). As noted in this figure no definite evidence of a response to cavitation reloading was found. Vertical displacements recorded on the EC-2 after the reflected wave were not sufficiently good to yield meaningful measurements.

Vertical velocities measured, after the reflected wave, at representative locations on the DD-593 are shown in Figure 3.16.

Horizontal velocities measured, after the direct shock wave, on the EC-2 bulkhead are shown in Figure 3.17. Note that VM-15 has a large superimposed vibration that obscures the bodily motion. Similar measurements made after the reflected wave show an insignificant response; a peak velocity of about 1 ft/sec was measured by VM-15.

3.8 DEVELOPMENT OF HULL DAMAGE IN EC-2

Deflection gages were installed in Hold 3 of the EC-2 to measure the development of side-frame and bottom deformation. A special effort was made to attach the support end of the gages as rigidly as possible to an integral element of the ship (Figure 2.19).

Deflection histories measured at the shock-wave phase are shown in Figure 3.18. In comparing MD-1 with MD-4, recall that MD-4 is attached to the side frame next to the engine-room bulkhead and to the first starboard bulkhead stiffener; it, therefore, measures side deformation on the attack (starboard) side very close to the bulkhead. No significant response occurred after the times shown in Figure 3.18. Set deflections measured before and after the test are also shown in Figure 3.18.

The motion-picture films taken by EG&G in the interior of the EC-2 were evaluated. Because of the small magnitude of the deformation, only the film from Camera 1 (Figure 2.13) could be read with sufficient accuracy to yield meaningful physical measurements. The resulting estimate of frame deformation at the MD-1 location is shown in Figure 3.18; cross-hatching is used to indicate the approximate accuracy of film reading.

Longitudinal strains in the shell plating on the starboard (attack) side were measured at about half-draft midway between frames. The resulting measurements are shown in Figure 3.19. The first portion of the records are plotted with an expanded time scale to show details and in order to show the close comparison between the two ST gages.

3.9 FINAL HULL DAMAGE

Slight damage to the attacked side of the EC-2 between the inner bottom and second deck was noticeable within the engine room and Hold 3 after Shot Wahoo. Systematic before-and-after measurements were carried out with a surveyor's transit, and damage contours representing frame deformations shown in Figure 3.20 and Figure 3.21 were derived. Squares indicate actual measurements; triangles indicate values faired from the vertical contours; circles designate set deflection measurements made by measuring the electrical resistance changes in the MD gages; and solid curves indicate an evaluation of the frame damage due to the test. As a result of the starboard side frame deformation many of the

brackets connecting the frames with the double bottom were buckled slightly (Figure 3.22). Notice that measurements were also made at the half-frames (or, at the shell plating); a typical damage contour for the plating is also drawn in Figure 3.20 as a dashed curve. It is apparent that, in addition to frame deformation, the side shell plating deformed between stiffeners. The amount of this dishing was measured at midframes on the starboard side in a number of cases, and these cases showed similar behavior; the amount of dishing increased with depth below the water surface down to the inner-bottom level. The dishing was, therefore, averaged for a number of cases and the resulting average dish is shown in Figure 3.23.

Hull damage in the port side and in the inner botiom was less than in the starboard side and proved to be too negligible for preparation of consistent damage contours.

Some damage was noticeable at the closure plates about the rudder shaft in the afterpeak region of the EC-2. Most of the bolts were sheared off. However, no hull dishing was noticeable in either the forepeak or afterpeak regions.

Bulkhead damage was essentially nonexistent at locations where the bulkheads could be examined.

Some damage was detected in the propeller-shaft tunnel of the EC-2 aft of Frame 134; forward of Frame 134 this damage was negligible. Aft of Frame 134 the shaft tunnel was bowed inward, largely on the starboard side, to such an extent that the width was reduced by about 6 inches (Figure 3.24). Catastrophic shock damage to the shaft bearings (Figure 3.25) was observed.

Divers were requested to examine the bottom of the EC-2, and visual observations of damage were reported. Slight plating dishes were described in the bottom between floors and longitudinals in the region between Frames 39 and 134; damage forward and aft of this region was entirely negligible. A washboard type of damage was reported for the ship's rudder. One split seam was described as open sufficiently to permit the "insertion of a fingernail"; this open seam was located at about Frame 120 at about the position of the starboard longitudinal and ran longitudinally for a total length of about 8 feet.

After the test, the EC-2 acquired a definite list to port (about 1° to 1.5°). The cause may have been a shift of the gravel ballast in Holds 2 and 4, perhaps supplemented by a drainage of water from the starboard tanks in Hold 1. (Water leakage from pipes in Hold 3 was observed.)

A careful examination of the hull of the DD-474 revealed no hull dishing that could definitely be ascribed to Shot Wahoo.

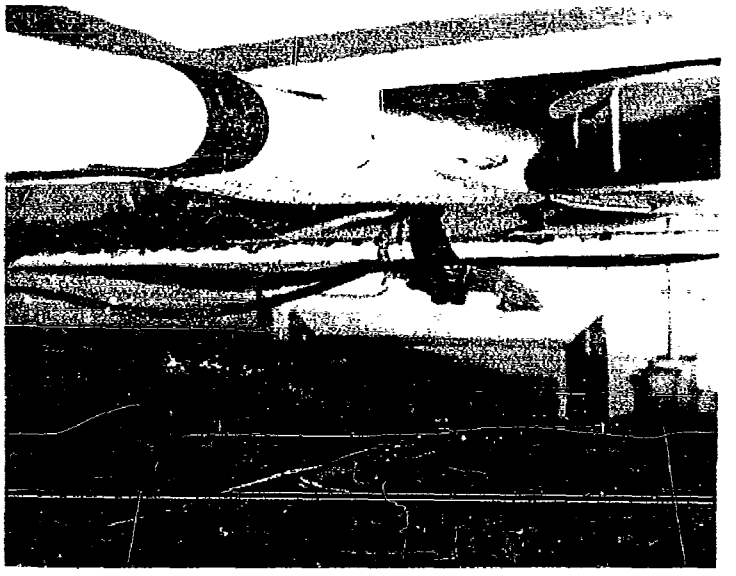

Figure 3.1 Damage caused when instrument platform cabinet bumped overhead in EC-2, Shot Wahoo.

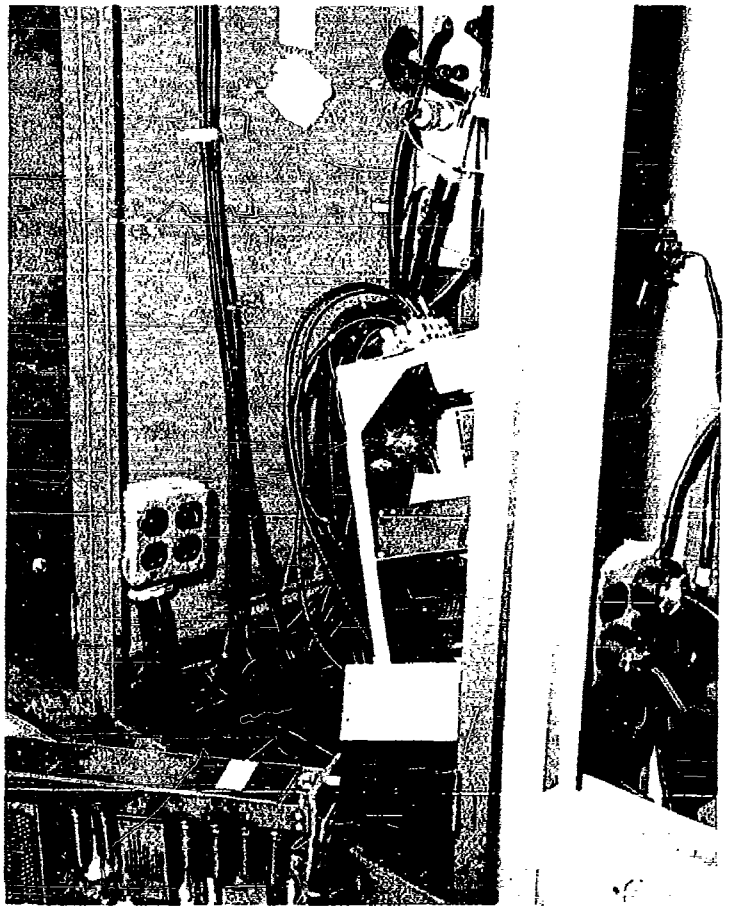

Figure 3.2 Damage to recording gear of instrumentation platform on EC-2, Shot Wahoo.

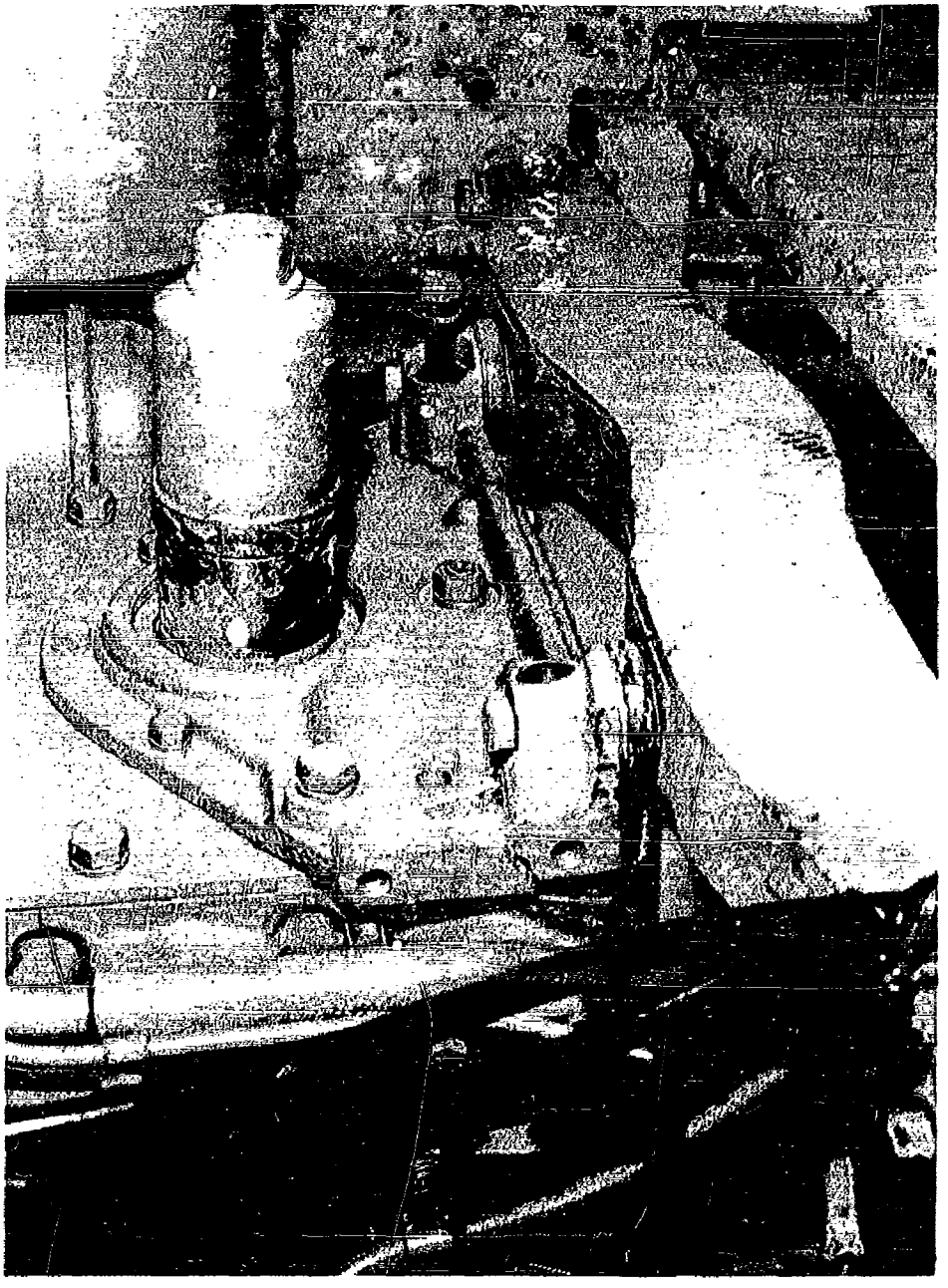

Figure 3.3 Damage to UERD generator in EC-2, Shot Wahoo.

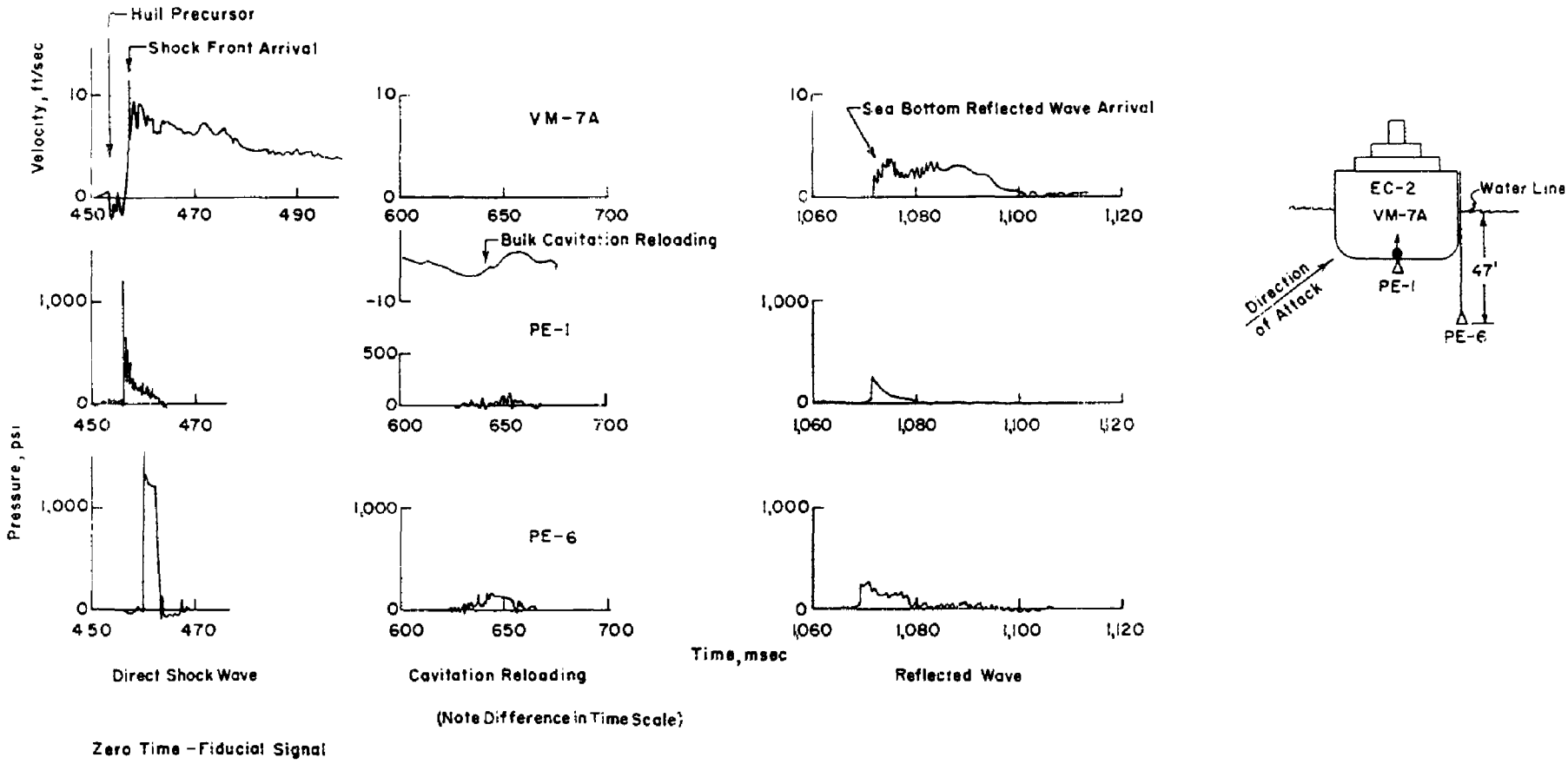

Figure 3.4 Effects of overall phenomena, EC-2, Shot Wahoo.

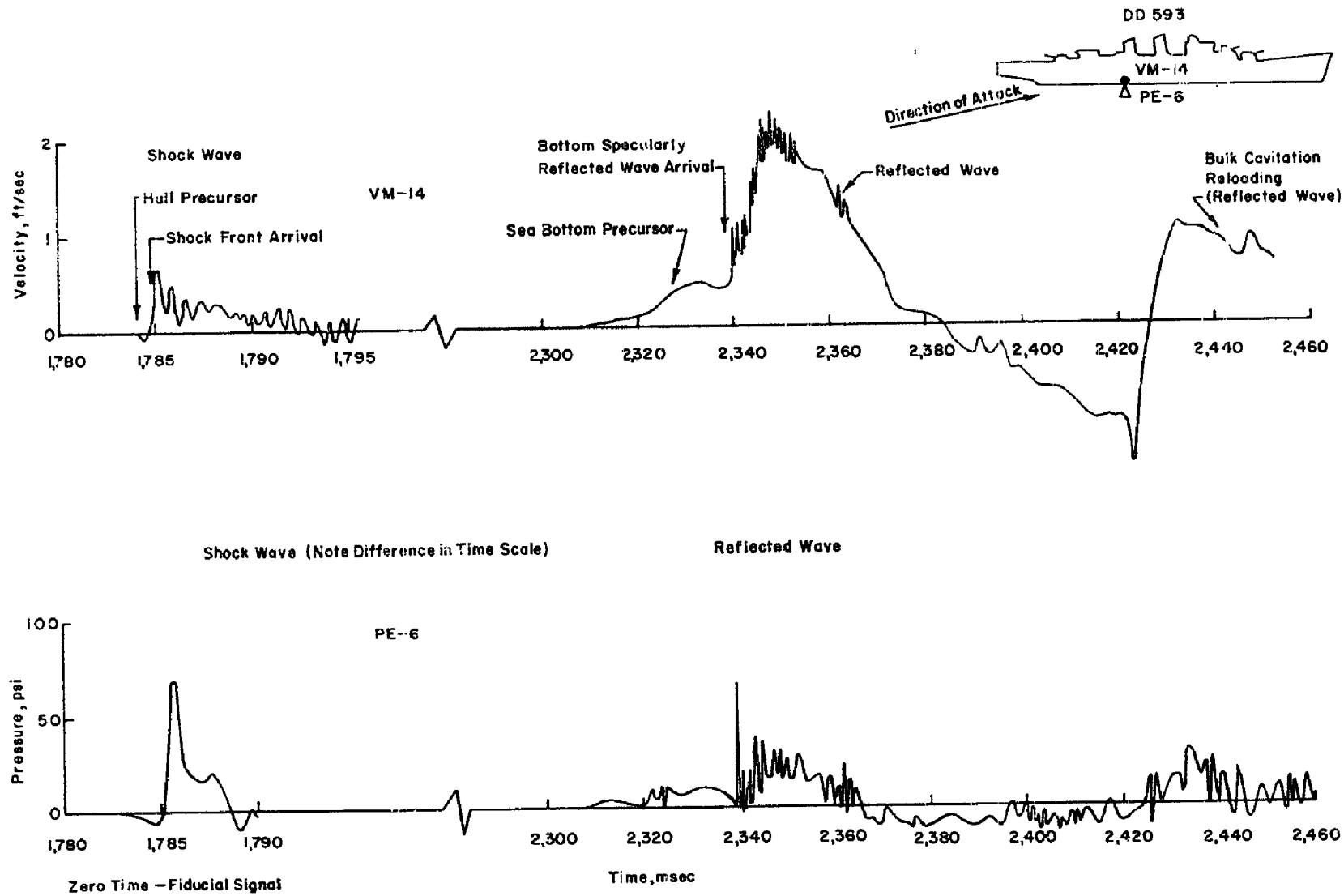

Figure 3.5 Effects of overall phenomena, DD-593, Shot Wahoo.

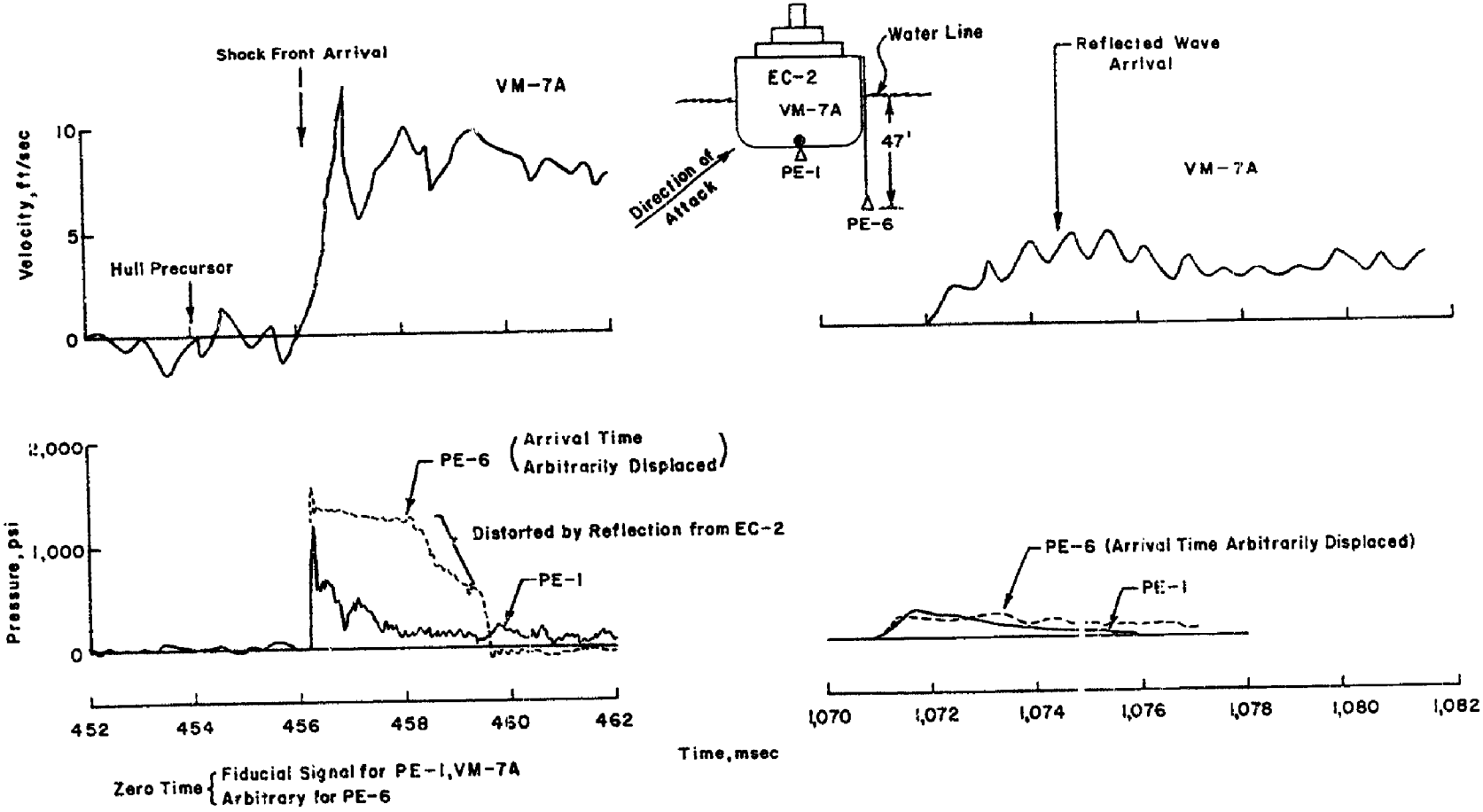

Figure 3.6 Hull loading and hull response, EC-2, Shot Wahoo.

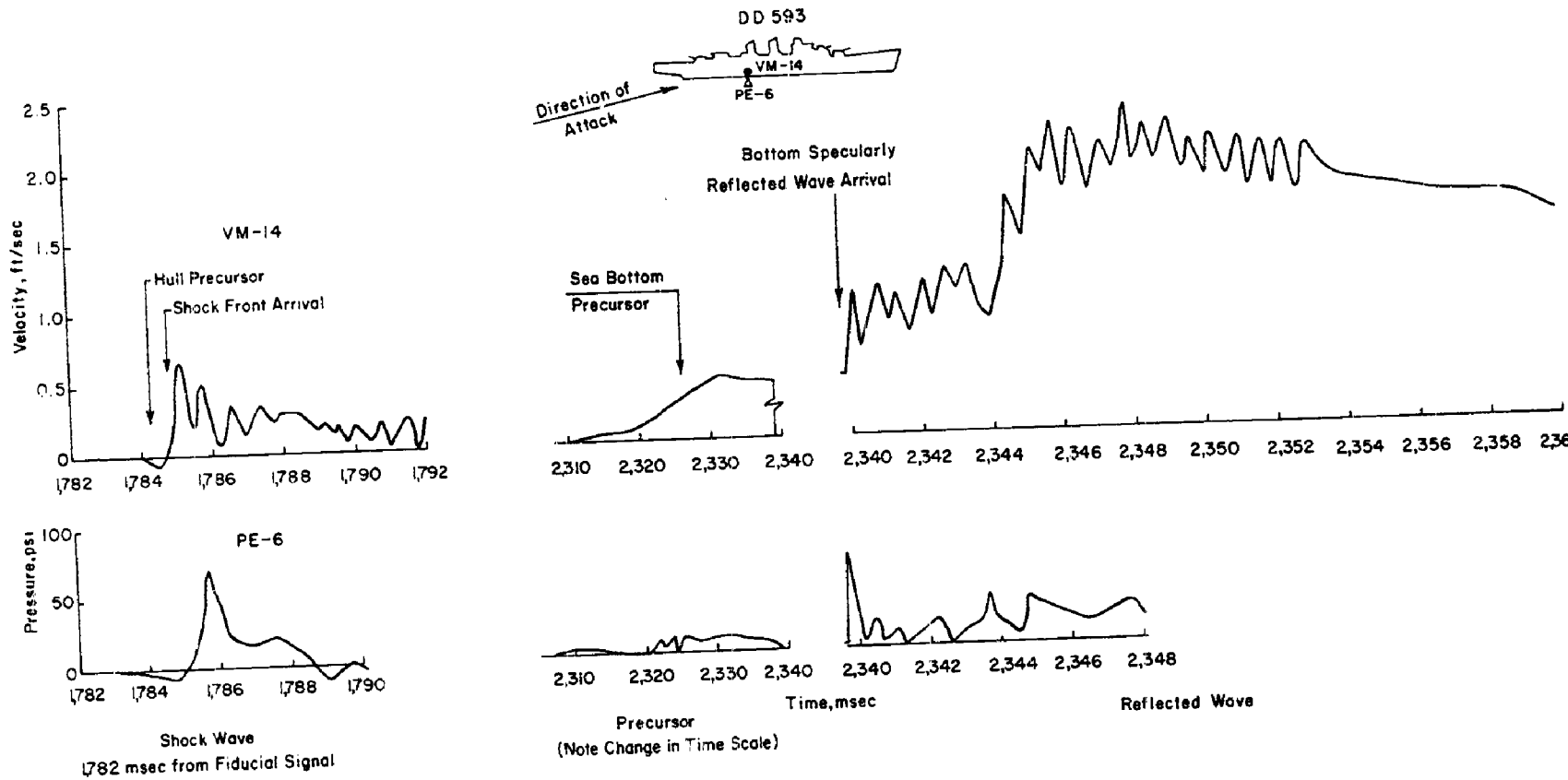

Figure 3.7 Hull loading and hull response, DD-593, Shot Wahoo.

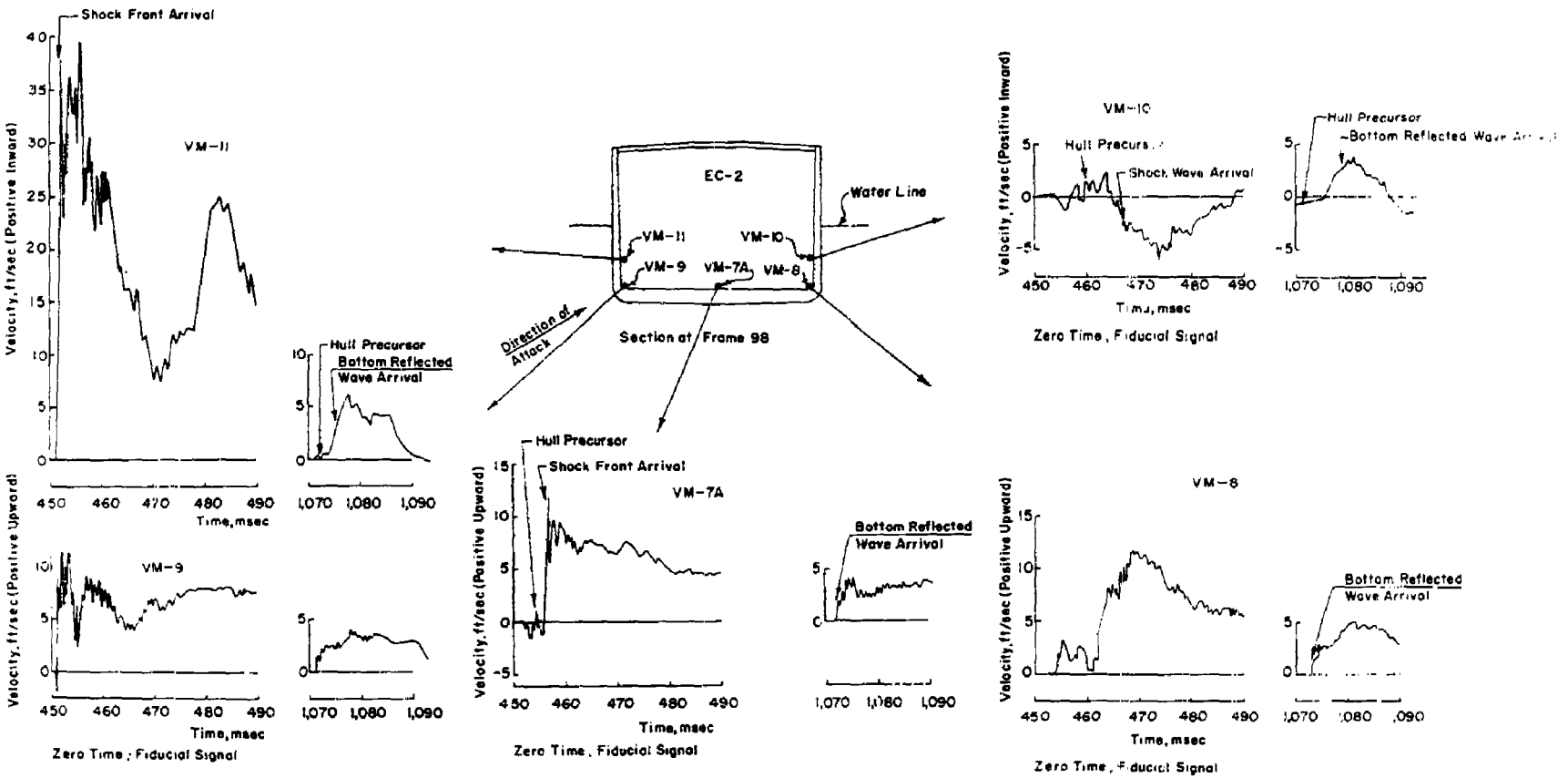

Figure 3.8 Cross-section distribution of hull response, EC-2, Shot Wahoo.

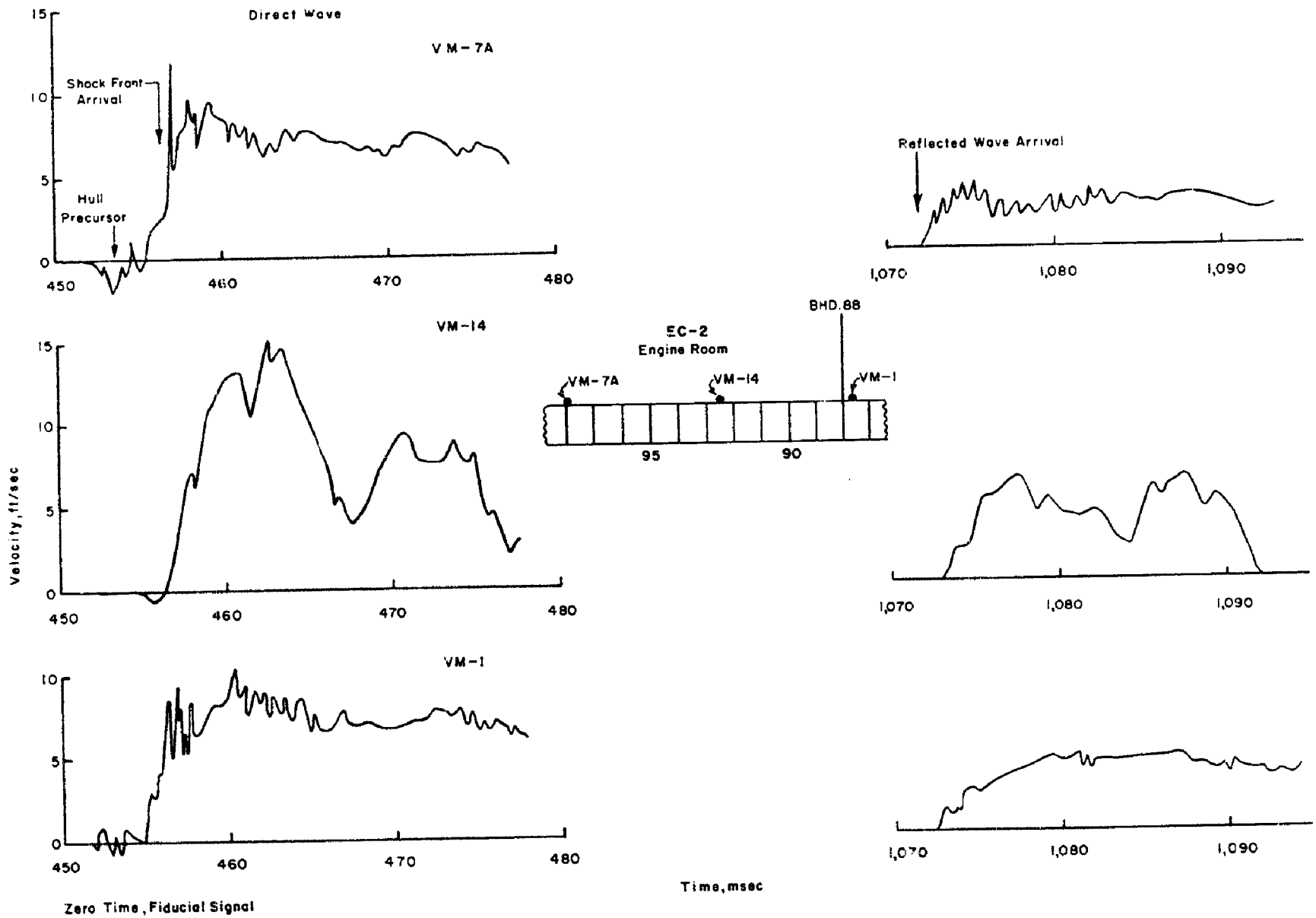

Figure 3.9 Velocities at EC-2 bottom, Shot Whoo.

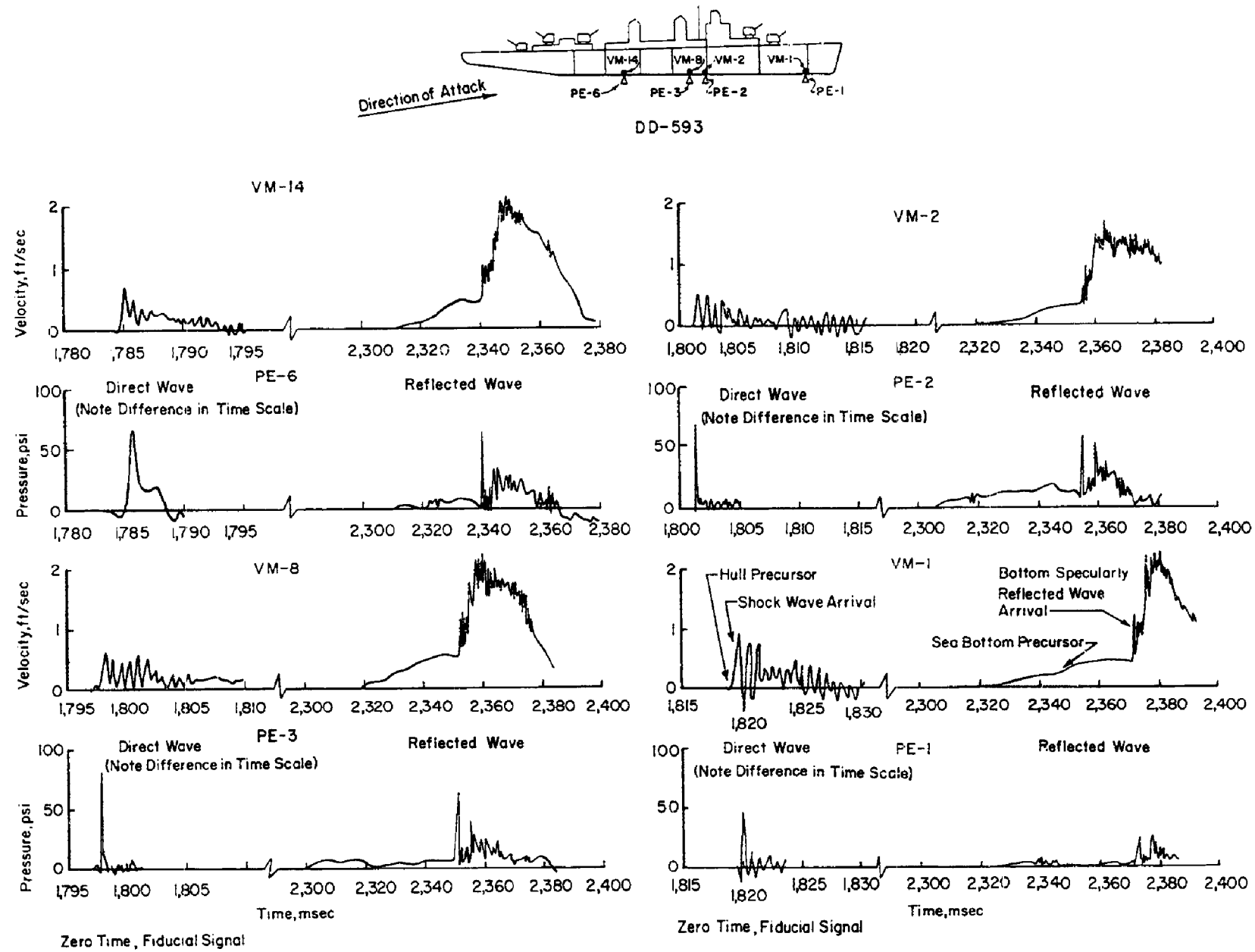

Figure 3.10 Longitudinal distribution of hull loading and hull response, DD-593, Shot Wahoo.

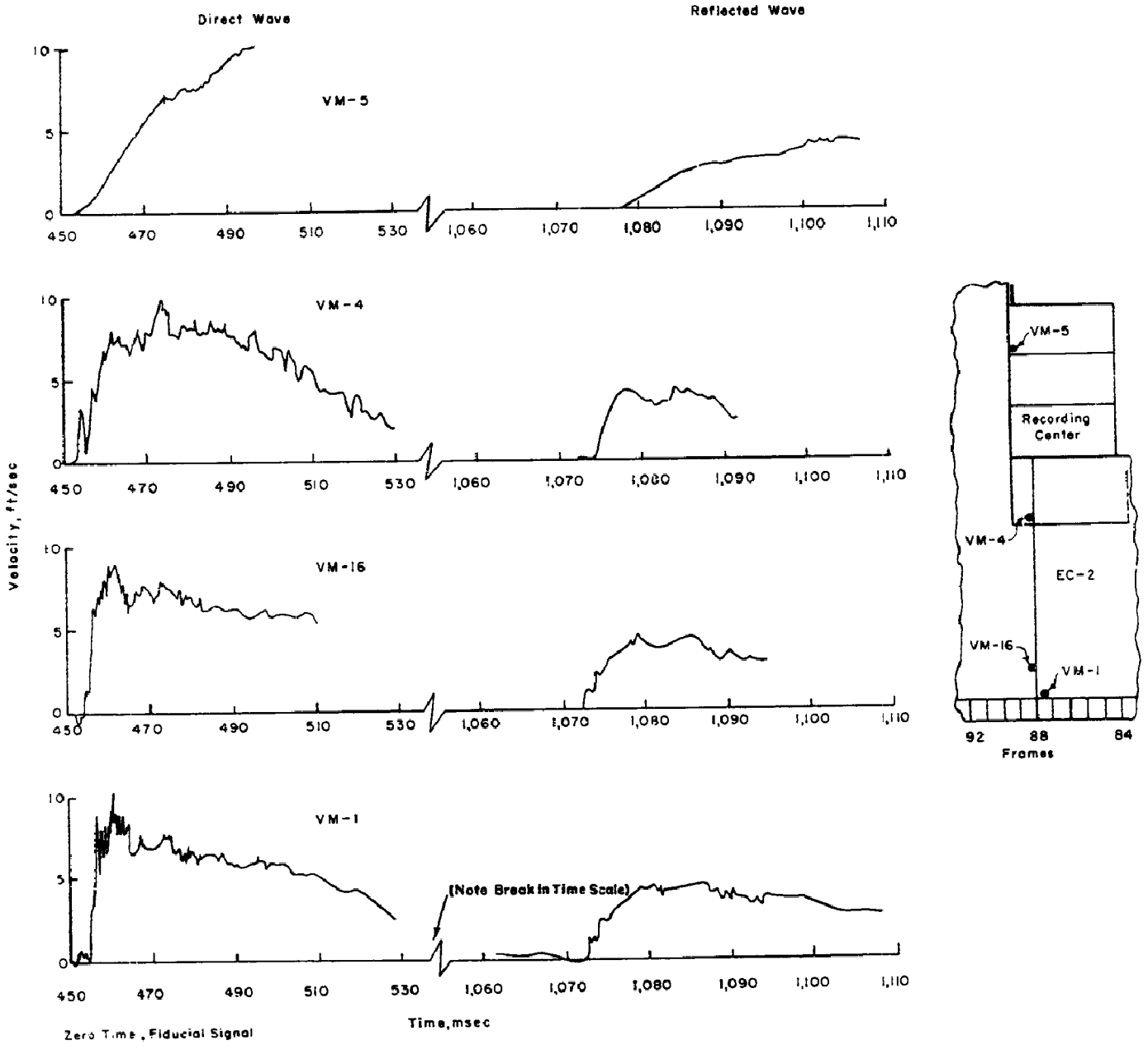

Figure 3.11 Vertical response distribution upward through EC-2 bulkhead, Shot Wahoo.

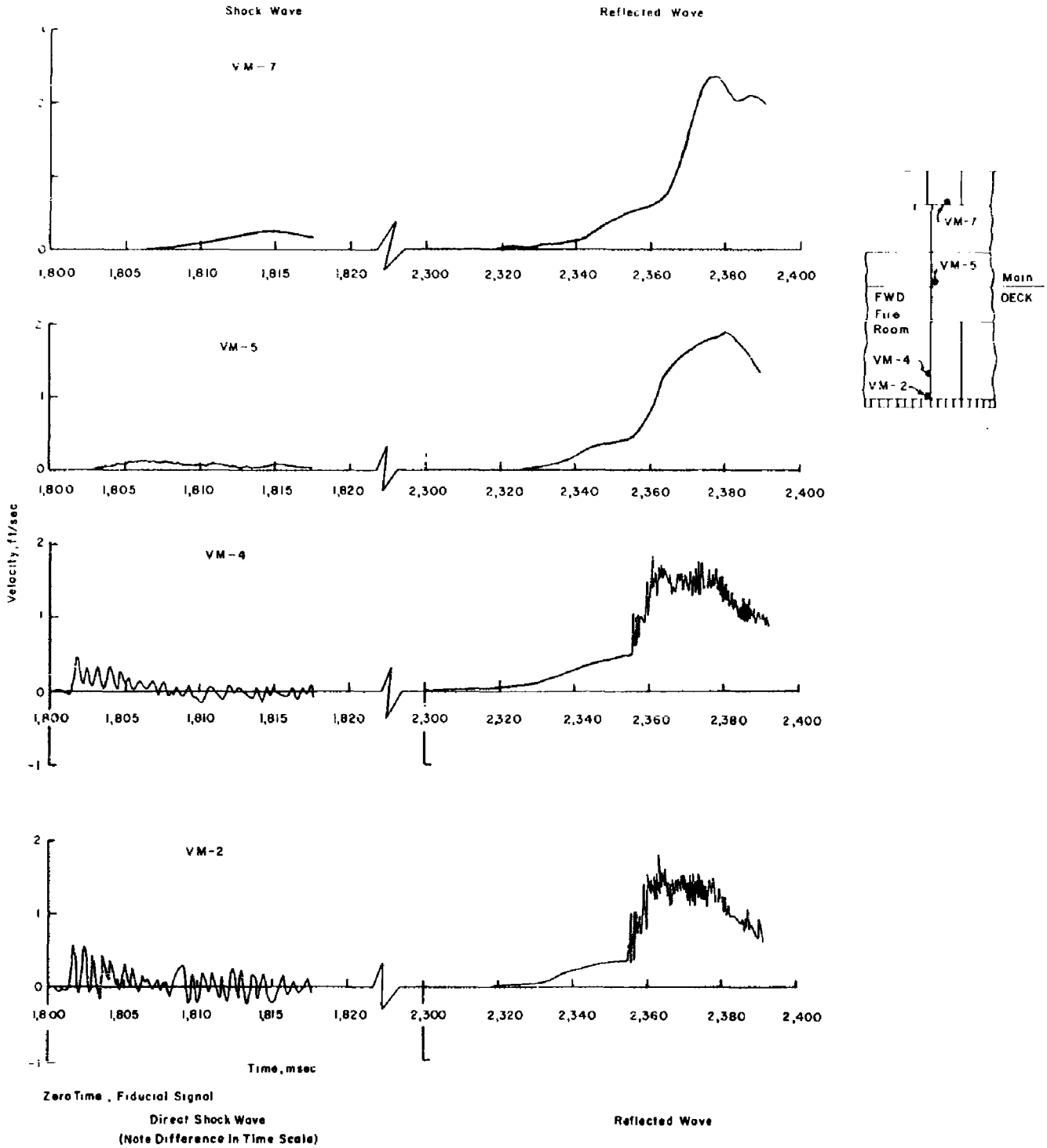

Figure 3.12 Vertical response distribution upward through DD-593 bulkhead, Shot Wahoo.

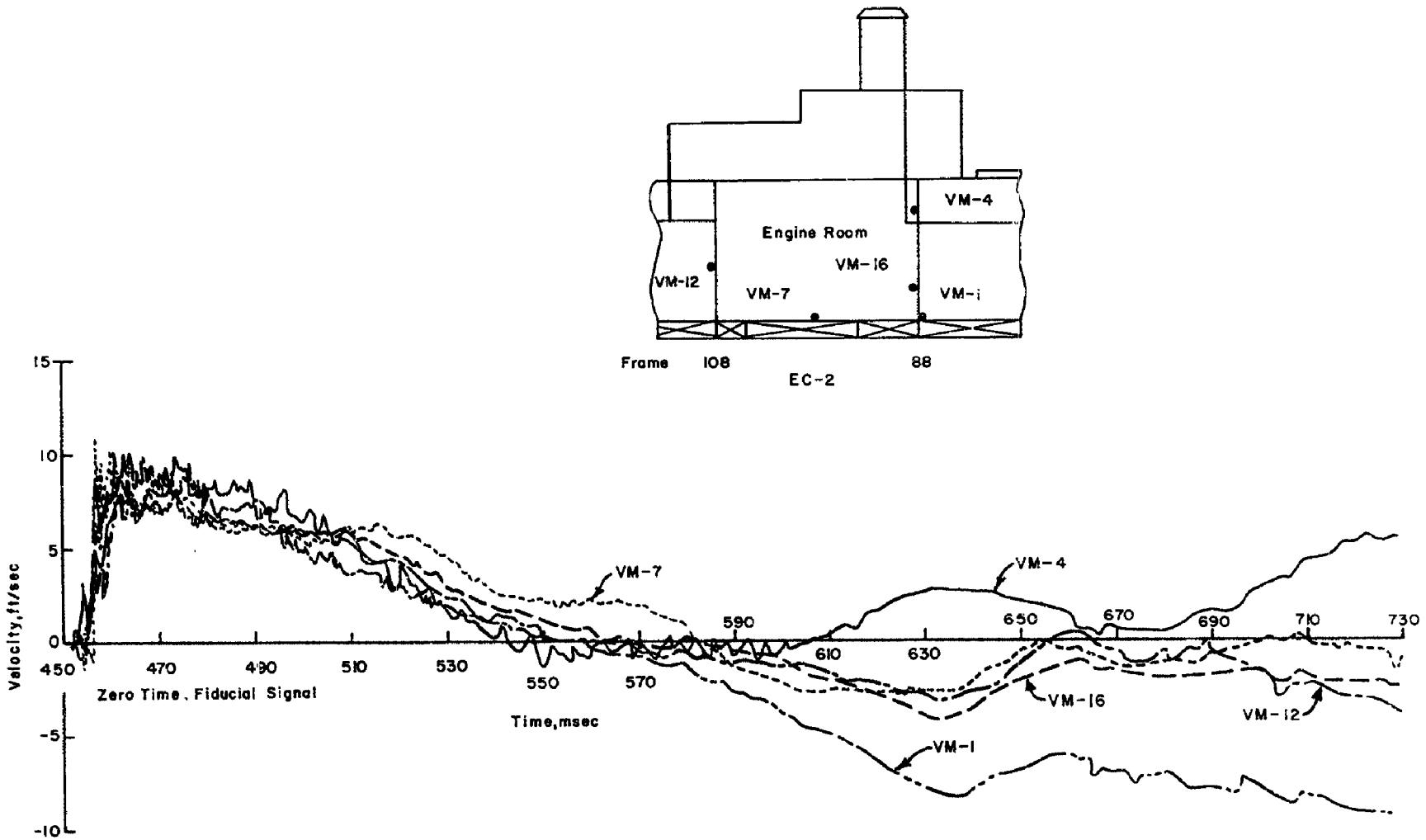

Figure 3.13 Typical vertical velocities of EC-2 after direct wave, Shot Wahoo.

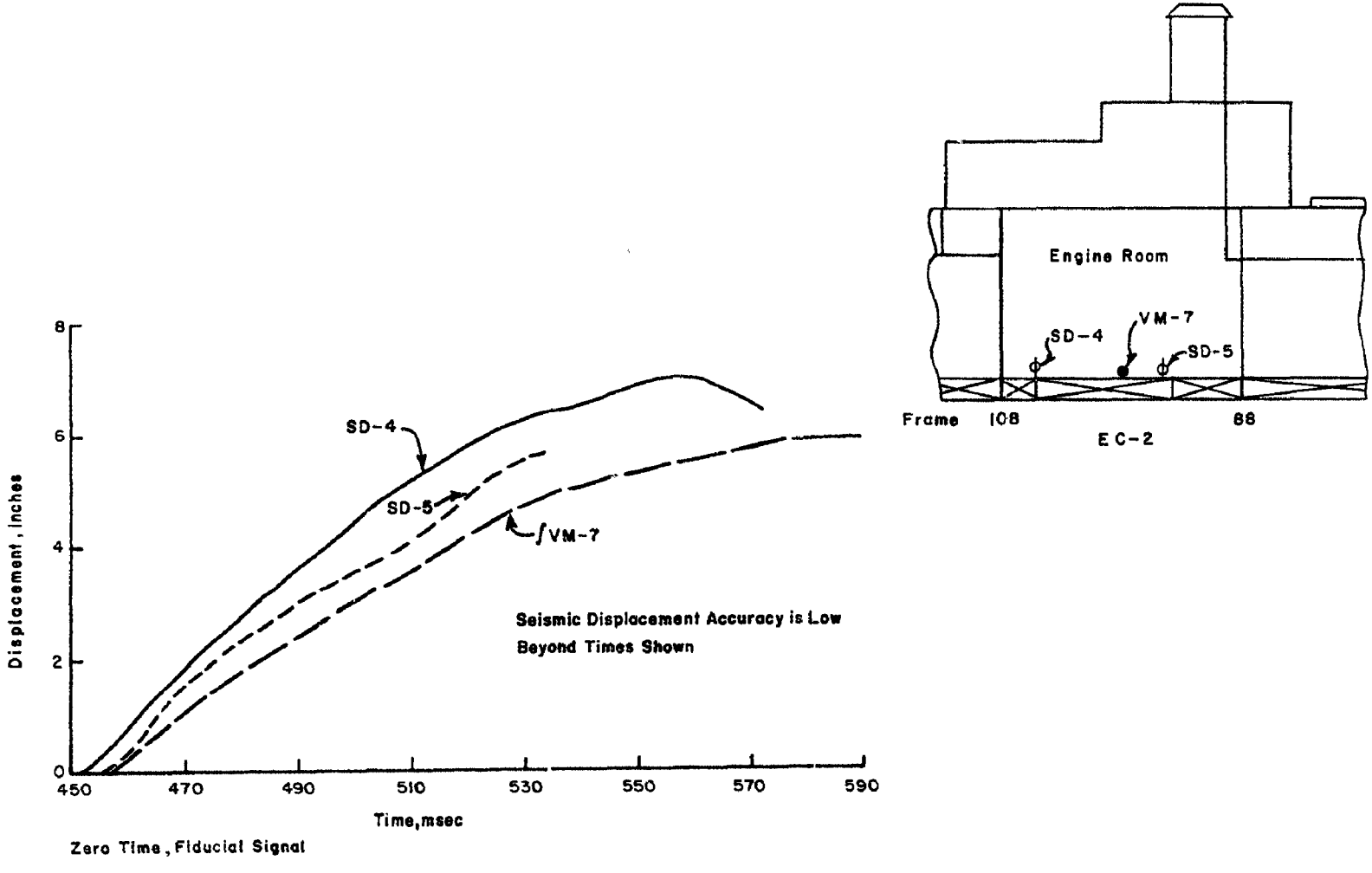

Figure 3.14 Vertical displacements of EC-2 after direct wave, Shot Wahoo.

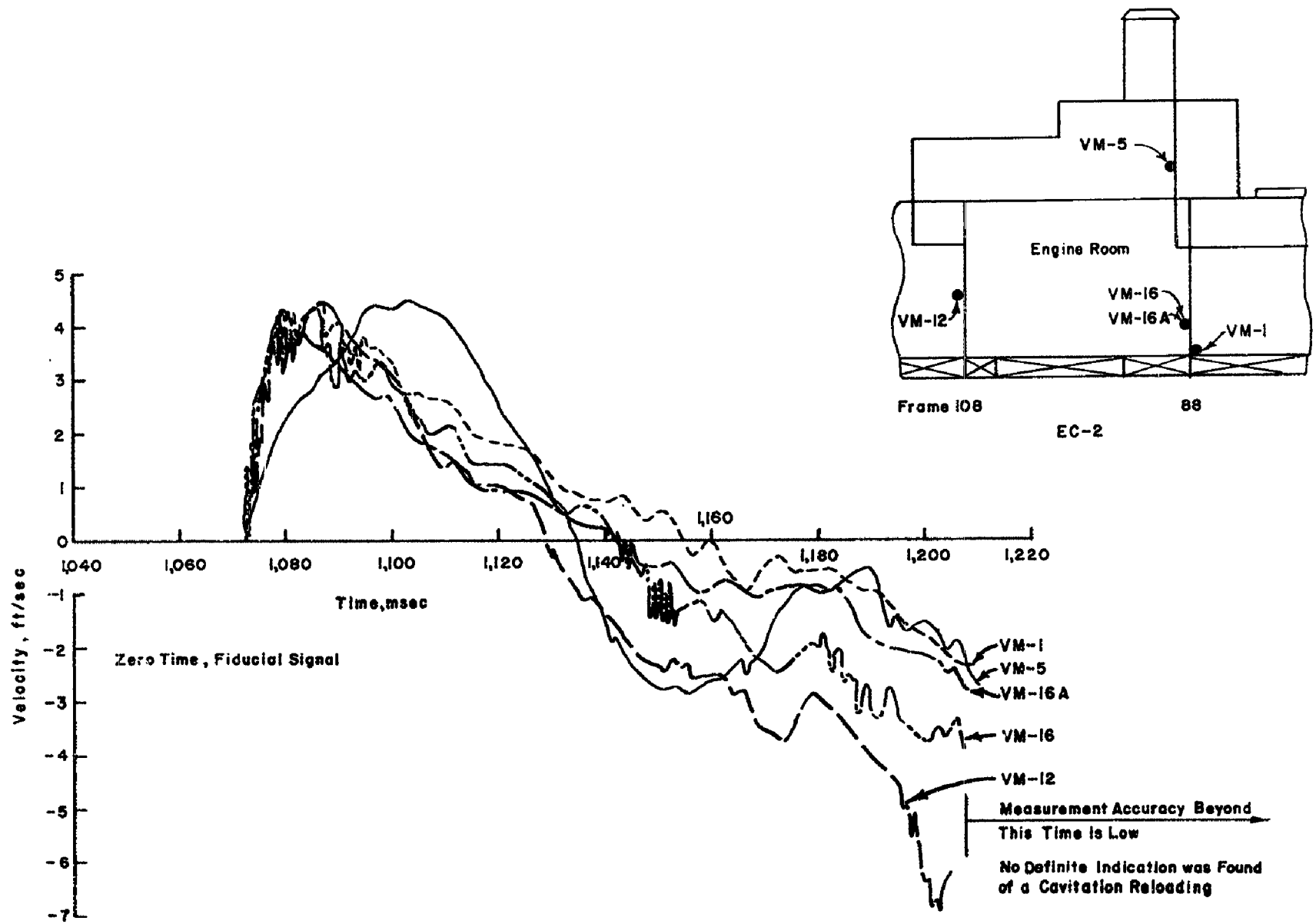

Figure 3.15 Typical vertical velocities on EC-2 after reflected wave, Shot Wahoo.

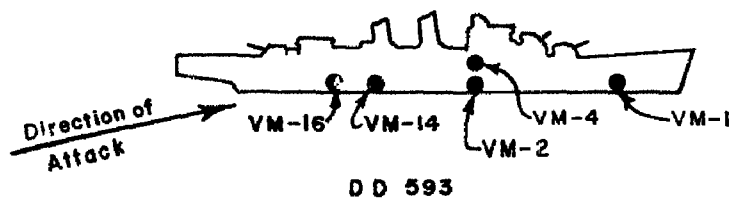

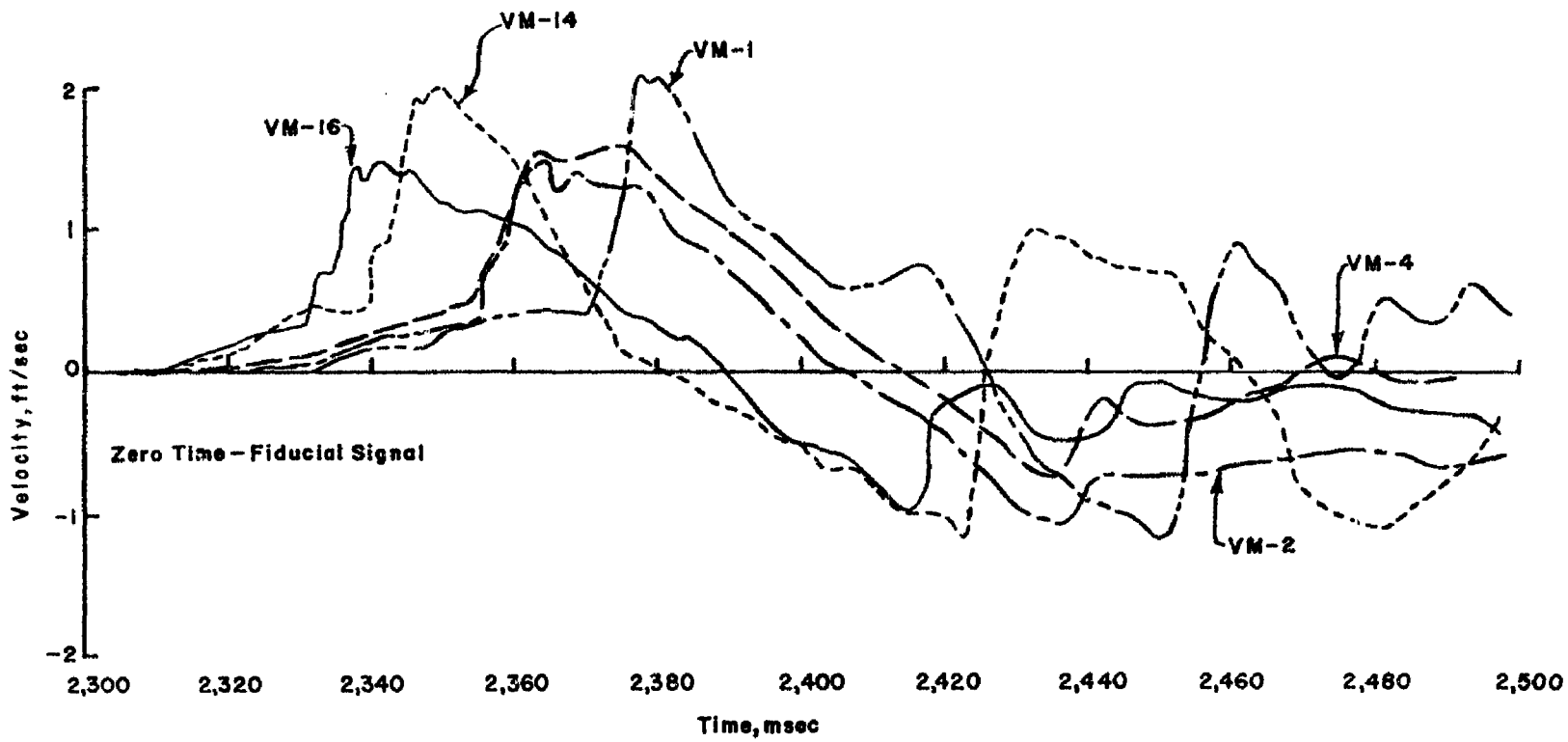

Figure 3.16 Vertical motion at various locations on DD-593 after reflected wave, Shot Wahoo.

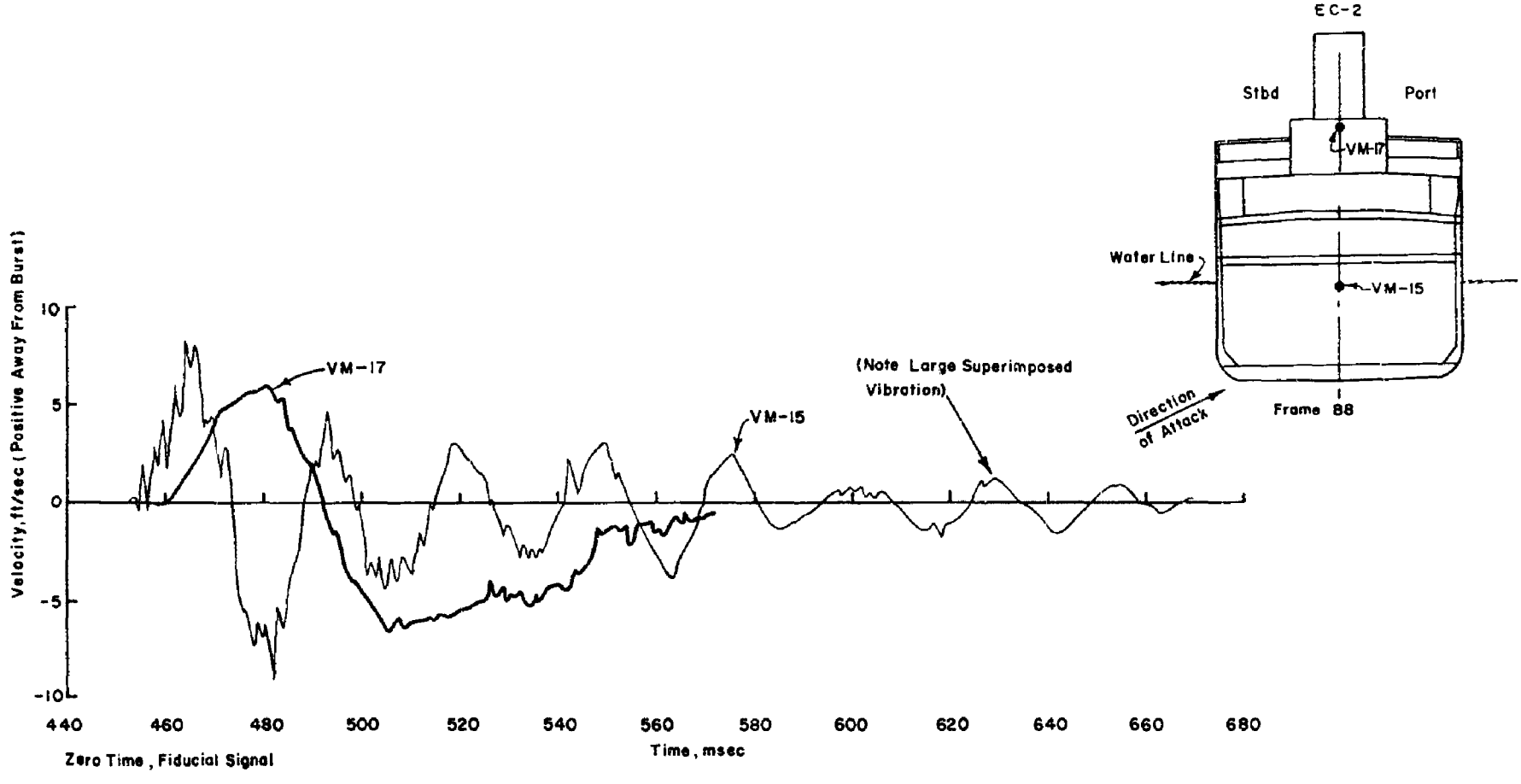

Figure 3.17 Horizontal velocities on EC-2 after direct wave, Shot Wahoo.

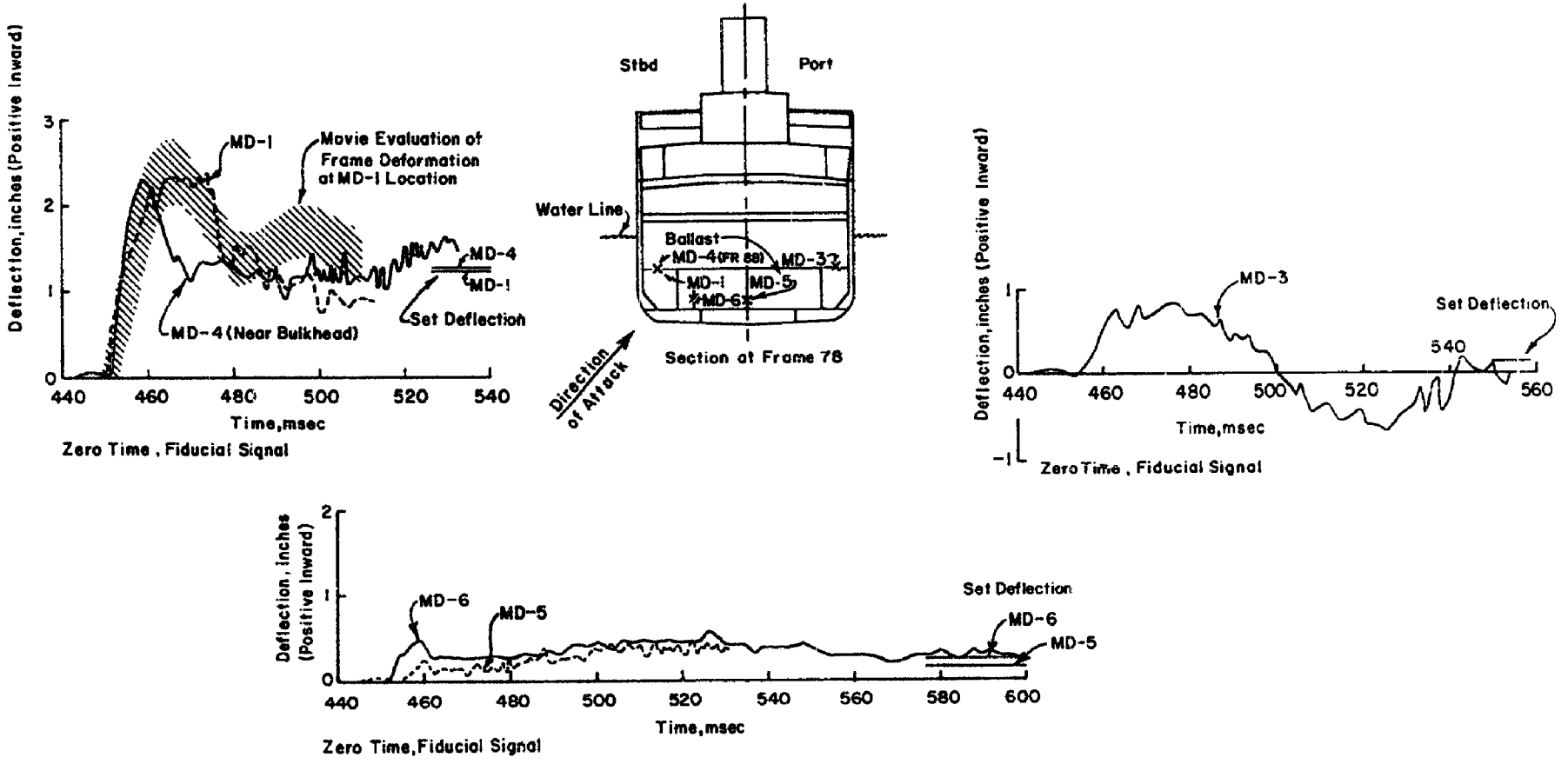

Figure 3.18 Development of hull damage in EC-2, Shot Wahoo.

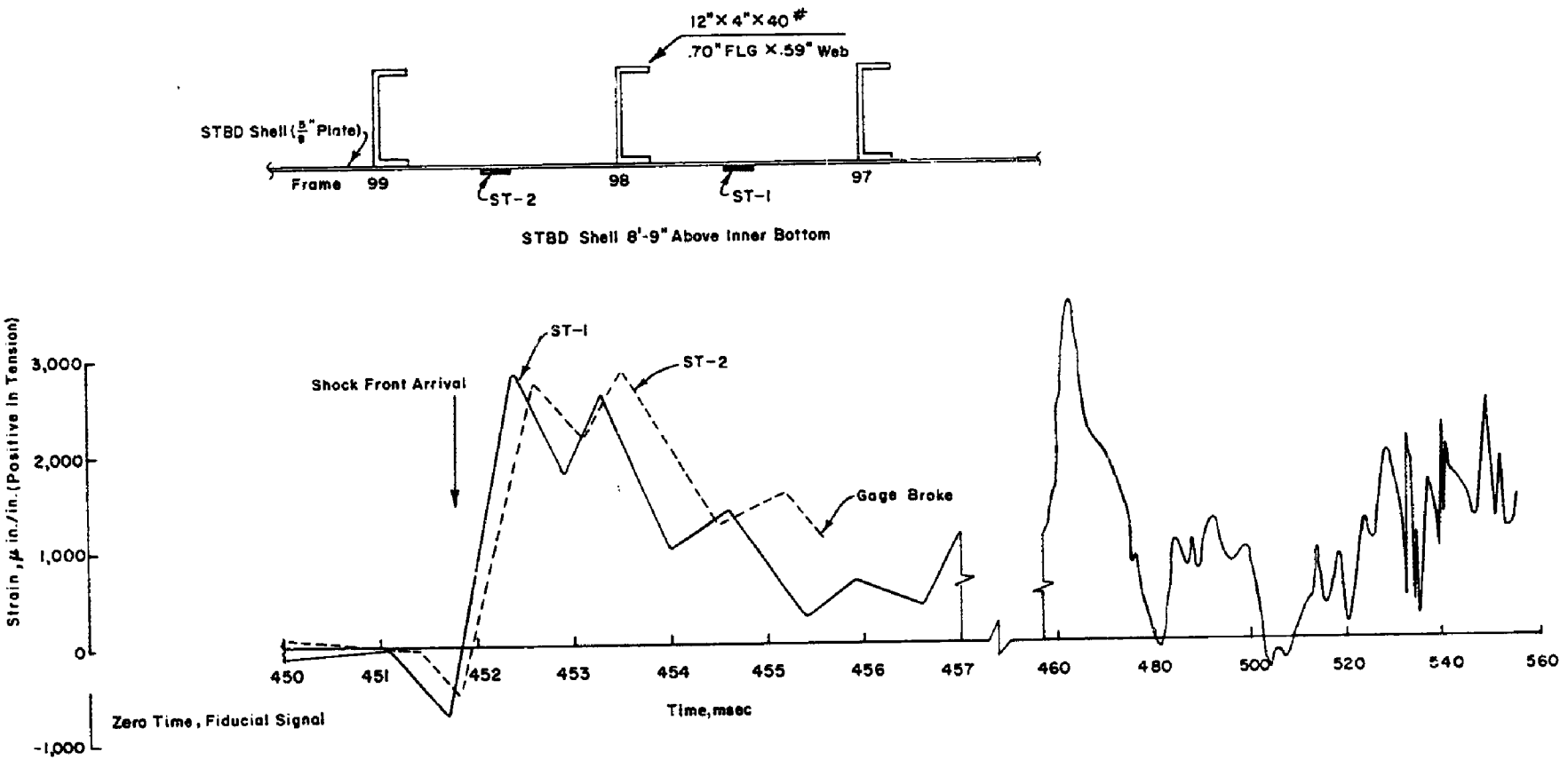

Figure 3.19 Longitudinal strains in shell plating on attack side of EC-2, Shot Wahoo.

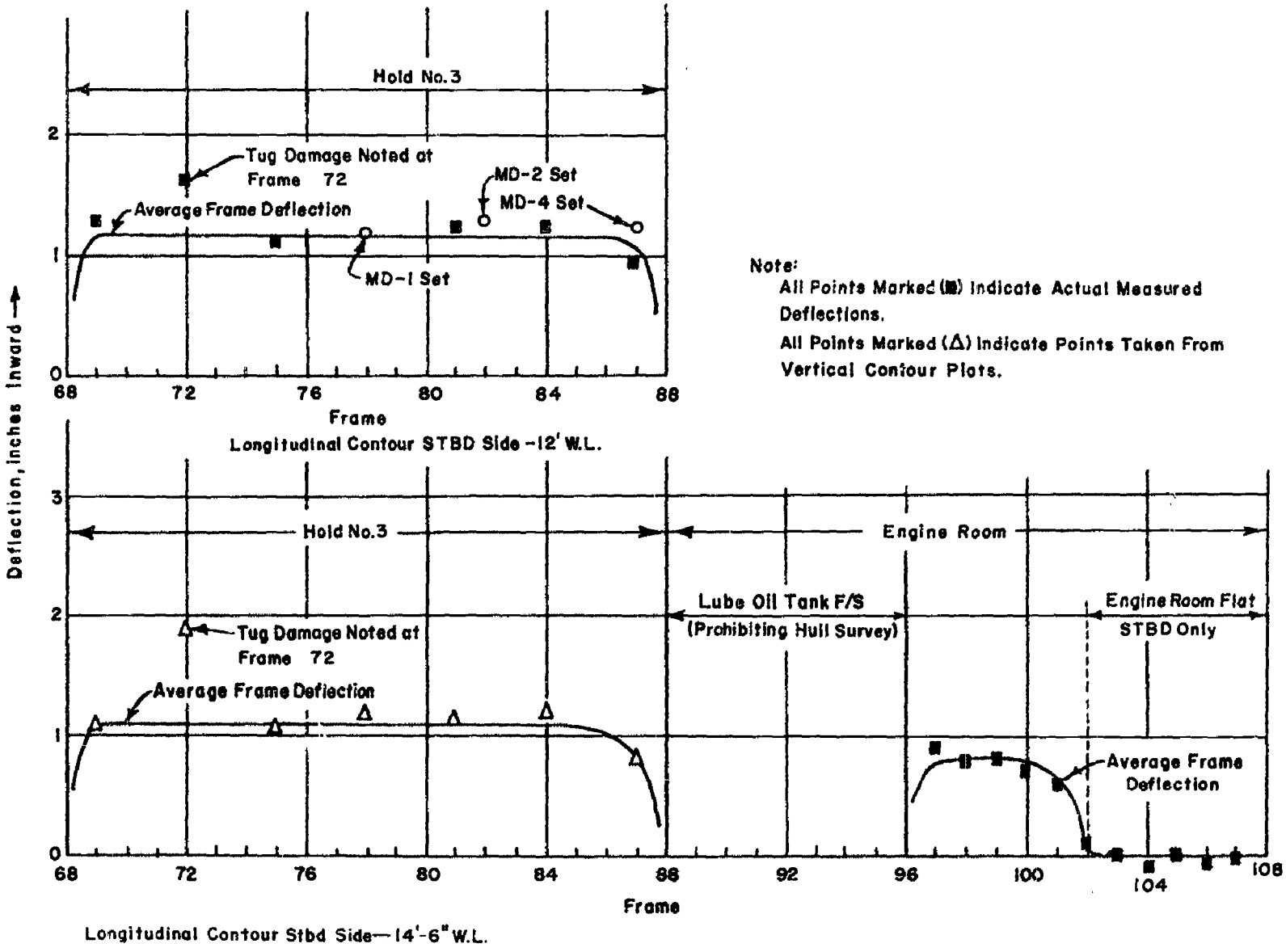

Figure 3.21 Longitudinal damage contours, EC-2, starboard side, Shot Wahoo.

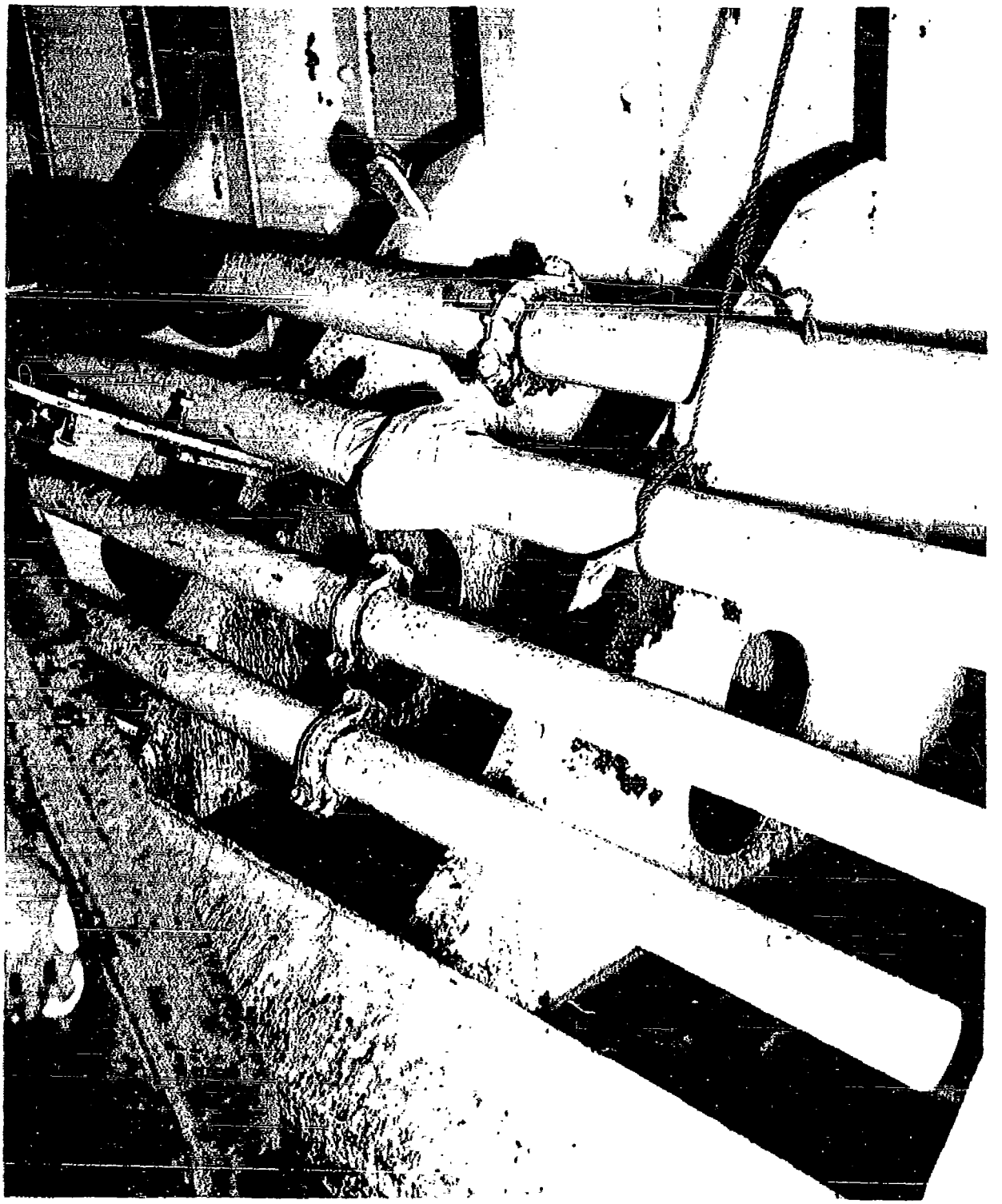

Figure 3.22 Buckled starboard side frame brackets in EC-2, Shot Wahoo.

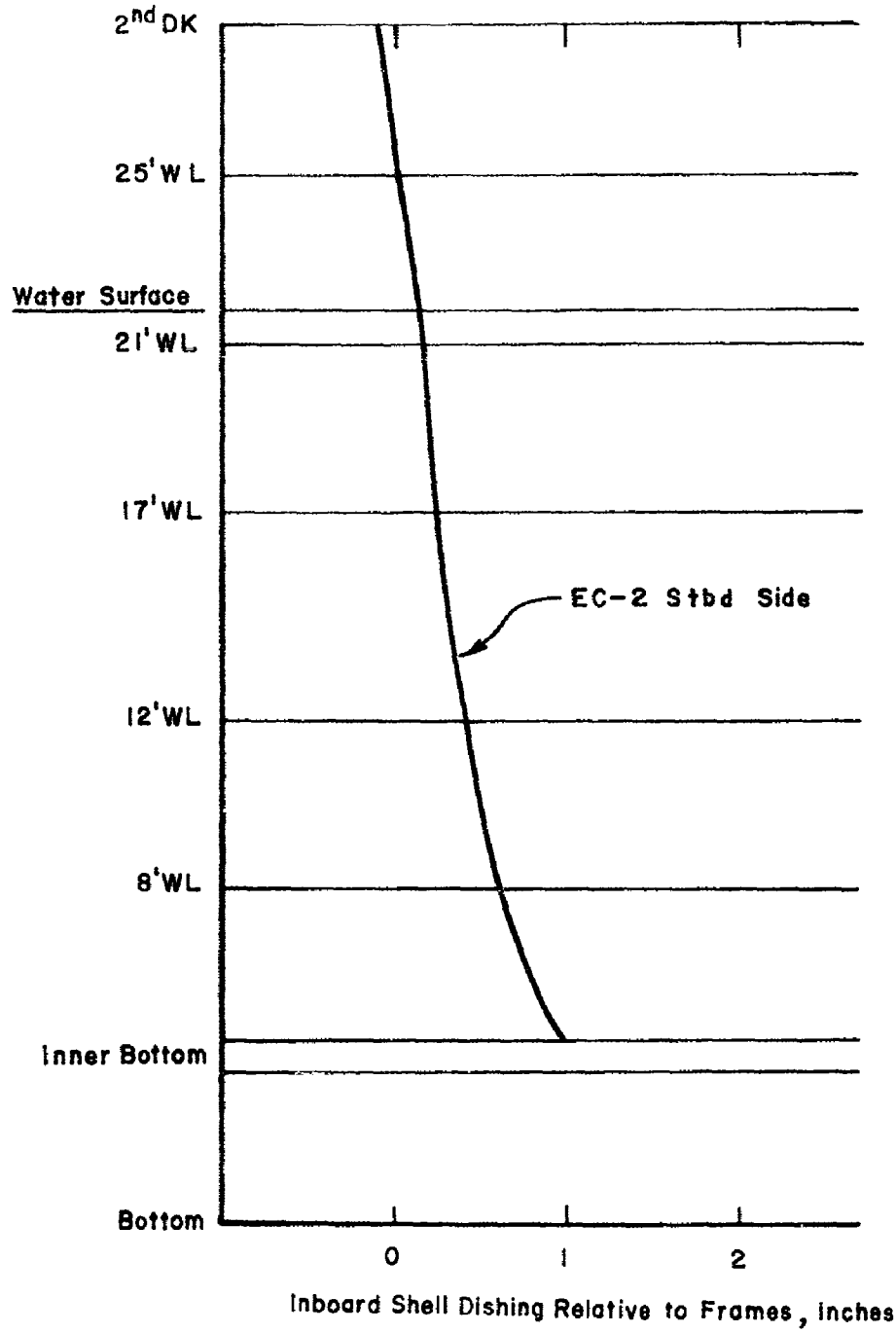

Figure 3.23 Average shell dishing between frames, EC-2 starboard side, Shot Wahoo.

Figure 3.25 Propeller-shaft bearing damage in EC-2, Shot Wahoo.

Figure 3.24 Propeller-shaft tunnel damage in EC-2, Shot Wahoo.

Chapter 4

DISCUSSION, SHOT WAHOO

4.1 PRELIMINARY REMARKS

Shot Wahoo was detonated at a burst depth of 500 feet at the site indicated in Figure 1.1. The nominal yield of 10 kt was confirmed by radiochemical analysis of water samples to within about 10 percent; such a deviation from the nominal yield is immaterial for present purposes. The analysis of the present report was therefore based on the assumption that the underwater effects arising from the explosion were equivalent to those of a 6.7-kt TNT charge exploded under the same conditions (Reference 11).

Sea conditions at the time of detonation were estimated, on the basis of information supplied informally by Project 1.13, to consist of 6-foot (crest to trough) ocean swells with a wavelength of about 300 feet and superimposed 3-foot (crest to trough) sea waves with a much shorter wavelength. The fiducial timing signal provided by EG&G was estimated to be available at the recording equipment within approximately 250 μsec of detonation; for the purposes of this report, therefore, the fiducial timing signal represented detonation time.

The underwater pressure and ship response measurements obtained from Shot Wahoo are summarized in Figure 4.1, which also shows elements of the test array. This array included some participating fleet ships as well as target ships. Project numbers are listed after each type of measurement. Other measurements of interest to Project 3.4 were also obtained. At nearly detonation time, bathythermograph measurements were obtained at the DD-593 by Project 1.13 (Reference 12). Together with previous observations in the general area, these measurements enabled estimates to be made of the sound speed structure throughout the area; such estimates are reproduced in Appendix A. Motion-picture coverage of the accompanying surface phenomena was obtained (Reference 13) by Project 1.3. Specific observations were made (Project 1.6) of the water waves produced by the underwater burst in the area of the test array (Reference 14). A survey of target-ship damage was made following the test; both equipment damage (Project 3.8, Reference 15) and hull damage (Projects 3.8 and 3.4).

The horizontal distance and the orientation of the key ships shown in Figure 4.1 were measured in three ways: an aerial photographic survey of the target array prior to shot time, radar screen scans near shot time, and shock-wave arrival time measurements at the ships. Of these, the last could be applied only in two cases, the EC-2 and DD-593, and the details of this effort are discussed in Appendix A. Evaluation of available data led to the estimates given in Table 4.1. The ship headings, or orientations, at shot time are expressed in terms of rotation from the nominal headings. The nominal headings, indicated in Figure 4.1, are either directly along the array lines or normal to the array lines.

Prior to analyzing the loading and response measurements obtained by Project 3.4, an effort was made to collect and summarize all pertinent phenomenological data (Program 1) obtained during Shot Wahoo (Figure 4.1) and, by comparing it with theoretical calculations, to adapt it to a form considered essential to a rational pursuit of Project 3.4 objectives. (The necessary information was supplied by key projects, such as 1.1 (Reference 16) and 1.5 (Reference 17), prior to the final publication of their own analyses.) The main results

of this Project 3.4 evaluation are expressed in this section; detailed justifications are presented in Appendix A.

Shot Wahoo generated four significant loading phases: direct shock wave, bottom-reflected pressure wave, and bulk-cavitation reloadings following both the direct and reflected pressure waves. The bottom-reflected wave assumed a particularly complex character beyond a critical range somewhat short of the DD-593 position. Beyond this critical range the first reflected-wave signal to arrive at positions near the water surface traveled partly through the sea bottom; the initial portion of the reflected-wave signal is designated a precursor. At a time corresponding to the first arrival of a signal traveling entirely through the water, i.e., a specular reflection, the bottom-reflected pressure wave exhibited a jump increase.

For the purpose of this report, the direct shock wave is characterized near the water surface by angle of attack, peak pressure, and surface cutoff time. Each of these is described below as a function of horizontal range from surface zero for depths below the water surface, which are of interest for surface ships.

The attack angles made at the water surface by the direct shock wave were computed by the use of refraction theory as described in Appendix A, and the results are plotted as a function of horizontal distance from surface zero in Figure 4.2. Experimental confirmation of these results could be obtained meaningfully in one case, the EC-2 by utilizing Project 3.4 shock-front arrival-time measurements along a transverse line (Appendix A). Insertion of this result into Figure 4.2 indicates a good agreement with the computed attack angles.

Direct wave peak pressures calculated by refraction theory for positions near the water surface are plotted as a function of range in Figure 4.3. For comparison, all available experimental data obtained near the water surface is also shown; the computed curve represents a satisfactory representation of all information. An objection to this statement might occur to the reader on the grounds that it should be expected, particularly at the more distant ranges, say, 15,000 feet, that the surface reflection would be anomalous (Reference 18) thereby reducing pressures well below the level to be expected merely on the basis of refraction theory. In fact, however, this does not occur; refraction causes peak pressure to be decreased and the attack angle to be increased just sufficiently so that the region of anomalous surface reflection does not commence until ranges at least greater than 15,000 feet are reached.

Surface cutoff times for depths near the water surface were also computed by refraction theory. Comparison with the experimental data in Appendix A, however, suggested that surface reflection effectively occurs at the troughs of ambient surface waves rather than from the average water level; recall that ambient surface waves totaling nearly 10 feet (crest to trough) were present at detonation time. This concept was, therefore, used to determine surface cutoff times at a depth of 13 feet below the average water surface: the results are shown as a function of range in Figure 4.4. Values at other depths can be estimated roughly by assuming proportionality with respect to effective depth (i.e., depth below the largest surface-wave troughs, or depth minus 5 feet).

The extent to which the above characterization of the direct shock wave is valid can be illustrated by comparison with Project 3.4 pressure histories, secured at the EC-2 position. A typical comparison is given in Figure 4.5; later portions of the experimental record are dashed, because they are influenced by reflections from the EC-2.

An effort was made to characterize the bottom specularly reflected shock wave, near the water surface, in a manner similar to that of the direct shock wave. The situation for the bottom-reflected shock wave is, however, more complex than that for the direct shock wave. In particular, the reader is reminded that beyond a range just short of DD-593 the bottom specular reflection is preceded by a precursor that has quite different characteristics. Attention is primarily confined to the specular reflection because this was, by far, the more

significant with respect both to peak pressure and to the consequent ship response.

The attack angles made, at the water surface, by the bottom specular reflection were computed from bottom contours and refraction theory as described in Appendix A. Results are plotted in Figure 4.6 for each of the array lines shown in Figure 4.1. Experimental confirmation was obtained, as shown in Figure 4.6, at EC-2 and DD-593 from arrival-time measurements given in Appendix A.

Peak pressures, near the water surface, were computed along the major array lines (Figure 4.1) for the bottom specularly reflected wave by the use of an experimentally determined bottom-reflection coefficient and ray-path (refraction) theoretical calculations as explained in Appendix A. These estimates are shown in Figure 4.7 together with experimental data obtained from gages not deeper than 100 feet. They may be expected to characterize the pressure jump occuring at the arrival time of the specular reflection in a rough sense, although deviations from the pressure level shown in Figure 4.7 can exist over time durations as long as several milliseconds. For example, there is no doubt that in the case of the reflected wave at DD-593 position the initial pressure jump, lasting 2 to 4 msec, is only about half of the pressure level given in Figure 4.7; this is suggested by the shallowest measurement obtained by Project 1.5 (Reference 17) and will be discussed later in Section 4.2.

Surface cutoff times for the bottom-reflected wave were computed as indicated in Appendix A and were plotted as a function of range along the two major array lines at a water depth of 13 feet; the results are indicated in Figure 4.8. Basically, the approach used here paralleled that used for the direct shock wave. Estimates at depths other than 13 feet can be made, therefore, by assuming proportionality with respect to depth below effective water surface.

Bulk cavitation occurred in Shot Wahoo following both the direct shock wave and the bottom-reflected shock wave. Observations on bulk cavitation were made from a movie camera mounted on an RB-50 aircraft 22,000 feet above surface zero, from Project 3.4 response gages on the EC-2 and DD-593, and from free-water-pressure gages located at various ranges near the water surface (Projects 1.1 and 3.4).

A presentation of all measurements of cavitation reloading time, following the direct shock wave, is made in Figure 4.9. Examination of this figure reveals that all types of measurements show a remarkable consistency and fall on the curve shown. The results which were derived from the movie film are explained in more detail in Appendix A. Figure 4.9 also includes the arrival times of the direct shock-wave front itself.

A similar investigation of bulk cavitation reloading following the bottom-reflected wave was carried out based on response measurements and on free-water pressure measurements; in this case, no supporting evidence could be found from the aerial movie films. Table 4.2 lists all available data on cavitation reloading times. Since absolute times were not available in all cases, the values listed are relative to reflected-wave arrival times at the gage location. Remarks are entered in Table 4.2 concerning estimates of peak pressure and attack angle characterizing the reflected wave at these positions; these will serve to remind the reader that the measurements were secured along different array lines and that no way of synthesizing the data is suggested.

Relatively little pertinent information is available from Shot Wahoo concerning loading phases beyond the four significant phases described above.

No observations were obtained, during Shot Wahoo, of the behavior of the gas bubble left in the water after detonation. However, simple theoretical estimates could be made concerning its early behavior, say, up to a time of about 0.2 the period, and the resulting mass flow of water near the water surface; as will be seen (Section 4.4) these estimates provide an insight into the bodily motion of the surface ship targets over a time period between cavitation reloading, caused by the direct shock wave, and arrival of the bottom-

reflected shock wave. No indication of a bubble pulse was found on Project 3.4 records.

It was known (Reference 14) that burst-generated water waves arrived at the EC-2 position: a 6-foot trough at about 24 seconds and, later, at least a 13-foot crest followed by a 15-foot trough. Records from Project 3.4, however, do not allow a measurement of the response of the target ship.

4.2 INITIAL HULL LOADING AND RESPONSE

When an incident-shock pressure wave impinges upon an underwater structure such as a ship, a complicated interaction ensues; as the hull deforms inward under the influence of the incident wave, the loading pressures are modified by the hull response. The initial phase of this interaction is relatively well understood for some conditions; later phases of the loading and response are complicated by the occurrence of cavitation in the water adjacent to the structure.

The most easily understood interaction phenomena that were documented in Shot Wahoo are the interaction of the direct shock wave with the EC-2 attacked side, i.e., the side facing the attack, and the interaction of the sea-bottom-reflected wave with the EC-2 bottom. The initial phase of the loading and response can be investigated in these cases by means of the Taylor theory (Reference 19). The simplified interaction model behind this theory utilizes the assumptions that the pressure in the water adjacent to the structure is controlled by plane-wave acoustic laws and that the structural response is controlled only by the loading pressure and by the inertia of the hull section of interest; in both cases it is implied that the phenomena at neighboring sections do not influence those at the local section of immediate interest. The equations appropriate for the slowly decaying shock waves of present interest are essentially those for incident pressure waves whose histories may be represented as step functions:

$$v_{plate} = 2\frac{p_m}{\rho c} \sin\beta \left[1 - e^{(-\rho c/m \sin\beta)t}\right]$$

$$p_{loading} = 2p_m e^{(-\rho c/m \sin\beta)t}$$

Where:

v_{plate} = velocity response normal to plane of structure

$p_{loading}$ = loading pressure adjacent to structure

p_m = peak free-water shock-wave pressure at location of structure

β = angle between incident ray and tangent at structural element of interest

ρ = water density

c = sound speed in water

m = mass/area of structure (plate)

t = time measured from shock-front arrival time at location of interest

Naturally, these equations need modification in those cases for which surface cutoff times (essentially terminating the shock wave) are less than the time it takes for the velocity to

approach its asymptotic value to within, say, 5 percent. The maximum velocity predicted by this theory when it applied to bottom structure is equal to the water particle velocity, a quantity which is defined in Section 4.4.

In the case of the initial interaction of the direct shock wave with the EC-2 attacked side, the only pertinent measurement was that of the velocity response of the side (VM-11). This response measurement is therefore reproduced in Figure 4.10, with a rather expanded time scale and is compared there with the theoretical estimate. The pertinent quantities utilized in the theoretical computation were taken from Section 4.1 except for the plate weight per-unit-area; this value was assumed to be 41.5 psf, because this represents an average weight distribution of both shell plating and stiffeners. A glance at Figure 4.10 indicates that the experimental velocity is somewhat lower than the theoretical velocity. Some insight into the reason for this is provided by noting that surface cutoff time at the gage position occurs near the end of the steeply rising portion of the theoretical velocity history; clearly, sections of the side above the gage position can achieve only considerably smaller velocities, and this may lead to a reduction in velocities at the gage position itself.

The interaction of the sea-bottom-reflected wave with the EC-2 bottom was measured by a pressure gage attached to the hull just below the keel (PE-1) and by velocity meters mounted to the inner bottom above the keel (VM-7 and VM-7A at a location corresponding to PE-1, and VM-14 some distance away). Theoretical calculations were based on pertinent quantities defined in Section 4.1 and on a weight per unit area, for the double-bottomed structure, of 224 psf. This estimate averages out all the structural features in the double bottom and takes into account the water ballast filling the double bottom to 75 percent. The loading pressure phenomena are presented in Figure 4.11 together with the theoretically calculated loading pressure based on the Taylor theory; an estimate of the incident pressure history is also indicated. Considering the gross simplification made in the structural characteristics of the double bottom, the comparison of theoretical and experimental loading pressures in Figure 4.11 is considered fair. The possible reasons for the differences will be discussed later.

The two velocity meters (VM-7 and VM-7A) mounted on the keel at a location corresponding to PE-1 produced almost identical measurements and, therefore, only one is used to give a comparison of the experimental with the theoretical response in Figure 4.12. The experimental record actually shows a response prior to the arrival of the shock front at the gage position, due to precursor waves through the steel bottom structure; the response level was small, however, and is neglected in Figure 4.12. Comparison of experimental and theoretical velocity response, is, as for the loading pressure, only fair. Some further insight into the validity of the theoretical assumption that structural restraint forces may be neglected is provided by calculating the velocity which would result from the experimental loading pressure (PE-1) if the assumption were true. Such a calculation is shown by the dashed curve in Figure 4.12, based on the impulse-momentum theorem and utilizing a weight per unit area of 244 psf. The deviation between the constructed velocity history (based upon the experimental loading pressure history and the impulse-momentum theorem) and the experimental velocity history indicates that structural restraint forces can be strictly neglected, at this location, only for a very short time and that, at times of the order of 2 to 3 msec after the commencement of the response, they play an appreciable role in reducing the velocity below levels otherwise to be expected.

The fact that the Taylor theoretical response curve falls midway between the experimental curve and the constructed curve, based on the impulse-momentum theorem, suggests that the removal of such structural restraint forces would have resulted in a much better agreement between the theory and experiment. Loading pressures would have been reduced and velocities correspondingly increased. That the structural restraint forces actually became prominent at such early times is undoubtedly due to the proximity of heavy weights in the

engine room to the gage location. One velocity measurement (VM-14) was secured at a location that was reasonably distant (about 6 to 7 feet) from heavy weights. Experimental velocities measured by VM-14 and VM-7A are compared in Figure 4.13. Notice that VM-14 shows a greater rise time and a somewhat greater peak velocity than does VM-7A. Comparison of VM-14 with the Taylor plate theoretical velocity (dashed curve) indicates close agreement.

When the shock pressure wave is incident upon a structural element at an angle β less than about 70°, the Taylor theory is no longer a useful tool in making estimates of the loading and response under long shock-wave attack conditions (Reference 6). Under such conditions, diffraction processes in the water play a significant role in raising the loading pressures at the point of interest above the level that would be expected merely on the basis of considering the response of an isolated local section; a high-pressure region tends to be found at relatively rigid portions of the ship structure, especially where the shock wave is normally incident, e.g., the leading edge of the EC-2 bottom. In such cases an empirical rule has been formulated to predict the peak velocity reached by the structural element (Reference 6):

$$v_m = 2\frac{p_m}{\rho c}\quad\frac{1+\sin\beta}{2}\quad f_1(z)\, f_2(t_s/\tau)$$

Where:

v_m = peak velocity of structural element normal to its plane

p_m = peak pressure

ρ = density of water

c = speed of sound in water

β = angle between incident ray and tangent at structural element of interest

$f_1(z) \simeq 1$, for long shock waves of present interest

t_s = surface cutoff time at point of interest

τ = characteristic time

f_2 = empirically determined function (Reference 6)

It is stressed that the rule is applicable only to certain bare structural elements of the hull itself; as in the case of the Taylor theory, structural restraint forces are neglected. The rule essentially coincides with the results of the Taylor theory in cases where the incident angle β is greater than about 70°. Pertinent measurements for the purpose of checking the validity of these rules were obtained in Shot Wahoo for the interaction of the direct shock wave with the EC-2 bottom and the interaction of the reflected wave with the DD-593 bottom. As a handy tool for carrying out the detailed discussion, peak bottom vertical velocities were estimated for a DD and for an EC-2 at a variety of hypothetical horizontal ranges, both for the direct wave and for the sea-bottom-reflected wave; the results are plotted in Figure 4.14. Values of the characteristic time τ utilized in the empirical rule were derived from References 6 and 20 and are 3.5 msec for the EC-2 and 1.2 msec for the DD. Corrections to account for variations in draft and differences between end-on and side-on attacks were taken into account in accordance with Reference 8.

The interaction between the direct shock wave and the bare hull structure of the EC-2 bottom in Shot Wahoo is best described experimentally by VM-14, which was located relatively far from heavy masses. It is this measurement which must be used for comparison with the empirical rule. The response measured by VM-14 is shown in Figure 4.15 where it may be directly compared with the response of VM-7, a meter located close to heavy masses. The experimental peak velocity, measured by VM-14 (13 to 15 ft/sec) compares very well with that expected on the basis of the empirical rule derived from EC-2 model experiments (Figure 4.14). The experimental peak velocity is, however, in excess of that derivable from the Taylor plate theory (8.5 ft/sec) by about 65 percent; in this case the Taylor plate velocity is equal to the water particle velocity.

The interaction of the reflected shock wave and the DD-593 bottom was measured in Shot Wahoo at two locations along the keel. At Frame 120½, a pressure gage (PE-6) was attached to the hull just under the keel and two vertical velocity meters (VM-14 and VM-15) were attached to the bottom nearby. At Frame 82½, corresponding measurements were obtained from PE-3 on the one hand and VM-8 and VM-9 on the other hand. A comparison of the response measurements obtained at each location by each pair of velocity meters indicated very close agreement. Moreover, both the loading and response were similar at the two locations. Therefore, the discussion is limited to the Frame 120½ location (PE-6 and VM-14). The loading pressure history measured by PE-6 and the velocity history measured by VM-14 have been presented in Figure 3.7.

Now it will be noticed that both the loading and the response arising from the arrival of the specularly reflected shock wave are superimposed on the loading and response arising from the sea-bottom-precursor pressure wave. The first step in studying the interaction resulting from the specular reflection was, therefore, to attempt to subtract from the records the loading and response due to the precursor. This was done simply by subtracting the levels established by the precursor just prior to the arrival of the specular reflection. The resulting velocity response to the specular reflection alone is shown in Figure 4.16. Also shown in Figure 4.16 is the velocity that would be expected at this location based upon the loading pressure history (PE-6), the impulse-momentum theorem, and the assumption that structural restraint forces played a negligible role in the interaction (the bottom weight per unit area was taken somewhat arbitrarily as 90 psf in accordance with Reference 20). The close qualitative comparison between the two curves indicates that, indeed, structural restraint forces were negligible during the most interesting phase of the interaction, i.e., 4 to 5 msec; the degree of quantitative agreement depends on the numerical value used for bottom weight, a more questionable value for the DD than for the EC-2. It is, therefore, proper on a DD to refer to such locations as VM-14 and VM-8 as bare hull structure.

The character of the response history has been overlooked thus far. However, the rise to a peak velocity does not occur smoothly but really consists of two separate rises spaced about 4 msec apart. It was just this behavior that led to the confidence, expressed in Section 4.1, that the free-water-reflected pressure wave at the DD-593 actually consisted of two corresponding jumps. In order to simplify the presentation of the reflected-wave characteristics, a gross treatment had been used, which ignored this complication; it was implicitly assumed that the full pressure rise had occurred immediately upon the arrival of this specular reflection. This same assumption was applied to the computation of the peak vertical bottom velocities, based on model test results, shown in Figure 4.14.

The fact that structural restraints on DD-593 near the VM-14 location are small up to a time at which the full peak bottom velocity is reached makes meaningful a comparison between the experimental peak velocity (1.5 ft/sec) and that predicted in Figure 4.14. As may be seen the comparison is close. The experimental peak velocity is, however, in

excess of that which would be deduced upon the basis of the Taylor plate theory by about 25 percent.

When a long shock wave directly impinges on any portion of a ship's hull (not only a bare hull section), the response in general depends not only upon the hull itself but also on the presence of heavy equipments at, or nearby, the location of interest. As shown in the preceding discussion, simple empirical tools allow at least the estimation of the initial velocity response for certain bare hull sections. In the more general case, however, such tools do not exist for nuclear bursts, although crude rules have been previously proposed to account for the effect of the mass of attached equipment in the case of short shock waves produced by HE attacks. Of course, the initial velocity response in the vertical direction will tend to lie between an upper bound, given by the response of the bare hull, and a lower bound, given by the vertical bodily velocity response of the ship as a whole; the latter type of response will be discussed in a succeeding section. Whether these bounds provide sufficient information for practical prediction methods depends on the degree of relative spread between them and the weight of the equipment in question.

The effect of equipments attached to the hull is more significant for the bottom than for any other portion of the hull, and all information accumulated by Project 3.4 in Shot Wahoo on ship-bottom peak vertical velocity responses is listed in Table 4.3. Note that the term "velocity jump" is employed in Table 4.3, in referring to the initial velocity response; this term (defined in Reference 20) refers to the change in velocity occurring over a relatively short time (at most 6 msec in the present case) following upon the arrival of the shock front at the location whose response is being measured. The purpose of its introduction is to minimize the ambiguity which occurs because of the fact that structural and sea-bottom precursor waves can arrive at the location of interest prior to the shock front arrival. The numerical values of experimental velocity jumps listed in Table 4.3 clearly do suggest a dependence of the velocity jump on the location of the gage.

Moreover, the experimental values listed in Table 4.3 suggest further tentative conclusions: (1) in the case of side-on attack the variation in shock severity across the width of the bottom, from leading to trailing edge, is relatively small if it can be said to exist at all (this remark applies to attack angles of at least 12°), and (2) in the case of end-on attack the experimental measurements listed in Table 4.3 do not in themselves imply any variation in shock severity along the length of the ship so long as the attack angle is greater than about 30°. Nevertheless, a comparison with C-2 model tests (Reference 8) suggests that some weakening may well have taken place from the extreme stern to Frame 148, the extreme aft position where a measurement was made; interpretation of the model results for a DD would lead, within the range of present interest, to the prediction that peak bottom velocity is reduced between the extreme stern and a position aft of Frame 148, and that thereafter it remains about the same. This is in agreement with Figure 4.14.

An explanation of the interaction process between a shock wave and the hull is more difficult in cases where the shock wave pressures are not transmitted to the location of interest directly but are diffracted around interposing sections of the hull. In any case the practical incentive to enter into this question does not exist; a glance at Figure 3.8 indicates, for example, that the peak velocity achieved at the shadowed side of the EC-2 is only about 10 percent of that of the attacked side in the case of an attack angle of 12° and about 50 percent in the case of an attack angle of 81°.

4.3 EARLY VERTICAL SHOCK TRANSMISSION UPWARD THROUGH SHIP

The manner in which shock motions are transmitted from the hull upward through the bulkheads and sides, and thence throughout the ship, is not well understood. Examination

of the early portions of velocity records obtained at meters located upward along the vertical centerline of bulkheads (Figures 3.11 and 3.12) suggest a few crude empirical conclusions for the case of nuclear attacks: (1) At a bulkhead, peak vertical velocities are of similar magnitude regardless of location. (2) At a bulkhead, the time to reach peak velocity increases with height of location above the bottom. (3) At a bulkhead, initial average accelerations decrease with height of location above the bottom by as much as a factor of 10, corresponding to the increase in time to reach peak velocity. The significance of these observations from a fundamental physical point of view is by no means obvious; indeed, the experimental presentation itself is beclouded because the EC-2 bulkhead is not continuous above the second deck level (corresponding to the location of VM-4) and the DD-593 bulkhead structural material changes from steel to aluminum above the main deck level (the location of VM-5).

The response measurements obtained in the EC-2 bulkhead (Frame 88) following the Wahoo direct shock wave appear to offer at once the simplest situation and the best documented. With attention restricted to the continuous portion of the bulkhead, the pertinent measurements are once again shown in Figure 4.17 where a special attempt was made to reproduce the details of the records faithfully. Moreover, in order to facilitate the understanding, the baselines of the measurements are located in such a fashion as to scale the actual vertical distance of the gage location above the bottom. In this form of presentation, therefore, the propagation front of an elastic signal traveling vertically upward through the bulkhead can be represented by a straight line with a slope corresponding to the propagation speed through steel (16. 6 ft/msec). Such a line is shown on Figure 4.17 with its origin corresponding to the first shock-wave arrival at the bulkhead centerline.

It is, of course, not surprising to note that a response is measured in each case prior to the time corresponding to shock-wave front arrival at the bulkhead centerline. These responses are due to structural precursor waves, originating at the time corresponding to shock front arrival at the leading edge of the ship. Precisely how the response at any gage location builds up is complicated by the multiple paths over which signals of various kinds can travel. However, it would appear that the main response is transmitted vertically upward along the bulkhead.

Particularly interesting is the close comparison between VM-1 and VM-16A. VM-1 was mounted to the inner bottom above the keel close to the bulkhead, whereas VM-16A was mounted directly on the bulkhead centerline itself (Figure 3.15). Apparently, at least in the case of such a massive double bottom structure as the EC-2 has, the response is essentially instantaneously transmitted, without distortion, from the double bottom to the bulkhead.

A close examination of the comparison between VM-16A and VM-4 suggests that the longer rise time empirically observed for gages located higher up along the bulkhead is not so much connected with the basic physical transmission of individual elastic waves upward through the bulkhead as it is due to the relatively greater magnitude of the response to structural precursor waves for higher as compared to lower positions. It is apparently this effect that leads to the observed increase in rise time with height above the bottom.

4.4 BODILY MOTION OF SURFACE SHIPS

The gross, or bodily, motions that could be determined from the response measurements obtained on the target ships in Shot Wahoo were the vertical motion of the center of gravity (heaving), pitching, and the horizontal motion of the center of gravity. Of these the first was best documented and most significant.

The vertical responses measured in the target ships show, in their initial and detailed characteristics, a considerable dependence upon the precise location of the gage. However, the gross response over relatively long periods of time is similar for nearly all gages.

Indeed, a simple examination of a number of superimposed response measurements gives a good impression of the overall vertical bodily motion of the target ships. Key evidence in this respect has already been presented in Figures 3.13 through 3.16.

Examination of Figure 3.13 suggests that the vertical bodily motion of the EC-2 following the direct shock-wave arrival is given typically by the gross characteristics of VM-16; this record is reproduced in Figure 4.18. The main characteristics of the EC-2 vertical motion following the direct shock wave may be described in simple terms as follows: an initial velocity (8.5 ft/sec) is established and thereafter the velocity decreases at constant deceleration (2.3 g) until cavitation reloading (182 msec after shock wave arrival) brings the velocity to about zero. This is emphasized by the idealized history shown by the dashed curve in Figure 4.18.

Such a behavior was previously found (Reference 6) in small-scale UERD model tests, and a simple physical concept was advanced. Bulk cavitation occurring in the water results in the separation of a surface water layer from the main body of water. This surface layer rises with an initial vertical velocity, and is thereafter subjected to a constant deceleration due both to the body force of gravity and to the pressure difference between the top and bottom surfaces of the layer; while a pressure of one atmosphere exists above the top surface, a pressure that is essentially zero (vacuum) must exist at the bottom surface of the layer. A cavitation reloading occurs when the layer is forced back upon the main body of water. If the depth of the separation surface, i.e., the water layer thickness, is not less than the draft of the ship, then a surface ship may simply be visualized as riding along with the water layer.

It is an easy matter to see how the concept fits together with the behavior of the EC-2 in response to the Wahoo direct shock wave. The layer thickness h was computed from the relation,

$$\Delta p = \rho h A$$

Where:

Δp = pressure difference (14.7 psi)

ρ = water density

h = layer thickness

A = portion of deceleration due to pressure difference (1.3 in the case of the EC-2 and the direct shock wave)

and a value of 25 feet was found. The water layer thickness was, therefore, about equal to the draft of the EC-2. Although this is believed to be a matter of pure coincidence it, nevertheless, means that the concept is applicable.

Continuing with the immediate discussion of the EC-2 bodily motion caused by the direct shock wave, it is natural next to take up the question of its bodily displacement. The vertical bodily displacement history of the EC-2 is shown in Figure 4.19; both the integral of the experimental velocity history, VM-16, and the computed displacement corresponding to the surface layer concept are shown. The agreement between these two curves is fairly close; differences are largely due to the idealizations employed. While the surface layer is following the motion indicated in Figure 4.19, the main body of water undergoes an upward swelling controlled by the expanding gas bubble left in the water following the burst. This upward swelling was computed, on the basis of the well-known incompressible fluid flow treatment and is also represented in Figure 4.19; for this computation it was estimated

that the bubble period was 5.0 seconds, and the maximum bubble radius was 400 feet. Cavitation reloading must be expected when this curve intersects the displacement history of the water layer; as shown this is to be expected at 209 msec after shock wave arrival. This is in fair agreement with the experimental cavitation reloading time at the EC-2.

Subsequent to bulk cavitation closure, the motion of the EC-2 must follow the mass flow of water controlled by the expanding gas bubble until the bottom-reflected wave arrives; further events become too complex to allow simple estimates. Although no sufficiently trustworth measurements were secured beyond the cavitation reloading time, theoretical estimates of this phase of subsequent vertical motion of the EC-2 are shown in Figure 4.20 as a matter of general interest. The overall estimates of the EC-2 motion are indicated as solid portions; estimates merely pertaining to the mass water flow are shown by dashed curves.

No further direct observations of the vertical bodily motion of target ships following the direct shock wave in Wahoo are available; the bodily motion of the DD-593 resulting from the direct wave could not be established. However, a number of plausible deductions can be made.

In the particular case of Shot Wahoo it seems plausible that the water particle velocity should represent a reasonable approximation to the initial bodily velocity; the thickness of the water layer is small compared to length of the free-water shock wave. In order to facilitate the discussion, therefore, the water particle velocity was computed for a variety of ranges; results are shown in Figure 4.21. Water particle velocity v_{wp} is defined by:

$$v_{wp} = 2 \frac{p_m}{\rho c} \sin \alpha$$

Where:

p_m = actual peak pressure near the water surface

α = attack angle near the water surface

ρ = water density

c = speed of sound in water

Quantities utilized in the computations were taken from Section 4.1. It is encouraging to note that the experimental initial vertical bodily velocity imparted to the EC-2 by the direct wave is in close agreement with the water particle velocity; this experimental value is shown in Figure 4.21 by a point.

The bulk cavitation reloading times deduced, over a wide range, in Section 4.1 may be used to compute surface layer thickness, if it is assumed that the initial velocity of the water layer equals water particle velocity and that the mass flow of water is controlled by the expanding gas bubble. For this purpose it is convenient first to translate the absolute cavitation reloading times (Figure 4.9) into times relative to shock-wave arrival; the results are shown in Figure 4.22. The method of computing surface layer thickness was identical to that previously illustrated for EC-2. Surface layer thickness estimates are presented in Figure 4.23; the experimental value directly deduced from the EC-2 response measurements is also shown there for comparison.

The sea-bottom-reflected wave gave rise to a vertical bodily motion of the EC-2, which had a character similar to that caused by the direct wave; the typical record is that of VM-16A shown in Figure 3.15. The initial vertical bodily velocity was 4.2 ft/sec, and the deceleration was 1.7 g; in this case, no reloading could definitely be detected on the experimental response records. The peak bodily displacement caused by the reflected wave is about 2 inches. Note (Figure 4.21) that the initial bodily velocity is somewhat less than the

water particle velocity (5.2 ft/sec). Apparently, the surface layer concept is still applicable to this case; the layer thickness would be about 47 feet.

The sea-bottom-reflected wave caused a vertical bodily response of the DD-593, which was obviously complicated by pitching (Figure 3.16). The character of the motion was investigated by integrating the velocity histories and utilizing these to construct displacement contours at various times (Figure 4.24). Clearly, the DD-593 vertical motion is predominantly composed of heaving and pitching. If the pitching is characterized by the relative displacement of the bow with respect to the center of gravity (Frame 103½), then the pitching history is characterized by the dashed curve shown in Figure 4.25. The heaving history (the vertical motion of the center of gravity) is characterized by the solid curve.

Further insight into the bodily motion of the DD-593 can be gained by replotting the observed velocity histories in such a way as to line up the shock wave arrival times at the various gage locations (Figure 4.26). To a first approximation, it appears that each section of the ship undergoes vertical bodily motion independently of the remaining sections. The sea-bottom precursor wave produces a slowly rising heaving velocity, which reaches about 0.4 ft/sec just prior to the arrival of the specular reflection wave front. The specular reflection wave, causing an increment in velocity of about 1.3 ft/sec, establishes an initial bodily velocity of about 1.7 ft/sec followed by a constant deceleration slightly in excess of 1 g, until cavitation reloading 83 msec later. Although it is clear that the surface layer concept is meaningless in this case, it may nevertheless be observed that the incremental initial bodily velocity is about equal to the water particle velocity (1.2 ft/sec) at the DD-593 position (Figure 4.21).

The vertical bodily response produced in surface ships by bulk cavitation closure, or reloading, can be estimated crudely for the EC-2, following the direct wave (Figure 3.13), and for DD-593, following the bottom-reflected wave (Figure 4.26). At the EC-2, it appears that reloading from bulk cavitation closure, following the direct wave, gave rise only to an insignificant response; the incremental bodily velocity was about 0.5 that caused by the direct shock wave, itself; the average, acceleration accompanying the velocity increment was only about 0.2 to 0.3 that accompanying the velocity rise caused by the direct shock wave. The DD-593 response caused by bulk cavitation closure, following the bottom-reflected wave, was appreciable; both incremental bodily velocity and accompanying accelerations were about equal to the corresponding responses caused by the specular reflection shock wave.

The available evidence on horizontal bodily motion of the target ships is limited to the EC-2 and the direct shock wave. Two horizontal velocity meters were located on a bulkhead, one near the vertical center of gravity and one up in the superstructure, and the records secured are shown in Figure 3.17. VM-15 shows a superimposed vibration, with a natural frequency of about 40 cps, which completely obscures the horizontal bodily motion of the ship; VM-17 shows a motion which, although it has possible shear and rolling components superimposed, is believed to be much closer to the actual horizontal motion of the ship itself. It is therefore estimated that the peak horizontal velocity of the EC-2 generated by the direct shock wave was about 6 ft/sec, or 70 percent of the peak vertical bodily velocity. The horizontal bodily motion of the EC-2, however, obviously has a character different from that of the vertical motion. For the first 30 msec, or so, following shock wave arrival, the ship acquired a horizontal velocity away from the burst with a maximum magnitude of 6 ft/sec. Subsequently, the ship acquired a velocity toward the burst, which was about equal in magnitude to that previously measured away from the charge. At the end of the movement away from the burst, the ship had attained a horizontal displacement of 1 inch, about 20 percent of the peak vertical bodily displacement.

4.5 HULL DAMAGE

The only appreciable hull damage on the EC-2 occurred on the starboard (attacked) side. Starboard frame deformation was measured about 9 feet below the water surface (Figure 3.18). The character of the attacked side-frame deflection history may essentially be summarized thusly: an initial peak deflection of 2.4 inches was achieved in about 15 msec following the shock wave arrival, and an outboard movement then ensued, which reduced the deflection level to about 1.2 inches. The level deflection shown by the deflection gages after the response to the shock wave agrees very well with the set deflection measured from these gages after the test. This implies that the EC-2 hull damage was caused essentially by the shock wave alone. The maximum set deflection of the attacked side frame was approximately 1.2 inches.

The above description of the deflection history is strikingly similar in general character to that applying to previously tested small-scale C-2 models (Reference 6). Quantitatively, the peak deflections d_m measured in the attacked side of the EC-2 may be compared with the energy density rule suggested by the C-2 model tests. The constant used in the rule depends upon the vertical span length of the frames between bottom and top restraints in the manner described in Reference 6. Taking account of the greater span in the EC-2 (25 feet) side frames than in the C-2 (17.5 feet), the rule becomes:

$$d_m \text{ (inches)} = 0.32E \text{ (ft-lb/in}^2\text{)}$$

where E is the incident shock-wave energy flux density at a water depth midway to the inner-bottom level, the depth at which the MD gages were located. This choice of depth roughly averages the energy density delivered to the entire span.

The evaluation of the measured free-water pressure histories carried out in Section 4.1 allows the estimate of the incident shock-wave energy flux density at a depth of 9 feet, shown in Figure 4.27 as a function of range; similar estimates are made for 13-foot depth and for the reflected wave for future convenience. Use of Figure 4.27 indicates that the energy density at the EC-2 position at a depth of 9 feet is 9.1 ft-lb/in^2. The application of the rule therefore yields a predicted peak deflection of 2.9 inches. Considering that a much more appreciable fraction of the total deformation energy is probably represented by plate dishing when the frame deformation is small than when it is large (as it was, relatively, in the model tests), this is an excellent agreement with the measured peak deflection (2.4 inches).

Since operational significance can only be attached to set deflections, it is useful to have a relationship between peak deflection and set deflection in order to apply the energy-density rule in practice. The previous small-scale model investigation (Reference 6) had indicated a very simple relationship between these quantities. Of particular importance was the observation that the value of set deflection depended only upon the peak deflection and in no way depended upon the precise manner in which this peak deflection came about. The empirical formula relating these two quantities was translated to full scale and is represented in Figure 4.28 as a dashed straight line; the behavior for small values of deformation must be considered unreliable because of experimental inaccuracies on the model scale. The experimental behavior found for the EC-2 is represented in Figure 4.28 as a point of the solid curve and is considered to be the best present estimate of the relationship between peak and set deflection for the side frames of merchant ships. This estimate, of course, ignores what are thought to be small differences between such slightly different ship types as EC-2 and C-2.

The survey (Figures 3.20 and 3.21) of the final EC-2 hull damage produced the following highlights. The maximum side frame deformation occurred at about the MD gage locations;

the frame deformation decreased above and below this location until it roughly vanished at the inner-bottom and second deck levels. Structural attachments to the attacked side reduced the deformation; this was noticeable at the bulkheads, at the forward water tanks (engine room) and even at the flat in the after portion of the engine room. The shell plating dished between the side frames; the amount of this dishing appeared to increase with depth below the water surface until the inner-bottom level was reached (Figure 3.23). Just above the inner bottom, the maximum dishing at the hull plating amounted to about 1 inch between frames.

4.6 ESTIMATION OF DD-474 AND DD-592 RESPONSE

Although the DD-474 and DD-592 response histories were not obtained in Shot Wahoo either by Project 3.4 or by any other project, certain gross motions that these ships must have undergone can be estimated. The effort in this regard was concentrated on the vertical heaving response of the center of gravity of the ships; this response is associated with the bulk cavitation resulting from the attack. In each case, only the predominant response associated either with the direct or reflected shock waves was considered. Idealized vertical bodily (heaving) velocity histories were constructed: first, by estimating the initial bodily velocity; second, by estimating the deceleration; and, third, by estimating the cavitation reloading time.

To some extent these estimates could be checked by computing the shock spectra corresponding to the estimated velocity histories, in the manner described in Section 2.3, and comparing these computational results with Project 3.3 measurements of the maximum response of reeds in the shock spectrum recorders installed on the ships (Reference 21). Although the electric motor drive installed to separate the reed responses produced by successive shock pulses, failed to operate, Project 3.3 nevertheless obtained maximum reed displacement measurements.

The DD-474 was subjected to the direct shock wave and to a bottom-reflected shock wave arriving 793 msec later. Of these it is sure (Figure 4.21) that the direct shock wave produced the stronger response. The initial vertical bodily velocity of the DD-474 following the direct shock wave is estimated to have been 5.2 ft/sec. It seems reasonable to believe that the surface layer concept is valid at the location of the DD-474 for the direct shock wave; therefore, it is estimated that the vertical bodily deceleration was 3.9 g and that the reloading time was 78 msec (Section 4.4).

Some rough confirmation of these estimates could be gained by comparing the corresponding computed shock spectrum with those spectra measured by Project 3.3 shock spectrum with those spectra measured by Project 3. 3 shock spectrum recorders with reeds having natural frequencies from 20 to 450 cps. The records in Reference 21 were examined and those that most likely reflect the vertical bodily response of the ship are plotted in Figure 4.29. A typical record was obtained at Frame $92\frac{1}{2}$ by a shock spectrum recorder mounted to the foundation of the flex plate (Project 3.3, Position 19). A comparison of the computed shock spectrum corresponding to the idealized velocity history estimated above with the typical shock spectrum measured by Project 3.3 is given in Figure 4.30. In considering these results it should be kept in mind that calculations and measurements, although each referring to the same natural frequencies, pertain only to a discrete set of natural frequencies. Straight lines connect the points for reading convenience and have no other significance. The comparison is considered to be fair and provides some qualitative reassurance as to the estimated bodily motion. However, it must be stated that the measured spectrum may reflect a superposition of responses to both direct and reflected shock waves, because reed response was only lightly damped. This superposition is more significant for the lower than for the higher frequency reeds. Moreover, the computed shock spectrum is not

particularly sensitive to the value of deceleration used but is, on the other hand, sensitive, at higher frequencies, to details of velocity changes that were idealized as jumps. Thus, only an order of magnitude check is involved.

The DD-592 was subjected successively to the direct shock wave and to a bottom-reflected shock wave arriving 677 msec later. In this case it was clear that the response to the bottom-reflected shock wave was predominant. A peak vertical bodily velocity of 2.2 ft/sec could be estimated from Figure 4.21. It is, however, by no means clear that the surface layer concept is in any way applicable to the DD-592 following the reflected wave arrival. Nevertheless, a crude estimate of 1.3 g was derived from the available experimental data for vertical bodily deceleration. The cavitation reloading time, similarly uncertain, was crudely estimated to be 105 msec.

The Project 3.3 shock spectra considered most apt to reflect the vertical bodily motion of the ship was examined, and the data is reproduced in Figure 4.31. A typical shock spectrum was obtained from a shock spectrum recorder located at Frame 106½ and mounted to the foundation of the reduction gear (Project 3.3 Position No. 21). A comparison of the shock spectrum, computed from the idealized estimated vertical bodily velocity history, with the typical Project 3.3 measurement is shown in Figure 4.32. The degree of comparison gives some grounds for reassurance concerning the correctness of the estimate, but again the comparison is not straightforward. The measured shock spectrum reflects a superposition of responses to both direct and reflected shock waves; the computed shock spectrum is rather insensitive to values of deceleration. On the whole, it must be said that the estimates for DD-592 are less reliable than those for DD-474.

4.7 LETHAL HULL DAMAGE RANGES

The close correlation of the EC-2 hull damage sustained in Shot Wahoo with small-scale model EC-2 tests previously conducted by UERD (Reference 6) allows the lethal hull damage range for merchant ships (EC-2), under Shot Wahoo conditions, to be estimated with some confidence. Corresponding information for destroyer targets is not available. However, plausibility arguments, based on the concept that hull damage is controlled by energy flux density, allow interim conclusions concerning lethal hull damage ranges for DD's.

For merchant ships, it appears that side-frame deformation is a controlling feature in estimating overall hull damage from an operational point of view. Lethal hull damage can be said to occur only when the hull is ruptured to an extent sufficient to lead to uncontrollable flooding of the ship. General experience in the field, however, indicates that hull rupture is not a suitable criterion for use in general predictions, since it depends upon many detailed features that are unknown to the experimenter. For this reason, a set deformation of the side frame at a level midway between the water surface and the inner bottom is chosen as a measure of the operational significance of merchant ship hull damage. The criterion selected is that a side frame deformation of at least 18 inches is lethal. This corresponds to a peak deflection (Figure 4.28) of 23 inches and a corresponding critical value of the energy flux density of about 75 ft-lb/in^2 at a depth of 9 feet below the water surface. Reference to Figure 4.27 indicates that a horizontal range of 1,100 feet, or less, lethal hull damage will be caused to merchant ships under Shot Wahoo conditions. It is stressed that this estimate of the lethal hull damage range does not depend critically upon the precise value of the criterion used to translate a set frame deformation into terms of operational significance. For example, if a 12-inch set deflection criterion had been utilized, a similar line of reasoning would have led to an estimated lethal hull range of 1,300 feet or less under Shot Wahoo conditions.

Basic experimental data on lethal hull damage ranges for destroyers is lacking, at least for deep underwater nuclear bursts of the Shot Wahoo type. However, it is believed that the

energy flux density concept is also applicable to destroyers and indeed there is some qualitative evidence of this as a result of an evaluation carried out for Shot Baker of Operation Crossroads in Reference 22. Numerical values derived in this British evaluation are not used here because of reservations as to the validity of the free-water-pressure estimates applied to the Shot Baker damage results.

Plausibility arguments can be used to derive a lethal hull range for DD's. Bottom deformation adjacent to the keel is considered to be the most significant feature of hull damage for DD's. Damage to the DD bottom may be roughly compared to damage to the EC-2 side; previous studies (Reference 23) suggested that, for long shock wave attacks, damage was essentially independent of the angle of incidence of the attack except insofar as this influenced the energy density itself. The concept of damage mechanism developed in Reference 6 suggested that the degree of damage was directly proportional to span length and inversely proportional to the yield stress. In comparing the DD bottom with the EC-2 side it is clear that the effective DD span length (a somewhat indefinite quantity for the DD) is less than for the EC-2 side and that, moreover, the high-tensile steel used for the DD bottom has a higher yield stress than the medium steel employed for the merchant ship's sides. These considerations suggest that a given energy flux density will produce less deformation in the DD bottom than in the EC-2 side. On the other hand, it seems reasonable to suppose that the critical value of hull deformation, for lethal hull damage, is less for the DD bottom than for the EC-2 side. In the absence of guides for weighing these opposing effects it was decided to assume the lethal hull range for DD's was the same as for the EC-2. This somewhat arbitrary decision led, incidently, to a choice of critical energy flux density for DD's of about 150 ft-lb/in^2 at a depth of 13 feet below the water surface (DD keel depth).

Lethal hull damage ranges (to midships) are considered to be roughly independent of the ship orientation to the attack. Any tendency in an end-on attack for midship damage to be less than that for a side-on attack at the same midship range is probably compensated for by relatively greater damage at the attacked end simply due to the fact that shock wave severity at the attacked end will be greater than at midships in accordance with the corresponding difference in ranges.

The estimates of lethal hull damage ranges given above are controlled entirely by the direct shock wave. Under Wahoo conditions, the reflected wave has no influence whatsoever (Figure 4.27). Surface waves generated by the burst are not expected to have any appreciable influence; the surface wave height (crest to trough) at 1,100 feet is judged to be about 60 feet on the basis of the 28-foot measurement secured (Reference 14) at the EC-2 position.

4.8 SAFE HULL DAMAGE RANGES

Safe hull damage ranges under Wahoo conditions can be estimated for merchant ships (EC-2) and destroyers in a very crude way. For this purpose, maximum safe damage is defined arbitrarily to be that amount that was sustained by the EC-2 as a result of the test. Some justification for considering that this degree of damage is safe is gained by noting (Figure 3.21) that tugs employed to handle the EC-2, before and after the test, produced damage, clearly unconnected with test damage, of a level comparable to that produced by the nuclear burst itself. By definition then, safe hull damage ranges for merchant ships under Shot Wahoo conditions are, in round numbers, 2,400 feet or greater.

To estimate safe hull delivery ranges for DD's, the same plausibility arguments followed in Section 4.7 for estimating lethal hull damage ranges are applied. Under Wahoo conditions then, the minimum safe delivery range for destroyers, from the standpoint of hull damage alone, is 2,400 feet, which leads to a choice of critical energy flux density for DD's of about 15 ft-lb/in^2 at a depth of 13 feet below the water surface (DD keel depth).

Under the definition used above, the minimum safe delivery range for DD's is controlled by the shock wave alone; the bottom-reflected wave has no influence (Figure 4.27).

TABLE 4.1 ARRAY AT DETONATION TIME, SHOT WAHOO

Ship	Horizontal Distance from Surface Zero to Center of Ships *	Orientation †
	feet	degrees
EC-2 (SS Michael Moran)	2,350	11
YC-1	3,400	–
YC-4	2,000	–
DD-474 (USS Fullam)	2,900	2
DD-592 (USS Howorth)	4,850	−9
DD-593 (USS Killen)	9,100	−6
DD-728 (USS Mansfield)	15,150	–
SSK-3 (USS Bonita)	18,450	–
DD-886 (USS Orleck)	30,900	–

* Taken to nearest 50 feet.

† Angle of ship heading (positive clockwise) from nominal orientation shown in Figure 4.1.

TABLE 4.2 MEASURED BULK-CAVITATION RELOADING TIMES FOLLOWING THE REFLECTED SHOCK WAVE, SHOT WAHOO

Values are relative to specularly reflected wave arrival times.

Array	Horizontal Range from Surface Zero	Experimental Relative Bulk-Cavitation Reloading-Time	Remarks
	feet	msec	
29	3,400	141 *	p_m = 185 psi, α = 69°
155	15,150	45 - 48 *	p_m = 76 psi, α = 13°
248	9,100	81 †	pm = 95 psi, α = 25°

* Project 1.1. † Project 3.4.

TABLE 4.3 INITIAL VERTICAL VELOCITY JUMP, BOTTOM HULL, SHOT WAHOO

Gage Location	Experimental Velocity Jump (ft/sec)	
	Centerline Location	Off Centerline Location
EC-2, Direct Shock Wave		
Frame 98; Stbd (VM-9, 9A)		13.8, 13.4
CL(VM-7, 7A)	12.3, 11.7	
Port (VM-8)		11.8
Frame 92½; near CL(VM-14)	13.8	
Frame 88; Stbd (VM-3)		9.7
near CL(VM-1)	9.9	
Port (VM-2)		9.6
EC-2, Sea-Bottom-Reflected Wave		
Frame 98; Stbd (VM-9, 9A)		3.3, 3.3
CL(VM-7, 7A)	4.4, 4.6	
Port (VM-8)		3.3
Frame 92½; near CL (VM-14)	4.5	
Frame 88; Stbd (VM-3)		3.5
near CL(VM-1)	3.3	
Port (VM-2)		3.0
DD-593, Sea-Bottom-Reflected Wave		
Frame 148, CL(VM-16)	1.6	
Frame 120½, CL(VM-14)	1.5	
Frame 119, near CL(VM-15)	1.5	
Frame 82½, CL(VM-8)	1.4	
Frame 81, near CL(VM-9)	1.5	
Frame 72, CL(VM-2)	1.5	
Frame 18, CL(VM-1)	–	

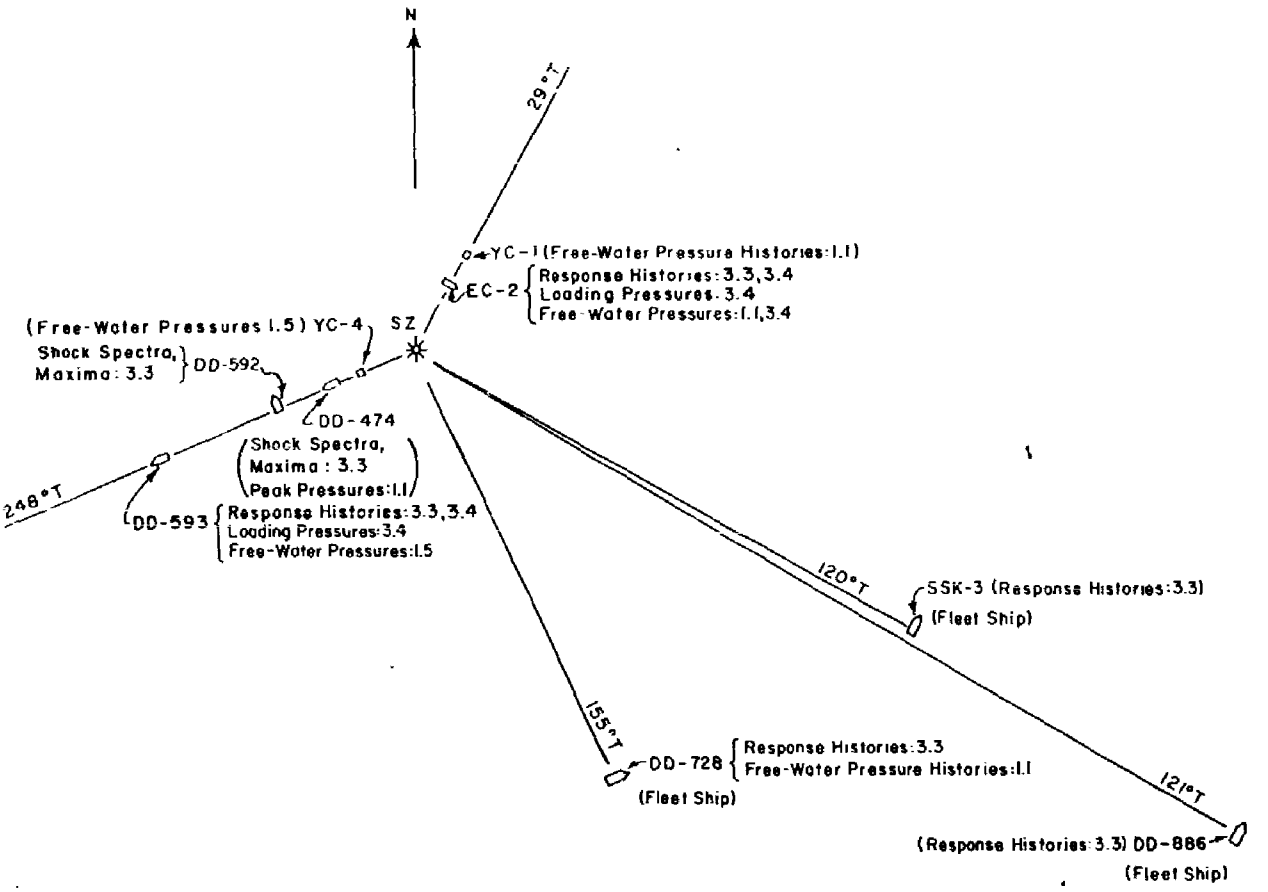

Figure 4.1 Test array and summary of underwater pressure and ship response measurements, Shot Wahoo.

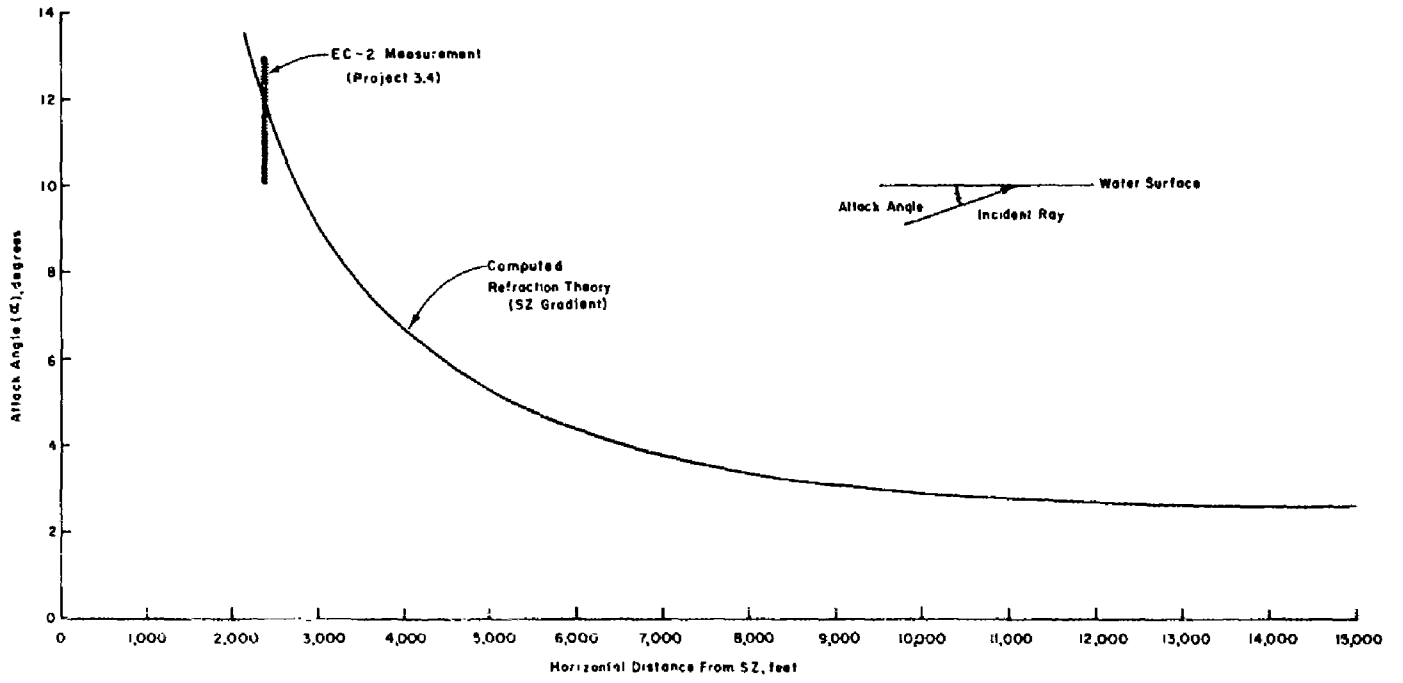

Figure 4.2 Direct shock wave attack angle at water surface versus range, Shot Wahoo.

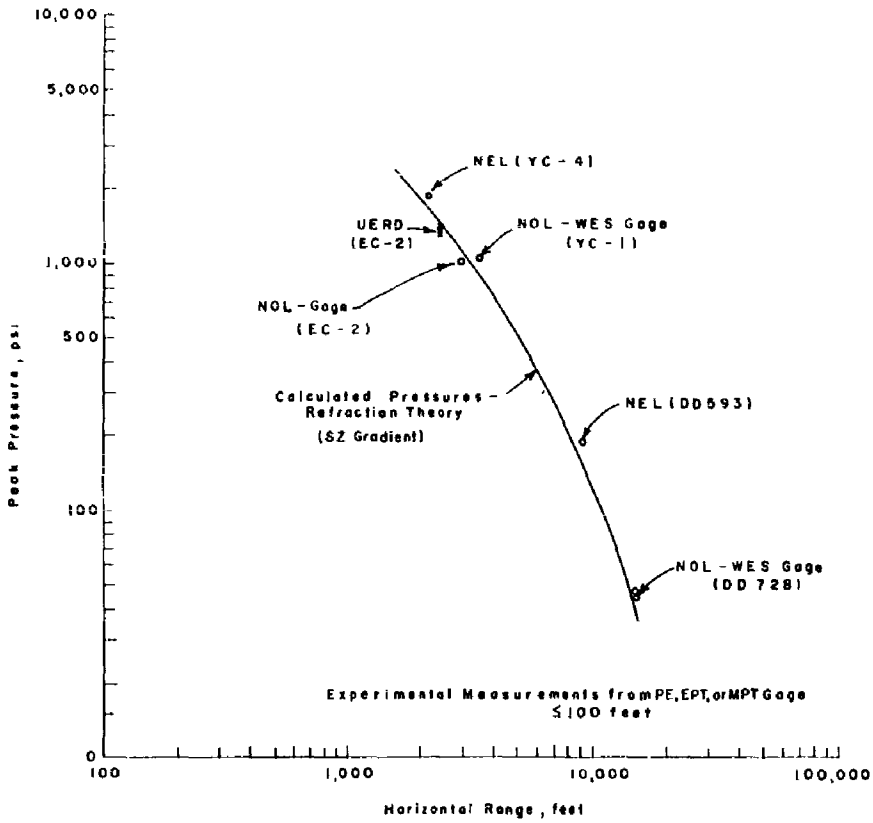

Figure 4.3 Direct wave peak pressure near water surface versus horizontal range, Shot Wahoo.

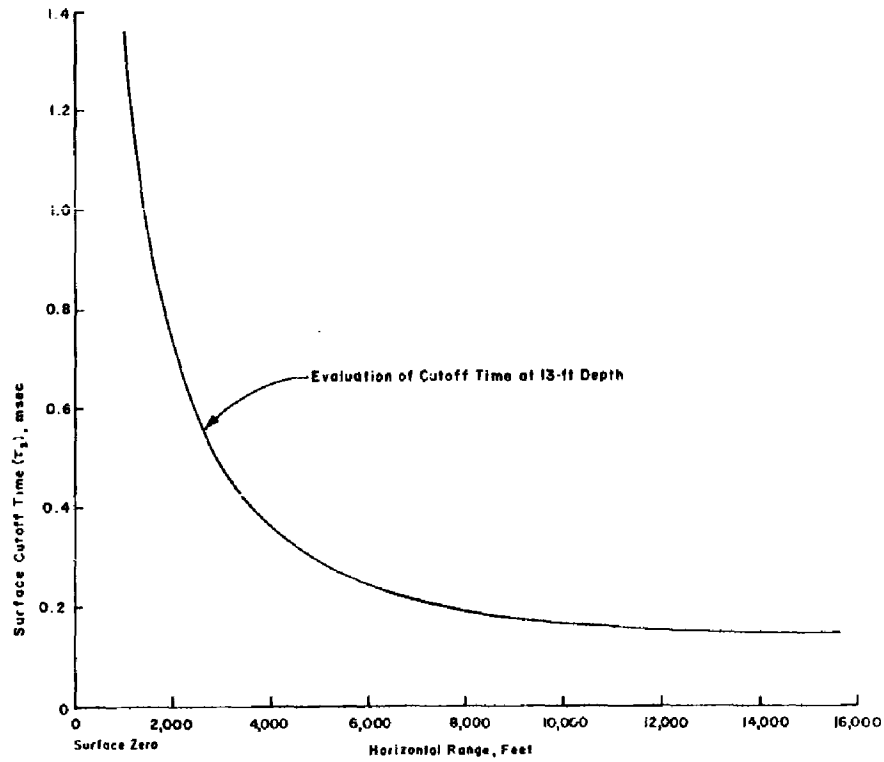

Figure 4.4 Variation of free-water surface cutoff time with horizontal range at 13-foot depth, direct wave, Shot Wahoo.

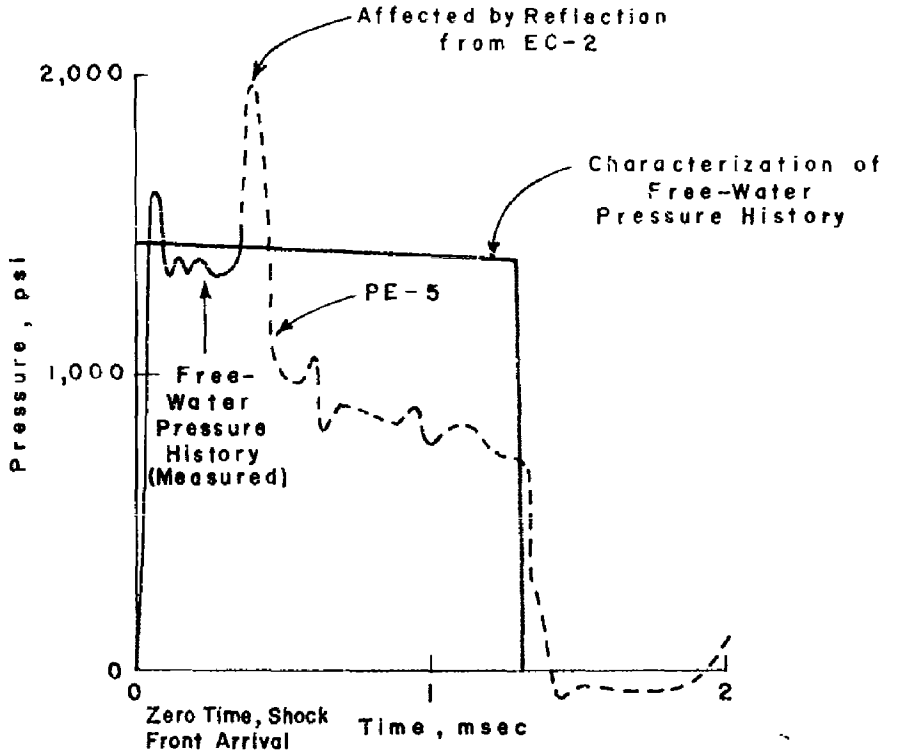

Figure 4.5 Comparison of experimental and estimated direct wave free-water pressure histories at EC-2, Shot Wahoo.

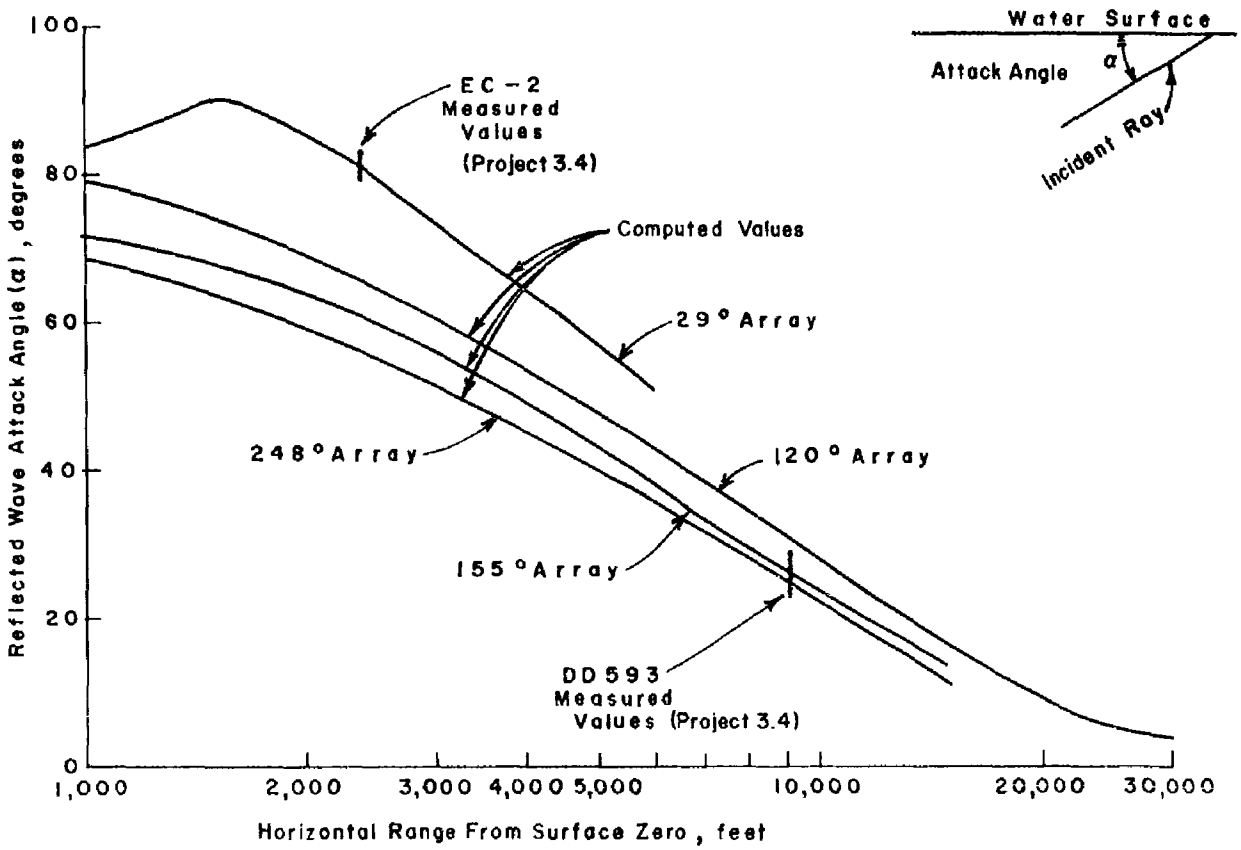

Figure 4.6 Variation of attack angle made between specularly reflected ray and water surface with horizontal range from surface zero, Shot Wahoo.

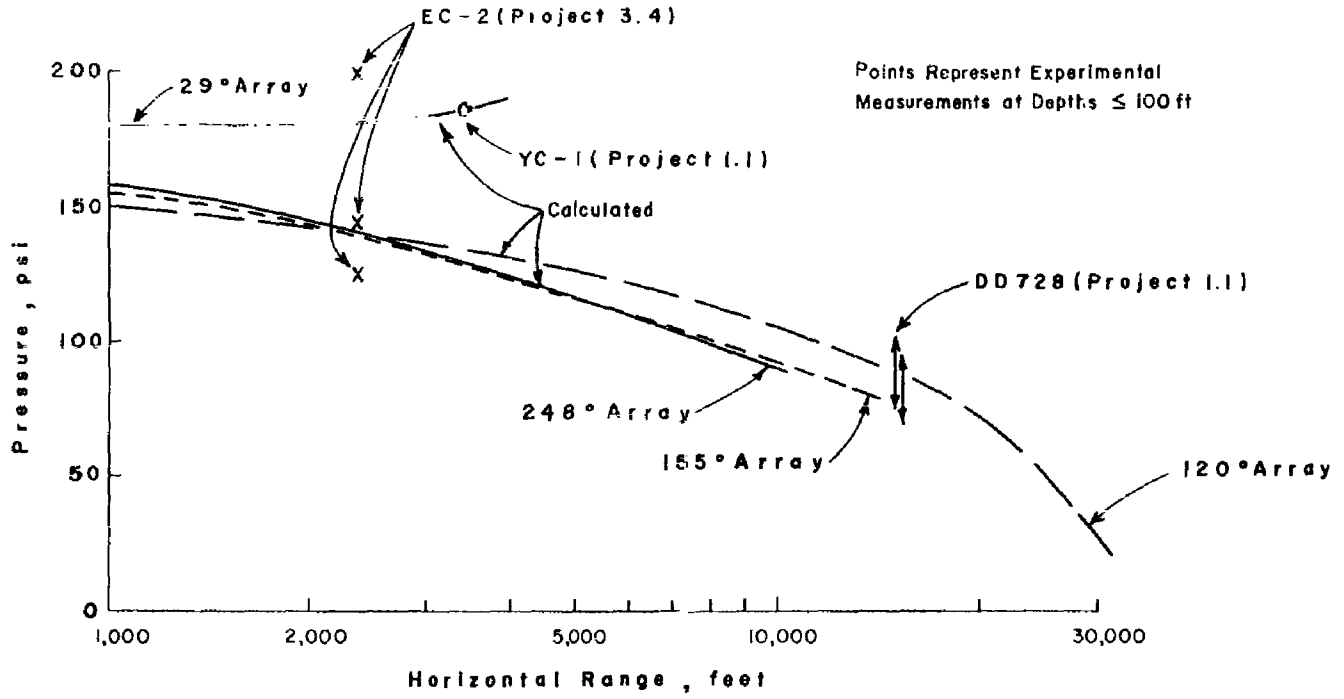

Figure 4.7 Peak pressure near water surface versus horizontal range, reflected wave, Shot Wahoo.

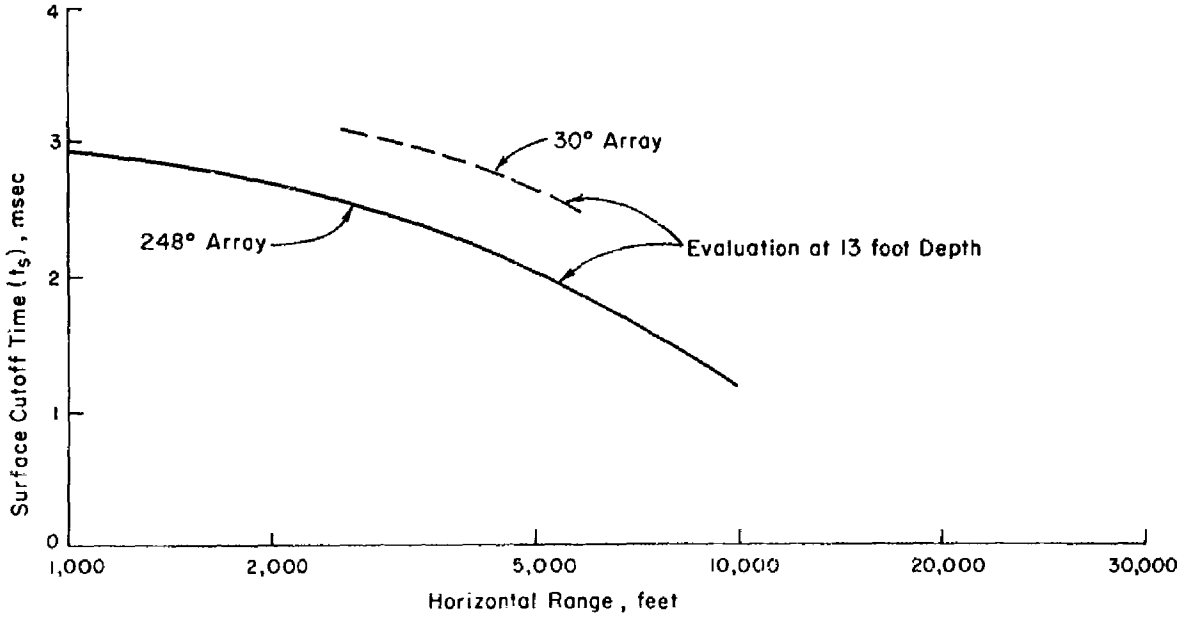

Figure 4.8 Computed surface cutoff time at 13-foot depth versus horizontal standoff, reflected wave, Shot Wahoo.

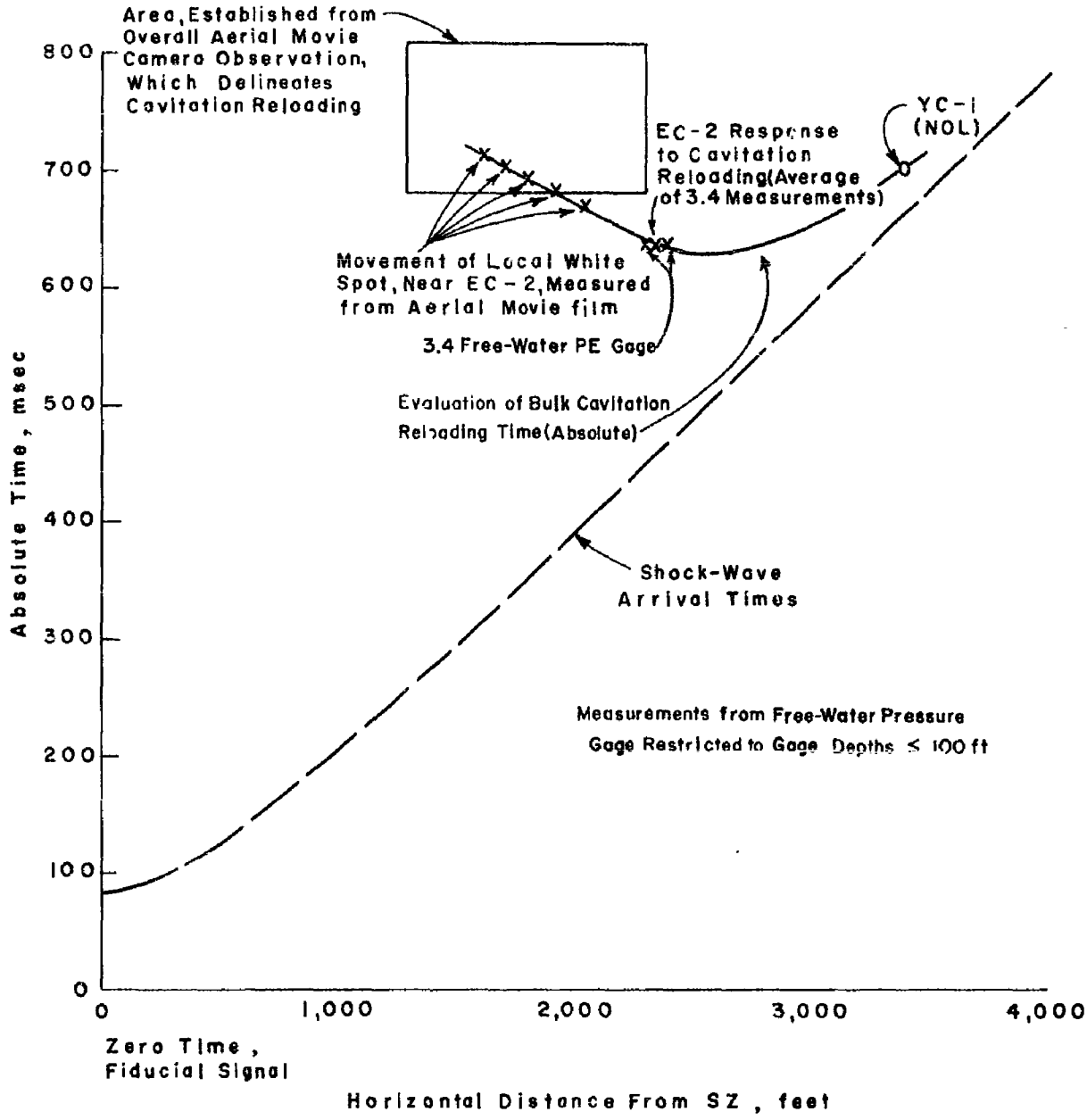

Figure 4.9 Observations on cavitation reloading absolute time, Shot Wahoo.

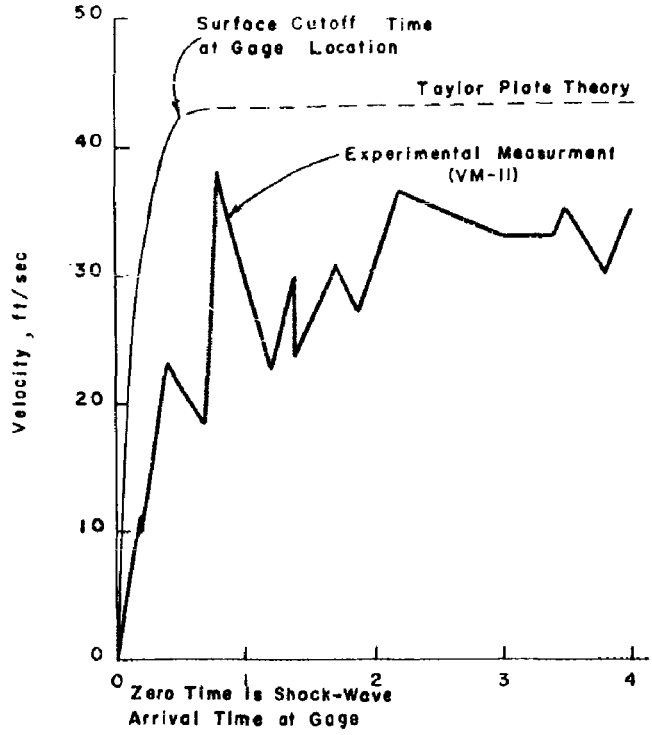

Figure 4.10 Interaction of direct shock wave and EC-2 attacked side, Shot Wahoo.

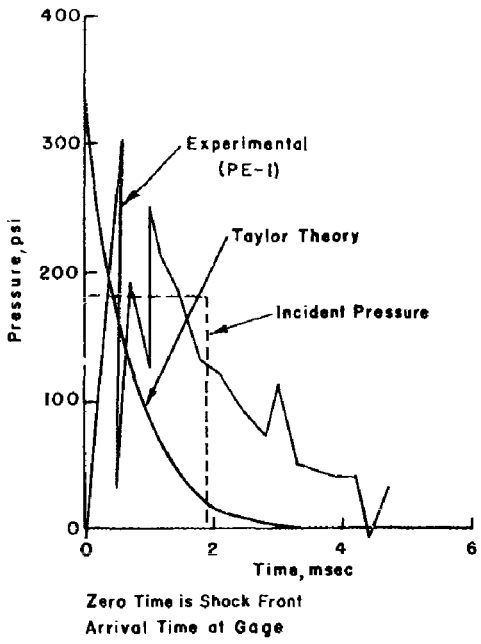

Figure 4.11 Interaction between reflected wave and EC-2 bottom, loading pressure, Shot Wahoo.

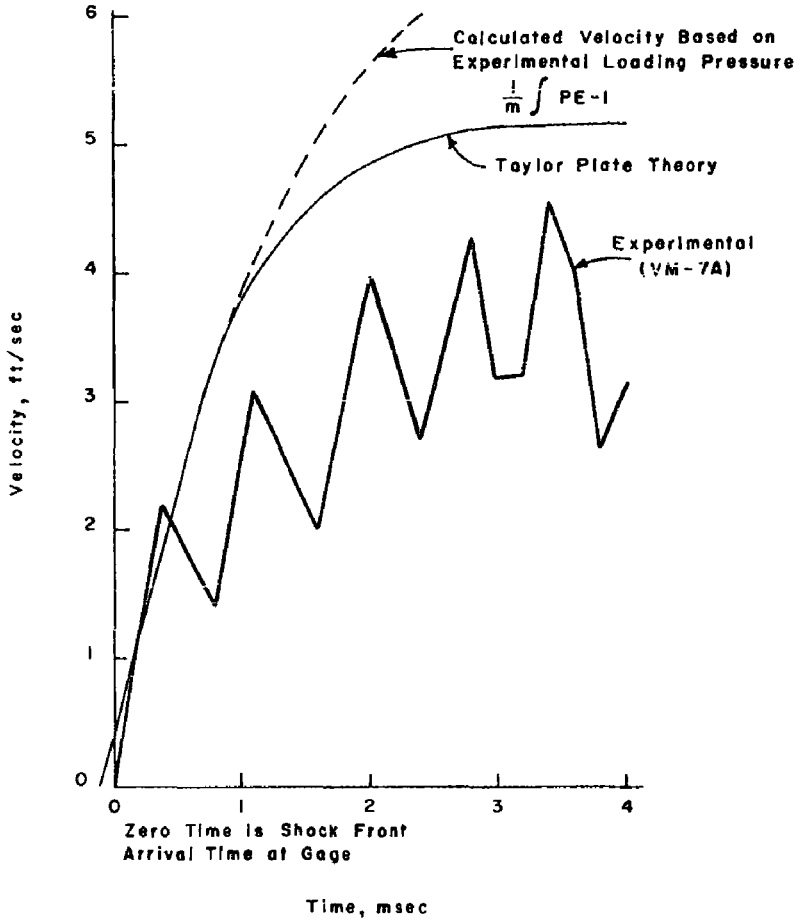

Figure 4.12 Interaction between reflected wave and EC-2 bottom, velocity response, Shot Wahoo.

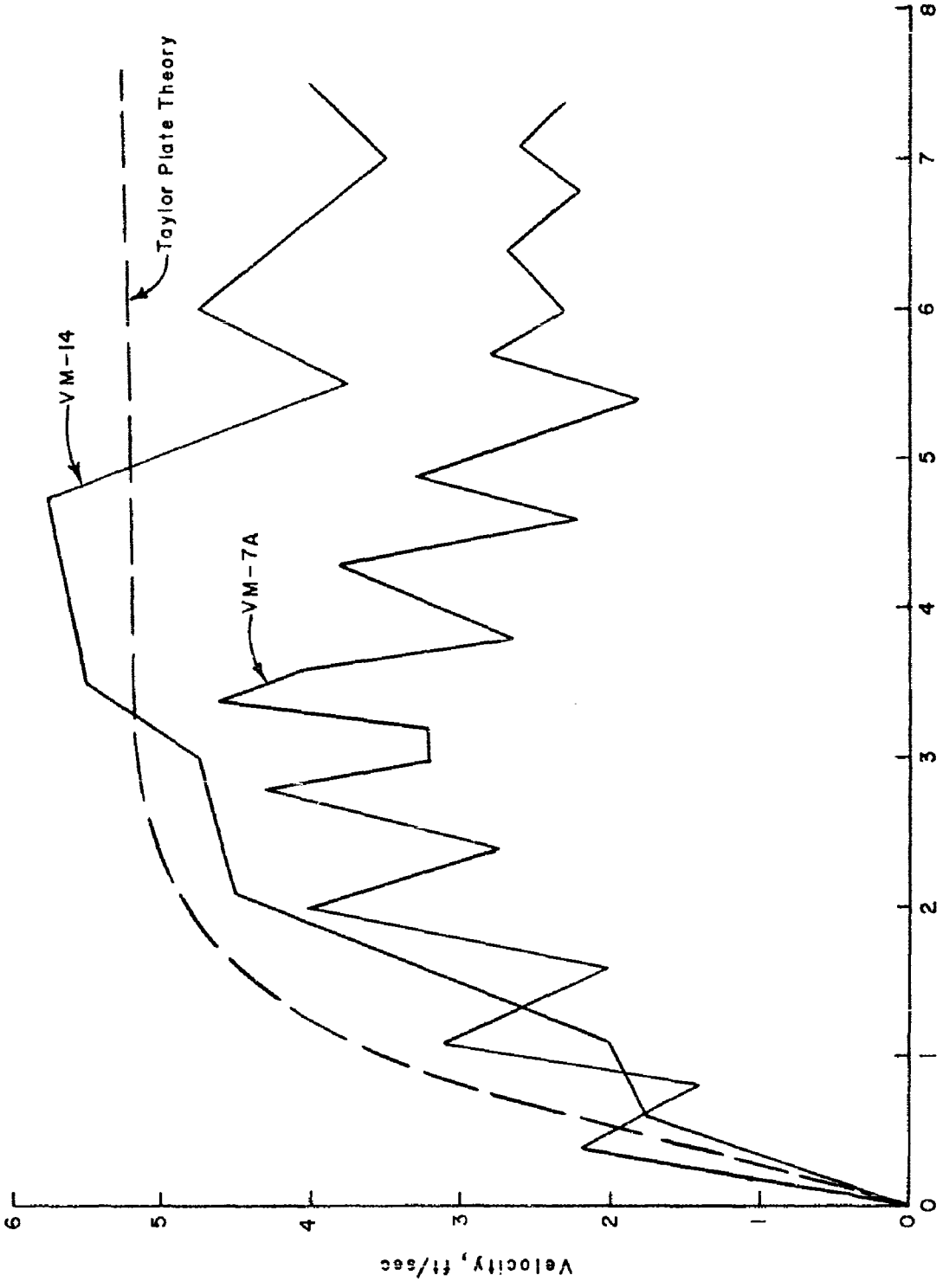

Figure 4.13 Vertical velocity response of EC-2 bottom to reflected wave, Shot Wahoo.

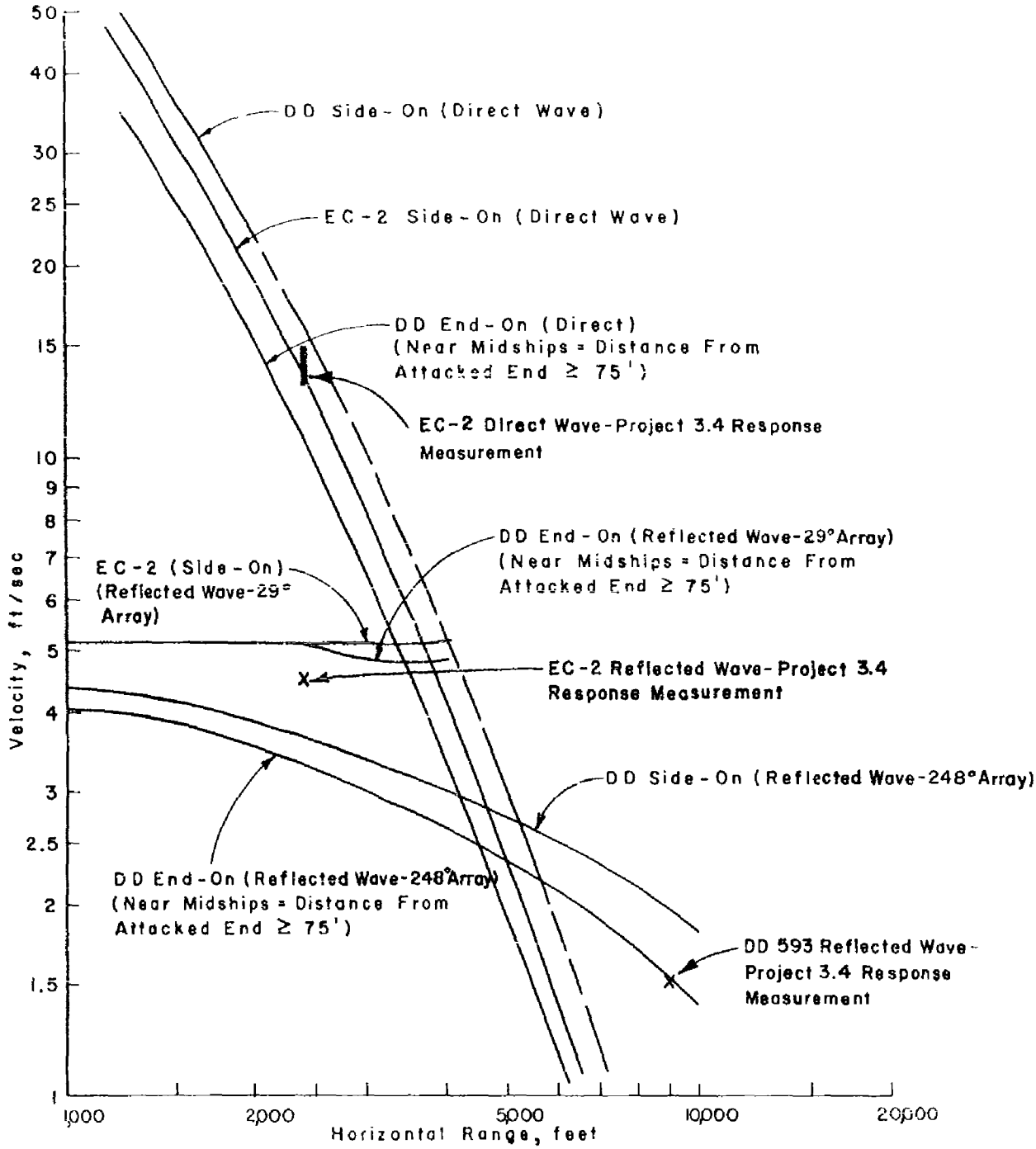

Figure 4.14 Vertical bottom velocity estimates for bare hull section, Shot Wahoo.

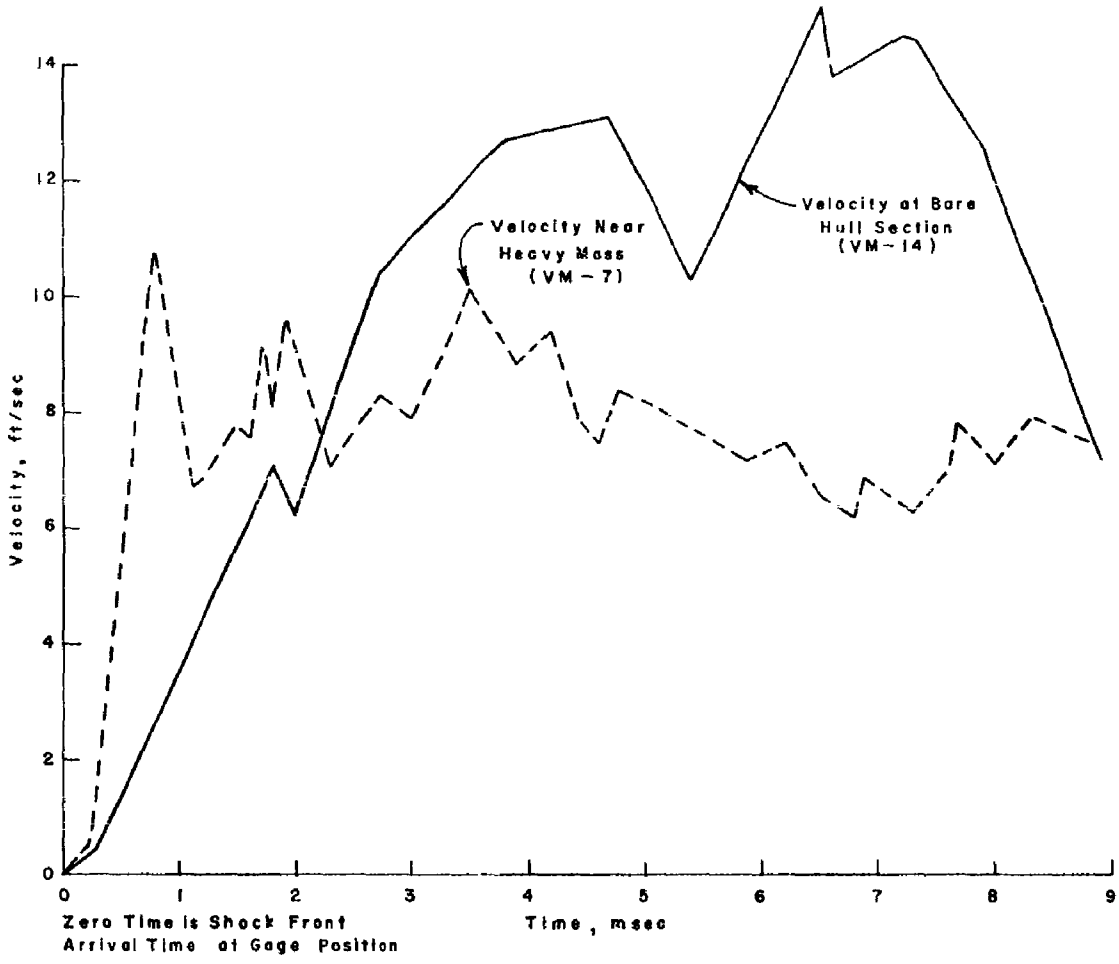

Figure 4.15 Initial vertical velocities measured at EC-2 bottom, direct shock wave, Shot Wahoo.

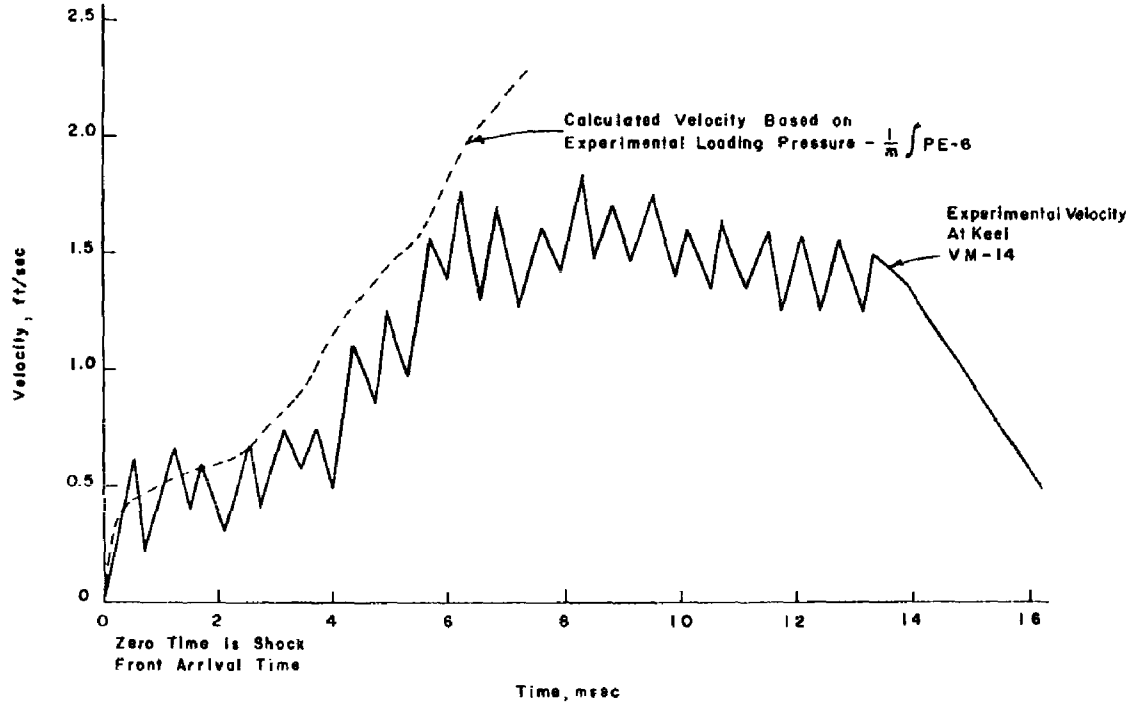

Figure 4.16 Vertical velocity response of DD-593 keel to reflected wave, Shot Wahoo.

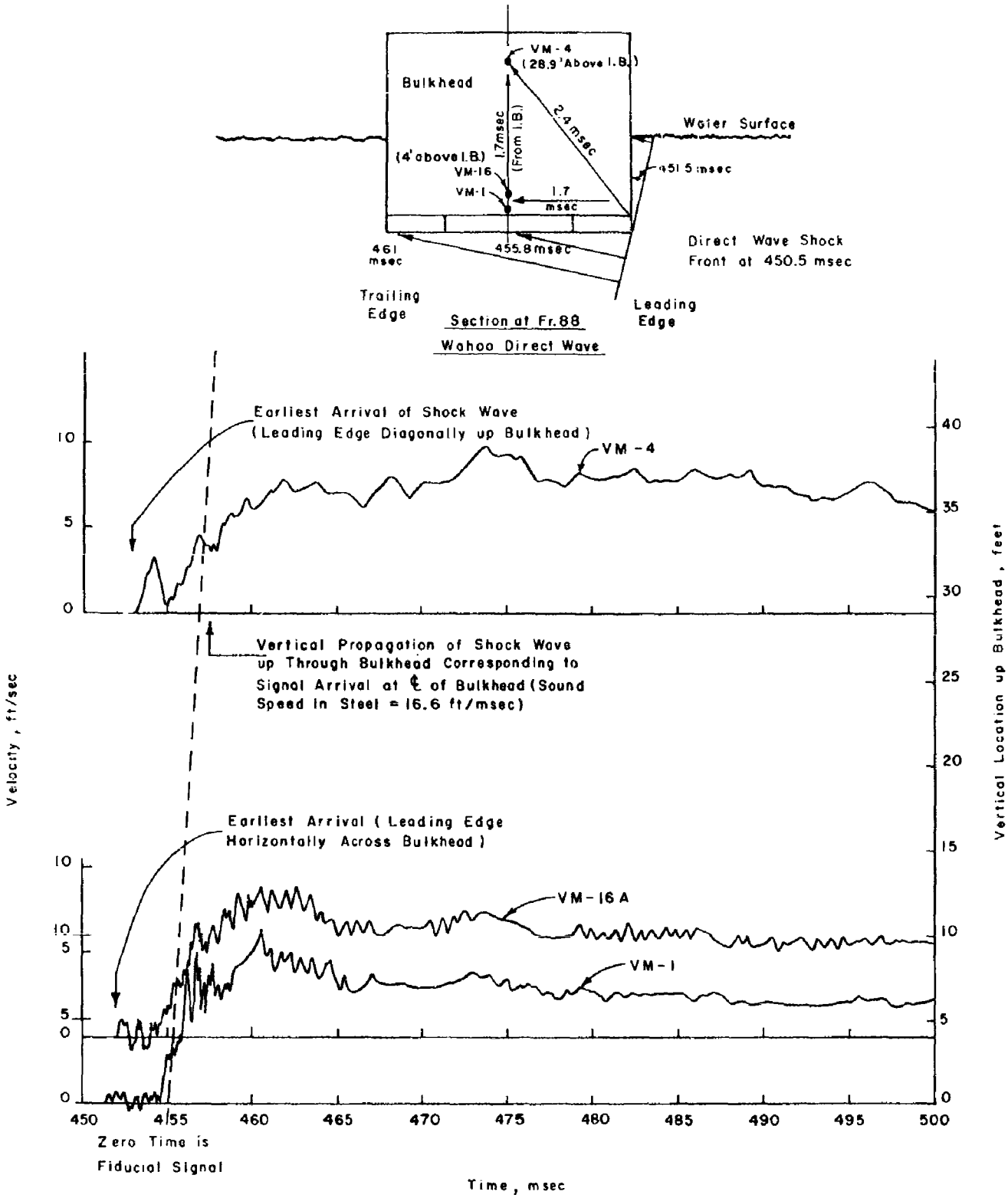

Figure 4.17 Response measurements up the EC-2 bulkhead at Frame 88, direct shock wave, Shot Wahoo.

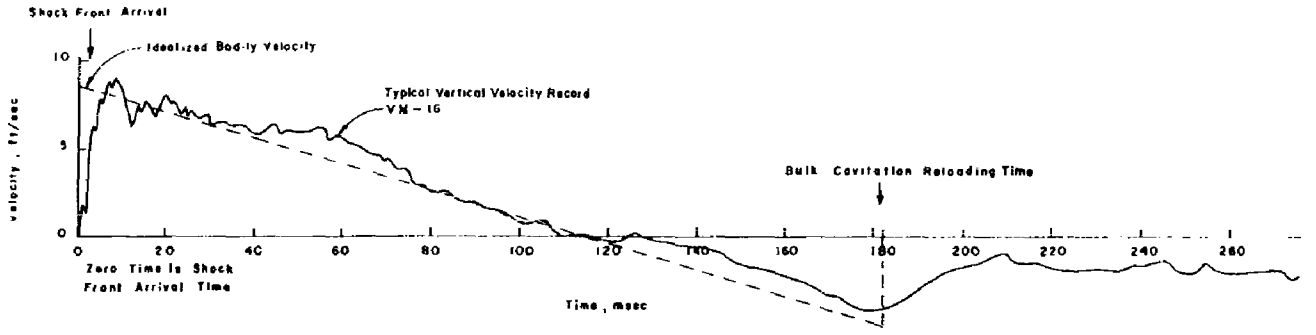

Figure 4.18 Vertical bodily velocity of EC-2 following direct shock wave arrival, Shot Wahoo.

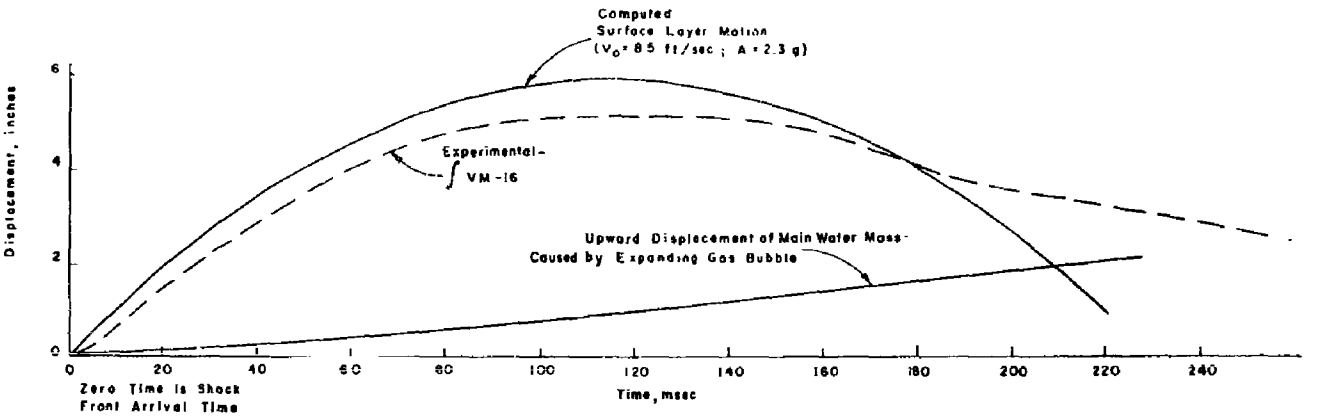

Figure 4.19 Vertical bodily displacement history of EC-2, Shot Wahoo.

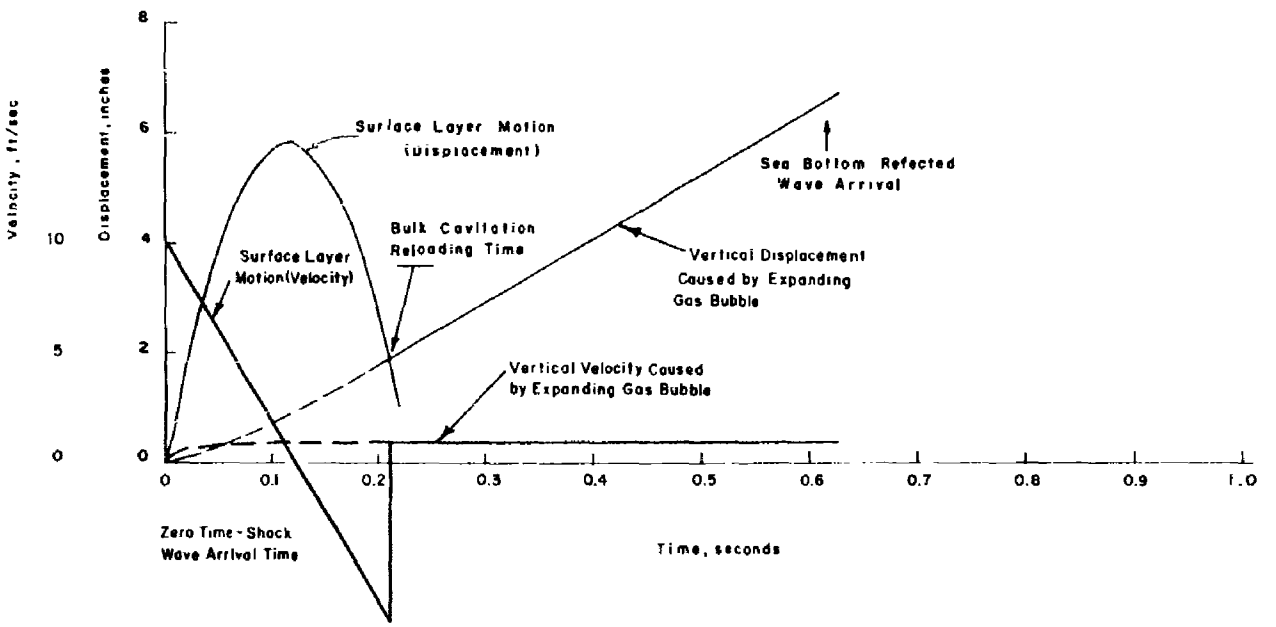

Figure 4.20 Vertical motion of EC-2, overall estimates.

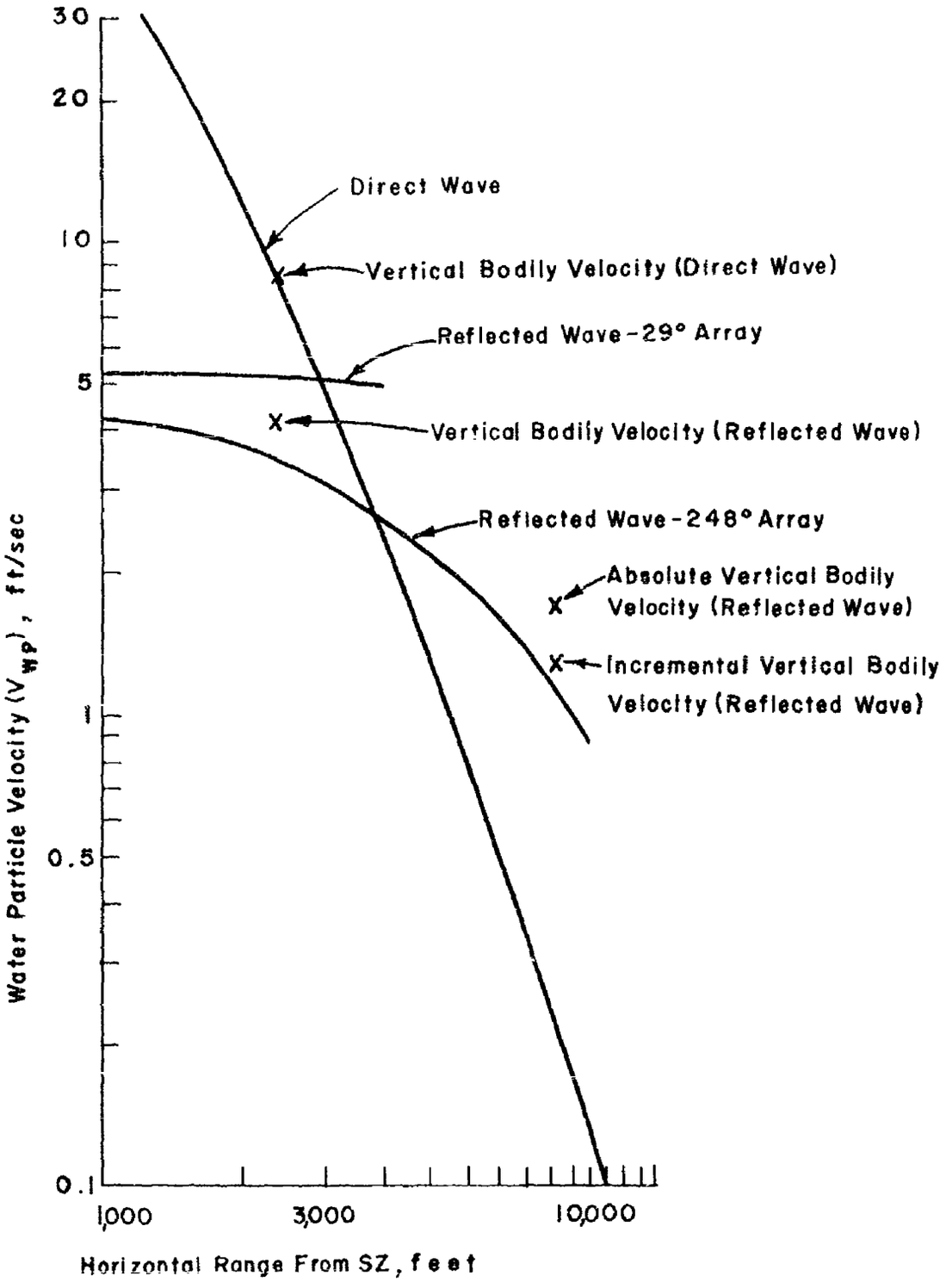

Figure 4.21 Water particle velocity versus range, Shot Wahoo.

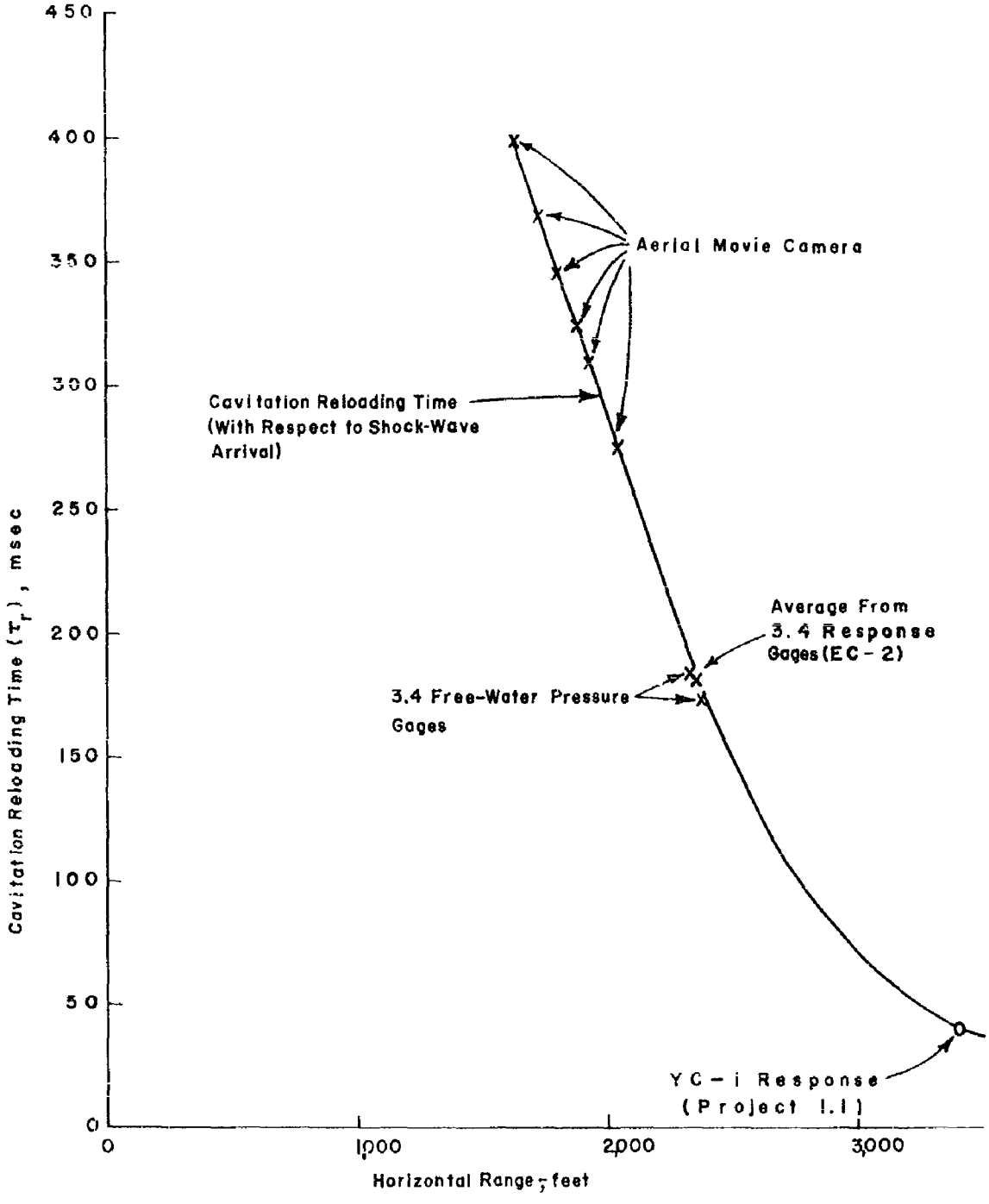

Figure 4.22 Bulk cavitation reloading time with respect to shock wave arrival time.

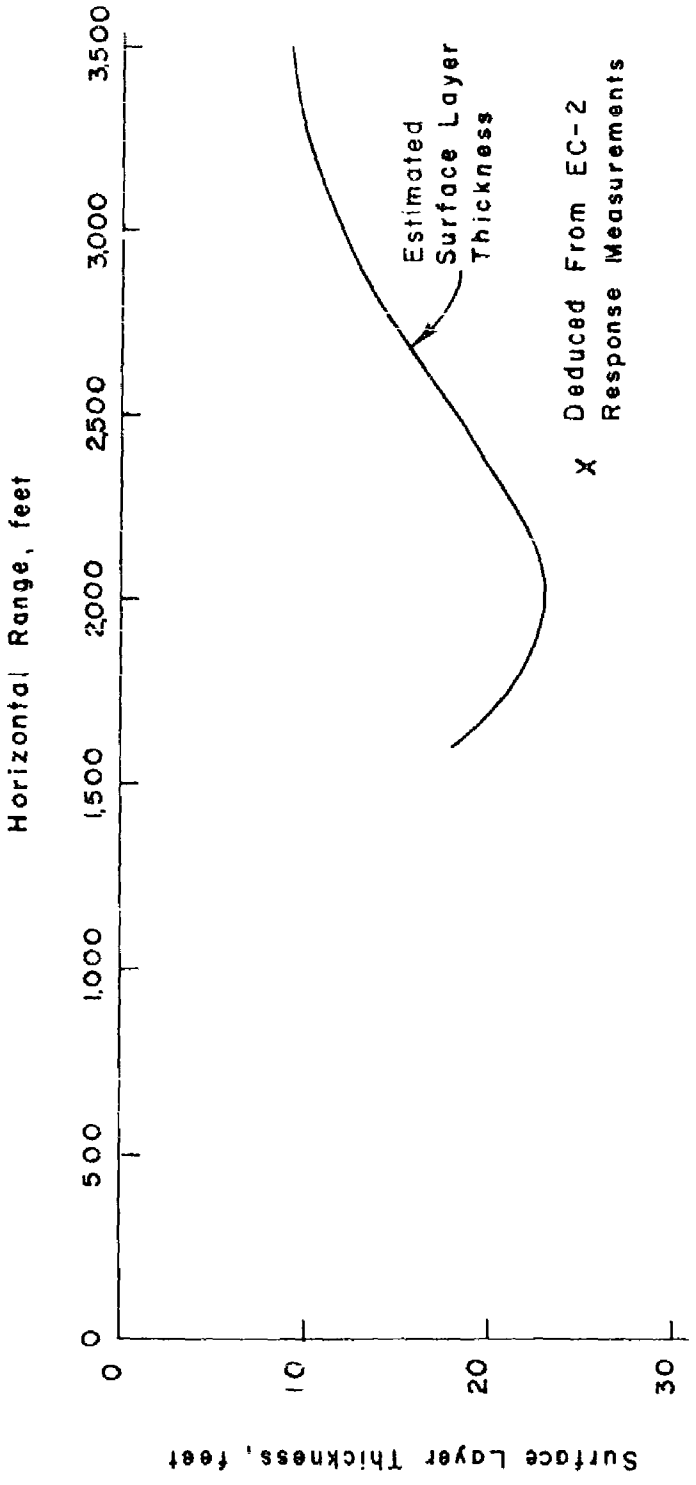

Figure 4.23 Surface layer thickness versus horizontal range, direct shock wave, Shot Wahoo.

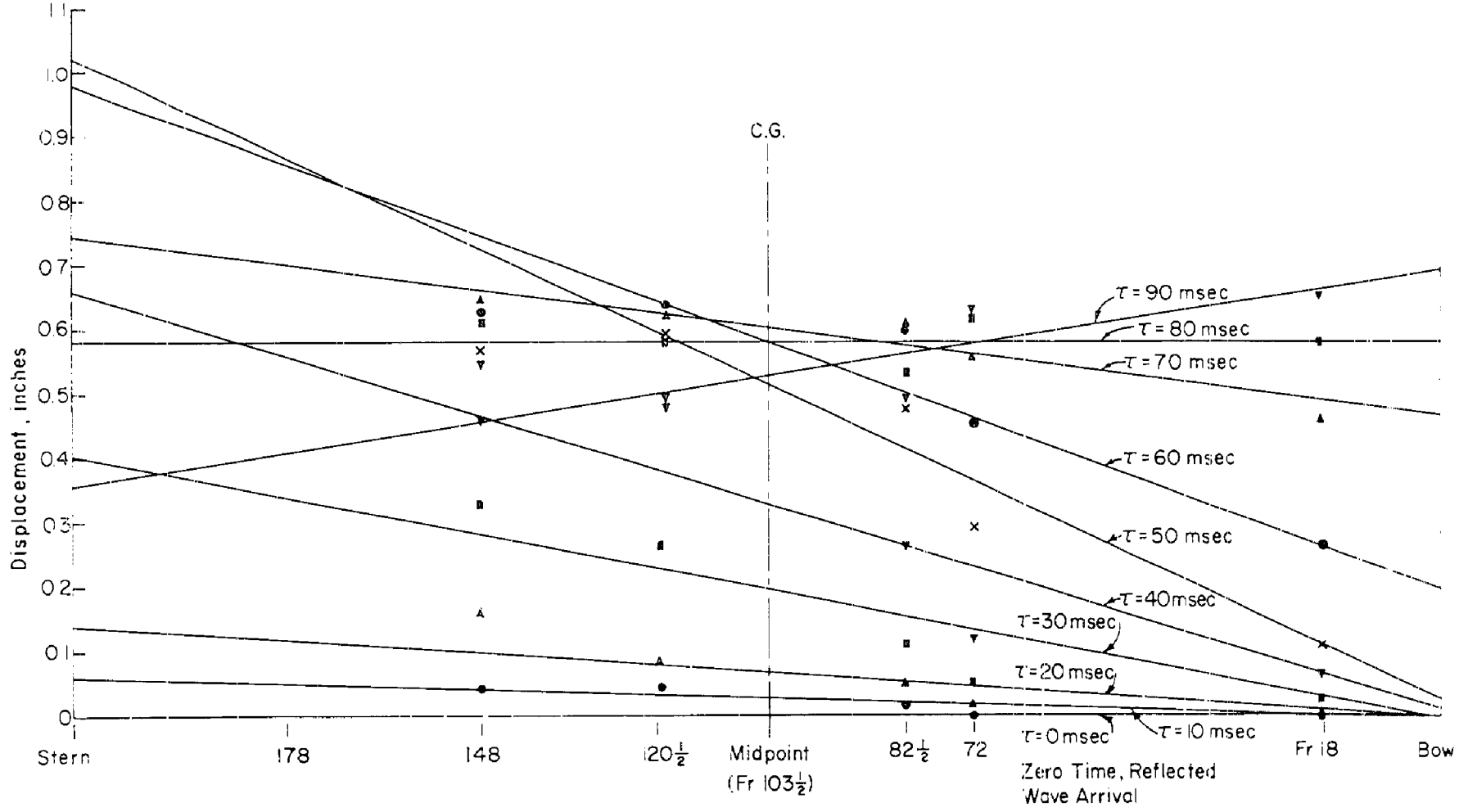

Figure 4.24 Vertical displacement contours for DD-593, sea-bottom-reflected wave, Shot Wahoo.

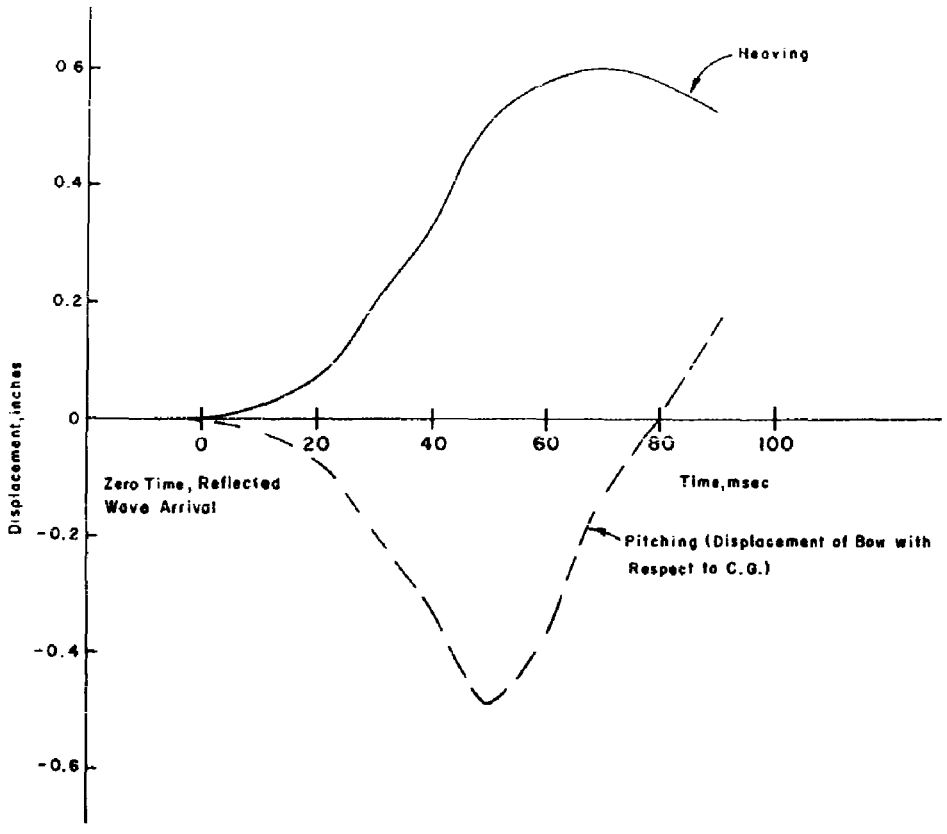

Figure 4.25 Pitching and heaving history of DD-593, sea-bottom-reflected wave, Shot Wahoo.

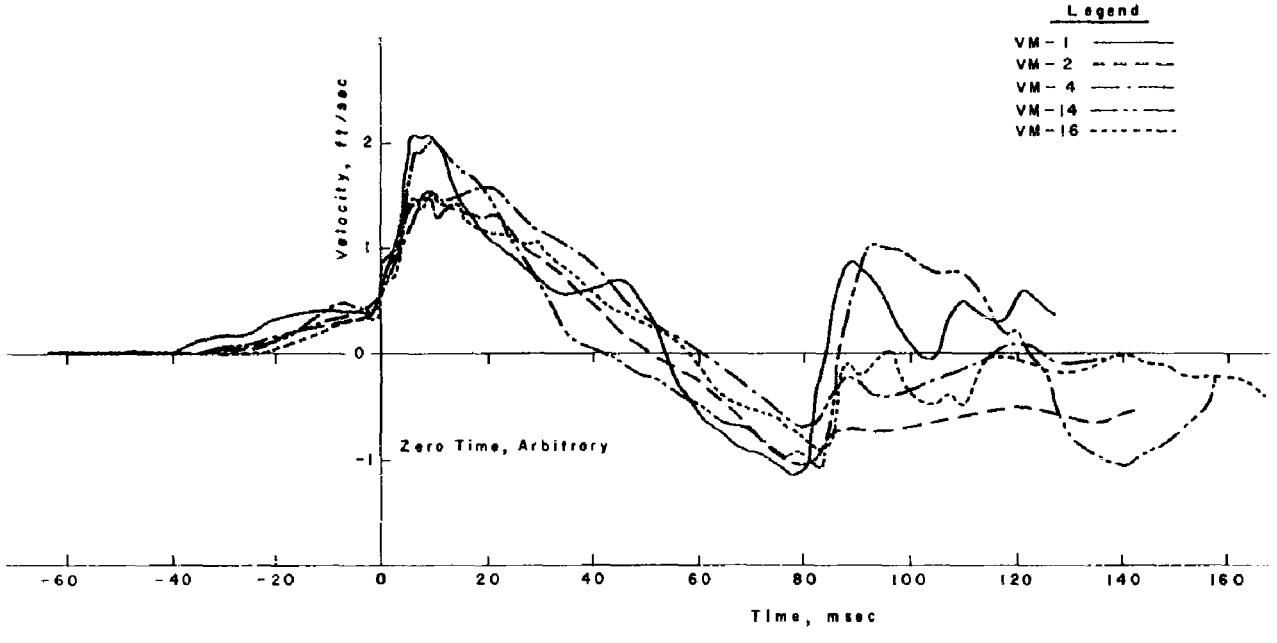

Figure 4.26 Vertical bodily velocity of DD-593 sections caused by reflected wave, Shot Wahoo.

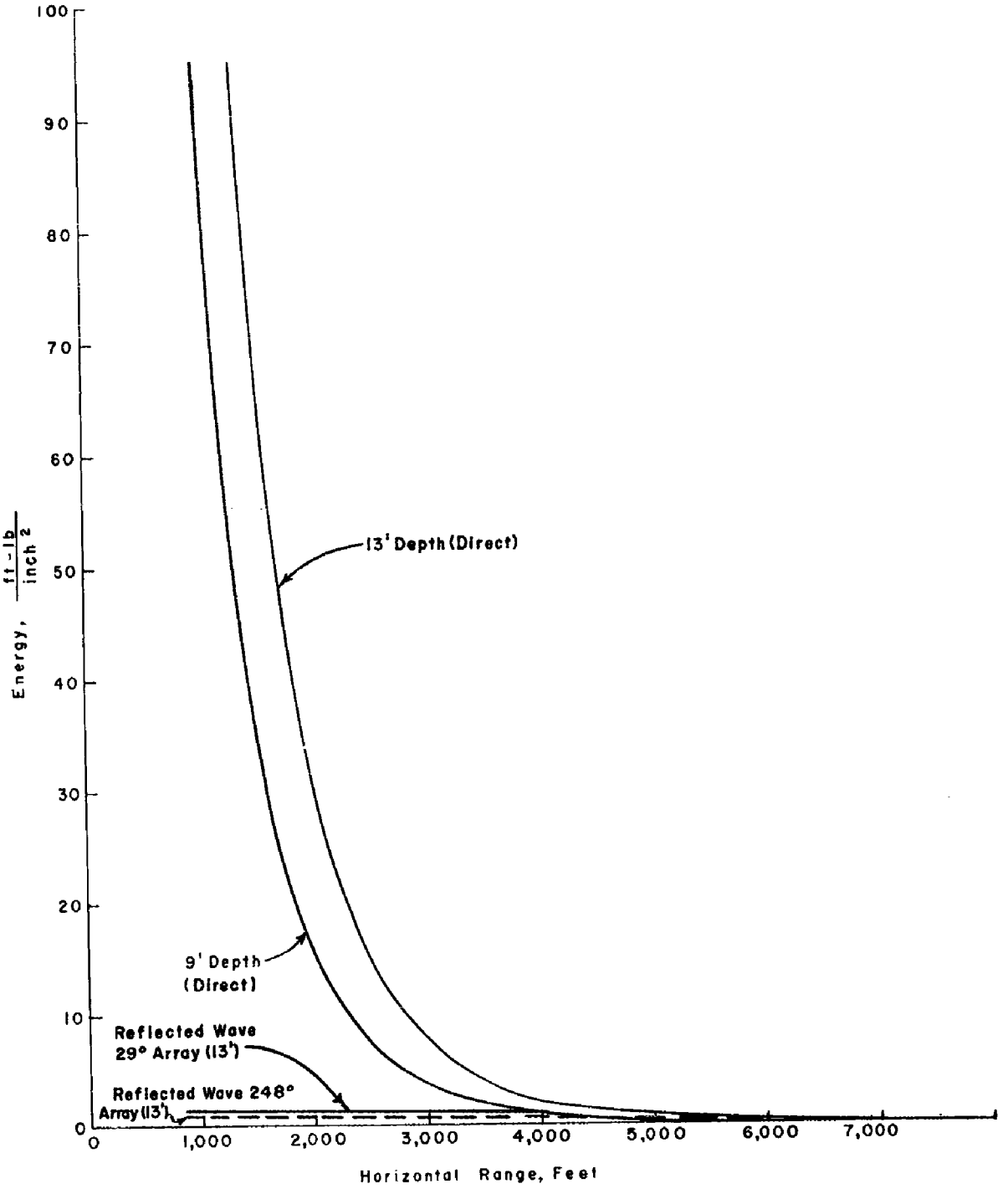

Figure 4.27 Shock wave energy flux density versus range, Shot Wahoo.

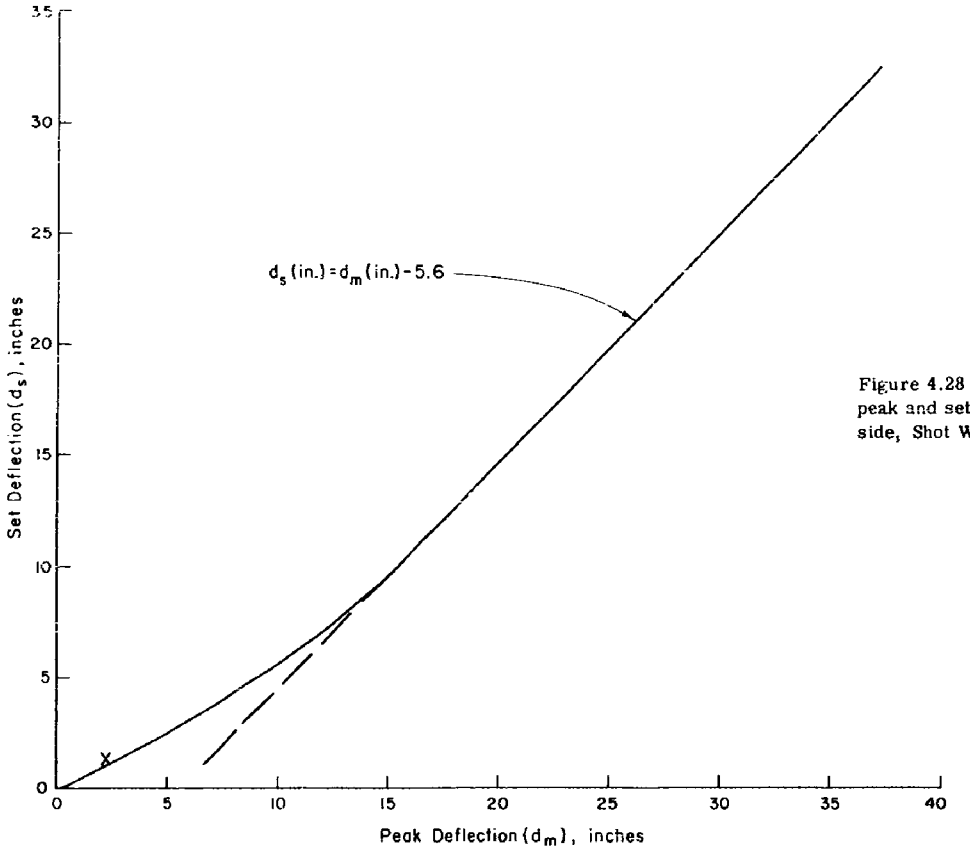

Figure 4.28 Relationship between peak and set deflections for EC-2 side, Shot Wahoo.

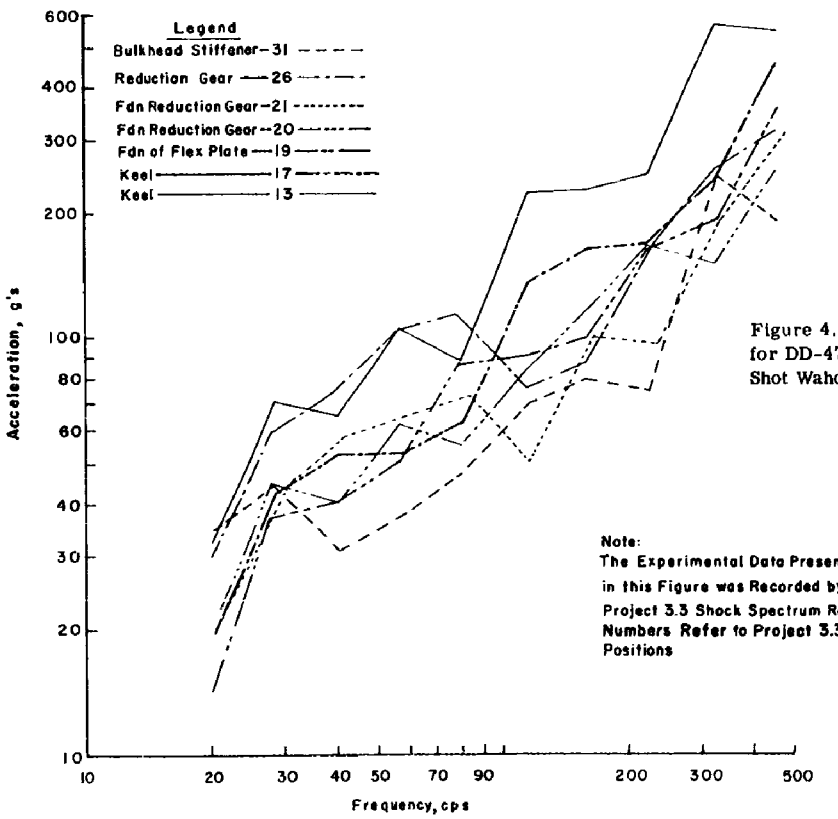

Figure 4.29 Typical shock spectra for DD-474 measured by Project 3.3, Shot Wahoo.

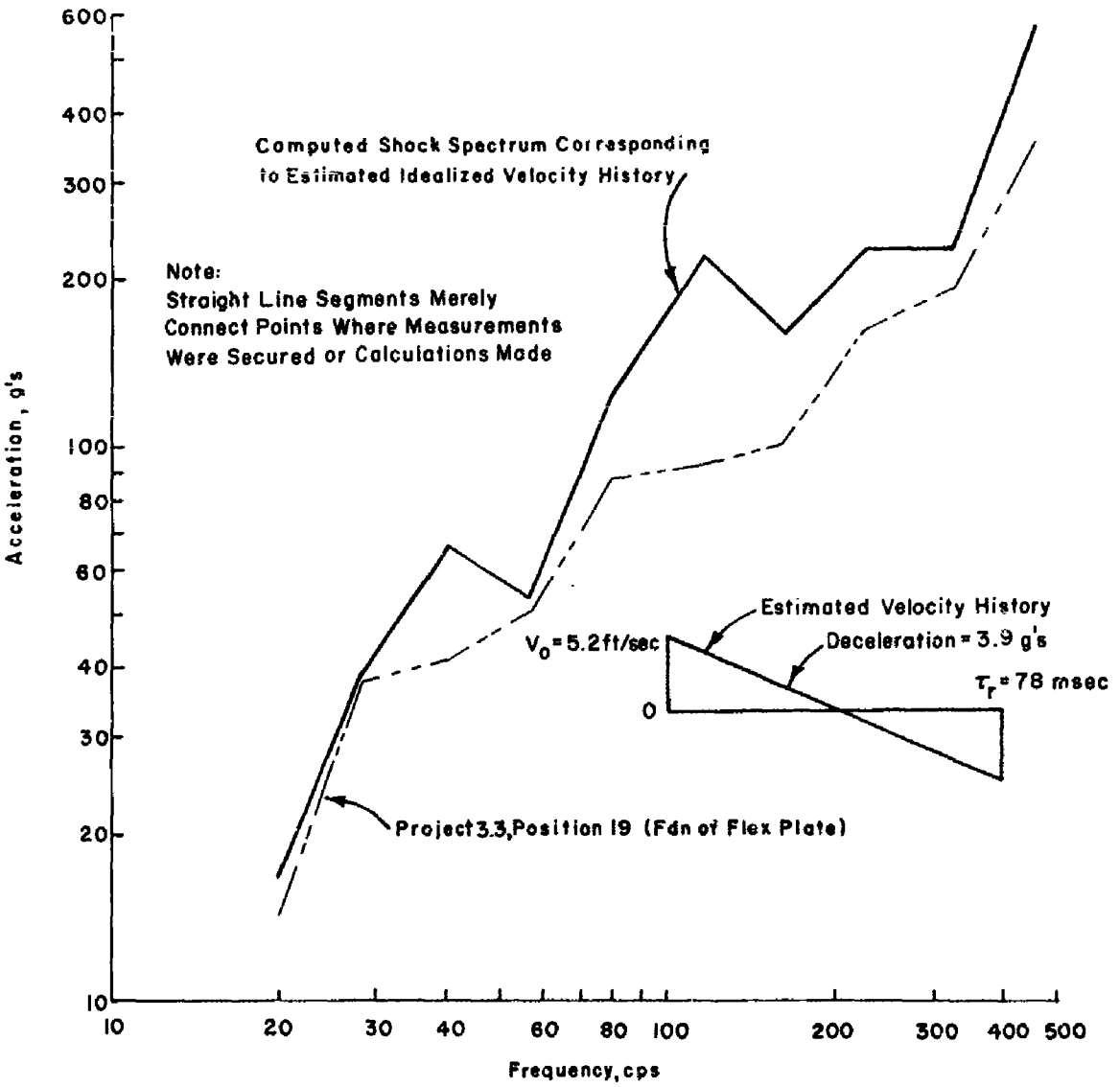

Figure 4.30 Comparison of computed shock spectrum with typical shock spectrum measured by Project 3.3 for DD-474, Shot Wahoo.

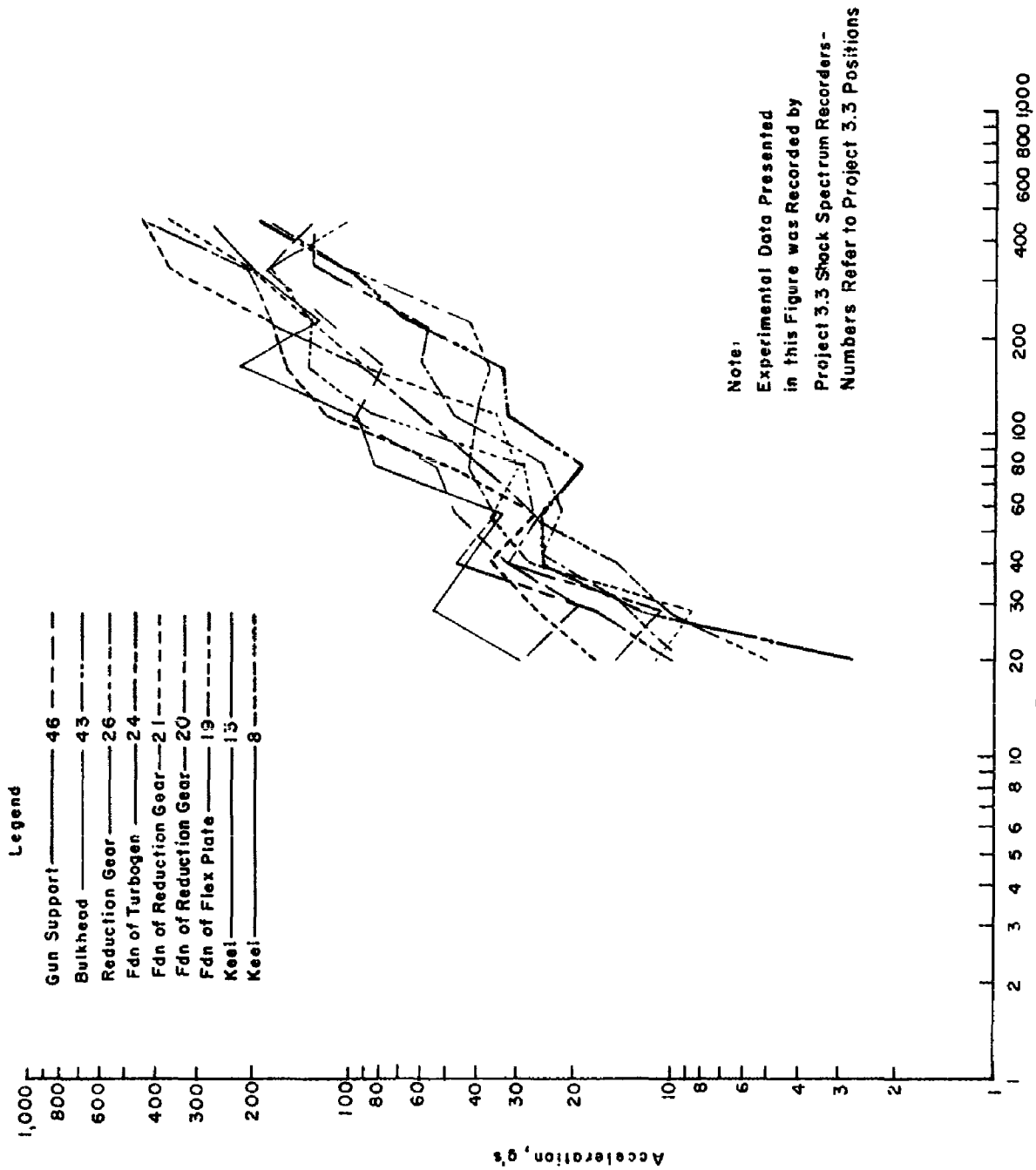

Figure 4.31 Typical shock spectra for DD-592 measured by Project 3.3, Shot Wahoo.

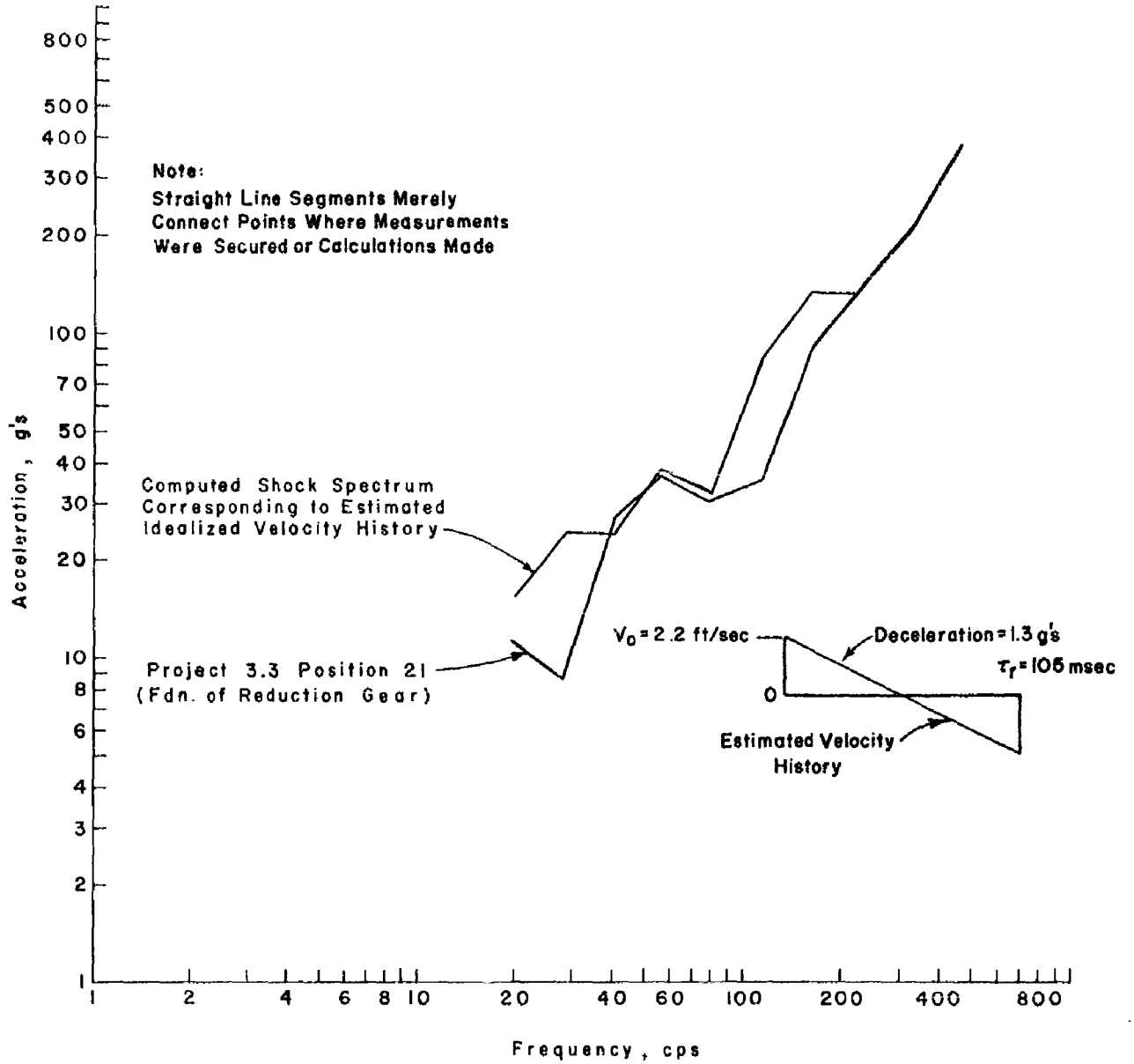

Figure 4.32 Comparison of computed shock spectrum with typical shock spectrum measured by Project 3.3 for DD-592, Shot Wahoo.

Chapter 5

RESULTS, SHOT UMBRELLA

5.1 PRELIMINARY REMARKS

During Shot Umbrella, records were obtained from all instrumented ships: DD-474, DD-592, DD-593, and the EC-2. The records for the most part were of good quality for the time period of major interest. The chief difficulty experienced was with the EC-2 records which, although of good quality for the time of chief interest, were unreadable after about $\frac{1}{3}$ second from the direct shock wave arrival. This recording difficulty apparently arose because of early bottoming of the air-ride springs supporting the instrumentation platform and later shock damage (loss of electrical contact) to the batteries (not placed on the platform) powering instrument relays.

Representative examples of the records obtained from the EC-2, DD-474, and DD-592 are shown in accordance with a scheme similar to that used to exhibit the Shot Wahoo test results (Chapter 3). However, records obtained from DD-593 (all were velocity measurements) are omitted; the maximum velocity measured (0.25 ft/sec) was too low to have any significance, and the velocity histories were obscured by the natural frequency of the meter. All records have been fully corrected in accordance with the procedures outlined in Section 2.3, and therefore represent physical measurements rather than raw data.

5.2 EFFECTS OF OVERALL RANGE OF UNDERWATER PHENOMENA

An overall impression of the effects of all observed underwater phenomena may be gained by glancing at Figures 5.1 through 5.3. The main phases of the loading and response are marked in the figures: a lagoon-bottom precursor pressure wave, the direct shock wave, a cavitation reloading subsequent to the direct shock wave, and the response of a ship (DD-474) to surface waves generated by the explosions.

Of these, it is clear that the direct shock wave is most significant. For this reason the few free-water pressure measurements obtained by Project 3.4 are shown on a greatly expanded time scale in Figures 5.4 and 5.5. Note that in the case of the EC-2 (Figure 5.4) pressure gages, portions of the free-water pressure histories may be distorted by reflections from the ship. In view of the relatively poor low-frequency response of Project 3.4 pressure-gage recordings, only pressures in excess of the precursor pressures are plotted. In those cases where measurements were obtained by Project 1.1 at identical locations, a satisfactory degree of agreement with similarly treated Project 1.1 measurements was achieved (Reference 16).

5.3 HULL LOADING AND HULL RESPONSE

The hull loading and hull response of the EC-2 immediately prior to, and immediately following, the arrival of the direct shock wave are illustrated in Figure 5.6. A free-water pressure record is also shown (dashed curve) for general comparison in Figure 5.6; an appropriate time shift was employed so that the rise time would coincide with that of the

loading pressure. Similar examinations of the early hull loading and response are made for DD-474 and DD-592 in Figures 5.7 and 5.8, respectively.

5.4 CROSS-SECTION DISTRIBUTION OF INITIAL HULL LOADING AND RESPONSE

The velocities and loading pressures measured over a cross section of the EC-2 hull just prior to and just following the direct shock wave are shown in Figure 5.9. Notice that in many cases the velocity records show large precursor effects, not only due to the lagoon-bottom-reflected wave but also due to structural-reaction waves in the target ship, arriving at a particular gage position prior to the arrival of the direct shock wave front itself.

Similar comparisons for the DD-474 and DD-592 are given in Figures 5.10 and 5.11, respectively. In examining these figures it should, of course, be realized that the DD-474 was attacked end-on whereas the DD-592 was attacked side-on.

5.5 LONGITUDINAL DISTRIBUTION OF INITIAL HULL LOADING AND RESPONSE

The EC-2 and DD-592 were attacked side-on. Under these conditions a systematic variation in the longitudinal distribution can hardly be expected. However, it is interesting to examine the experimental evidence from the viewpoint of examining what differences arise merely from the exact location of the gage along the structure.

The EC-2 was instrumented by Project 3.4 only in the engine room and Hold 3; there is thus no information leading to a comparison of the response of the EC-2 along the entire length of the ship. However, the effect on bottom velocities of the exact location of the velocity meter in relation to heavy masses along the bottom of the ship is shown in Figure 5.12. It is stressed here that: VM-7A was located close by large machinery masses, VM-14 was located in an open area of the bottom (relatively far away from large weights), and VM-1 was near a bulkhead and only a few feet from the large ballast mass in Hold 3.

DD-592 was instrumented by Project 3.4 along nearly its entire length. It, therefore, provides further examples of the variation caused in bottom velocities merely by the precise location of the meter along the hull structure. Such examples are given in Figure 5.13.

DD-474 was attacked end-on, and a systematic study of the resultant variation in loading and velocities is given in Figure 5.14.

5.6 RESPONSE DISTRIBUTION UPWARD THROUGH SHIP

An indication of the great differences in the early phase of the response upward along the bulkhead of the EC-2 is given in Figure 5.15. A similar study of the early response distribution up the bulkhead of the DD-474 is given in Figure 5.16. The DD-592 is omitted because of the low response levels.

In Shot Umbrella some evidence was obtained concerning the mechanism by which shock motions are transferred from bulkheads (and from sides) to deck platings. This is illustrated in Figure 5.17 over longer time periods chosen to illustrate the flexural motion of the deck.

5.7 BODILY MOTION OF TARGET SHIPS

Some insight into the bodily motion of the target ships may be gained in Shot Umbrella, as it was in Shot Wahoo, simply by comparing the responses measured at representative locations.

The vertical velocities measured at various representative locations on EC-2 resulting from the direct shock wave are reproduced over a long time interval in Figure 5.18. Vertical

displacement histories of the EC-2 measured at various locations are shown in Figure 5.19. In addition, a typical velocity record (VM-4 from Figure 5.18) was integrated and is also shown in Figure 5.19 to demonstrate the degree of consistency between Figures 5.18 and 5.19.

A similar examination of the measurements secured on the DD-474 can be made by reference to Figures 5.20 and 5.21. Again, typical velocities were integrated and are shown in Figure 5.21 to demonstrate the comparison with displacements at nearby locations.

An examination of the response measurements obtained from DD-592 is not profitable in terms of establishing bodily velocities, by reason of the small response levels and the short reloading time.

Horizontal velocities measured on the EC-2 are shown in Figure 5.22. Note that the VM-15 has a large superimposed vibration that obscures the bodily motion.

Horizontal velocities secured in the DD-592 were too small to allow a reasonable interpretation of horizontal bodily motions.

5.8 DEVELOPMENT OF HULL DAMAGE IN EC-2

Deflection gages were installed in Hold 3 of the EC-2 to measure the development of side-frame and bottom deformation. A special effort was made to attach the support end of the gages as rigidly as possible to an integral element of the ship (Figure 2.19). During Shot Umbrella, no motion-picture films were attempted, nor were any shell-plating strain measurements attempted.

The development of hull damage in the EC-2 was very similar to that observed during Shot Wahoo. The deflection histories measured at the shock wave phase are shown in Figure 5.23. In comparing MD-2 with MD-4, recall that MD-4 was attached to the side frame next to the engine-room bulkhead and to the first port bulkhead stiffener; therefore, it measured side deformation on the attack (port) side very close to the bulkhead. Set deflection measurements obtained at the deflection gages themselves are also shown in Figure 5.23.

5.9 FINAL HULL DAMAGE

Hull damage on the EC-2 as a result of Shot Umbrella was slight and very similar in character to that found after Shot Wahoo. A damage survey was conducted in accordance with the description given in Section 3.9, and the results for the attacked side are presented in Figures 5.24 and 5.25 (following the same scheme as described in Section 3.9).

The general damage picture in the EC-2 was essentially the same as that after Shot Wahoo; however, previous damage was, of course, accentuated.

Divers were again requested to examine the bottom of the EC-2. On this occasion they were provided with a rule and straight edge and requested to measure any bottom-plating dishes. With one exception, they reported that bottom-plate dishes between floors (or frames) did not exceed $\frac{1}{4}$ to $\frac{1}{2}$ inch (Holds 2, 3, 4, and the engine room) and at the ends of the ship (Holds 1 and 5) were too negligible to be measured. The single exception was a local dish at about Frame 120 toward the port edge; here a series of lobes measured about $1\frac{1}{2}$ inches in depth.

An examination of the DD-474 revealed no hull dishing that could definitely be ascribed to Shot Umbrella.

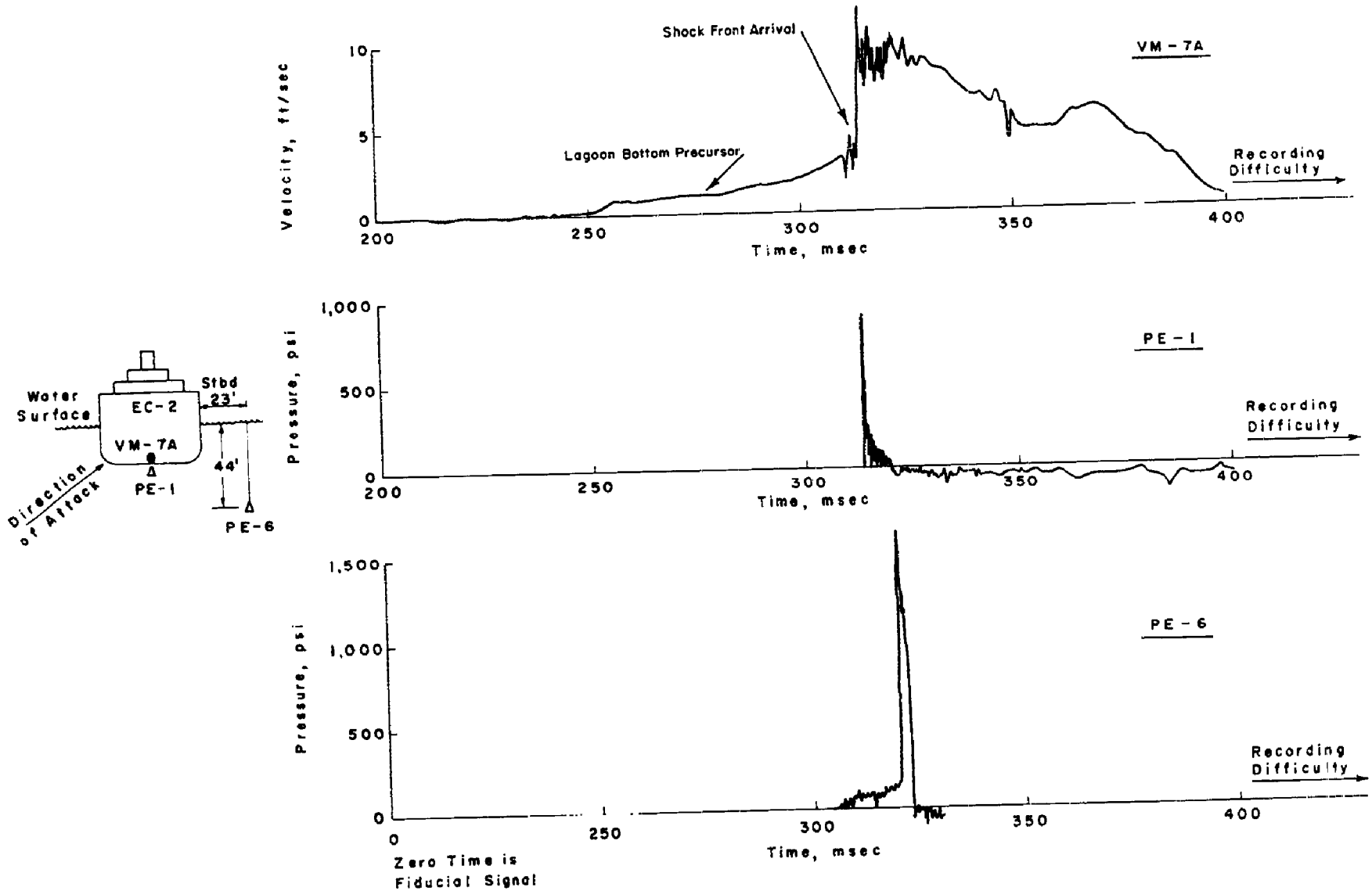

Figure 5.1 Overall effects of underwater phenomena, EC-2, Shot Umbrella.

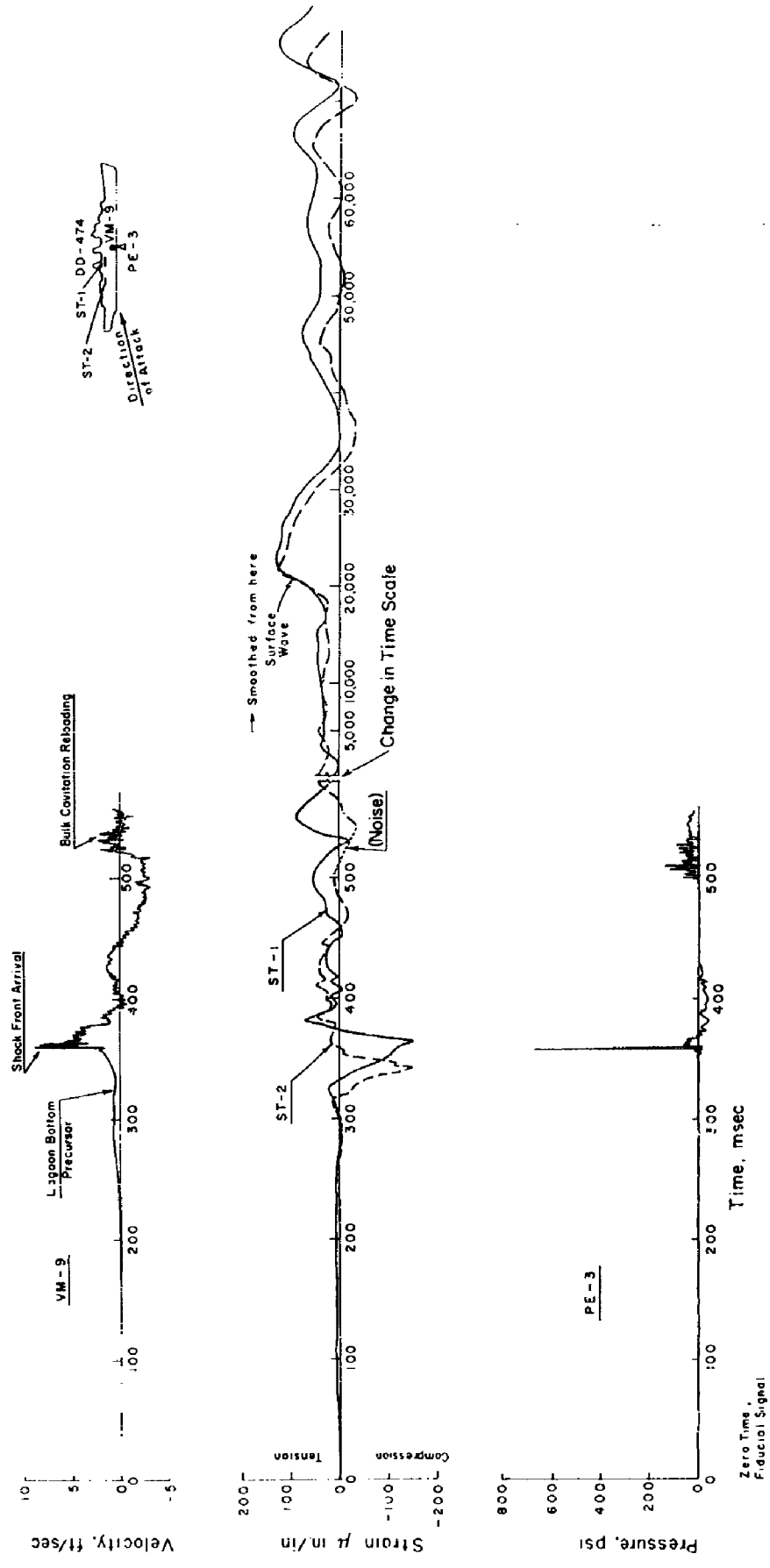

Figure 5.2 Overall effects of underwater phenomena, DD-474, Shot Umbrella.

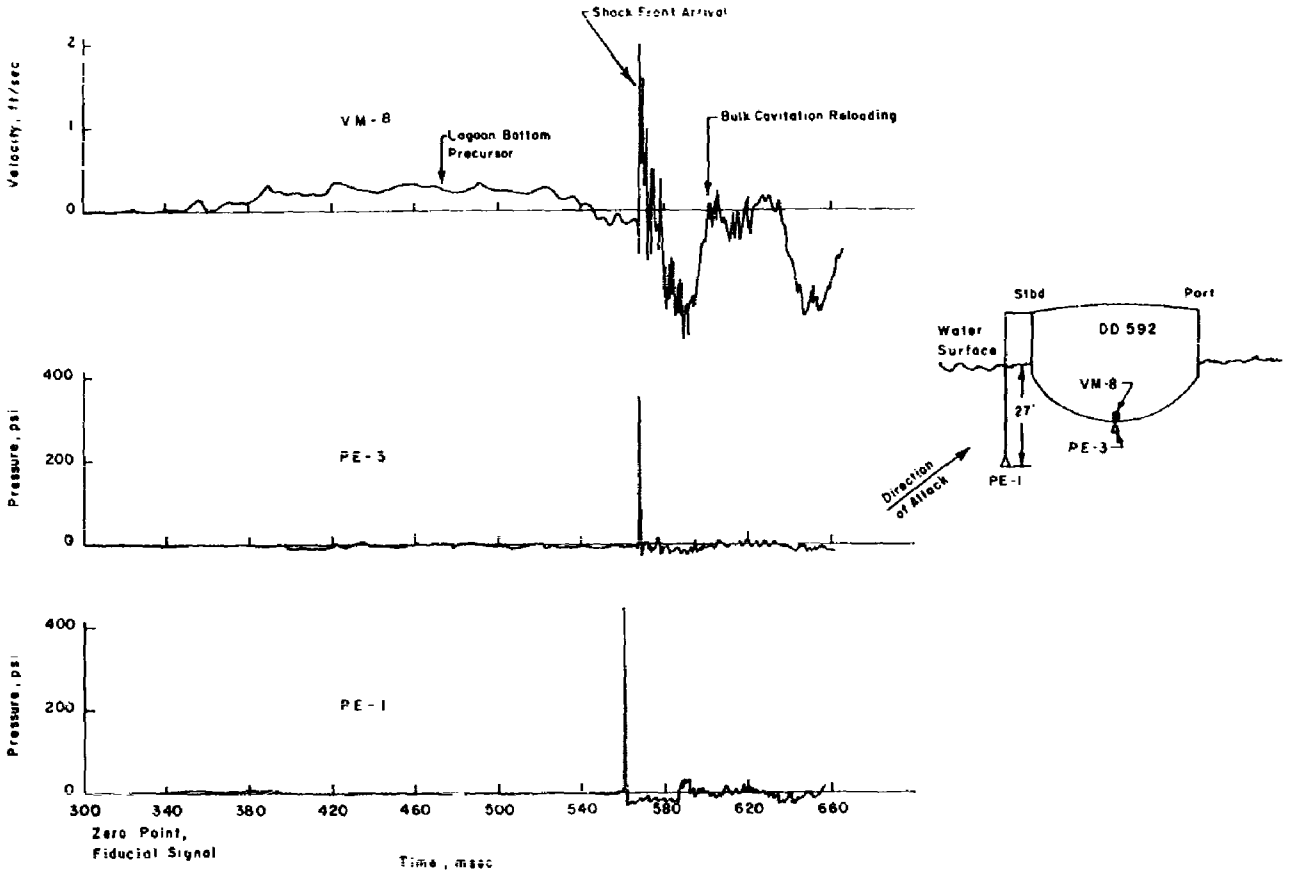

Figure 5.3 Overall effects of underwater phenomena, DD-592, Shot Umbrella.

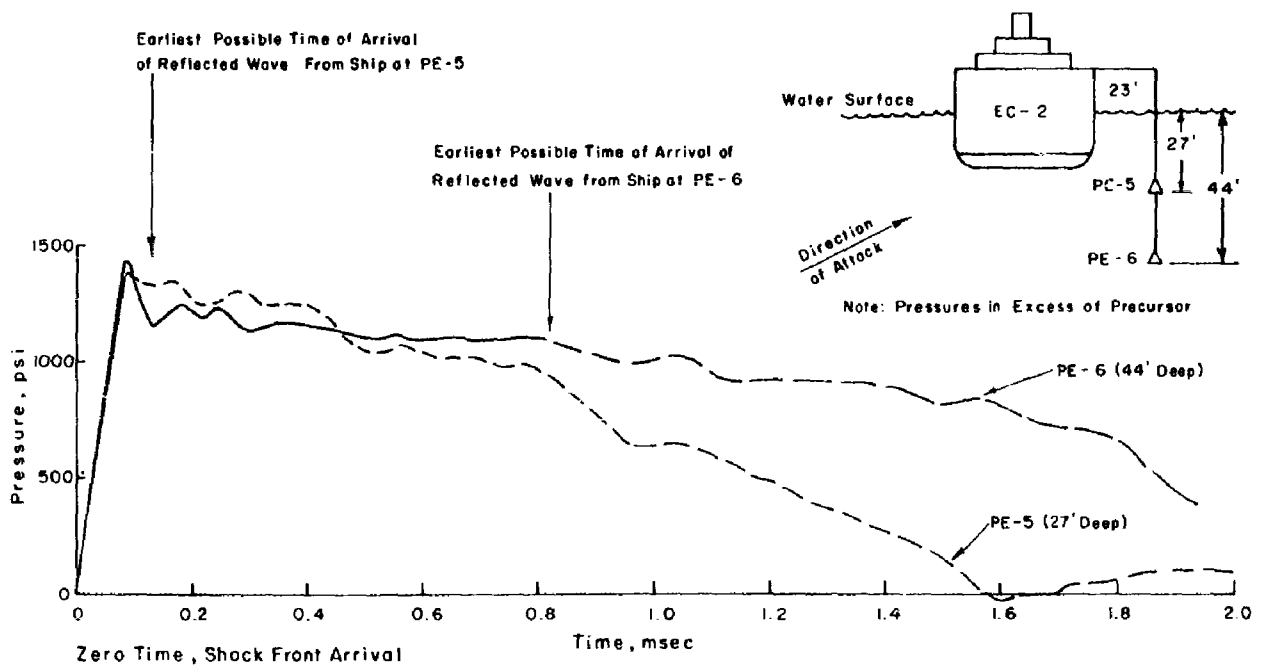

Figure 5.4 Free-water direct shock waves, EC-2, Shot Umbrella.

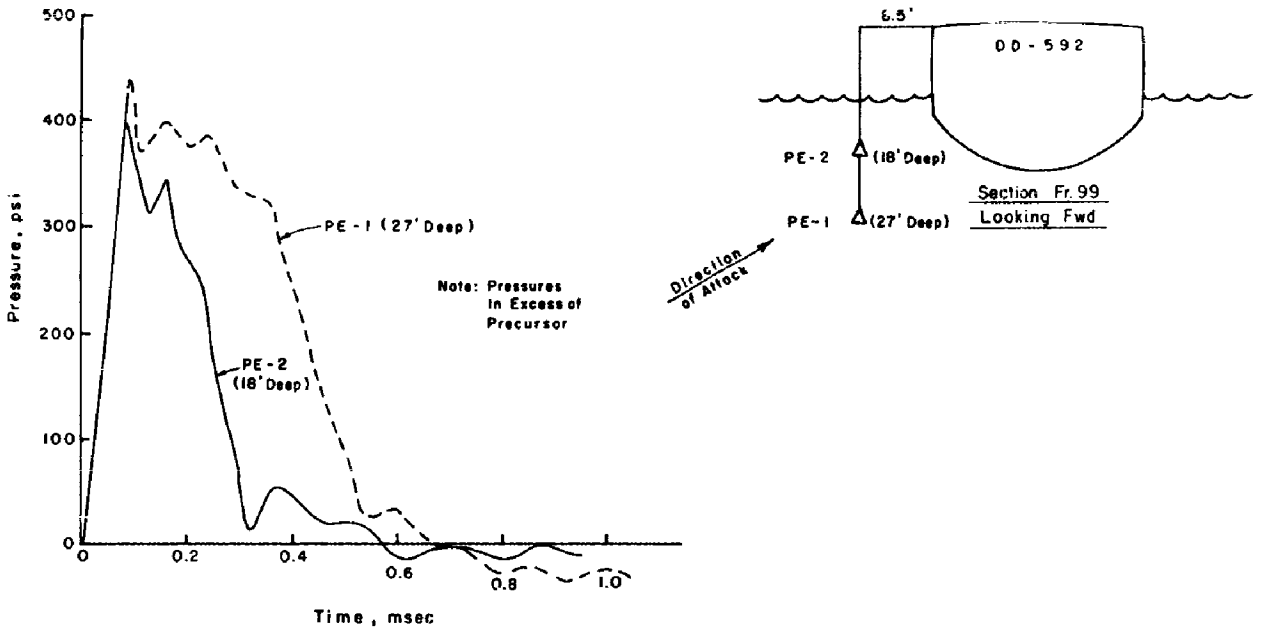

Figure 5.5 Free-water shock wave pressure history, DD-592, Shot Umbrella.

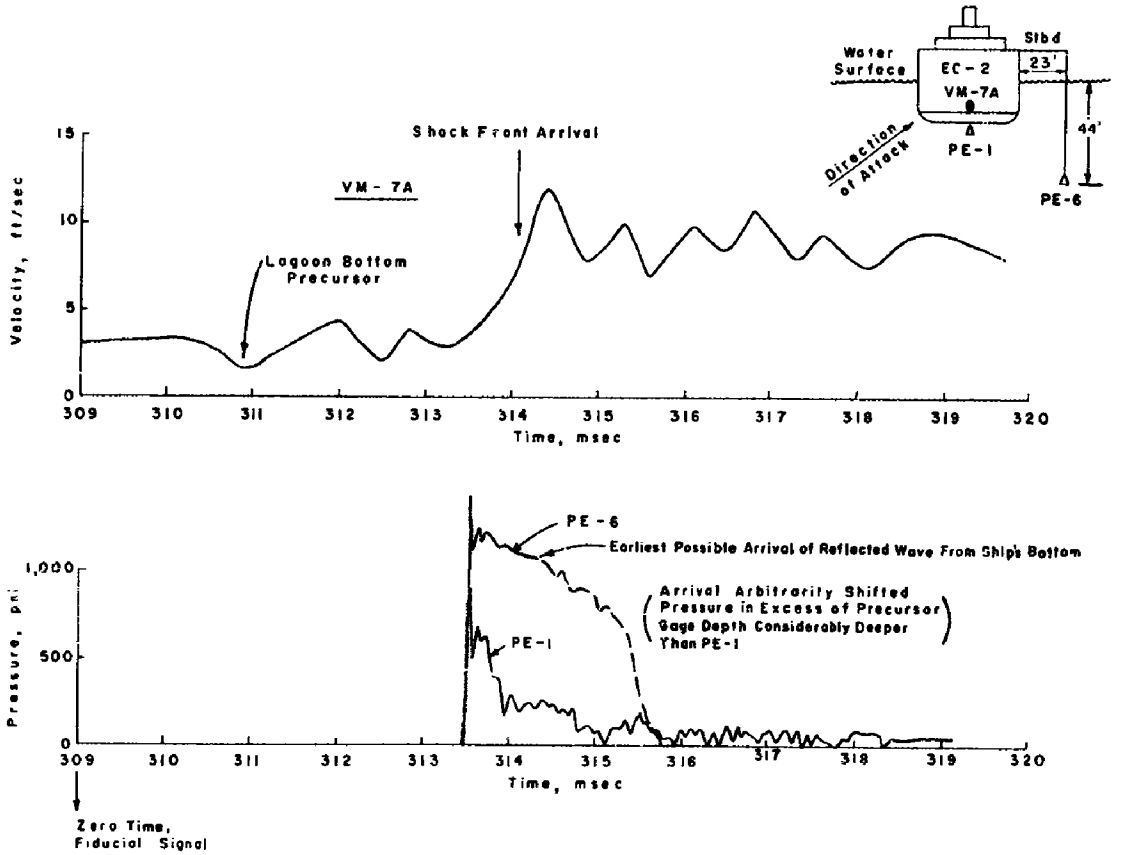

Figure 5.6 Initial hull loading and hull response, EC-2, Shot Umbrella.

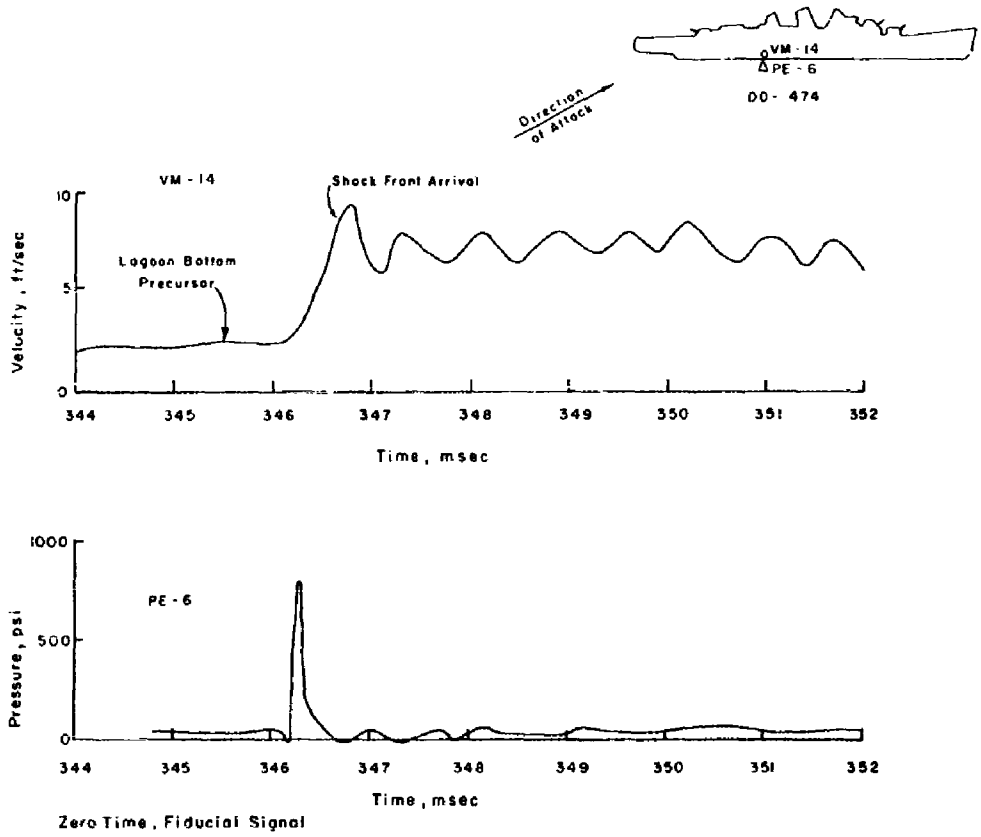

Figure 5.7 Initial hull loading and hull response, DD-474, Shot Umbrella.

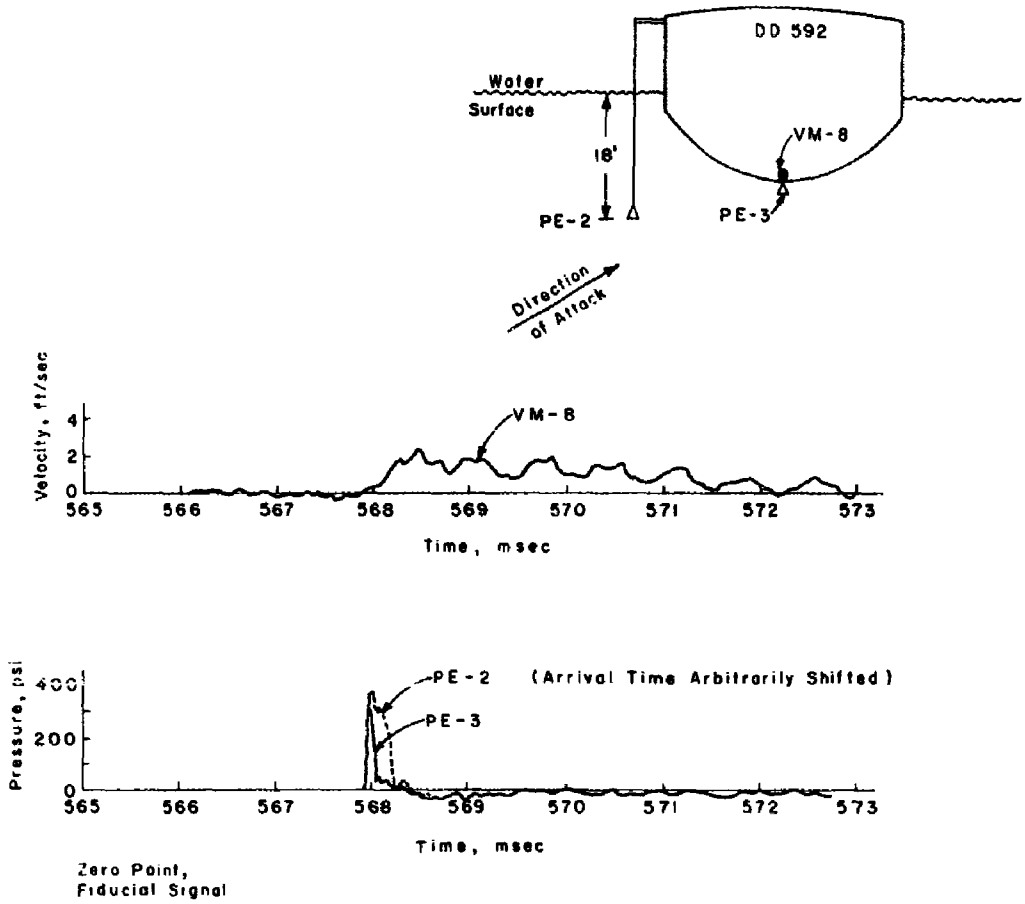

Figure 5.8 Initial hull loading and hull response, DD-592, Shot Umbrella.

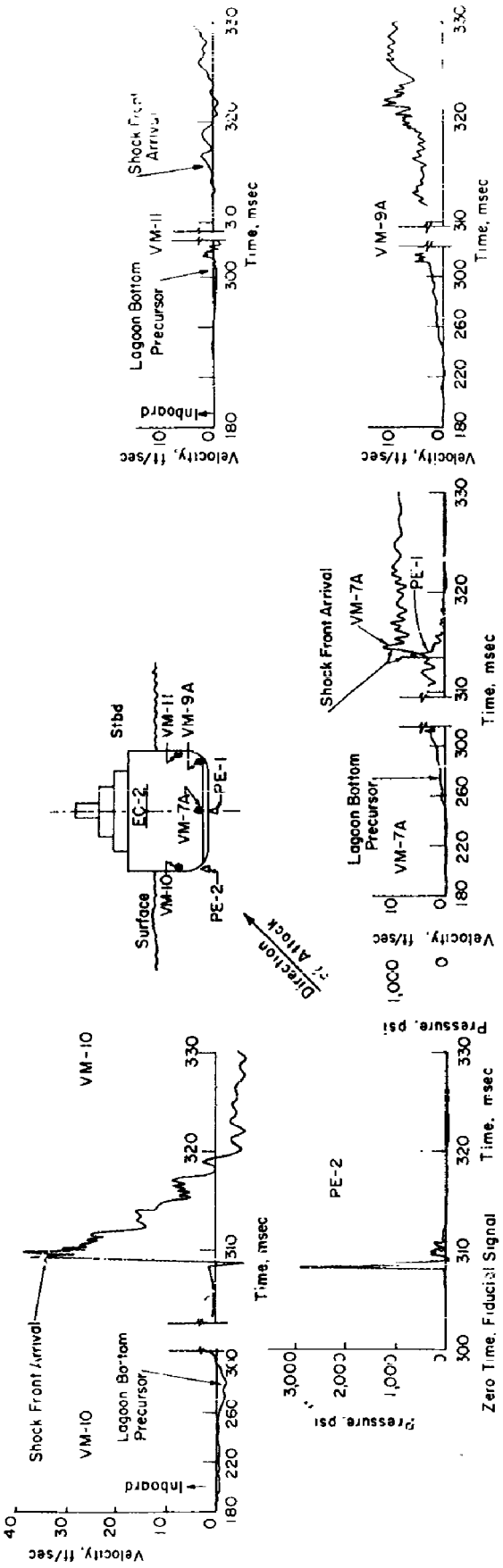

Figure 5.9 Cross-section distribution of initial hull loading and response, EC-2, Shot Umbrella.

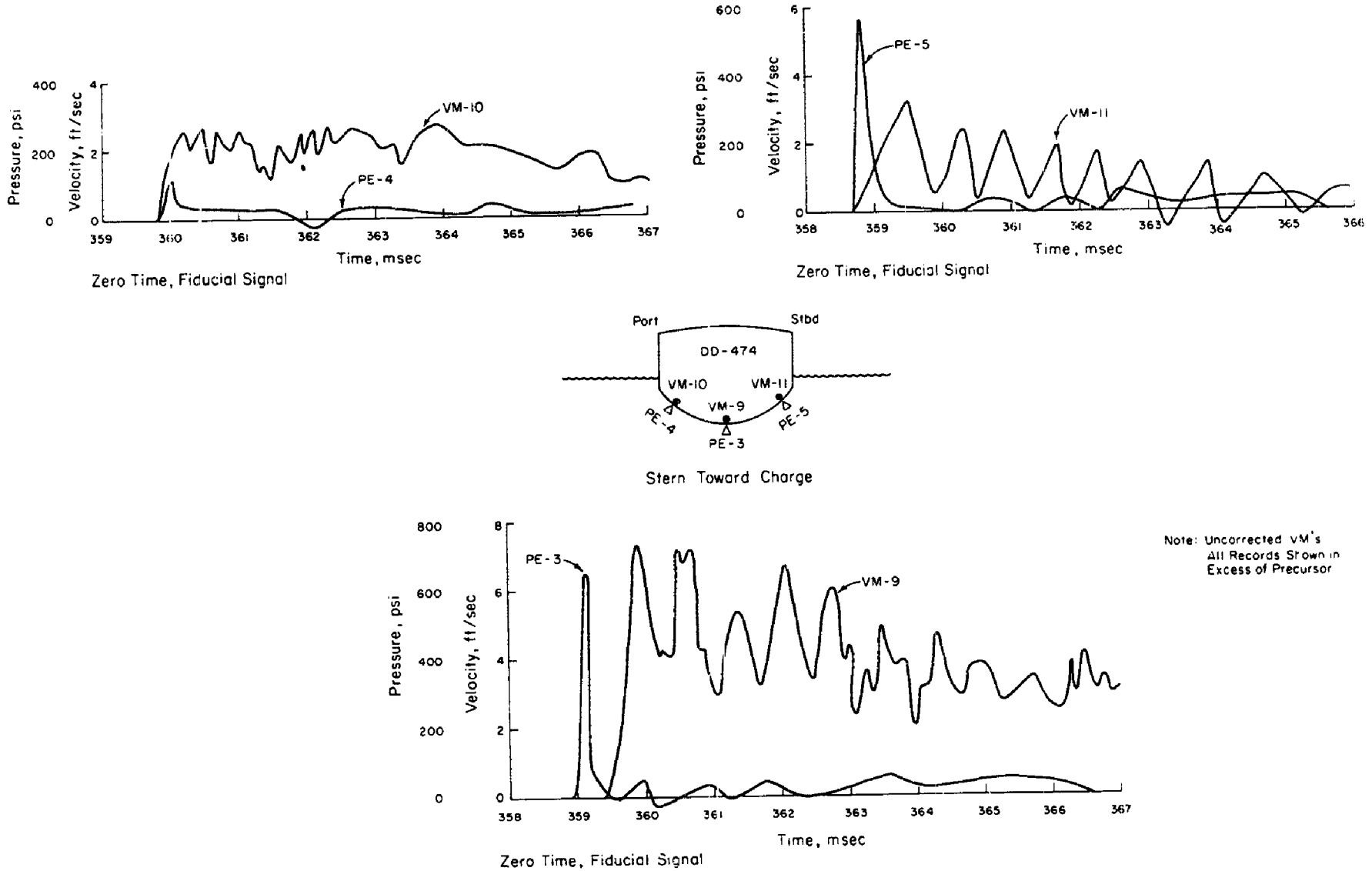

Figure 5.10 Cross-section distribution of initial hull loading and response, DD-474, Shot Umbrella.

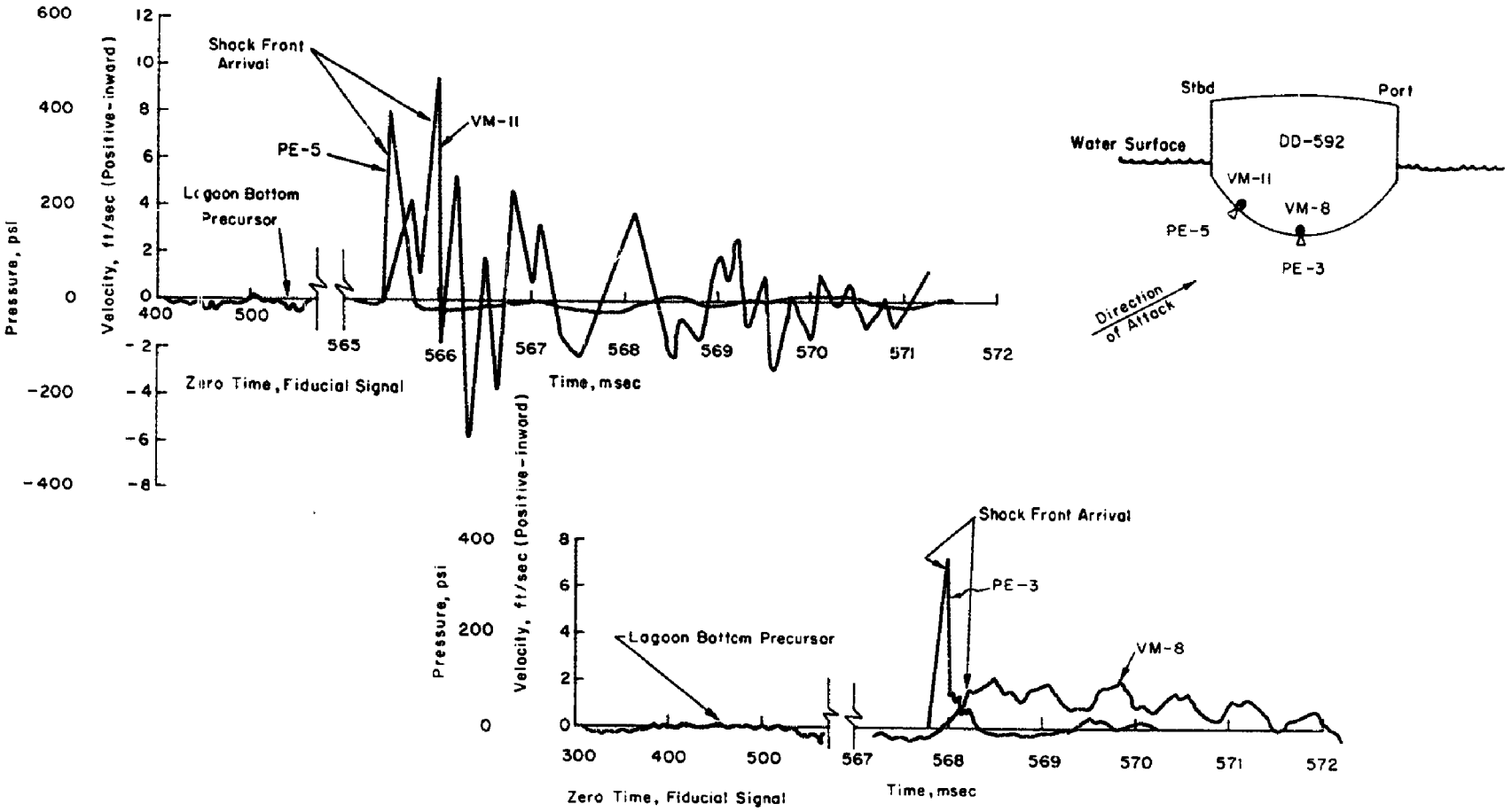

Figure 5.11 Cross-section distribution of initial hull loading and response, DD-592, Shot Umbrella.

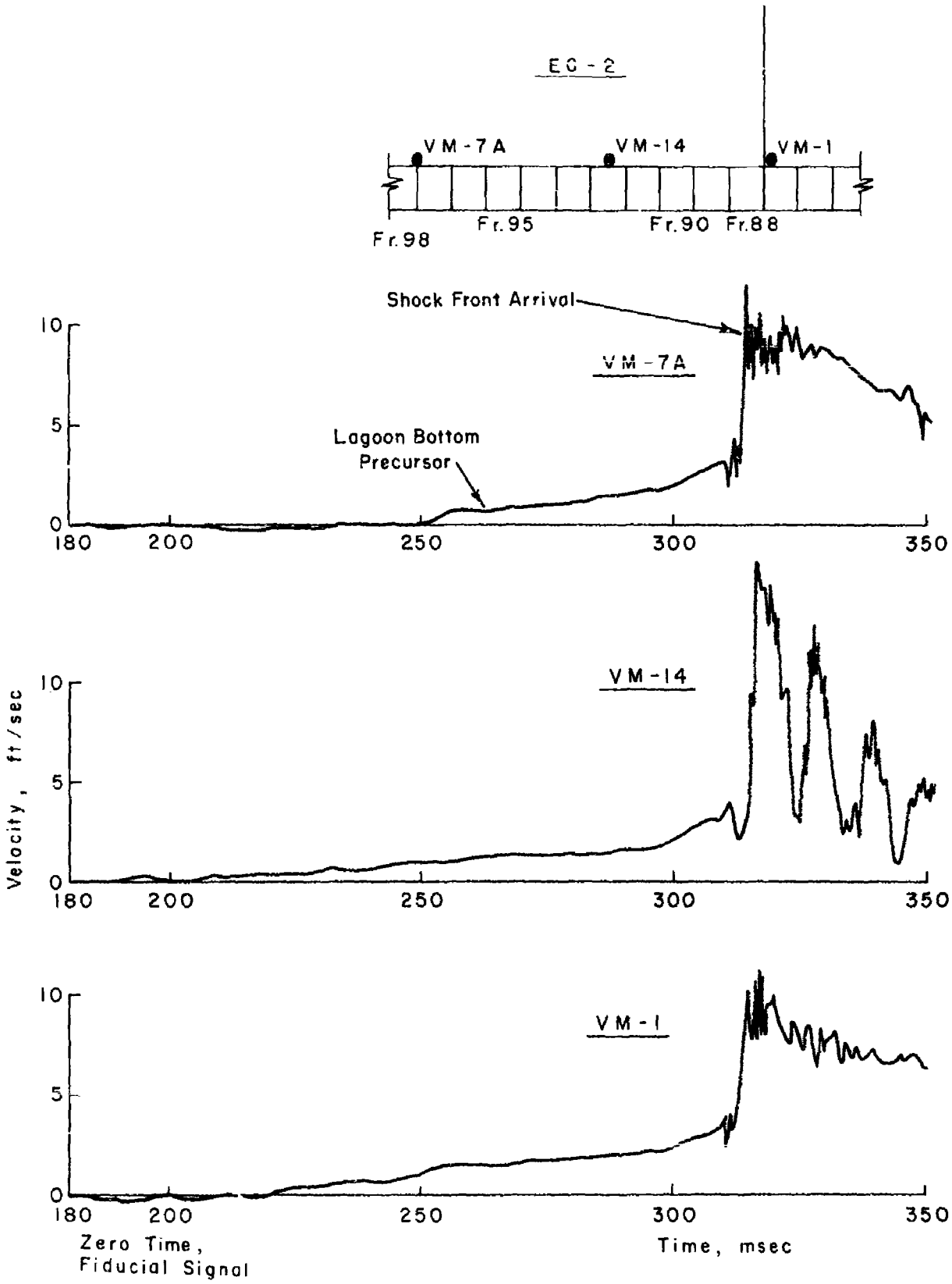

Figure 5.12 Bottom velocities at various locations along keel, EC-2, Shot Umbrella.

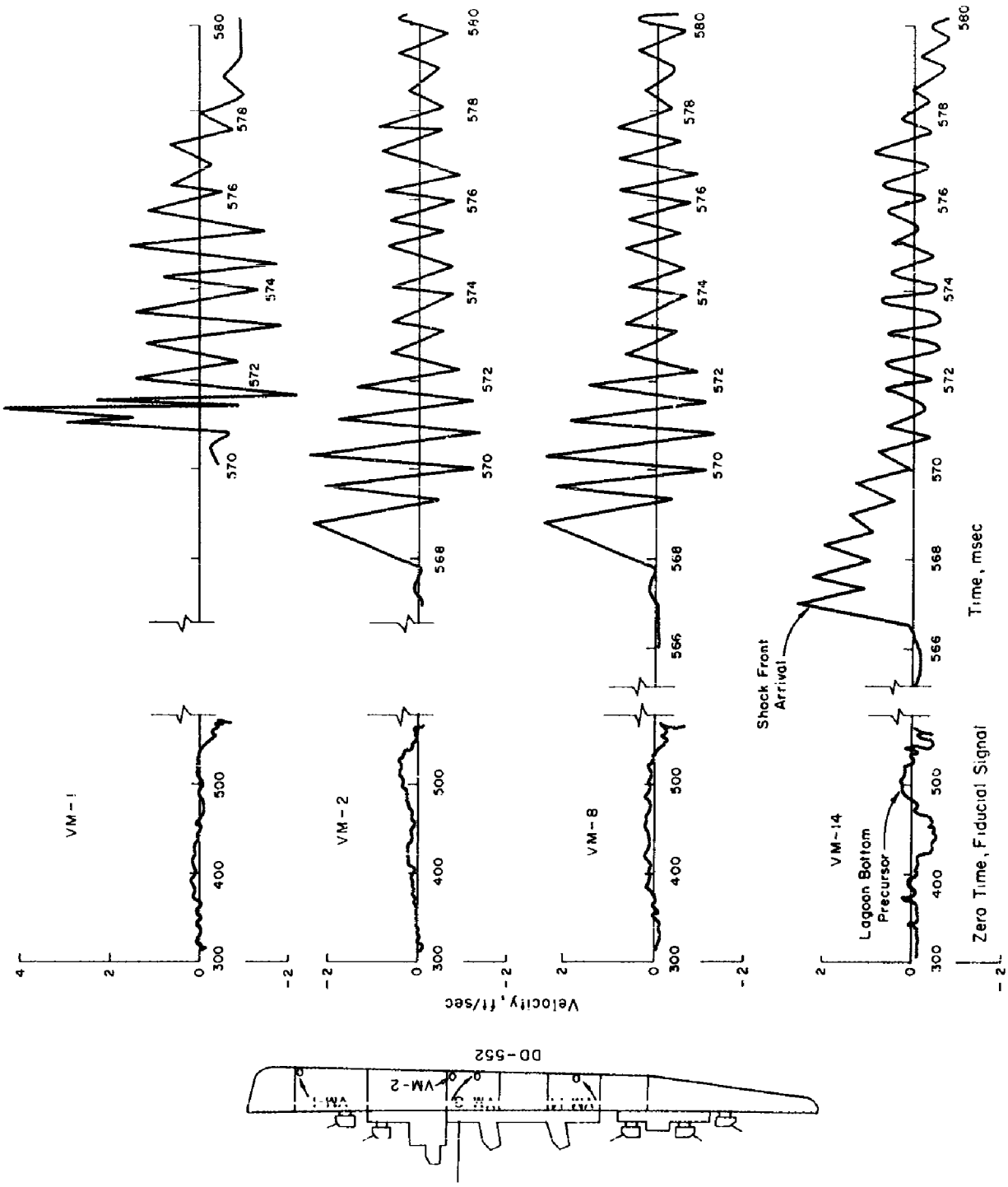

Figure 5.13 Longitudinal distribution of bottom velocities along keel, DD-592, Shot Umbrella.

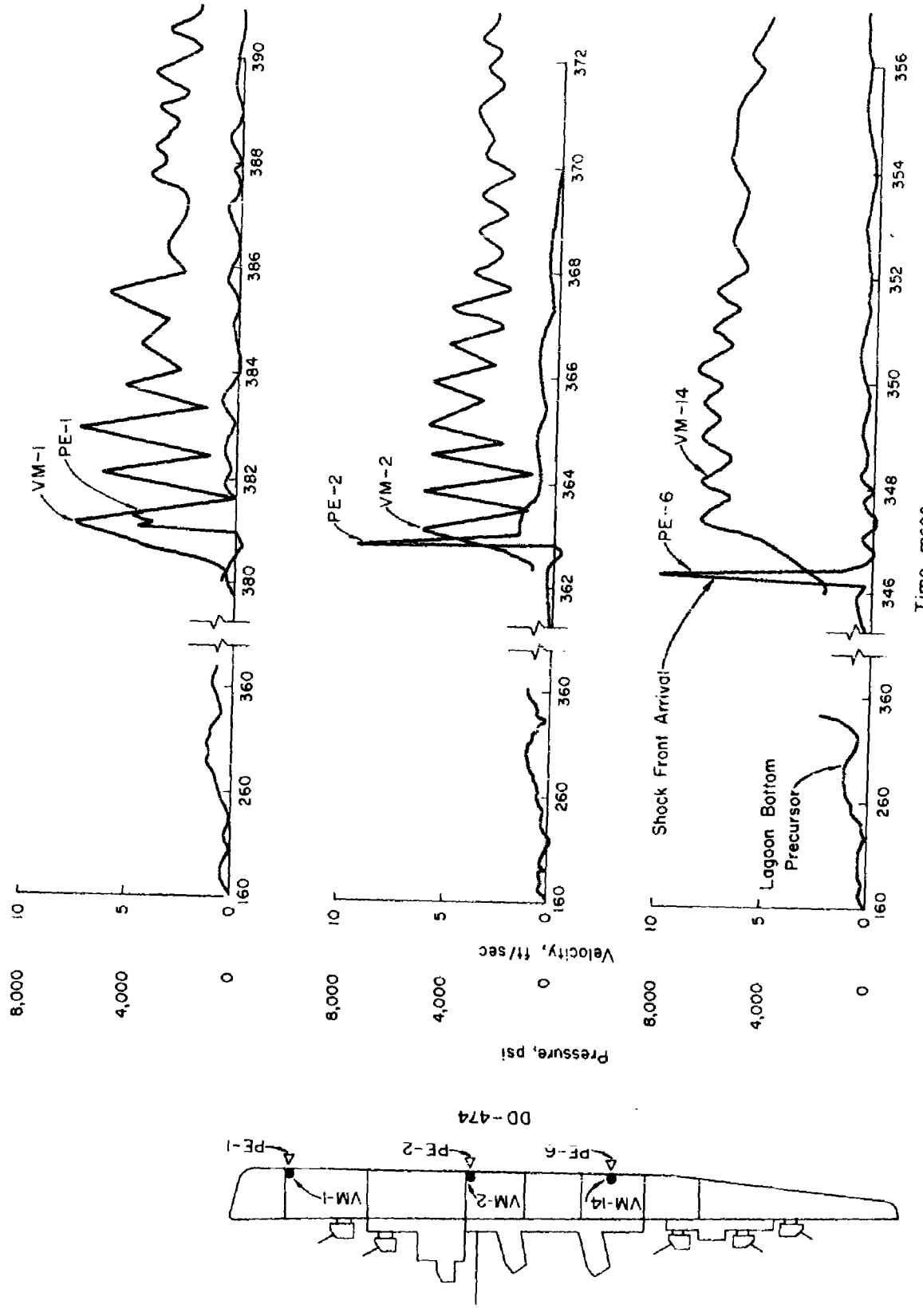

Figure 5.14 Longitudinal distribution of hull loading and response, DD-474, Shot Umbrella.

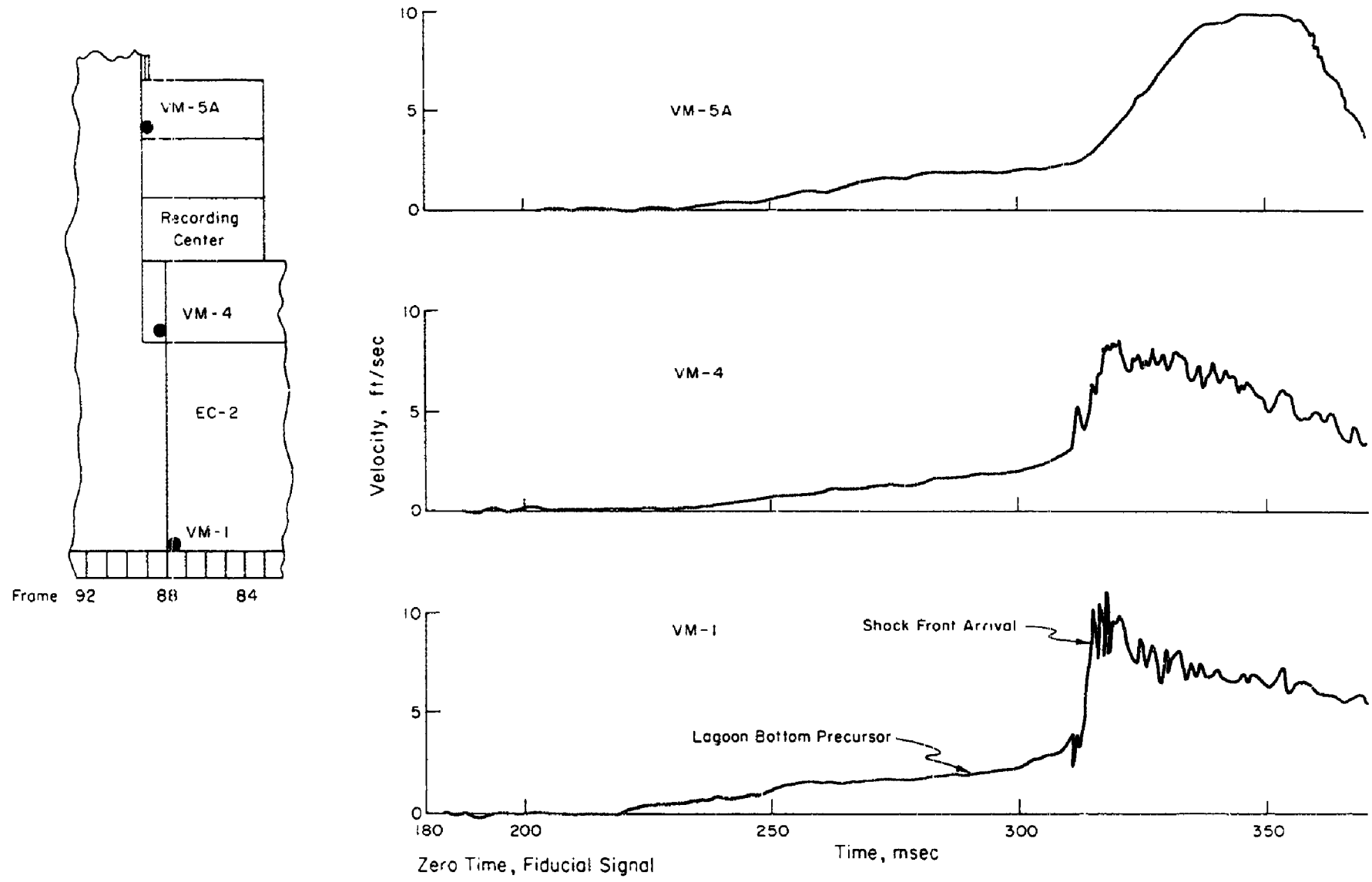

Figure 5.15 Early response distribution upward along bulkhead, EC-2, Shot Umbrella.

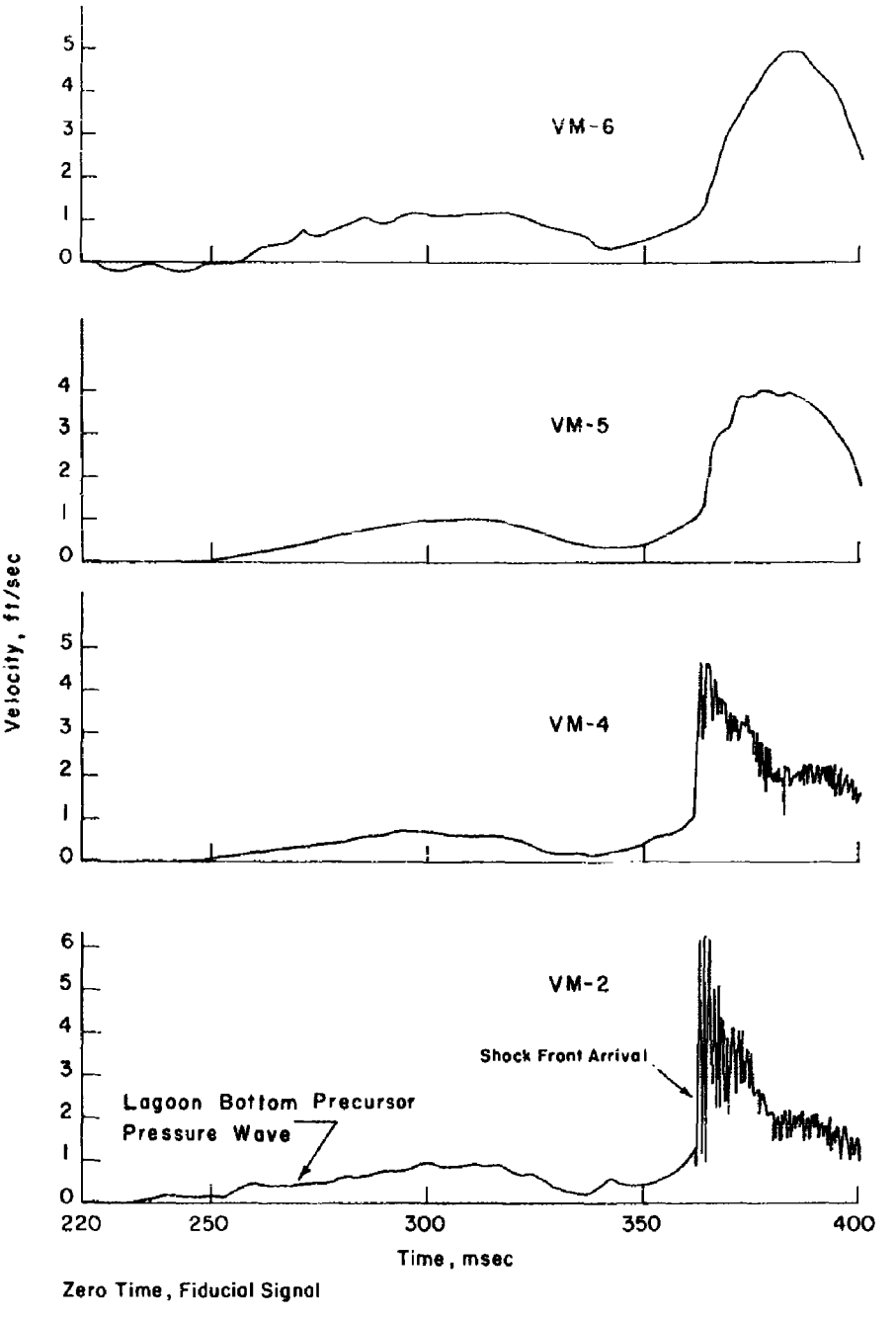

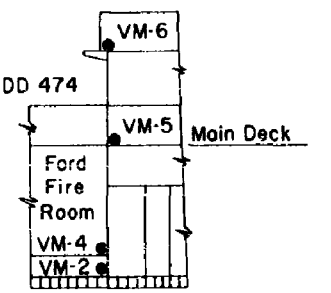

Figure 5.16 Early response distribution upward along bulkhead, DD-474, Shot Umbrella.

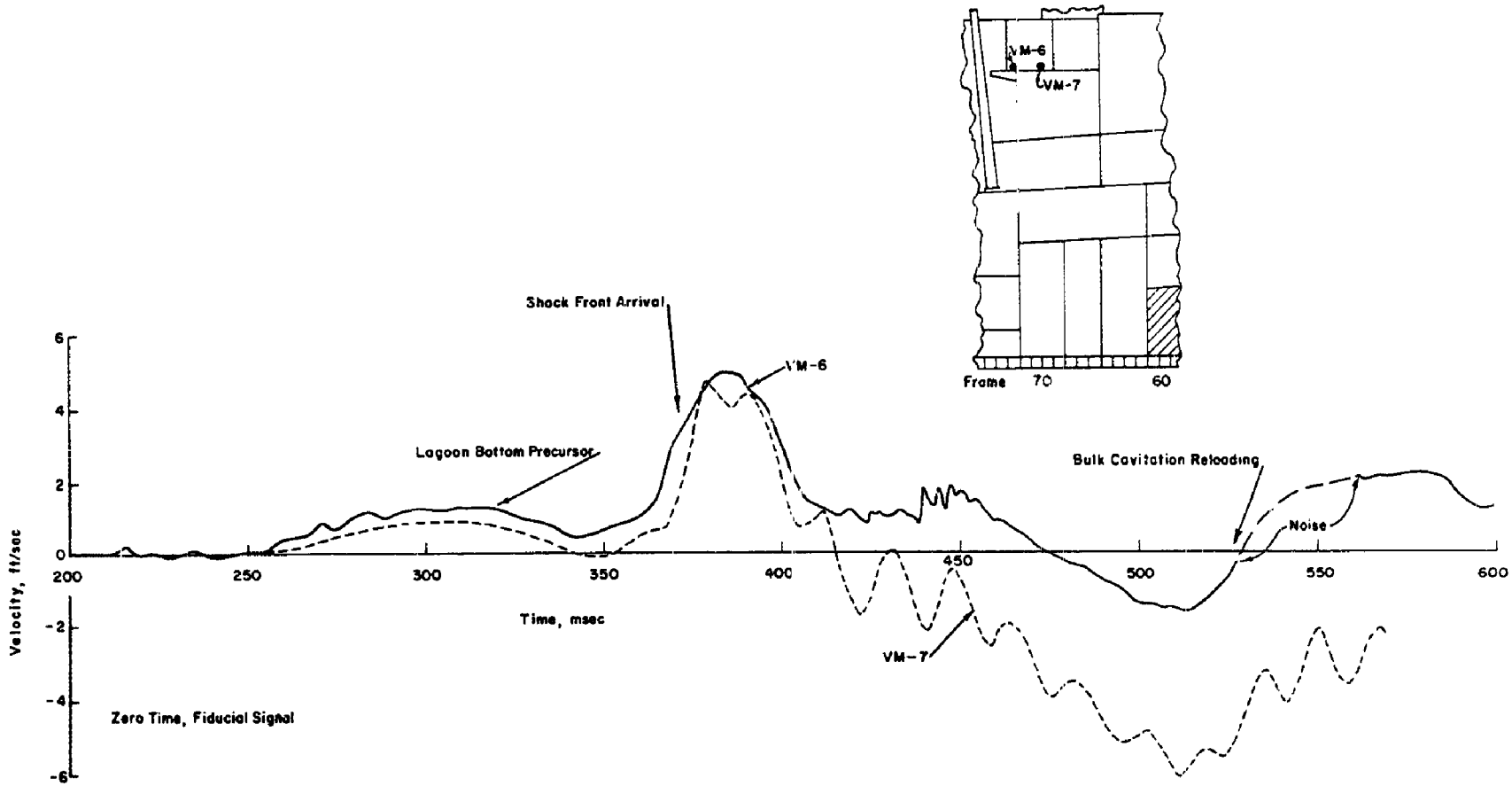

Figure 5.17 Comparison of bulkhead velocity and deck plating velocity, DD-474, Shot Umbrella.

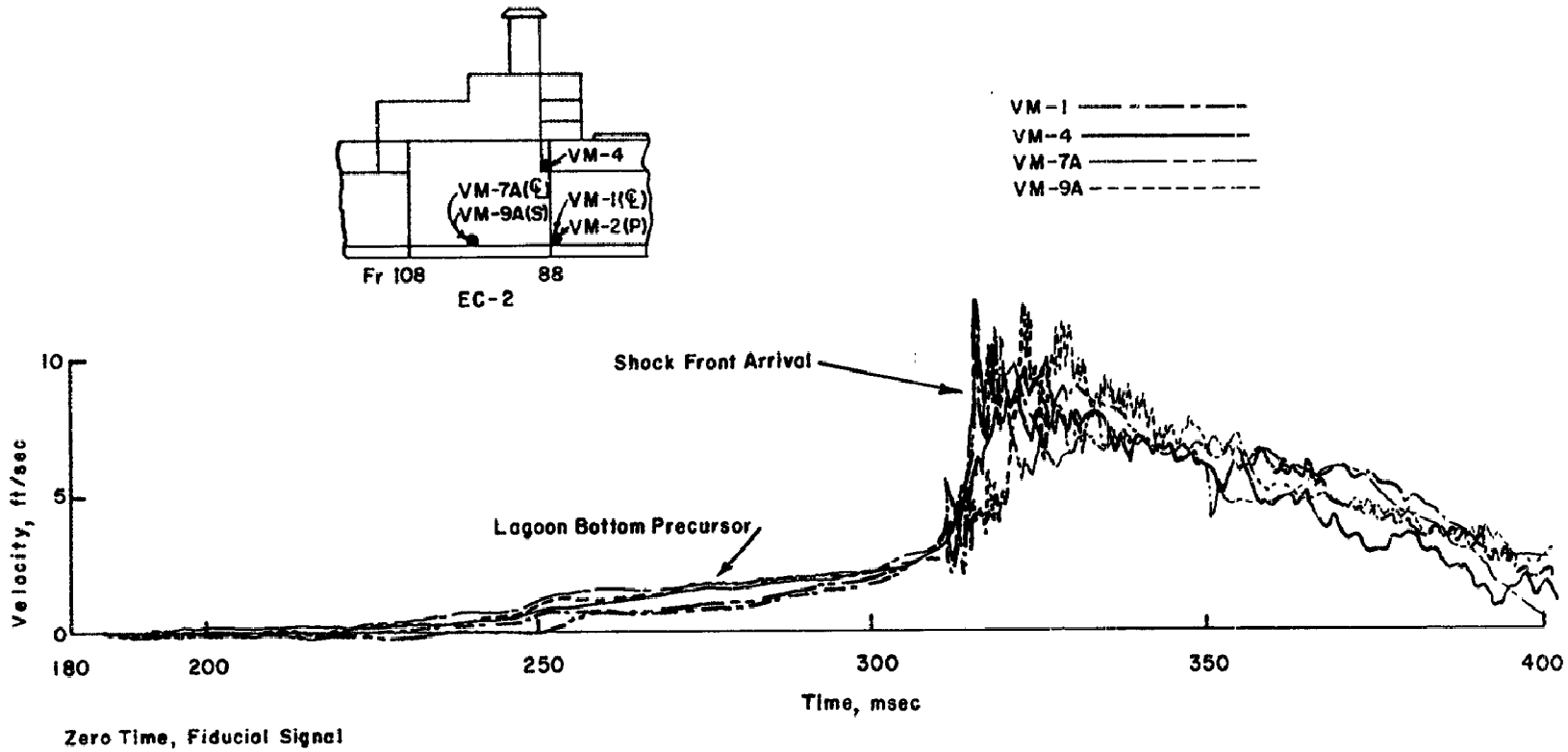

Figure 5.18 Vertical velocities at various locations on EC-2, Shot Umbrella.

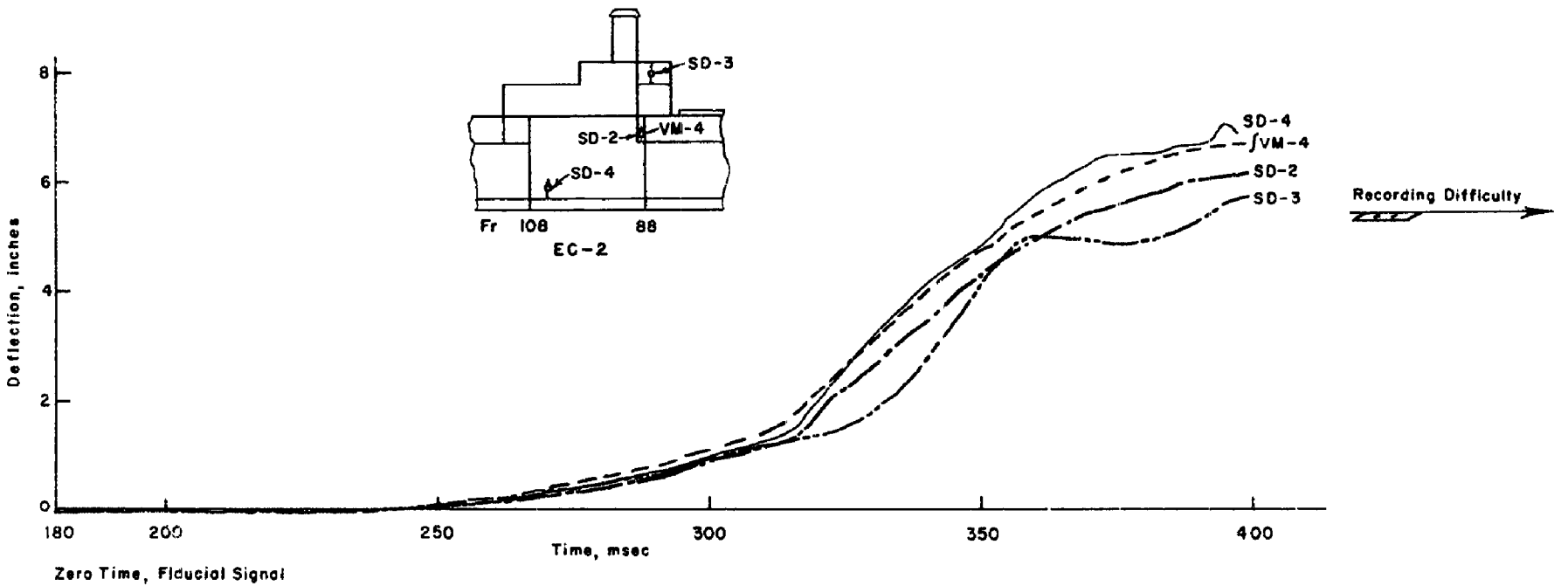

Figure 5.19 Vertical displacement histories, EC-2, Shot Umbrella.

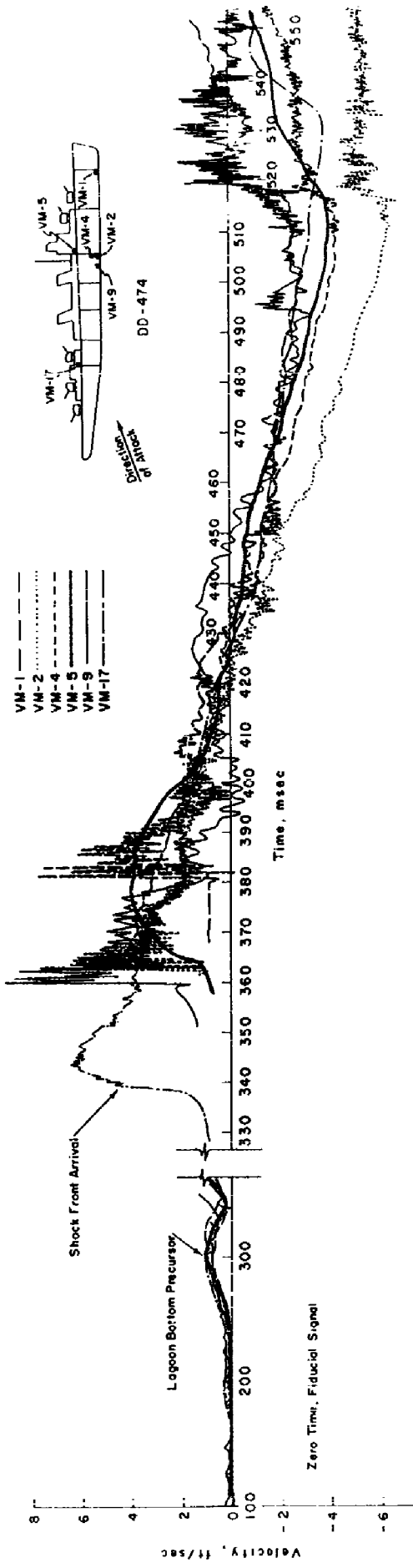

Figure 5.20 Vertical bodily velocities at various locations, DD-474, Shot Umbrella.

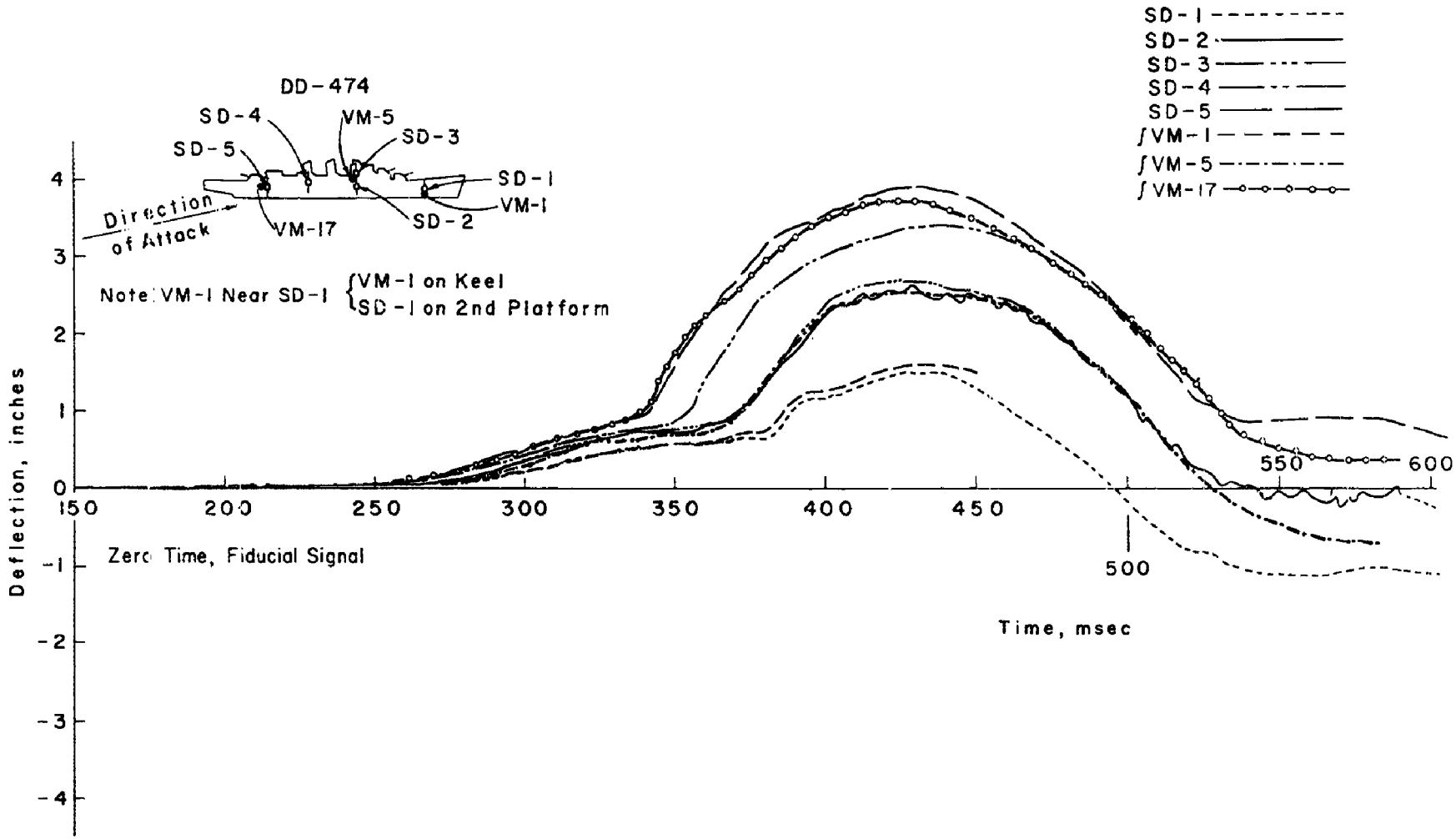

Figure 5.21 Vertical displacements at various locations, DD-474, Shot Umbrella.

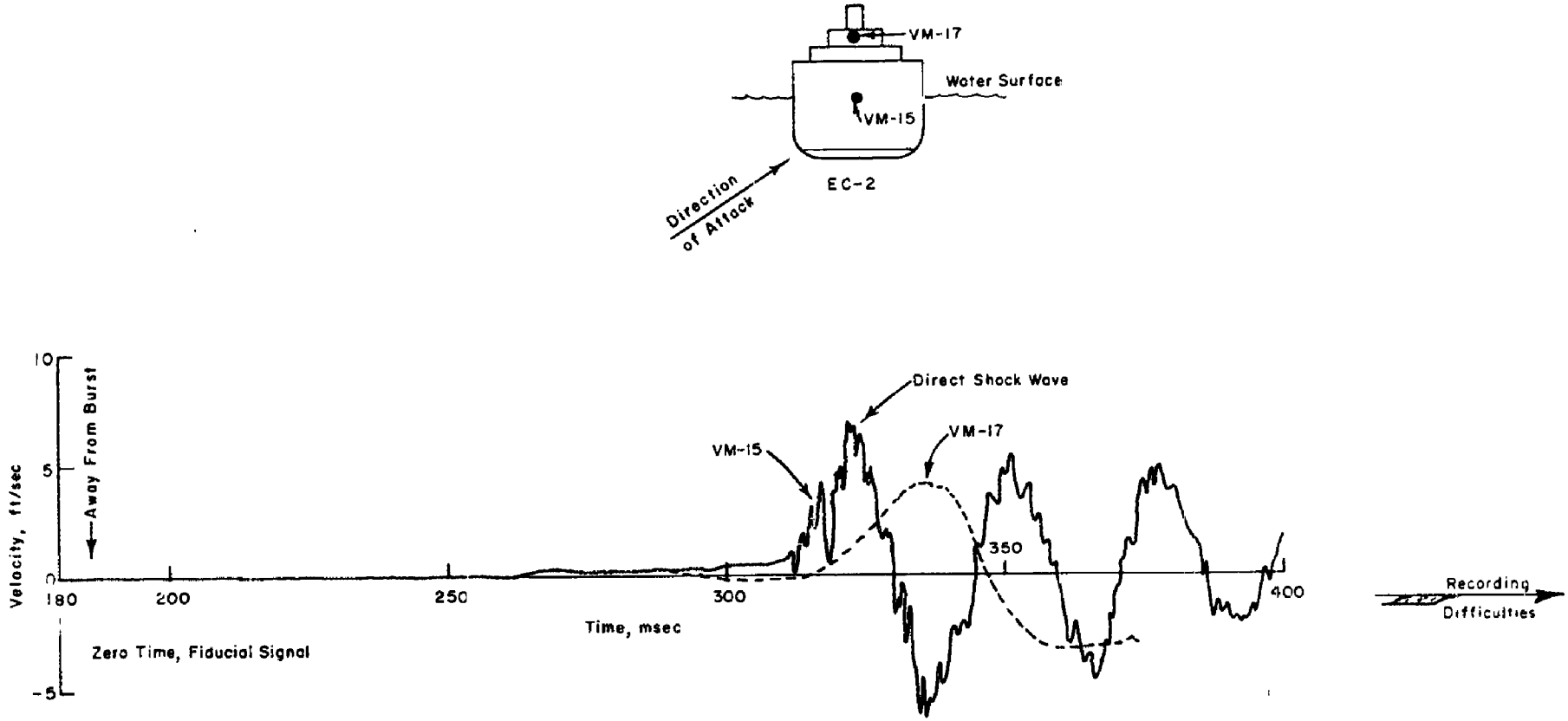

Figure 5.22 Horizontal bodily motion, EC-2, Shot Umbrella.

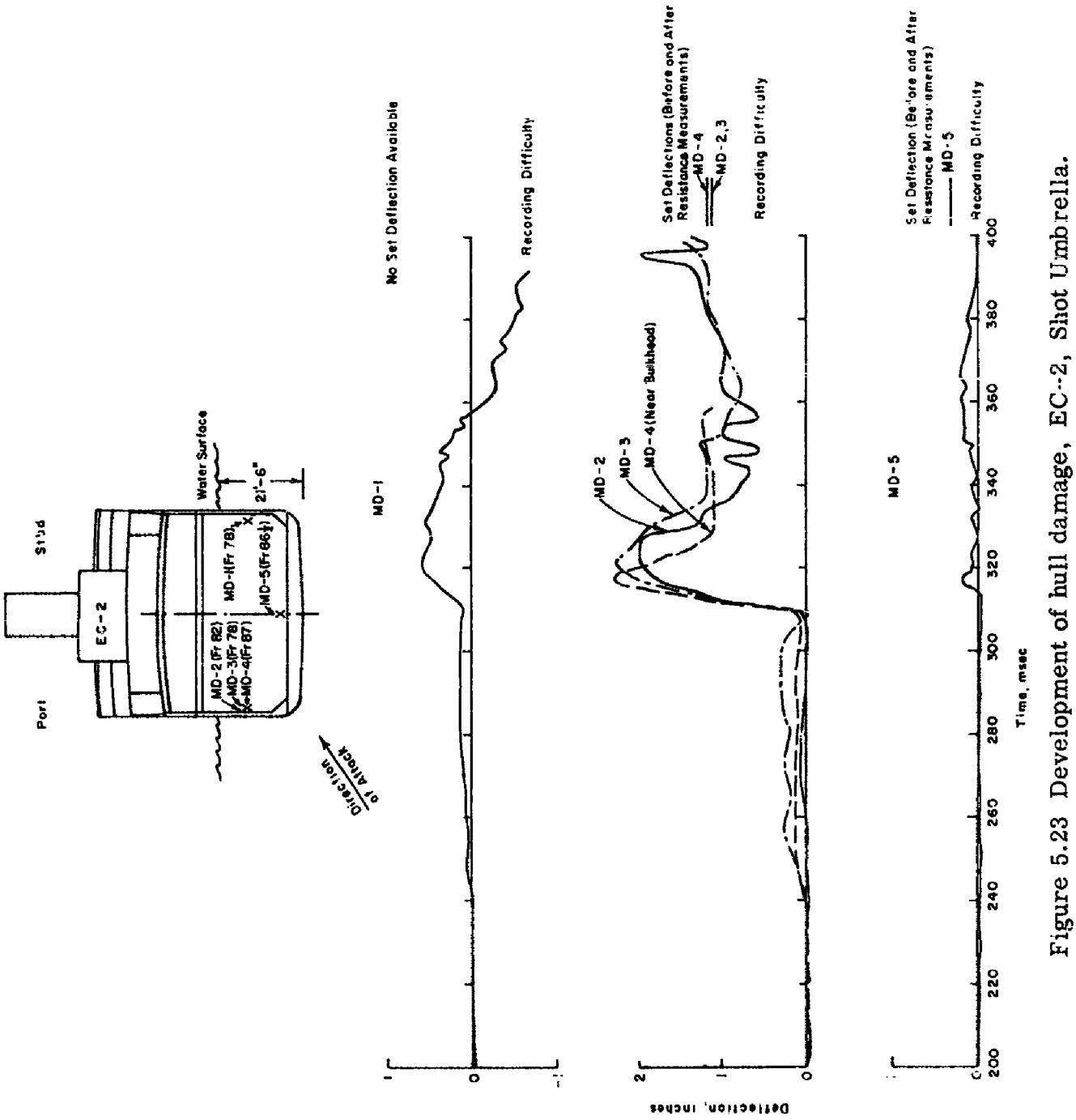

Figure 5.23 Development of hull damage, EC-2, Shot Umbrella.

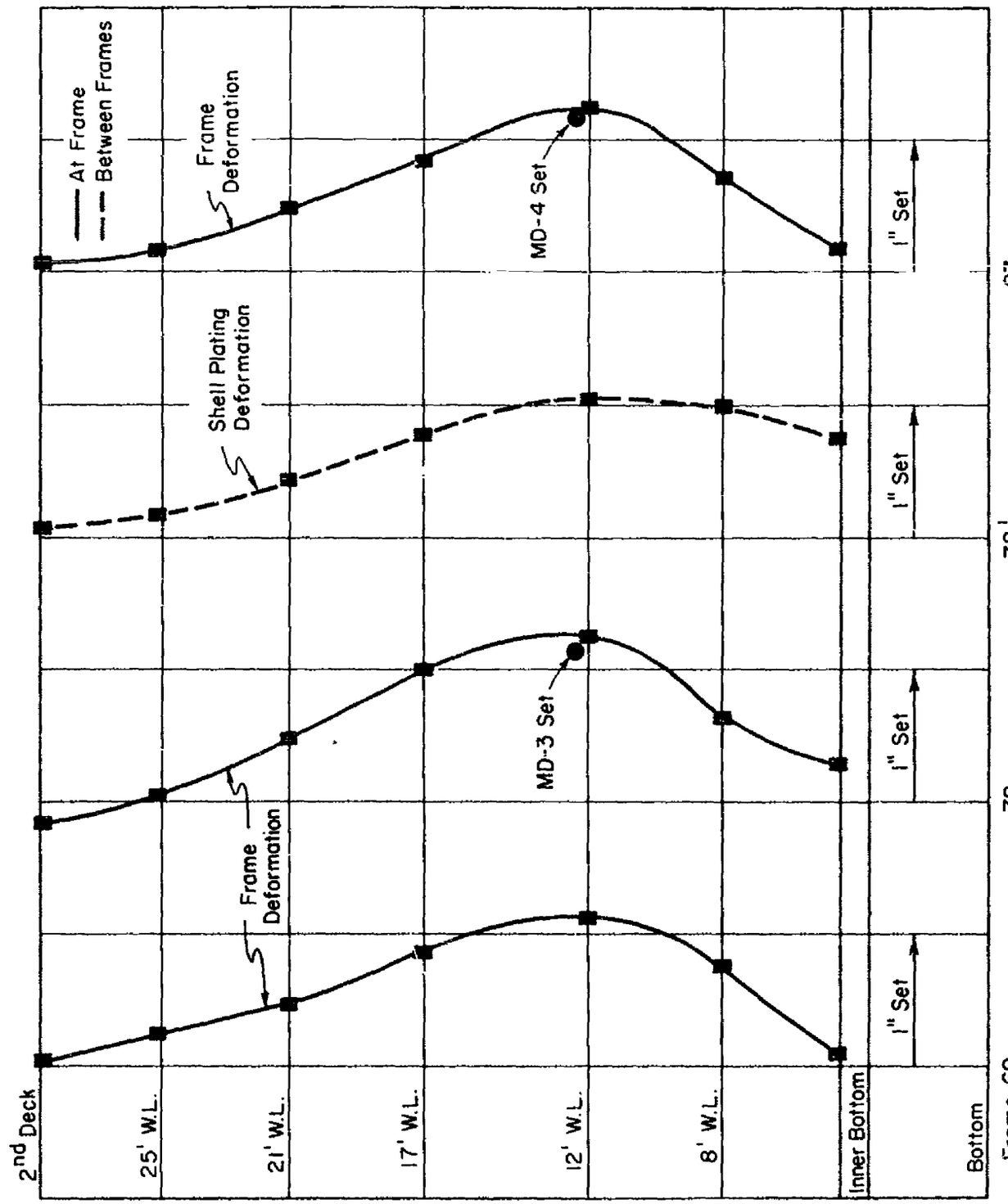

Figure 5.24 Typical vertical port side damage contours in Hold 3, EC-2, Shot Umbrella.

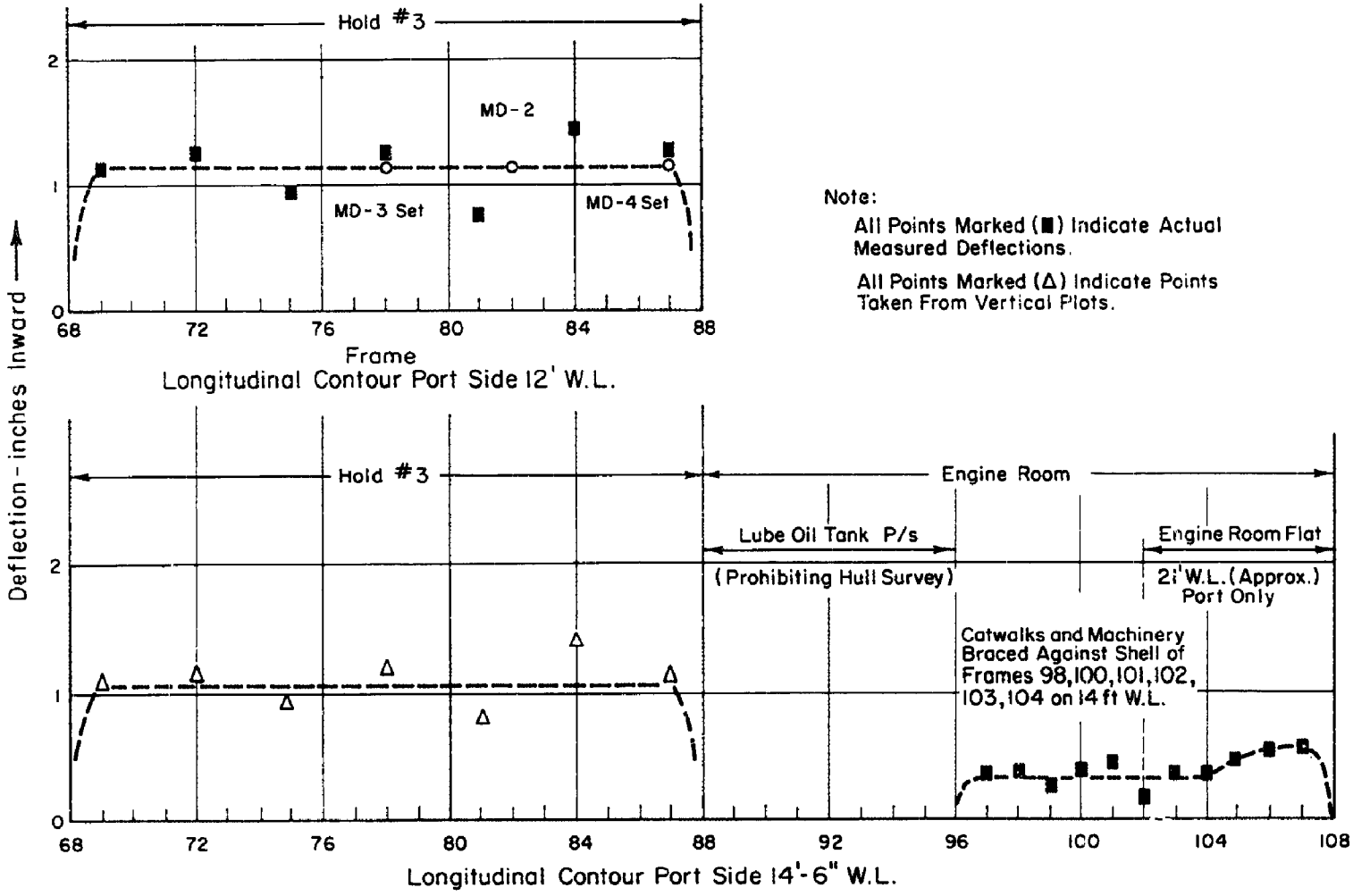

Figure 5.25 Longitudinal damage contours, port (attacked) side, EC-2, Shot Umbrella.

Chapter 6

DISCUSSION, SHOT UMBRELLA

6.1 PRELIMINARY REMARKS

Shot Umbrella was detonated, at a burst depth of 150 feet, at the site indicated in Figure 1.1; the device was placed on the lagoon bottom. A yield of about 10 kt was confirmed by radiochemical analysis of water samples to within sufficient accuracy for present purposes. It was assumed, as for Wahoo, that the underwater effects of this burst were equivalent to those of 6.7 kt of TNT exploded under the same conditions (Reference 11). Sea conditions just prior to detonation time were roughly comparable to those prevailing for Shot Wahoo. The fiducial timing signal supplied by EG&G was estimated to be available at the recording equipment within approximately 250 μsec of detonation; for the purposes of the present report, therefore, the fiducial timing signal represented detonation time.

The underwater pressure and ship response measurements obtained from Shot Umbrella are summarized in Figure 6.1, which also shows key elements of the test array. The project which obtained the results is indicated by number after each type of measurement. Other observations of direct interest to Project 3.4 were also made. It was estimated that isothermal conditions prevailed in the lagoon and that the speed of sound in the water was 5,050 ft/sec. Motion-picture coverage of the accompanying surface phenomena was obtained (Reference 13). Specific observations were made of the water waves produced by the underwater burst in the area of the test array (Reference 14). A survey of target ship damage was made following the test, both equipment damage (Project 3.8, Reference 15) and hull damage (Projects 3.8 and 3.4).

The horizontal distance and heading of the target ships of interest to Project 3.4 were determined in two ways: (1) an aerial photographic survey of the target array made prior to shot time and (2) shock wave arrival time measurements at the ships. Application of the second method is discussed in Appendix B. Evaluation of available data led to the estimates listed in Table 6.1. The ship headings, or orientations, are expressed in terms of rotation from the nominal headings, indicated in Figure 6.1.

Prior to analysis of the loading and response measurements obtained by Project 3.4, an effort was made to adapt Program 1 phenomenological data to a form convenient for application to surface ship targets. The necessary information was supplied by Project 1.1 prior to final publication of its own analysis. The main results of the Project 3.4 evaluation are presented in this section; detailed justifications are presented in Appendix B.

During Shot Umbrella, the most significant underwater loading phase, insofar as effects on surface ships are concerned, was the direct shock wave (Figures 5.1 through 5.3). At the target ships instrumented by Project 3.4, other loading phases were, however, noticeable: the lagoon-bottom precursor pressure wave and the bulk cavitation following the direct shock wave.

The evaluation of the free-water pressure data had the objective of characterizing the direct wave, near the water surface, as a function of range from surface zero. This characterization was accomplished by a description of attack angle, peak pressure, and pressure decay with time.

The attack angles α made at the water surface by the direct shock wave front could not be meaningfully estimated from the experimental arrival-time measurements because of the shallow angles of attack and the associated inaccuracies. Consequently, the nominal geometric attack angles are accepted.

The evaluation of the experimental data (Reference 16) concerning the variation of peak pressure near the water surface with horizontal range from surface zero is shown in Figure 6.2. Peak pressures measured by Project 3.4 are also shown and indicate a good agreement with this evaluation of Project 1.1 data. The peak pressures represent shock-wave pressures: these are essentially absolute overpressure, since precursor pressures were relatively small. Peak pressures vary little with depth, at least down to depths of about 30 feet, the maximum depth of Project 3.4 interest.

Experimental pressure histories near the water surface are of short duration and, for the most part, have the shape illustrated in Figure 6.3. A key quantity characterizing the shape is the equivalent decay time constant, suggested by a comparison with free-water shock waves produced by HE charges. For simplicity two types of approximation were used, as illustrated in Figure 6.3, for the equivalent decay time constant: a lower bound, θ_e, matching the duration, or surface cutoff time, and an upper bound, θ_u, matching the initial slope. Naturally, at any given range from surface zero the equivalent decay time constant varies with depth below the water surface; evaluations of this variation for both types of approximation are given in Figures 6.4 and 6.5. The consequent variation of decay time with range is indicated, for depths of 13 and 22 feet, in Figure 6.6.

Bulk cavitation occurred following the direct shock wave. Observations on bulk cavitation were made from movie cameras mounted on an RB-50 aircraft 25,000 feet above surface zero, from free-water pressure gages (Project 1.1) located at various ranges near the water surface, and from Project 3.4 response gages located on the key target ships.

A presentation of all measurements of bulk cavitation reloading time is given in Figure 6.7. A detailed description of the movie film analysis is given in Appendix B. Examination of this figure reveals that all types of measurement show a remarkable consistency and fall on the curve shown. The dashed curve, representing the direct wave arrival times, is included in Figure 6.7 in order to orient the reader.

Some pertinent information was available concerning phenomena other than the underwater loadings. Water waves generated by the burst were measured at the DD-474 position; these consisted of an 11-foot crest at about 21 seconds, then an 11-foot trough at about 30 seconds, followed by smaller waves (Reference 14). Measurements of the corresponding DD-474 bending strains were obtained by Project 3.4.

An analysis of the Project 3.4 records obtained on the EC-2, DD-474, and DD-592 was carried out in such a fashion as to obtain information concerning the interaction of the direct shock wave with the surface ships, the transmission of the shock throughout the target ships, the bodily motion of the target ships, the development of hull damage in the target ships, and the estimation of safe and lethal hull damage ranges under Shot Umbrella conditions. No analysis of DD-593 records was attempted because of the negligible response levels measured there (Section 5.1).

6.2 INITIAL HULL LOADING AND RESPONSE

The interaction of an incident shock pressure wave with an underwater structure (ship) is understood less well under conditions such as Shot Umbrella than it is under conditions such as Shot Wahoo. Basically, this is due to two characteristics of Shot Umbrella: (1) the incident pressure wave resulted from a nonlinear surface bottom reflection and (2) the attack angle at the water surface was essentially glancing.

One situation in which the interaction phenomena were documented in Shot Umbrella may perhaps be interpreted in a naive way: the interaction of the direct incident shock wave with the EC-2 attack side. Simplifying assumptions made for this particular situation are that the shock wave is normally incident on the EC-2 attack side and that it can be considered a simple shock wave, within the short distances of interest for the interaction with the structure. Under these assumptions it would seem possible that the initial phase of the loading and response can be investigated by means of the Taylor theory in a similar manner to the application to Shot Wahoo. If the incident shock-wave pressure history is characterized by peak pressure and by the equivalent decay time constant introduced in Section 6.1, then the appropriate equations are reproduced below for convenience:

$$v(t) = \frac{p_m}{\rho c} \sin\beta\, e^{-t/\theta} \frac{1}{z' - 1} \left[e^{t/\theta\ (z'-1)/z'} - 1 \right] ; \quad t \le t_c .$$

Where:

$v(t)$ = velocity response normal to plane of structure

$z' = z \sin\beta$

β = angle between incident ray and tangent to structural element of interest

$z = \frac{m}{\rho c \theta}$

m = mass/area of structural element

ρ = water density

c = speed of sound in water

p_m = peak pressure

θ = equivalent decay time of shock wave

$t_c = z'/(z'-1)\ \theta\ \ln z'$ (t_c is the time at which the loading pressure vanishes and is sometimes called the cavitation time)

At times greater than cavitation time t_c, the above relationship ceases to have physical meaning. In applying this equation to the EC-2 attacked side, consideration had to be given to the choice of equivalent decay time constant θ that best represented the experimental incident shock-wave pressure history (see Figure 6.3 for an example of a nearby pressure history) up to cavitation time, keeping in mind that the cavitation time itself depends on θ. A trial calculation indicated that choice of the upper bound θ_u, 2.5 msec at the EC-2, would yield $t_c \cong 0.4$ msec and, hence, that this choice gave the best representation of the pressure history. The resulting calculation of the expected velocity history of the EC-2 attacked side is shown in Figure 6.8. The pertinent quantities utilized in the theoretical computation were taken from Section 6.1, except for the plate weight per unit area; for this quantity 41.5 psf was used, since this represents an average weight distribution of both shell plating and stiffeners. The only pertinent measurement secured during Shot Umbrella was that of the velocity response of the attacked side (VM-10). This response measurement is therefore reproduced in Figure 6.8, with a rather expanded time scale; the baseline of this record was adjusted so that the velocity shown represents the increase in velocity, above the level established by the precursor, caused by the shock wave. The agreement of the theoretical and experimental velocity histories is good and is considered encouraging for this type of naive treatment.

Most of the experimental data secured in Shot Umbrella covering the interaction

phenomena pertained to loading and response measurements on the bottoms of the ship hulls. Under the nearly glancing incident attack angles obtained in Shot Umbrella, the Taylor theory is, of course, no longer a useful tool. Under these conditions the empirical rules formulated to predict peak velocities reached by the structural element under Shot Wahoo conditions (see Reference 6, and the corresponding discussion for Shot Wahoo) may conceivably be useful for Shot Umbrella if two simplifying conditions hold: (1) the structural element is of the type in which structural restraint forces can be neglected for time periods of interest, and (2) the attack is not so glancing that the structural response depends on the pressure level p_m in a nonlinear way. Actually, the last assumption can hardly be true and the empirical rule is introduced merely in the hope that, at pressure levels of interest, the deviation from linearity is not overwhelming.

The empirical rule is reproduced below:

$$v_m = 2\frac{p_m}{\rho c}\ \frac{1 + \sin\beta}{2}\ f_1(z)\ f_2\left(\frac{t_s}{\tau}\right)$$

where the basic variables have been previously defined (Section 4.2) and the empirical functions f_1 and f_2 are given in Reference 6. In view of the lack of previous experience in applying this rule to a situation like Shot Umbrella a somewhat arbitrary procedure was used. It had been previously hypothesized (Reference 6) that the characteristic time τ, although insensitive to the shock wave decay time for long shock waves, decreased with decay time for short shock waves; indeed, it had been suggested that τ might be approximately equal to the Taylor cavitation time t_c for normal incidence. Acceptance of this interim notion led to the conclusion that, under Shot Umbrella conditions, $f_2 \simeq 1$. With this guiding philosophy, bottom peak velocities were computed from the rule and are presented in Figure 6.9 as a function of range; the indicated range of values corresponds to the use of upper and lower bound estimates for the decay time constant. Corrections to account for variations in draft and differences between end-on and side-on attacks were not made, in view of the considerable uncertainty in applying the small amount of information available on these questions (Reference 8) to Umbrella conditions.

Experimental information on the interaction between the direct shock wave and the bare hull structure of the EC-2 bottom is best described experimentally by VM-14, located relatively far from heavy masses; this was demonstrated in Section 4.2. The peak velocity jump measured by VM-14 was 12 to 14 ft/sec, a value noted on Figure 6.9 where it compares well with the estimate made on the basis of the empirical rule.

Experimental evidence on the interaction between direct shock wave and the bare hull structure of the DD's is available at several locations on DD-474 and DD-592. That these locations on the keel at midsections of the DD's may indeed be considered elements of the bare hull was demonstrated in Section 4.2, the discussion for Shot Wahoo. However, a demonstration that a similar behavior exists in the case of Shot Umbrella is made in Figure 6.10 for DD-474; a comparison is given between VM-14 and the velocity to be expected from the loading impulse computed from PE-6 on the basis that only the mass (a weight per unit area of 90 psf) controls the response. The levels of both velocity and pressure records were adjusted to make them relative to the repcursor. The comparison shown in Figure 6.10 again illustrates that for the first 2 msec, or so, structural restraint forces may be neglected at such locations on the DD's. Peak experimental jump velocities at bare hull portions of the DD bottoms were: 7.1 to 8.2 ft/sec for DD-474 and 2 to 2.8 ft/sec for DD-592. The values are entered into Figure 6.9 and indicate reasonably good agreement with the computed values. The largest deviation occurs for DD-474, attacked end-on: this would not exist at all if the same type of adjustment for the end-on computed curve had been made as for Shot Wahoo.

The general agreement of the experimental peak bottom velocities at bare hull sections with the computed values in Figure 6.9, while encouraging, should not be considered a proof that the interpretation difficulties implicit in the empirical rule are, indeed, completely clarified by the somewhat arbitrary procedure employed; the role of coincidence in producing agreement is difficult to judge without more information. At any rate, from a pragmatic point of view it seems reasonable to utilize the computed curve at least as a device for interpolating and extrapolating experimental values to other ranges of general interest.

Peak bottom velocities measured in Shot Umbrella again show a dependence on the precise location of the meter, whether mounted on the bare hull or mounted near heavy masses or bulkheads. This is demonstrated in Table 6.2 where all information accumulated by Project 3.4 in Shot Umbrella on ship bottom velocity responses is listed. Note that the term "velocity jump" is employed in referring to the initial velocity response. This term is defined in the same way as in Section 4.2, under the Shot Wahoo discussion. Again, as in Shot Wahoo, no systematic dependence on position along the length of the ship was noted; valid information on variation over the ship width was too sparse to justify any conclusion in this direction.

6.3 VERTICAL SHOCK TRANSMISSION UPWARD THROUGH SHIP

During Shot Umbrella, the transmission of shock motions from the hull upward through the bulkheads was similar to that for Shot Wahoo. Examination (Figures 5.15 and 5.16) of the early portions of velocity records obtained at meters located upward along the vertical centerline of bulkheads suggests essentially the same crude empirical conclusions as in the case of Shot Wahoo: (1) bulkhead peak velocities are of similar magnitude regardless of location, (2) the time to reach peak velocity for locations along the bulkhead increases with height of location above the bottom, and (3) average initial acceleration, for locations along the bulkhead can decrease, with height above the bottom by factors of 10, because of the corresponding increase in times to reach peak velocities. The above empirical conclusions pertain to the response due to the direct shock wave itself. In Shot Umbrella, where response levels to the lagoon-bottom precursor waves were relatively significant, it can be observed that the response to the precursor is essentially independent of location. Thus the increase in time to reach peak velocity with height of bulkhead location above the bottom is limited to the direct shock wave itself, i.e., it is associated with the steep front of the shock wave (hardly a surprising conclusion).

The manner in which shock motions are transmitted from the bulkheads, and from the sides, to decks is complicated by the many equipment items fastened to the deck. An example, is, however, suggested by the comparison over a long time period of two velocity histories mounted in the sea cabin of the DD-474 superstructure (Figure 5.17); one velocity meter was mounted directly over the bulkhead and one was mounted to an adjoining deck plate. As might be expected, the deck plating lags the bulkhead response rather systematically. Moreover, it is hardly surprising to note the superimposed vibration shown by the deck plate velocity meter VM-7; this suggests that the natural frequency of the plate in this particular area is about 55 cps.

6.4 BODILY MOTION OF SURFACE SHIPS

The analysis of bodily motion in Shot Umbrella is restricted to the EC-2 and DD-474; response levels on the DD-592 and DD-593 were too low to allow a profitable pursuit of this matter for these ships. Observations could be made on the response to the lagoon-bottom precursor, the direct shock wave, and the surface waves generated by the burst. With respect to the response to the direct shock wave, information was available on heaving,

pitching, and horizontal motion. Of all these, the heaving motion in response to the direct shock wave was the best documented and the most significant.

The character of the vertical surface-ship response to the precursor pressure wave can be seen in Figures 5.18 to 5.21. Note that the magnitude of this response, although smaller than that due to the direct shock wave, is appreciable. Moreover, note that the response distribution throughout each ship is roughly uniform. Both velocity and displacement essentially increase gradually until shock front arrival; the DD-474 velocities show a dip but rise once more to reach about their maximum level just prior to the shock front arrival. For the EC-2 maximum responses to the precursor wave were about 2.5 ft/sec and 1.3 inches for heaving velocity and displacement, respectively. Corresponding measurements for DD-474 were about 1 ft/sec and 0.5 to 0.8 inch. The response to the precursor pressure wave is so gradual that it can hardly be considered to have practical implications for surface ships. For example, maximum accelerations are less than 1 g.

The vertical responses to the direct shock wave were measured at representative locations in the target ships. Although these differ in their initial detailed characteristics, they suggest a similar gross behavior when examined over relatively long periods of time. A simple examination of a number of superimposed response measurements, therefore, gives a good impression of the overall vertical bodily motion of the surface ships. This is particularly true of side-on attacks, and key evidence in this response has already been presented in Figures 5.18 and 5.19.

Examination of Figure 5.18 suggests that the vertical bodily motion of the (side-on) EC-2, caused by the direct shock wave, can be described in simple terms; an increase in velocity of 6 to 7 ft/sec due to the shock wave established a total initial velocity of 8.5 to 9.5 ft/sec and thereafter the velocity decreased at constant deceleration (2.2 to 2.7 g) until cavitation reloading; cavitation reloading itself was not observed on Project 3.4 records because of recording difficulties.

The vertical bodily motion of the EC-2 in Shot Umbrella is strikingly similar to that observed in Shot Wahoo and suggests that, despite the far more complicated character of the Shot Umbrella situation, the surface layer concept discussed in Section 4.4 is generally applicable. The water layer thickness at the EC-2 position was estimated, from the observed deceleration, to be about 20 to 30 feet, probably in excess of the EC-2 draft.

Looking at the vertical bodily motion of the EC-2 in terms of displacements provides some opportunity to deepen the understanding of this motion. A typical displacement history of the EC-2 is SD-2 (Figure 5.19), and this displacement history is reproduced for convenience in Figure 6.11. The surface layer concept was employed to compute the displacement, based upon the values of initial bodily velocity and surface layer thickness quoted above; the results are also shown. The computed curves allow an estimate of the later motion and, in particular, an estimate of cavitation reloading time. Conditions existing in the main body of water are, of course, far more complicated in Shot Umbrella than in Shot Wahoo. However, rough calculations suggest that the expanding gas bubble itself has a negligible influence, via the resultant upward swelling of the main body of water, on the cavitation reloading time at the EC-2 position. Moreover, it hardly seems conceivable that the upward swelling of the water caused by the precursor pressure wave continues. Therefore, the surface layer concept in the Shot Umbrella case would suggest crudely that cavitation reloading occurs when the bodily displacement has returned to zero at a time 230 to 255 msec. This is in reasonable agreement with the experimental cavitation reloading time of 245 msec (Figure 6.7).

The direct shock wave gave rise to a vertical bodily response of DD-474, attacked end-on rather than side-on, which was obviously complicated by pitching (Figures 5.20 and 5.21). The character of the motion was investigated by utilizing the displacement measurements to construct displacement contours at various times (Figure 6.12). Clearly, DD-474

vertical motion is predominantly composed of heaving and pitching; no significant excitation of the flexural, or whipping, modes was observed as a result of the end-on attack (see also, Figure 5.2 in this connection). If the pitching is characterized by the relative displacement of the bow with respect to the center of gravity (Frame 103½), then the pitching history is characterized by the dashed curve shown in Figure 6.13. The heaving history (the vertical motion of the center of gravity) is characterized by the solid curve.

Further insight into the bodily motion of DD-474 can be gained by replotting the observed velocity and displacement histories at each of three sections where measurements were obtained in such a fashion as to line up the shock-wave arrival times; the three sections were Frame 146, Frames 72 through 82, and Frame 18. The results are shown in Figures 6.14 through 6.16. Notice that selected typical velocity histories have been integrated to demonstrate the degree of consistency with displacement measurements. To a first approximation, each section of the ship can be viewed as undergoing vertical bodily motion independently of the remaining sections and the motion of each section is therefore discussed separately.

The DD-474 aft section response (Figure 6.14) suggests that the increase in vertical velocity (4.5 ft/sec) due to the shock wave establishes an initial bodily velocity of 5.5 to 6 ft/sec and that thereafter the velocity decreases at constant deceleration (1.9 g) until cavitation reloading at 195 msec. The surface layer thickness suggested by the surface layer concept is 35 to 42 feet. A computed displacement history, based on the surface layer concept, is also shown in Figure 6.14 and indicates fair agreement with the measured displacement, if any possible upward swelling of the main body of water is neglected.

The DD-474 midsection response (Figure 6.15) suggests that the increase in vertical velocity (3 to 3.5 ft/sec) due to the shock wave establishes an initial velocity of 4 to 5 ft/sec and that thereafter the velocity decreases at constant deceleration (1.8 to 2 g) until cavitation reloading at 155 msec. The corresponding surface layer thickness is 37 to 50 feet. Again, a computed displacement history, based on the surface layer concept, shows fair agreement with the measured displacements (Figure 6.15).

A similar evaluation of the DD-474 forward section response (Figure 6.16) leads to a velocity increment of 2.7 to 3.2 ft/sec, an initial bodily velocity of 3.5 to 4 ft/sec, a deceleration of 2.1 to 2.3 g, a reloading time of 130 msec, a surface layer thickness of 29 to 37 feet, and a computed displacement history in reasonable agreement.

As in Shot Wahoo it is useful to compare initial vertical bodily velocity to the water particle velocity v_{wp}; under Shot Umbrella conditions, however, it seems advisable to define water particle velocity by a slight generalization of the definition utilized in Shot Wahoo. At any pressure gage location, the experimental impulse is a direct measure of the average vertical velocity of the water particles lying above the gage:

$$v_{av,\ h} = \frac{I_h}{\rho h}$$

Where:

$v_{av,\ h}$ = average vertical velocity of water particles above gage depth, h

I_h = shock wave impulse at gage position ($\int_o^{t_s} p\,dt$) measured from shock-wave arrival ($t = 0$) to surface cutoff time (t_s), and

ρ = water density

The water particle velocity is defined as:

$$v_{wp} = \lim_{h \to o} \frac{I_h}{\rho h} .$$

Notice that, under conditions such as Shot Wahoo in which neither the free-water surface nor the bottom influences the character of the direct shock wave up to surface cutoff time, the impulse reduces at shallow depths roughly to $p_m t_s$, where $t_s \simeq (2/c)\ h \sin \alpha$, and the above definition of water particle velocity becomes identical to that introduced previously in Section 4.4.

The method by which the experimental data (given in Reference 16) was interpreted, so as to yield the indicated limits, is illustrated in Figure 6.17 where the quantity $I_h/\rho h$ is plotted as a function of depth at several ranges of interest. It may be noted (Reference 16) that precursor pressures do not contribute appreciably to the impulse. The experimental results essentially fall in straight lines; as illustrated in the figure, these were extrapolated to the surface and the limit values were utilized for estimates of water particle velocity. The consequent variation of water particle velocity with range from surface zero is shown in Figure 6.18.

The experimental values of vertical bodily velocity, both the initial bodily velocity and the velocity increment due to the shock wave, are plotted in Figure 6.18 for comparison with the water particle velocity. That the initial bodily velocity is higher than the water particle velocity is hardly surprising, since the bottom precursor contributes to the former but not significantly to the latter. That the incremental initial bodily velocity tends to be somewhat less than the water particle velocity may be explained by the surface layer concept; the layer depth at both ships is about 20 to 40 feet and reference to Figure 6.17 therefore suggests that, for such a depth, the average layer velocity increment (and, hence, the ship velocity increment) should be lower than the water particle velocity, by about a corresponding amount.

The bulk cavitation reloading times deduced over a width range in Section 6.1 may be used to compute surface layer thickness over a similar range if estimates of initial bodily velocity based on Figure 6.18 are employed. Noting that precursor velocities tend to be about a third of incremental bodily velocities, initial bodily velocity was estimated by multiplying water particle velocities by a factor of $1^1/_3$. It is convenient first to translate the absolute cavitation reloading times (Figure 6.7) into times relative to shock wave arrival (Figure 6.19). The method of computing surface layer thickness was essentially identical to that previously used for Shot Wahoo. Final surface layer thickness estimates are presented in Figure 6.20 where experimental values directly deduced from surface ship decelerations are also shown for comparison.

The vertical bodily response produced in Shot Umbrella surface ships by bulk cavitation closure could only be estimated crudely for DD-474 (Figures 6.14 through 6.16). It appears that reloading caused by bulk cavitation closure gave rise to an incremental bodily velocity almost as large as that caused by the direct shock wave but that the accompanying accelerations were less than 0.5 those associated with the direct shock wave.

The available evidence on horizontal bodily motion of the target ships is limited to the EC-2. Two horizontal velocity meters were located on the bulkhead, one near the vertical center of gravity and one up in the superstructure. The records secured have already been shown in Figure 5.22. VM-15 shows a superimposed vibration with a natural frequency of about 30 cps which completely obscures the horizontal bodily motion of the ship. VM-17 shows a motion which, although it has possible shear and rolling components superimposed, is believed to be much closer to the actual horizontal motion of the ship itself. It is therefore estimated that the peak horizontal velocity of the EC-2 was about 4 ft/sec. This amounts to about 60 percent of the peak incremental vertical velocity, or about 45 percent of the peak absolute vertical bodily velocity. The horizontal bodily motion of the EC-2, however, obviously had a different character from that of the vertical motion. For the first 30 msec or so following shock wave arrival, the ship acquired a horizontal velocity away from the burst

and suffered a maximum horizontal displacement of 0.8 inch, 10 to 15 percent of the peak vertical displacement. Subsequently, the ship acquired a velocity toward the burst that was about equal in magnitude to that previously measured away from the burst.

The surface waves generated by the burst gave rise to a response at DD-474, attacked end-on, which was measured by two strain gages attached to the main deck (centerline) in such a way as to record longitudinal bending strains at approximately the node and antinode positions for the first (two noded) flexural vibration mode of the ship (Figure 5.2). The strain gages measured the quasi-static bending of the ship in response to the surface waves. The first mode flexural vibration period of a DD is about 0.5 second; the measured strains were about equal at the node and antinode locations; and the strain histories are similar to the surface-wave histories (Reference 14). Taking the neutral axis for longitudinal bending at a height of 15 feet above the keel, it was estimated that the maximum girder (keel) strain caused in the DD-474 by a 22-foot surface wave (crest to trough) was about 300 μin/in.

6.5 HULL DAMAGE

The hull damage to the EC-2 in Shot Umbrella was strikingly similar to that in Shot Wahoo. Again, the only appreciable damage occurred to the attacked side (port for Shot Umbrella, starboard for Shot Wahoo). The port side had been left essentially undamaged as a result of Shot Wahoo.

The results of deflection measurements of the starboard frame deformation at a depth of about 9 feet below the water surface are shown in Figure 5.23. The character of the attacked side frame deflection history may be summarized thusly: an initial peak deflection of 2.2 inches was achieved in about 10 to 15 msec following the shock wave arrival. An outboard movement then ensued which reduced the deflection level to about 1 inch. The level deflection shown by the deflection gages after the response to the shock wave agrees fairly well with the set deflections measured from these gages after the test; this implies that the EC-2 hull damage was caused by the shock wave alone. The maximum set deflection of the attack-side frame was approximately 1.1 inch. The above description of the deflection history parallels that of Shot Wahoo in every respect, except for minor changes in the numerical values.

Once again, the energy-density rule introduced in previous small-scale EC-2 model tests (Reference 6) may be checked, this time with a distinctly different type of experimental situation from previous applications. The shock-wave energy flux density is estimated, at several depths below the water surface, as a function of range in Figure 6.21; experimental values from Reference 16 were utilized, as were some extrapolations. Reference to Figure 6.21 indicates that the estimated shock wave energy flux density at the EC-2 position at a depth of 9 feet is 17.5 ft-lb/in^2. The application of the rule discussed in Section 4.5 therefore yields a predicted peak deflection of 5.6 inches—a value in excess of the experimental peak deflection by 150 percent.

Although the comparison of experimental peak deflection with the rule is not as good as it was in the case of Shot Wahoo, it must be recognized that the situation for Shot Umbrella is considerably more uncertain for several reasons. First, although considerably more experimental measurements were obtained in Shot Umbrella than in Shot Wahoo, few were obtained at the shallow depths of interest for surface ship response. Therefore, the extrapolations which led to the curves shown in Figure 6.21 are subject to some uncertainty.

Second, in applying the empirical rule, the value of shock wave energy flux density to be utilized is an average of free-water shock wave energy flux density over the vertical expanse of the entire side (between the inner-bottom level and the water surface); this averaging is done automatically for long shock-wave attacks, such as Shot Wahoo, by choosing the value

of the midpoint of this vertical expanse. In the Shot Umbrella situation the average energy density may differ from this; sufficient experimental evidence to judge the significance of this is not available.

Third, it seems rather unlikely that the side-frame deformation is appreciably influenced by the precursor pressures occurring before the direct shock wave, and it seems possible that only the pressure increase over and above the precursor level has significance. The energy that is shown in Figure 6.21, of course, reflects the Project 1.1 procedure of computing energy from total overpressure (above hydrostatic values); the alternate procedure of computing energies from pressure in excess of the precursor level would have reduced the energy estimates by perhaps 15 percent.

Considering the uncertainties peculiar to Shot Umbrella, together with the suggestion made in Section 4.5 that a larger fraction of the total deformation energy is represented by plate dishing when the frame deformation is small than when it is large (the situation for the model tests), the degree of agreement of experimental peak deflection and empirical rule is judged to be acceptable. Certainly from a practical point of view it appears that the empirical energy-density rule is a useful tool in estimating hull damage under Shot Umbrella conditions, as well as under Shot Wahoo conditions.

The survey (Figures 5.24 and 5.25) of the final EC-2 hull damage after Shot Umbrella leads to conclusions very similar to those of the Shot Wahoo damage survey. The maximum frame deformation (on the attack side) was again at about the MD gage locations. Structural attachments reduced the degree of damage noticeably. The shell plating dished between frames and the amount of this dishing increased with depth below the water surface until the inner-bottom level was reached. Just above the inner bottom the maximum dishing between frames amounted to about 1 inch.

6.6 LETHAL HULL DAMAGE RANGES

The energy flux density rule allows the lethal damage range for merchant ships under Shot Umbrella conditions to be estimated. As in the case of Shot Wahoo, plausibility arguments are introduced to derive conclusions concerning lethal hull damage ranges for destroyers as well. Some verification of these estimates can be obtained in Shot Umbrella by the introduction of an equivalent shock factor based on the peak pressure and the equivalent decay time constant of the direct shock waves and an appeal to HE experience relating shock factor with hull damage ranges.

For merchant ships (EC-2), the energy flux density rule and the damage criteria introduced in Section 4.7 suggests that at a depth of 9 feet a critical value of energy flux density is about 75 ft-lb/in^2. Lethal hull damage will therefore be caused to merchant ships under Shot Umbrella conditions at ranges of 1,200 feet or less.

Applying the same argument for predictions of lethal hull damage ranges for destroyers outlined for Shot Wahoo in Section 4.7, the lethal hull damage to DD's will occur under Shot Umbrella conditions at ranges of 1,200 feet or less.

As remarked in Section 6.1, the short shock wave produced in the Shot Umbrella situation is reminiscent of the pressure waves produced by HE charges. It was for this reason that the direct wave pressure measurements were evaluated in terms of an equivalent decay time constant. The shock factor used in HE test analysis to relate attack severity with surface ship hull damage, actually the maximum shock factor (S. F.) is defined by:

$$\text{S.F.} = \sqrt{W/R}$$

Where:

W = charge weight in pounds of TNT

R = distance from the charge center to the nearest point on the hull

The maximum shock factor can equally well be expressed in terms of peak pressure and decay time constant, as

$$\text{S.F.} = 3.11 \times 10^{-4} \ (p_m)^{0.35} \ (\theta)^{0.5}$$

Where:

p_m = peak pressure, psi

θ = decay time constant, msec

In Shot Umbrella, use of an equivalent decay time constant allows the introduction of an equivalent maximum shock factor. Needless to say, however, the word "equivalent" should be interpreted with some caution. For example, the typical HE charge produces local damage as compared to the wide spread damage caused by nuclear attack.

Now, HE experience with surface ships suggests that, for side attacks with charge depths less than venting depth (to restrict attention to the shock wave effects above), lethal hull damage will result at a maximum shock factor of 0.8 to 0.9 for both merchant ships and destroyers. Application of this HE experience to Shot Umbrella, by use of Figure 6.22, leads to an estimate of 1,100 to 1,400 feet for the greatest range at which lethal hull damage results to merchant ships and destroyers under Shot Umbrella conditions.

The close agreement between the two methods of estimating lethal hull damage ranges provides some confidence in the accuracy of the estimates. It should, incidentally, be realized that the comparison between these two methods is a comparison of different criteria, rather than a comparison of two basically different methods. In fact, the maximum shock factor, as used in typical HE attack conditions, is a direct measure of shock-wave energy flux density; roughly speaking, shock wave energy flux density is proportional to the square of the maximum shock factor.

It may have been noticed that attention in the above discussion is restricted to the direct shock wave effects; possible effects of the surface waves generated by the burst are neglected. That the surface waves have no significant effect on the lethal hull damage range, under Shot Umbrella conditions, is felt to be justified by the estimate, based on Reference 14, that at 1,200-foot range the surface wave crest-to-trough height is less than 35 feet.

6.7 SAFE HULL DAMAGE RANGES

As in Shot Wahoo (Section 4.8), safe hull damage for merchant ships is arbitrarily defined to be that amount of hull damage which was sustained by the EC-2 in Shot Wahoo. Since the same amount of damage was sustained by the EC-2 in Shot Umbrella, this leads, by definition, to the estimate that safe hull damage ranges for merchant ships under Shot Umbrella conditions are 1,700 feet or more.

Employing the same criterion as applied in Shot Wahoo, an estimate of the minimum safe hull delivery range for DD's under Shot Umbrella conditions is 1,700 feet. It is interesting to notice (Figure 6.22) that the equivalent maximum shock factor at this range is 0.34 to 0.52. HE test experience would suggest that this estimate is about the right order of magnitude.

TABLE 6.1 SHIP LOCATION AND ORIENTATION, SHOT UMBRELLA

Ship	Standoff *	Orientation †
	feet	degrees
EC-2	1,700	7
DD-474	1,900	6
DD-592	2,950	−8
DD-593	7,800	−7

*Standoff to midship position, rounded off to nearest 50 feet.

† Angle of ship heading (positive clockwise) from nominal orientation indicated in Figure 6.1.

TABLE 6.2 INITIAL VERTICAL VELOCITY JUMP, BOTTOM HULL, SHOT UMBRELLA

Gage Location	Experimental Velocity Jump (ft/sec)	
	Centerline Location	Off Centerline Location
EC-2 Shock Wave		
Frame 98 Starboard (VM-9A)		8 to 9.5
CL(VM-7A)	8 to 10	
Port (VM-8)		–
Frame 92½ near CL(VM-14)	12 to 14	
Frame 88 Starboard (VM-3)		5
near CL(VM-1)	7 to 9	
Port (VM-2)		6 to 7
DD-474 Shock Wave		
Frame 120½ CL(VM-14)	7.1	
Frame 119 near CL(VM-15)	8.2	
Frame 82½ CL(VM-6)	6.3	
Frame 81 near CL(VM-9)	7.4	
Frame 72 CL(VM-2)	5.4	
DD-592 Shock Wave		
Frame 120½ CL(VM-14)	2.8	
Frame 82½ CL(VM-8)	2.5	
Frame 81 near CL(VM-9)	2.0	
Frame 72 CL(VM-2)	2.5	

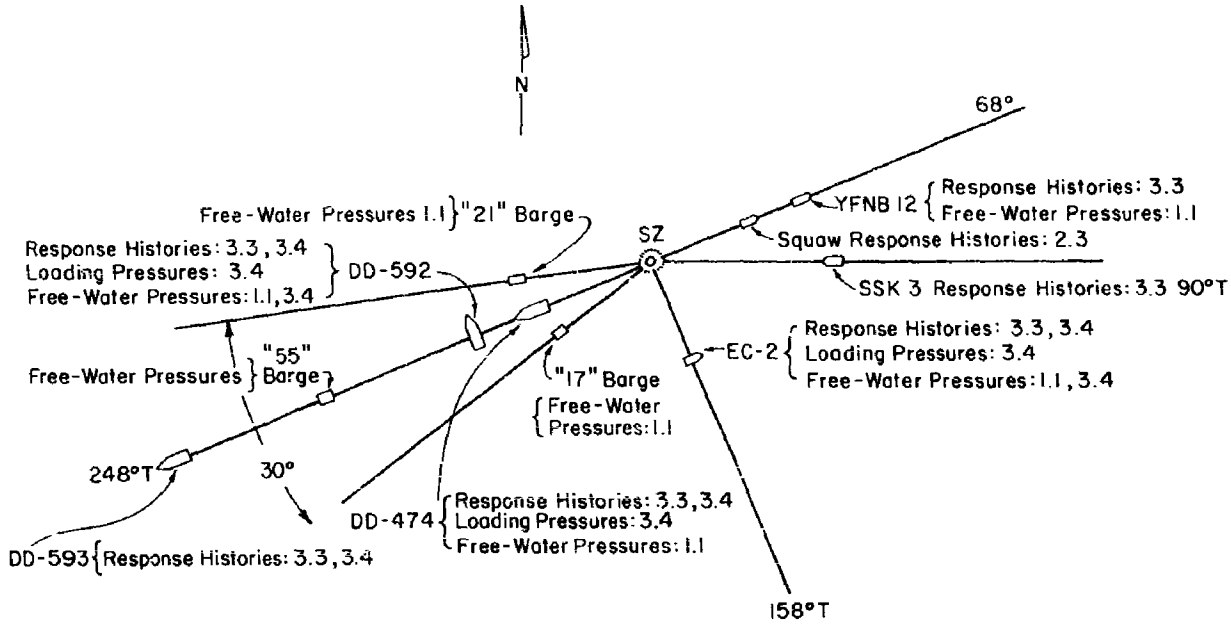

Figure 6.1 Target array and summary of underwater pressure and ship response measurements, Shot Umbrella.

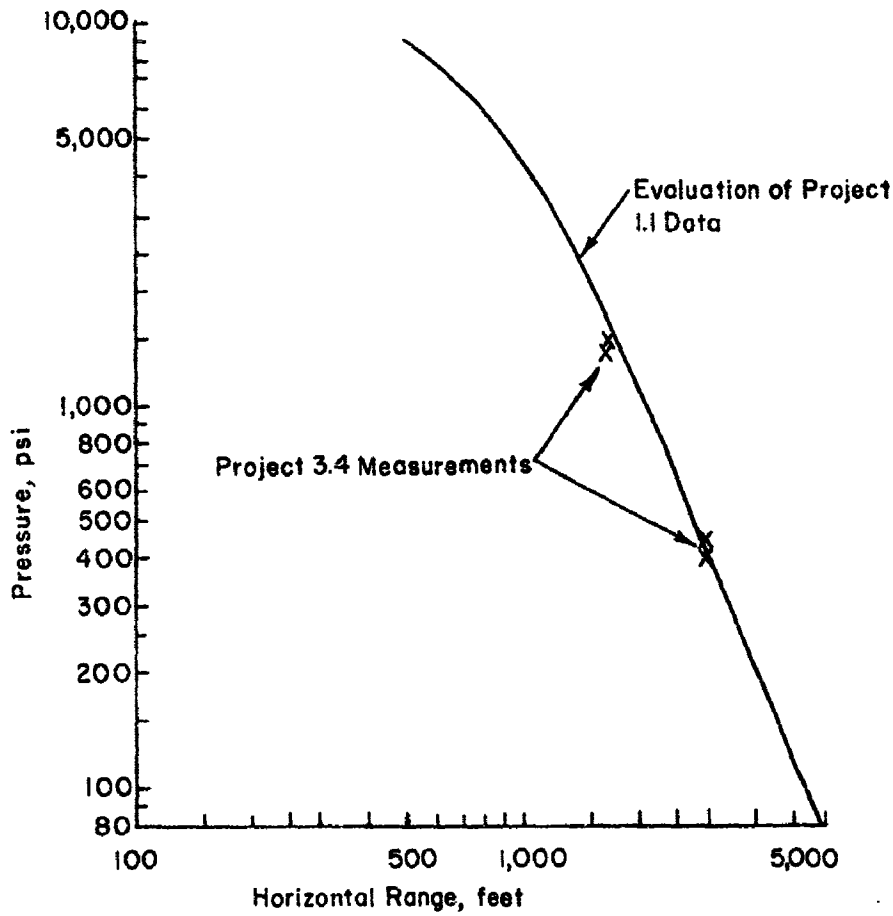

Figure 6.2 Peak shock wave pressure near water surface versus horizontal range, Shot Umbrella.

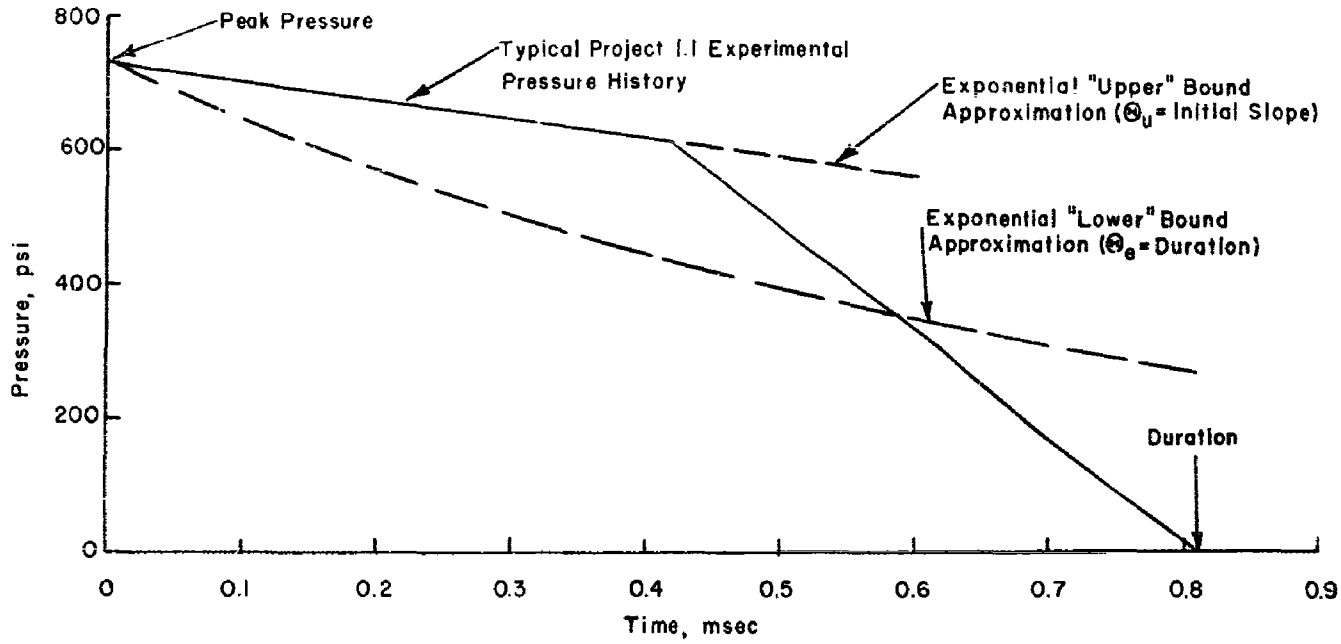

Figure 6.3 Estimation of equivalent decay time constant, Shot Umbrella.

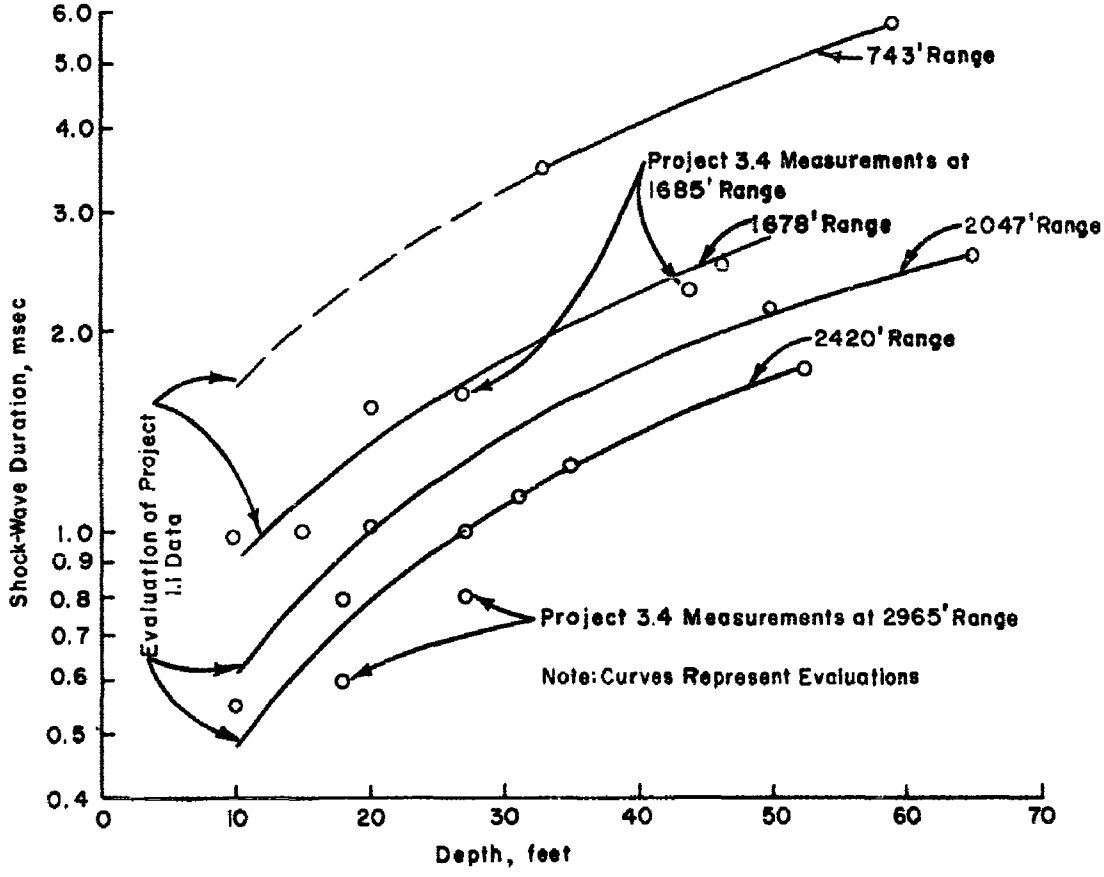

Figure 6.4 Shock wave duration at various ranges as a function of depth, (equivalent decay time constant lower bound approximation), Shot Umbrella.

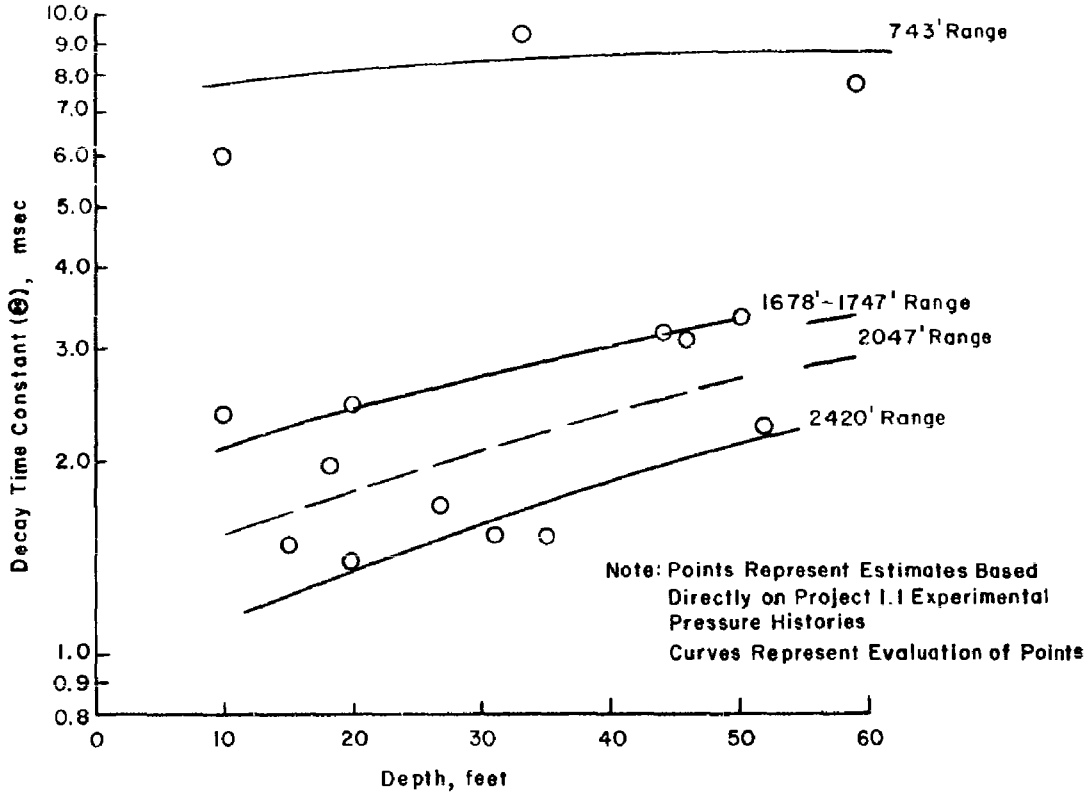

Figure 6.5 Equivalent decay time constant (upper bound approximation), Shot Umbrella.

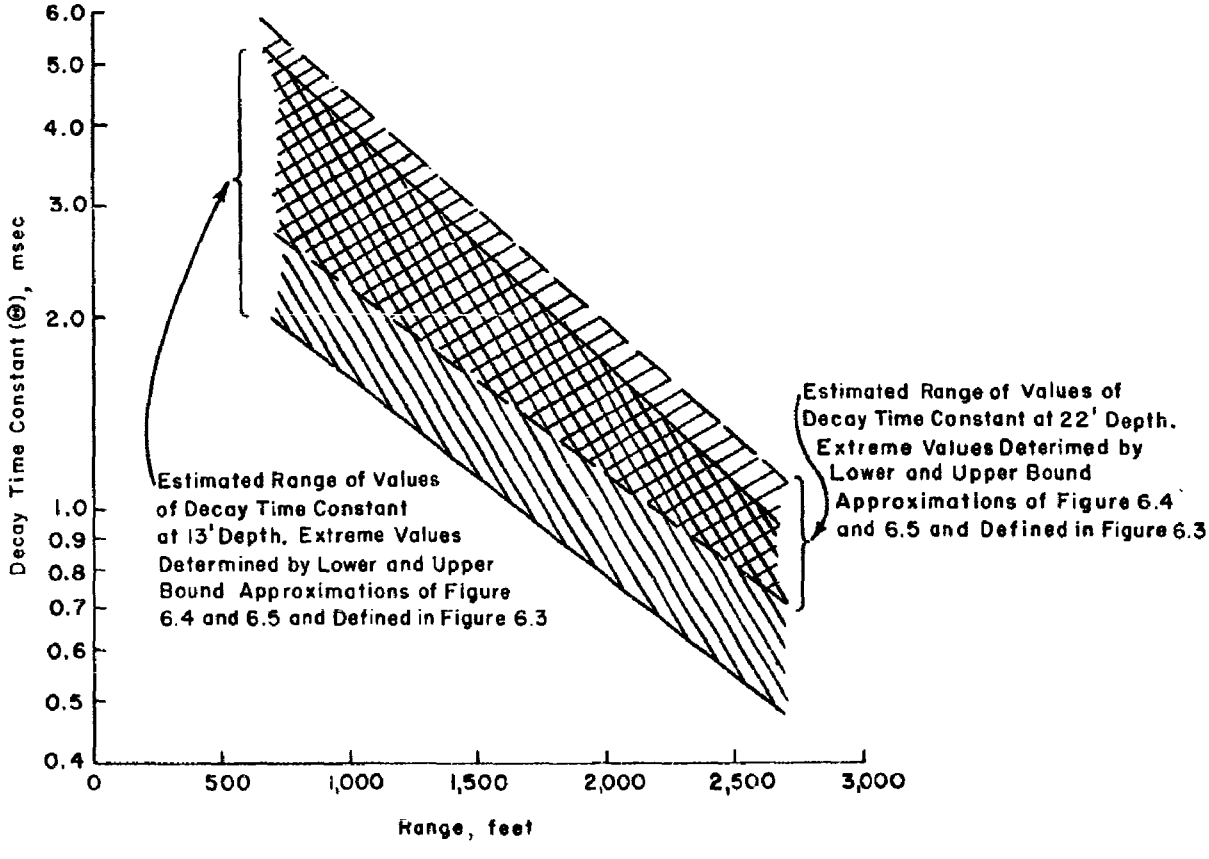

Figure 6.6 Equivalent decay time constant approximation versus range, Shot Umbrella.

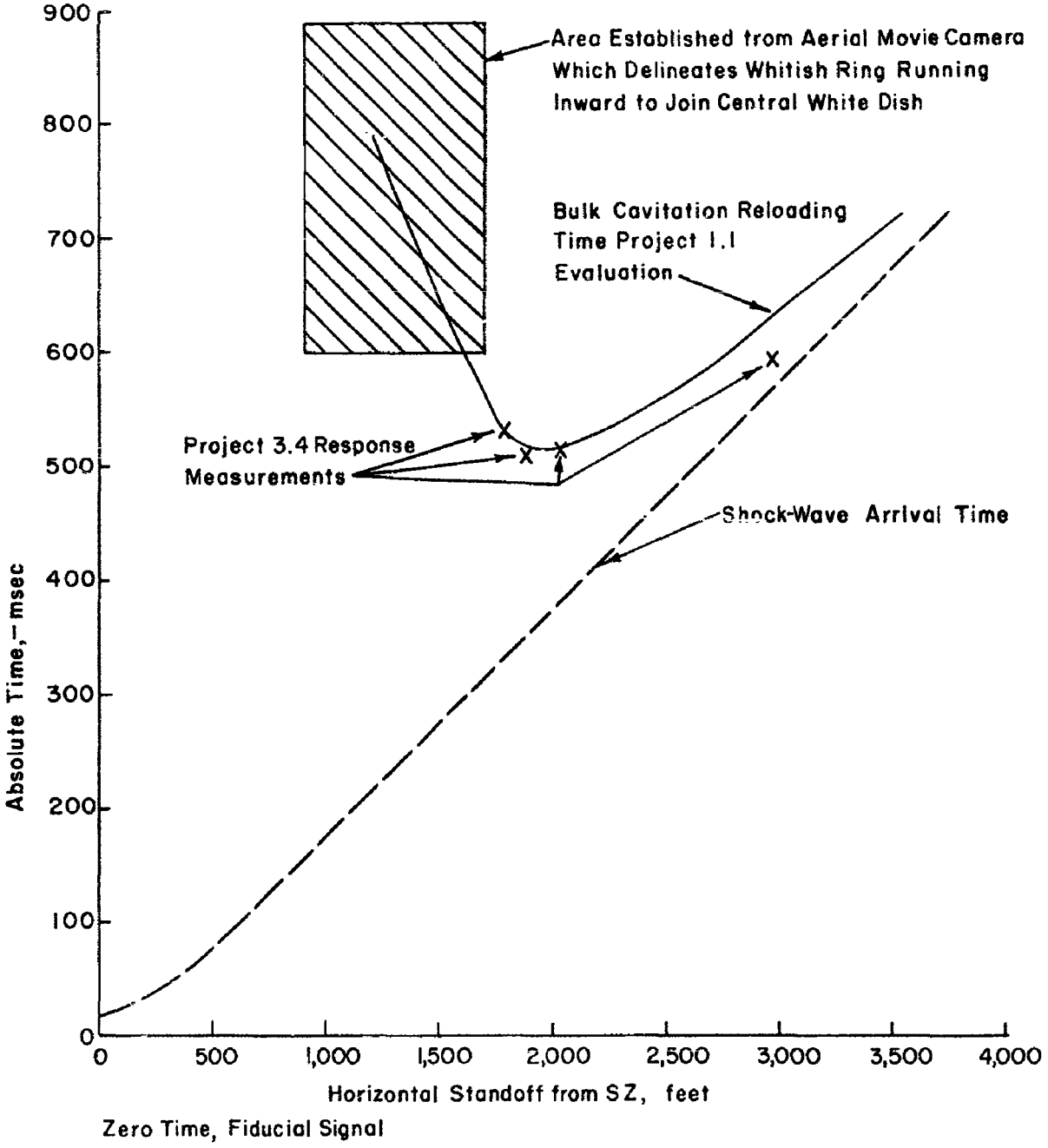

Figure 6.7 Observations on cavitation reloading time, Shot Umbrella.

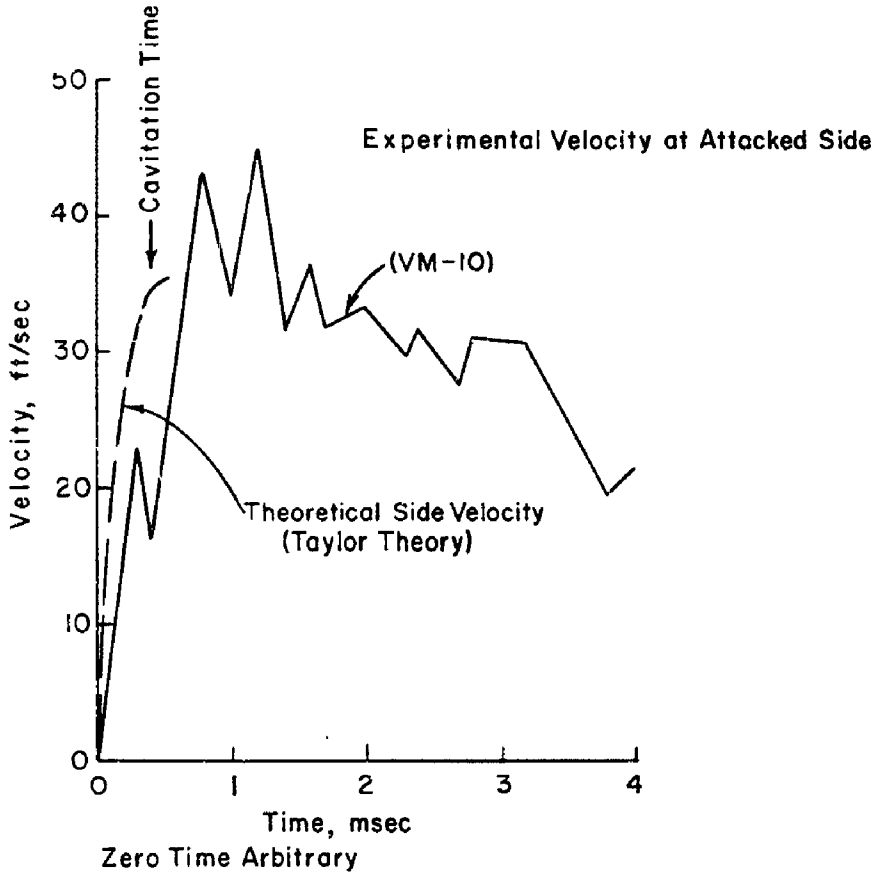

Figure 6.8 Interaction at EC-2 attack side, Shot Umbrella.

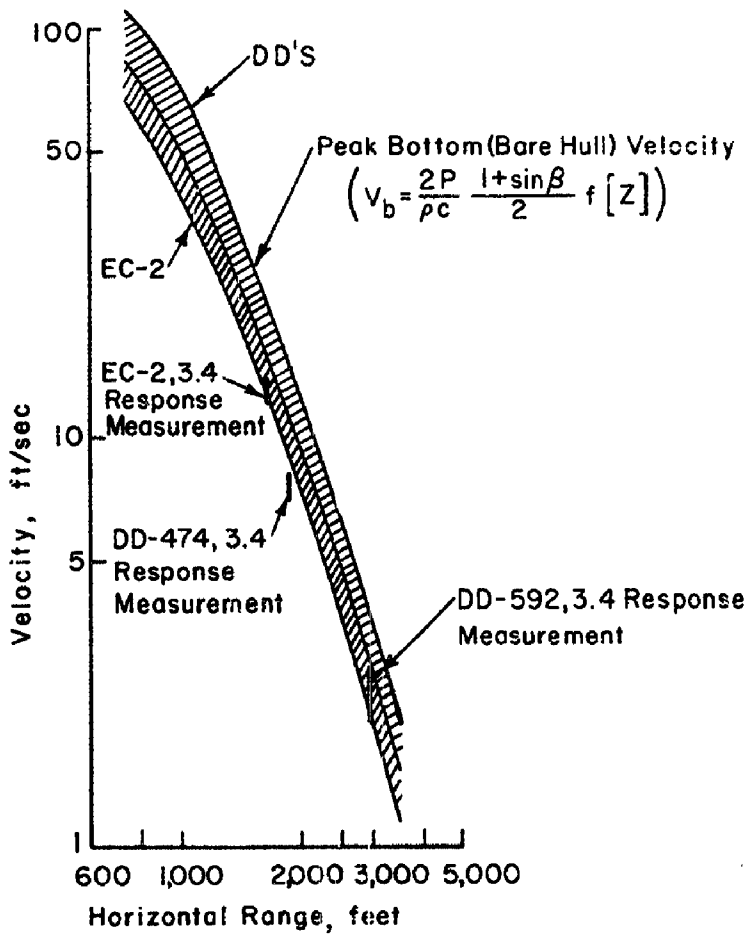

Figure 6.9 Peak vertical bottom velocities at bare hull sections of DD's and EC-2, Shot Umbrella.

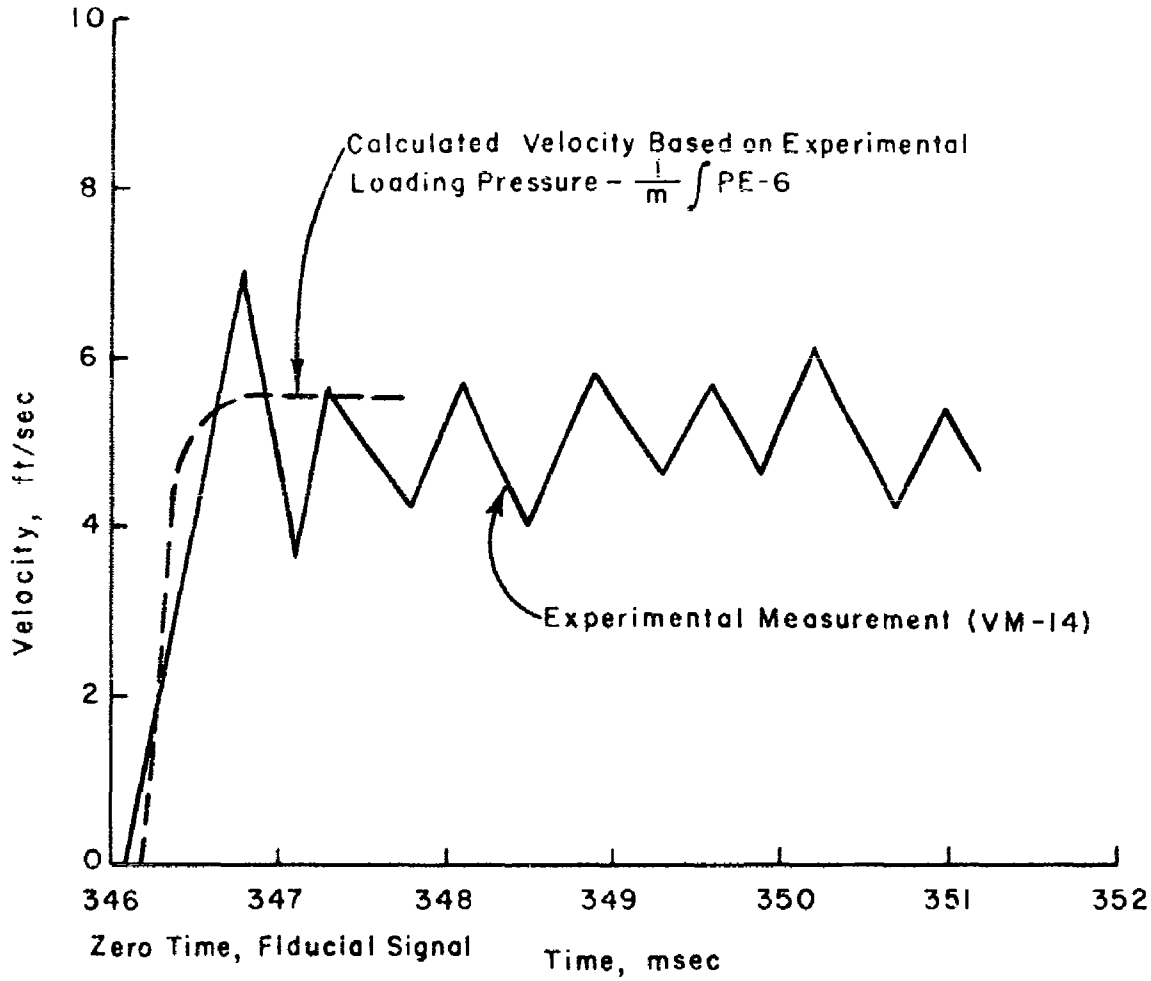

Figure 6.10 Interaction between direct shock wave and DD-474 bottom, Shot Umbrella.

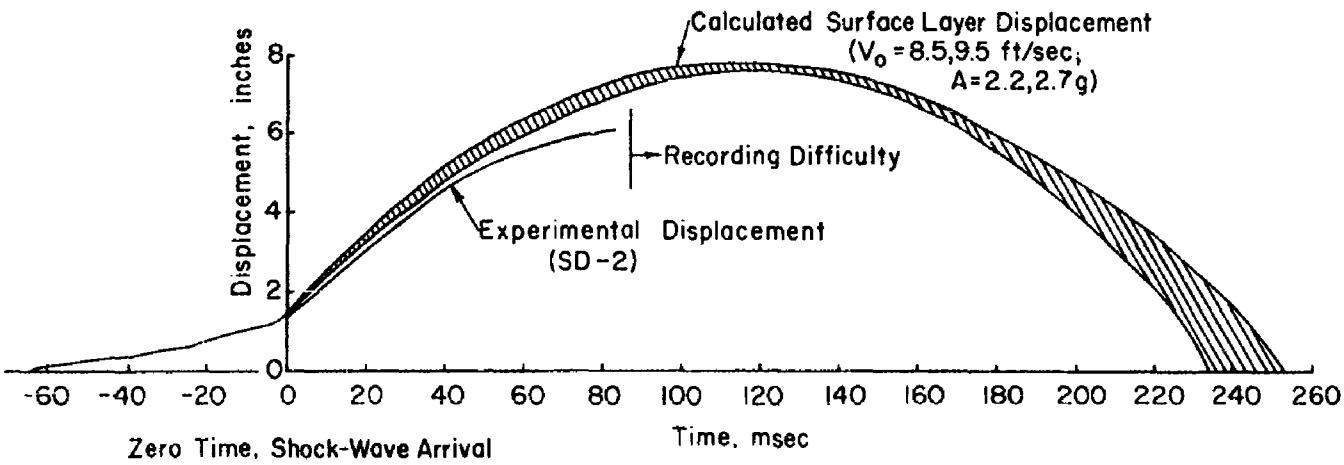

Figure 6.11 Vertical bodily displacement history, EC-2, Shot Umbrella.

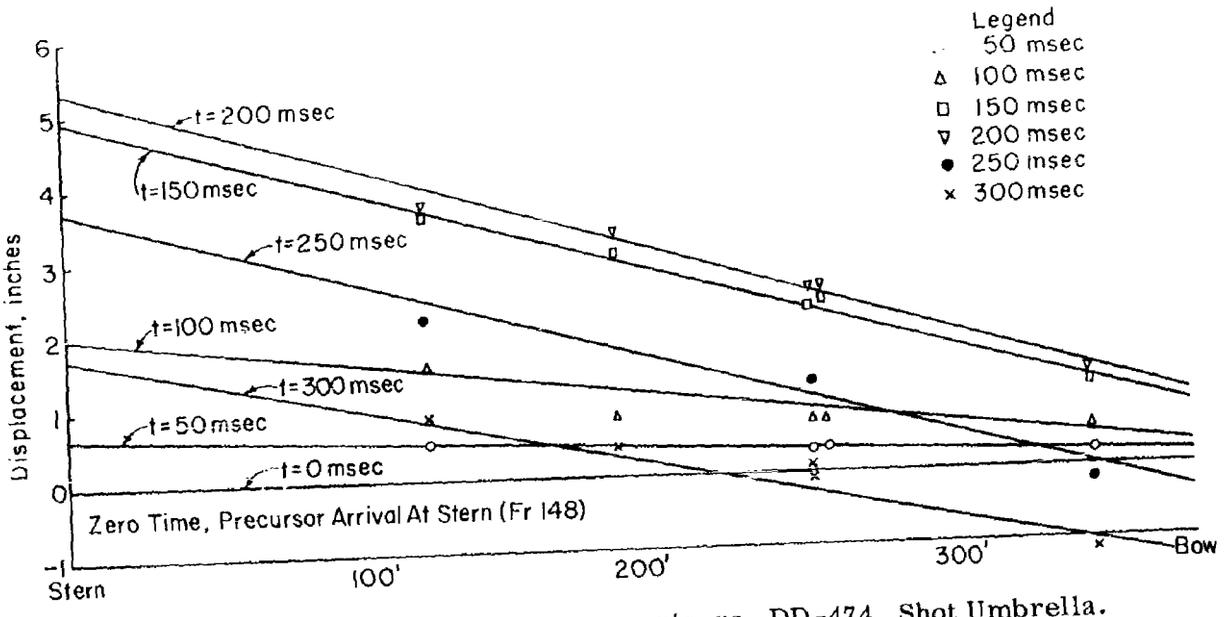

Figure 6.12 Vertical displacement contours, DD-474, Shot Umbrella.

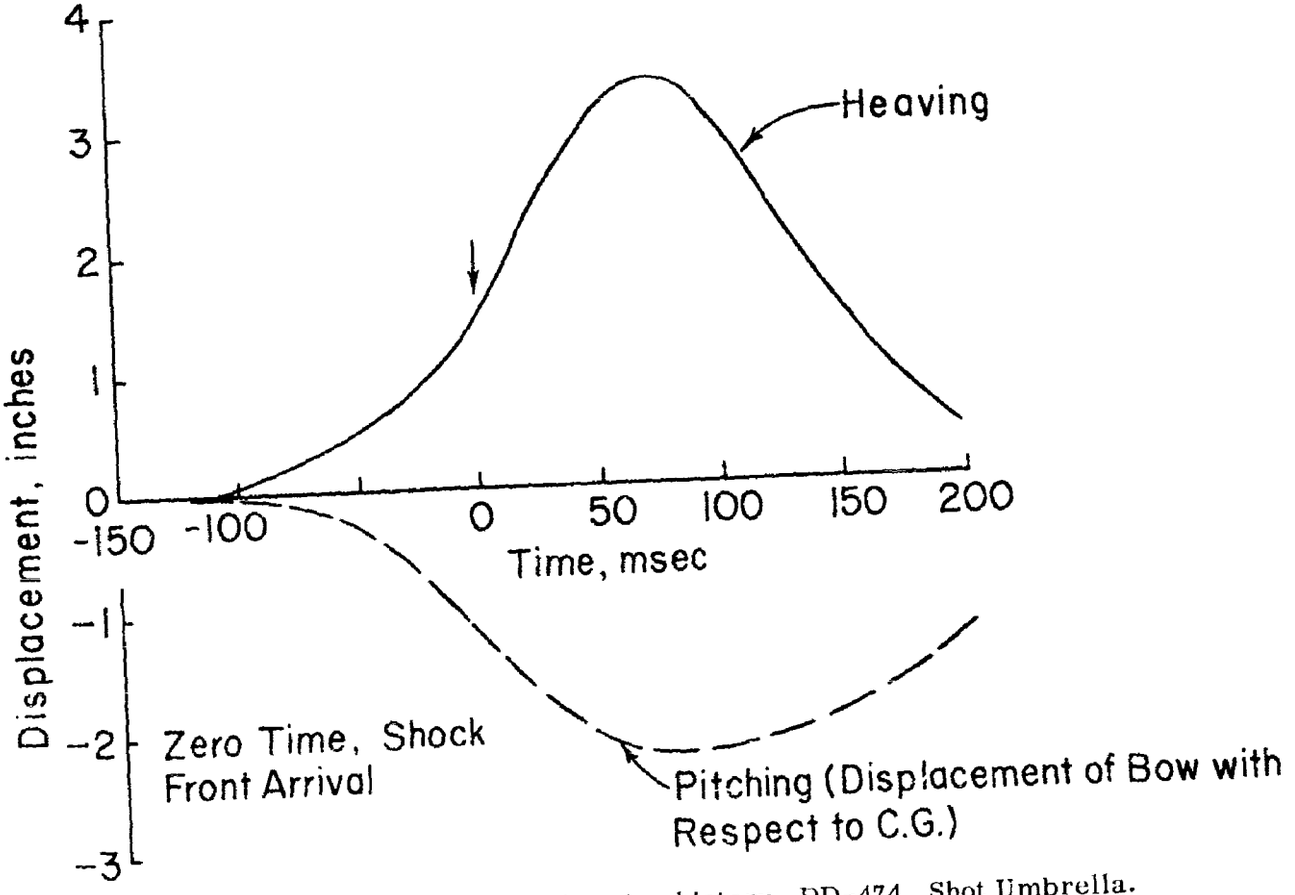

Figure 6.13 Pitching and heaving history, DD-474, Shot Umbrella.

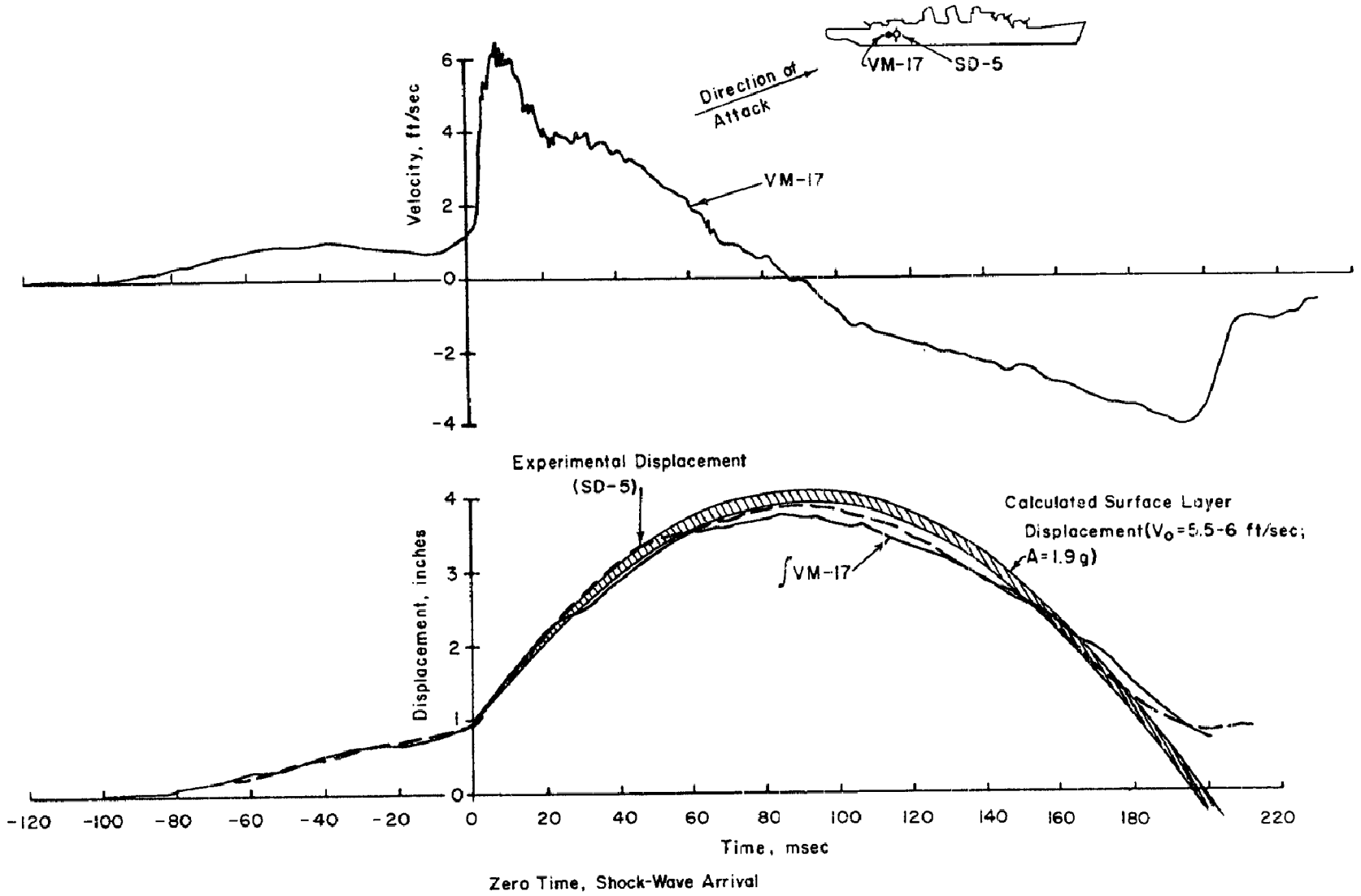

Figure 6.14 Vertical bodily motion of DD-474, stern (Frame 148), Shot Umbrella.

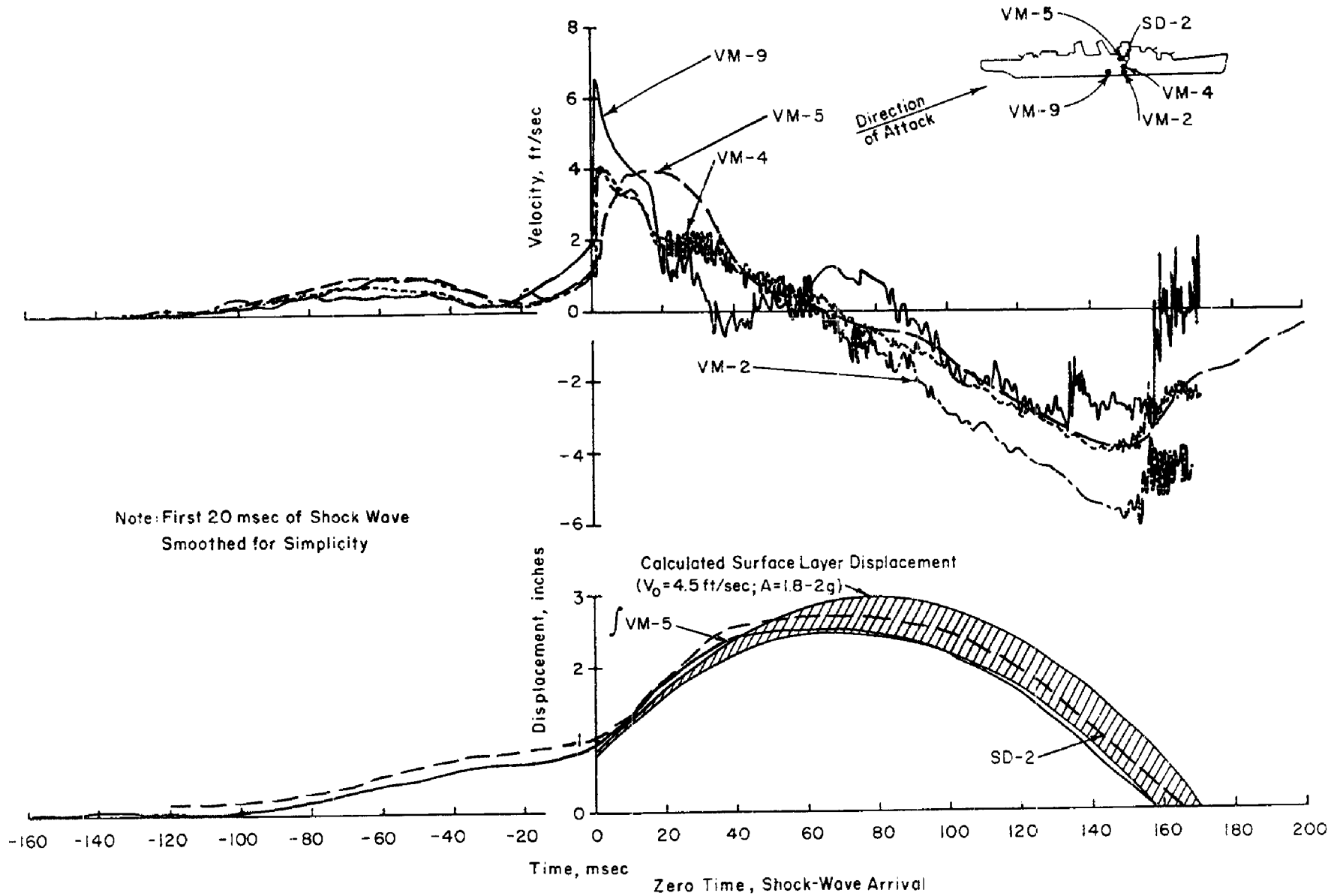

Figure 6.15 Vertical bodily motion of DD-474, midships (Frames 72 through 82), Shot Umbrella.

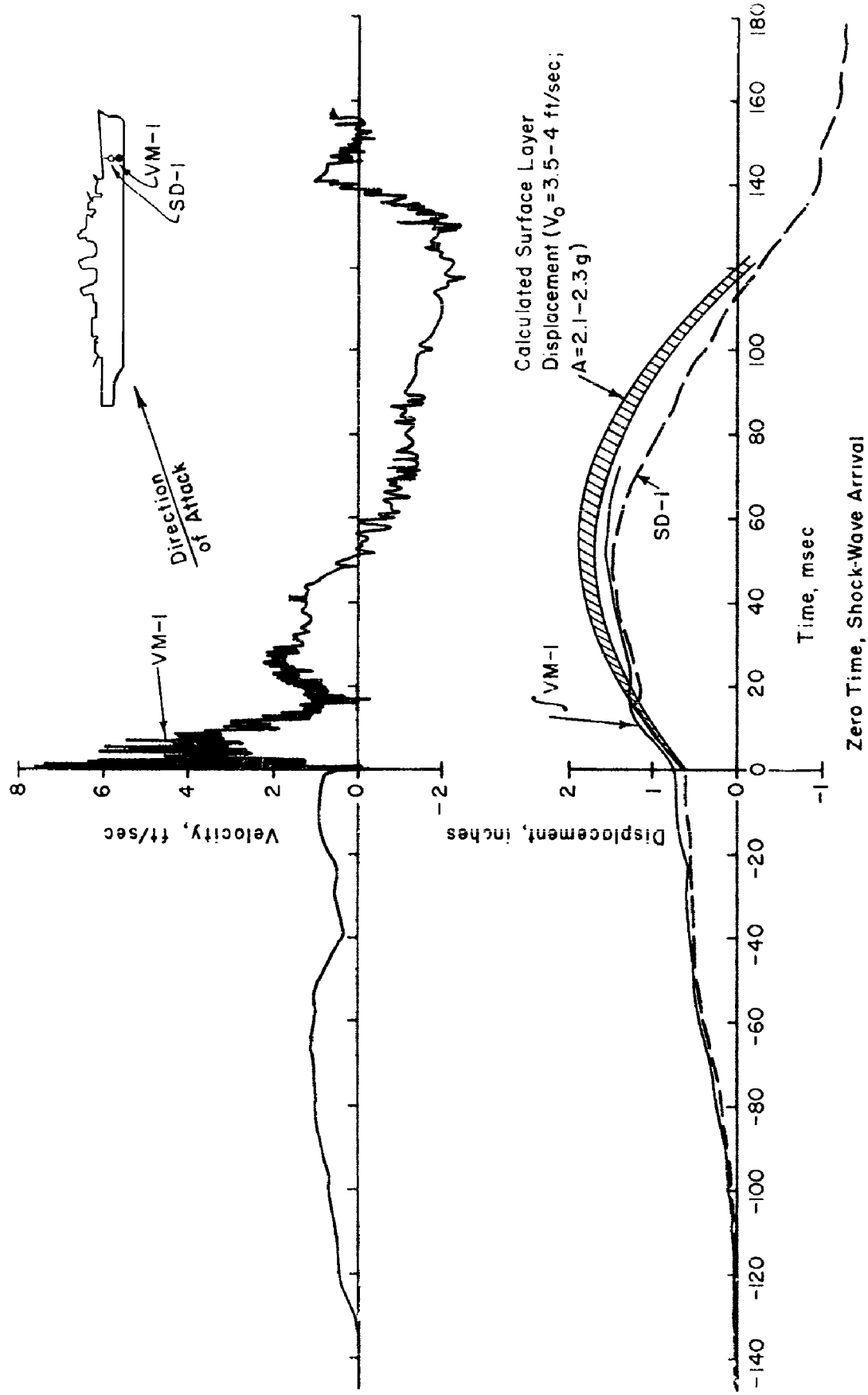

Figure 6.16 Vertical bodily displacement of DD-474, bow (Frame 18), Shot Umbrella.

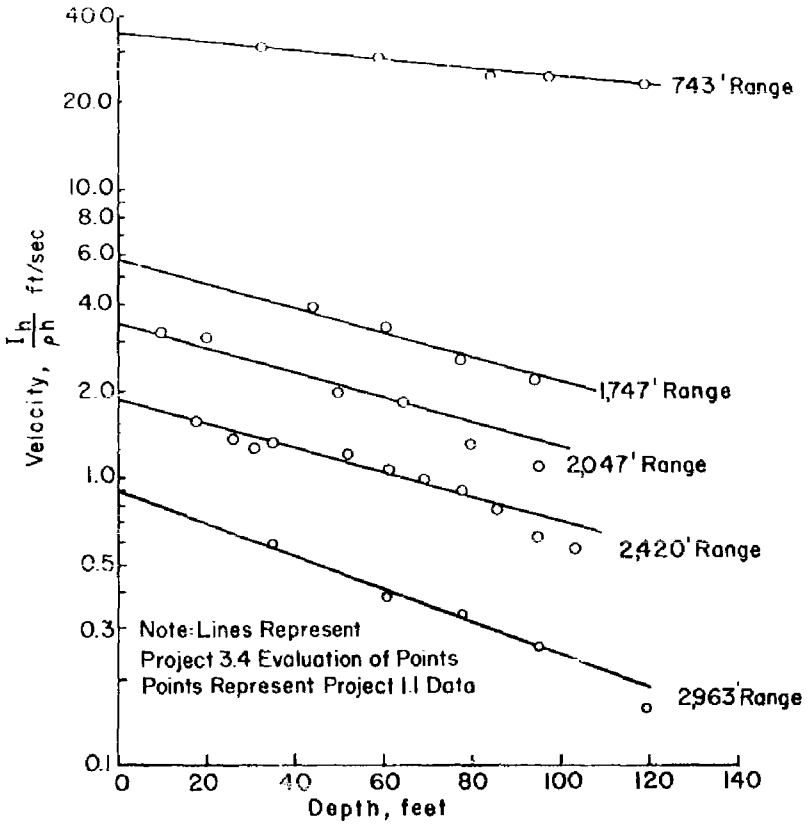

Figure 6.17 Average water layer velocity versus depth, Shot Umbrella.

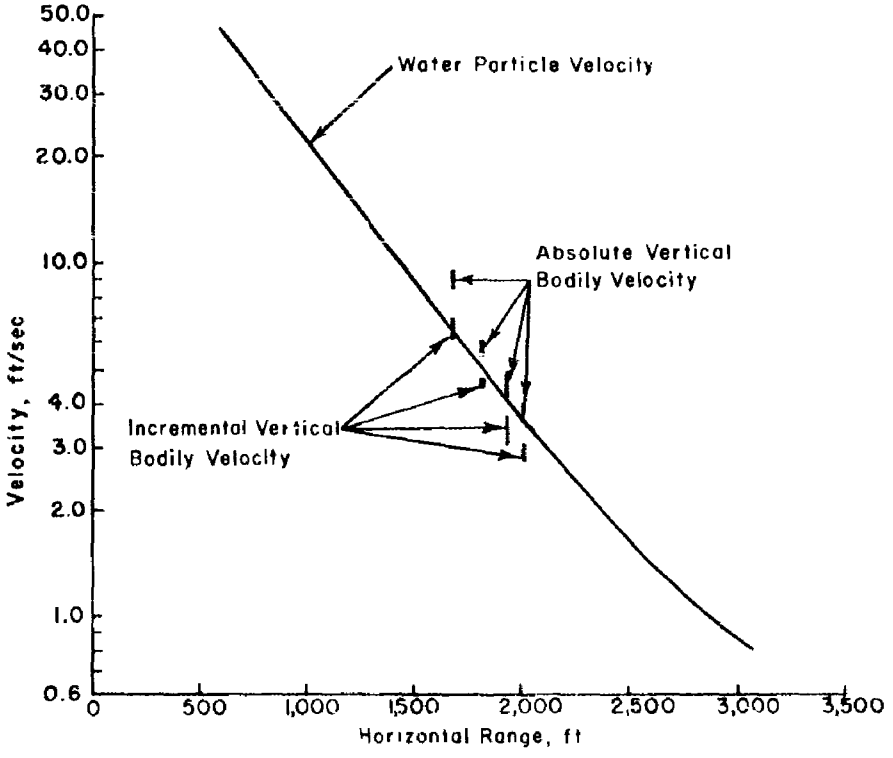

Figure 6.18 Vertical bodily and water particle velocity versus range, Shot Umbrella.

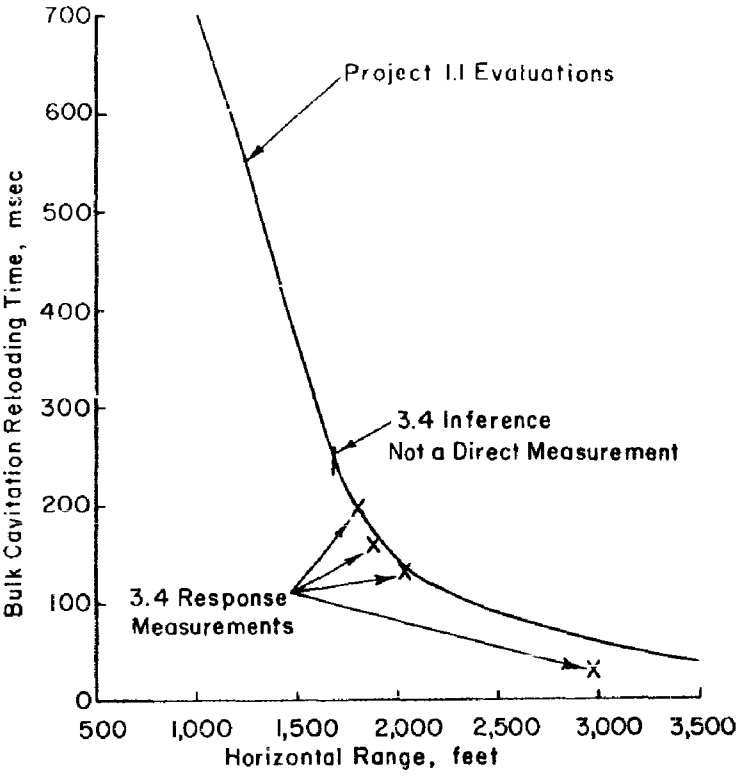

Figure 6.19 Bulk cavitation reloading time (with respect to shock wave arrival time), Shot Umbrella.

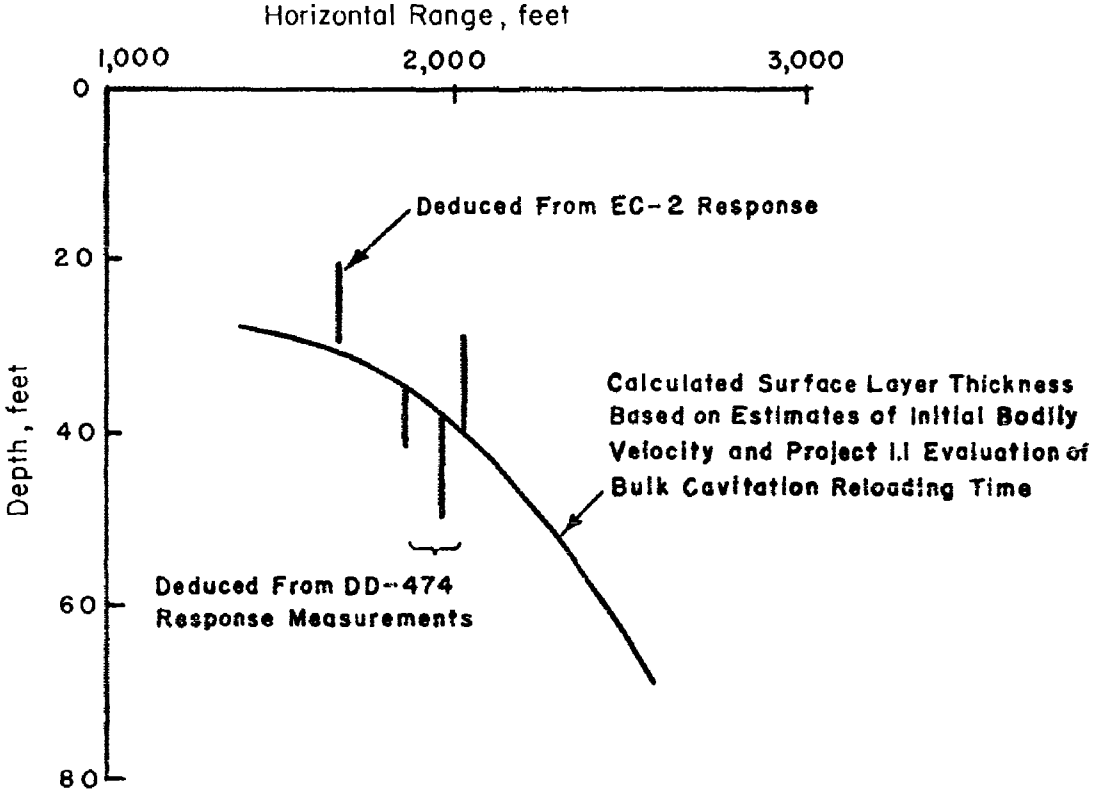

Figure 6.20 Surface layer thickness versus horizontal range, Shot Umbrella.

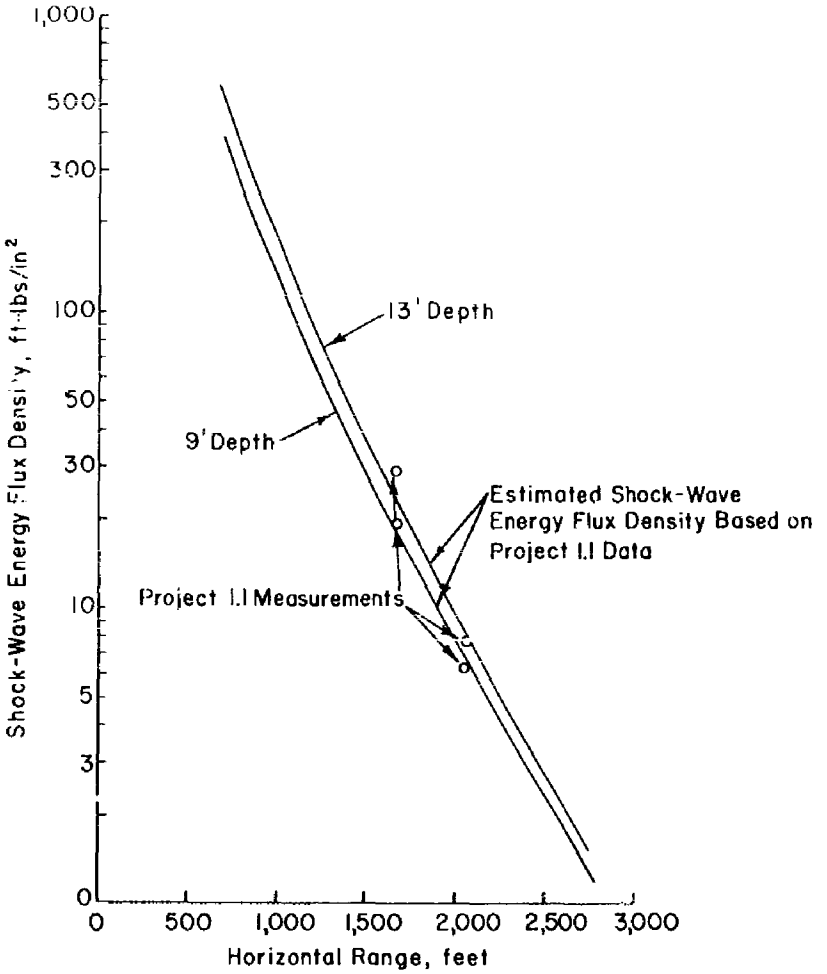

Figure 6.21 Shock wave energy flux density versus horizontal range, Shot Umbrella.

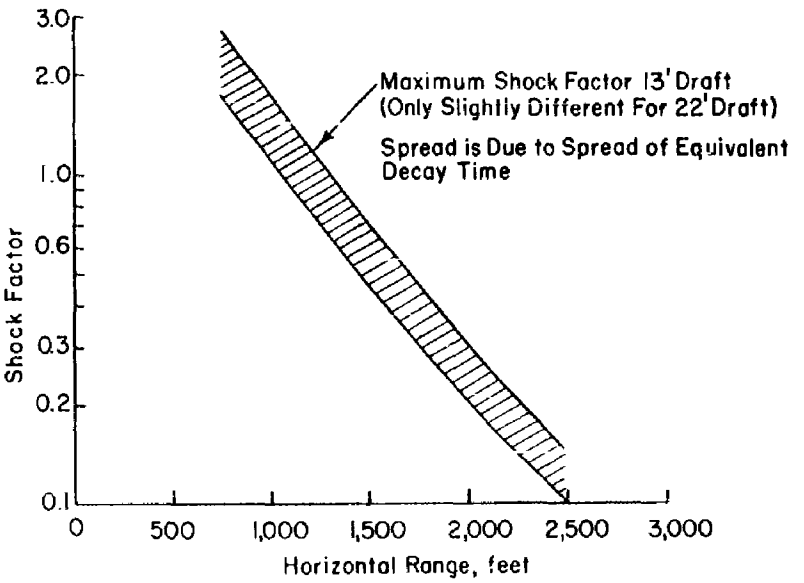

Figure 6.22 Equivalent shock factor versus range, Shot Umbrella.

Chapter 7

CONCLUSIONS

The conclusions in this chapter refer to underwater nuclear bursts and are specifically concerned with Shot Wahoo and Shot Umbrella conditions. The terms "Shot Wahoo conditions" and "Shot Umbrella conditions" include yield, shot geometries, bottom reflections, thermal-gradient characteristics and target ship types.

From the standpoint of hull damage, the following safe delivery ranges for destroyers have been demonstrated: 2,900 feet under Shot Wahoo conditions and 1,900 feet under Shot Umbrella conditions. Minimum safe delivery ranges, from the standpoint of hull damage alone, are controlled by the direct shock wave under both Shot Wahoo and Umbrella conditions and are estimated to be 2,400 feet under Shot Wahoo conditions and 1,700 feet under Shot Umbrella conditions. For these estimates, destroyer hull deformation comparable, in its operational significance, to that sustained by the EC-2 is considered to be the maximum amount which can be called safe.

The lethal ranges for the EC-2 from the standpoint of hull damage are controlled by the direct shock wave under both Shot Wahoo and Umbrella conditions and may be estimated by use of the energy-density rule. The assumption that a 1.5-foot deformation of the attacked side frames represents lethal damage leads to the estimate that under both Shot Wahoo and Umbrella conditions a horizontal range of 1,100 to 1,200 feet, or less, is lethal.

Checkpoints for small-scale UERD model experiments were obtained from both Shots Wahoo and Umbrella. However, no direct correlation with the UERD full-scale HE tapered-charge tests (Project 3.1 for Operation Hardtack) is possible because of the loss of data on the DD-592 in Shot Wahoo.

In Shot Wahoo, the direct shock wave was by far the most significant loading phase at the EC-2 position. The bulk cavitation reloading and the bottom-reflected wave effects were small by comparison. Bottom velocity jumps caused by the shock wave were two times as great as those caused by cavitation reloading and three times as great as those caused by the sea-bottom-reflected wave. Hull damage was caused by the direct shock wave alone.

In Shot Wahoo, the most significant loading phases at the DD-593 were the bottom-reflected wave and the subsequent bulk cavitation reloading. Responses produced by the direct shock wave were negligible by comparison; vertical velocity jumps caused by the reflected wave were 2 to 3 times as great as those caused by the direct shock wave. Response severities produced by the bottom-reflected wave and the subsequent bulk cavitation reloading were about equal, both with respect to peak velocities and associated accelerations.

In Shot Umbrella, the direct shock wave was the most significant loading phase for surface ships within the range of primary interest. Bulk cavitation reloading following the direct shock wave produced, at the DD-474, vertical velocity increments almost as great as those produced by the direct shock wave, but the associated accelerations were less than 0.5 of those due to the shock wave itself. Lagoon-bottom precursor pressure waves gave rise to vertical displacements and velocities of the target ships which were each about 30 percent of the total displacements and velocities, respectively. However, the accelerations associated with the motions were negligible.

Surface waves generated by Shot Wahoo and Umbrella did not cause any significant effects

on the surface ship targets. In Shot Umbrella, 22-foot surface waves (crest to trough) gave rise to girder strains less than 300 μin/in in the DD-474, attacked end-on. It is doubted that surface waves would exercise any significant influence on lethal hull damage ranges under either Shot Wahoo or Umbrella conditions.

Under side-on attack, the largest hull responses are produced at the attacked side. In the EC-2, the direct shock wave in each test gave rise to a peak velocity of the attacked side frame about three times greater than the maximum peak velocity measured at the bottom; the response of the shadowed side was small in comparison to that of the bottom. Variation of response across the bottom itself tended to be small.

Under side-on attack, the vertical bottom velocities are by no means uniform over the length of the ship. Despite the uniformity of the loading, the velocity response is appreciably dependent upon precise location along the structure and the proximity of this location to heavy masses. Peak bottom velocities at bare hull locations can be more than 50 percent greater than those at locations near heavy masses and bulkheads.

Under end-on attack, vertical peak bottom velocities depend on precise location at the hull structure and its proximity to heavy masses. Peak bottom velocities at bare hull sections tended to be uniform along most of the length of the ship. At the extreme attacked end itself, however, it is believed that they are higher than over the rest of the ship; the basis of this belief is indicated by the next conclusion.

Peak vertical bottom velocities at bare hull sections of midships appear to be 30 to 40 percent less for end-on attack than for side-on attack. This decrease is consistent with crude inferences drawn from previous UERD small-scale model test experience.

Peak vertical velocities measured at bare hull sections of the target ships were, with one exception, distinctly higher than corresponding water particle velocities; the exceptional case was the EC-2 bottom response to the Shot Wahoo bottom-reflected shock wave where the incident pressure wave was nearly normal to the bottom, and the peak bottom velocity was about equal to water particle velocity. The amount of the increase over water particle velocity was: 65 percent for the EC-2 and the Shot Wahoo direct shock wave, 25 percent for the DD-593 and the Shot Wahoo bottom-reflected wave, 100 percent for the EC-2 in Shot Umbrella, 100 percent for the DD-474 in Shot Umbrella, and 100 to 200 percent for the DD-592 in Shot Umbrella.

Vertical keel peak velocities at bare hull sections may be predicted with reasonable accuracy by use of the empirical rule proposed on the basis of previous small-scale UERD model tests. This applies to both Shot Wahoo and Umbrella conditions.

Peak vertical velocities tend, with the exception of bare hull sections themselves, to be uniform throughout the ship, under both Shot Wahoo and Umbrella conditions. However, the time to reach peak velocity increases considerably with the height of location above the bottom and, for this reason, average initial accelerations can be appreciably less for high locations than for bottom locations. Along bulkheads this diminution in acceleration can involve a factor of 10, or more. On decks a further diminution is likely to occur for positions that are away from the bulkheads and sides of the ship.

The bodily motion of surface ships caused by shock waves consists predominantly of vertical motion. Even for the shallowest side-on attack condition, the EC-2 in Shot Umbrella, the bodily velocity increment in the vertical direction was more than 50 percent greater than that in the horizontal direction, while the maximum vertical displacement was more than six times the maximum horizontal displacement.

Vertical bodily motion of surface ships in response to shock waves, even in end-on attacks, consists almost entirely of heaving and pitching; flexural motions are negligible. Pitching is caused primarily by arrival time differences of the shock wave and by variations in free-water shock wave strength along the ship. For this reason, individual sections of the ship may, to a first approximation, be considered to respond only by heaving,

independently of the remaining portions of the ship.

The vertical heaving motion of surface ships caused by shock waves consists of a rapid rise in velocity, followed by a slow deceleration. The increment in initial peak vertical bodily velocity is approximately equal to the water particle velocity. Later ship motion is controlled by the motion of a surface layer of water, split off from the main body of the water by bulk cavitation. Deceleration is controlled by the thickness of the water layer. In general, the vertical bodily motion of the surface ships confirmed the concepts previously advanced in connection with the small-scale UERD model tests.

Hull damage in both Shots Wahoo and Umbrella was essentially limited to the attacked side and was confined, vertically, between the inner-bottom and second deck levels. Maximum side-frame deformation tended to occur at a level about midway between the water line and the inner bottom but was reduced by structural restraints introduced by bulkheads and flats. In each test the maximum attacked side-frame deformation amounted to about 1 inch. Maximum side-plating deformation, between frames, occurred just above the inner bottom and decreased with height above this level. In each test the maximum plating dish amounted to about 1 inch.

The general character of the EC-2 hull damage, under both Shot Wahoo and Umbrella conditions, is very similar to that found in small-scale UERD tests with C-2 models. The magnitude of the side damage may be predicted, with an accuracy sufficient for predicting lethal ranges, by use of the energy-density rule proposed on the basis of these small-scale tests.

Appendix A

DETAILED EVALUATION OF UNDERWATER PRESSURE PHENOMENA, SHOT WAHOO

An evaluation of all available information concerning test conditions and underwater pressure phenomena was carried out to create a suitable background for Project 3.4 analysis of surface-ship loading and response. Data was made available to UERD by other projects, particularly Project 1.1, prior to final publication of their own results.

The UERD conclusions have been summarized in the main text; detailed justifications are presented below.

A.1 TEST CONCLUSIONS

Estimates of the ranges of the EC-2 and DD-593 were made from measured direct shock wave arrival times and calculations utilizing refraction theory.

Direct shock wave arrival times measured by bottom gages (pressure gages attached to the hull and velocity meters) along the EC-2 and DD-593 centerlines are plotted as a function of distance from the stern of the ship in Figures A.1 and A.2, respectively. Notice that in Figure A.1 a few helpful measurements made by Project 3.3 are included. The experimental points are connected by straight lines called centerlines so that arrival times can be derived at the midship locations (Frame 91 for the EC-2 and Frame 103½ for the DD-593).

Bathythermograph measurements carried out in the test area allowed Project 1.13 (Reference 12) to estimate sound speed in the water; such estimates formed the basis of the calculation effort and are therefore reproduced in Figure A.3 at key locations. In addition, numerical values of the sound speed gradient actually utilized in computations are shown for the surface zero condition and an average gradient condition.

The arrival time of the direct shock wave front at various ranges along the water surface was computed. The first step in such a computation is to estimate sound signal arrival times from refraction theory; this was done by machine computation (IBM 650) employing a ray path technique similar to that of Reference 24. For this purpose the sound velocity structure of the water was assumed to be horizontally stratified in accordance with the surface zero condition shown in Figure A.3; the choice of this condition is justified by the ray paths thus computed and shown in Figure A.4. The second step in the computation of shock wave arrival times involved a correction to the sound signal arrival times to allow for the finite amplitude of the shock wave; to employ this type of correction the peak pressure at the point of interest was estimated to correspond to that expected in isovelocity water. The computed shock wave arrival times are presented as a function of range from surface zero in Table A.1.

The computational results together with Figures A.1 and A.2 allow the midship positions of the EC-2 and DD-593 to be located. The estimated locations (Table 4.1) differ only slightly from the results of the aerial photographic survey.

Experimental direct shock wave arrival times measured at the EC-2 bottom along a transverse line were also plotted in Figure A.1. These measurements formed the basis for the estimate of the direct shock wave attack angle at the EC-2 (Figure 4.2).

Measurements of bottom-reflected wave arrival times at various key ship locations were compiled and used to check sea-bottom depths, estimated from a prior oceanographic survey (Reference 25), and to deduce other associated information. Experimental reflected-wave arrival times at the EC-2 measured at various positions are plotted in Figure A.5. A similar presentation of experimental reflected wave arrival times at various positions along DD-593 is given in Figure A.6. However, in this case, two types of reflected-wave arrival times are considered: the arrival time of a precursor wave traveling for part of its path through the bottom material and the arrival time of the specular reflection ray traveling entirely through the water. The greater inaccuracy involved in estimating precursor-wave arrival times is indicated in Figure A.6 by the use of lines rather than points.

Concentrating for the moment on the specular reflection, experimental arrival times at midship positions on EC-2 and DD-593 are estimated in Column 4 of Table A.2. Other projects participating in Shot Wahoo secured measurements of reflected wave arrival times with respect to direct shock wave arrival times; these are also incorporated in Table A.2, in Column 3. The experimental arrival times could be translated to times after detonation by use of Table A.1; the results are noted in Table A.2, in Column 5.

With the aid of the prior oceanographic survey (Reference 25), bottom contours could be constructed for the various array lines, and reflected wave arrival times could be computed by means of ray path refraction theory in a manner similar to that utilized for the direct shock wave. An example of such a bottom contour is given in Figure A.7 along the gradient of the bottom slope, i.e., the 29° array. Note that the bottom slopes by an angle of 17°. Typical ray paths are also shown in Figure A.7, and symbols are introduced in order to simplify the discussion. A ray is emitted from a point Z, the burst, and impinges upon the bottom, forming an angle β with respect to the bottom normal. Specular reflection produces a ray, also making an angle β with respect to the bottom normal, which extends to a point of interest P and forms an attack angle α with respect to the water surface. The first such ray to arrive at P travels essentially in the propagation plane formed by Z, P, and I, the burst image. The image point I was considered, in the computations, to shift in the discrete fashion indicated in the figure to account for the curvature of the bottom. In the particular case of the bottom contour shown in Figure A.7, the propagation plane is vertical. In other directions, however, the propagation plane ZIP is not vertical although still intersecting the water surface at the line P-SN, where SN is the projection of the bottom normal through Z; a rough allowance for this effect was made in the computations.

Otherwise, in general, the computations of reflected wave arrival times were carried out in a manner similar to that used for the direct wave. Two minor qualifications have to be made, however, for the sake of accuracy. The sound speed gradient in the water was taken as an average sound speed gradient defined in Figure A.3. This seemed somewhat more generally pertinent than the surface zero gradient structure used for the direct wave computations. Corrections to the sound signal arrival times to allow for the finite amplitude of the shock wave were made only for that part of the ray path lying between the burst and the bottom and were made on the basis of isovelocity estimates of peak pressure just before the ray impinged upon the bottom.

The results of the computed reflected-wave arrival times are listed in Column 5 of Table A.2. Within the framework of the computational procedure, it is believed that the degree of agreement between experimental and computed arrival times indicates that the actual bottom depths were essentially identical with those found in the prior oceanographic survey.

Two byproducts of the computational effort involved in connection with reflected wave arrival times have interest for present purposes. The first of these is the correlation of the angle between the specularly reflected wave and the bottom normal with horizontal range from surface zero along each of the array lines (Figure A.8). The second byproduct is the correlation of the attack angle made between the specularly reflected ray and the water surface with horizontal range from surface zero; this has been presented in Figure 4.6 for all pertinent array lines.

The information, both experimental and computational, on the bottom-reflected wave provides some indication of the sound speed through the upper layer of the bottom. The arrival times of the sea bottom precursor reflected wave at the DD-593 (Figure A.6) were extrapolated back, using an extreme line, to intersect with the line established by the specular reflection arrival times. Since the DD-593 was very closely alined (in its heading) along the 248° array line, the intersection must represent an upper bound estimate of the critical range from surface zero at which a bottom precursor wave can first be distinguished and must, therefore, correspond to an upper bound estimate of the critical bottom reflection angle at which total reflection first commences. The upper bound estimates of the critical range is about 8,800 feet. Use of Figure A.8 enables an upper bound critical bottom reflection angle to be estimated as 48° . The sound speed in the bottom is related to the critical bottom reflection angle by

$$\sin\beta_{crit} = \frac{c_W}{c_B}$$

Where: c_W = sound speed in water

c_B = sound speed in bottom

It is, therefore, deduced that the sound speed in the upper layer of the bottom is at least 6,600 ft/sec. The estimate of 8,000 ft/sec made in previous study (Reference 26) is, therefore, certainly not in conflict with present evidence.

A.2 DIRECT SHOCK WAVE

An effort was made to describe the direct shock wave near the water surface as a function of range. Although the aim of this effort was primarily to establish the shock wave characteristics at water depths of about 30 feet or less, some attention had to be paid to much deeper depths.

The two major stations at which most experimental information was obtained were the EC-2 and DD-593.

Experimental results (Projects 1.1 and 1.5) concerning the peak pressure at these locations are reproduced in Figures A.9 and A.10. Also shown in Figures A.9 and A.10 are calculated peak pressure curves. These calculations were based on refraction theory and the sound gradient structure at surface zero given in Figure A.3. As may be seen, the comparison between experimental and theoretical information is fairly good and serves to establish the peak pressure level near the water surface.

The calculation method was also used to describe peak pressure near the water surface as a function of range and the result shown in Figure 4.3 is considered in satisfactory agreement with all available experimental evidence.

In a similar way the calculated and experimental values of surface cutoff times were plotted as a function of depth at the EC-2 and DD-593 positions (Figures A.11 and A.12). In the case of the DD-593 the pressure does not drop abruptly and the corresponding uncertainty in reading cutoff time is indicated by the use of lines rather than points to represent the data. Comparison of the calculated (dashed) curve and experimental data at the EC-2 (Figure A.11) indicates rather good agreement at large depths but also indicates that at more shallow depths the actual cutoff time can be as much as, say, 35 percent less than the computed value. It is believed that the reason for this is the uneven water surface; recall that ambient surfac waves totaling nearly 10 feet (crest to trough) were present at detonation time. If the direct shock wave is effectively reflected from the troughs rather than from an average water level, then it would be expected that the predicted cutoff times should be altered as indicated by the solid curves in Figures A.11 and A.12. These curves are considered to be the best estimates of cutoff time; note the good agreement with EC-2 experimental measurements. The presence of ambient surface waves may also help to explain the slow rate of pressure dropoff in the DD-593 measurements. Surface reflection at certain positions must have taken place, locally, at essentially glancing incidence thereby leading to a nonlinear overall effect. At any rate, the simplified evaluation represented by the solid curves of Figures A.11 and A.12 appeared sufficient for present purposes, and the concept was used to compute surface cutoff times as a function of range in Figure 4.4.

A.3 BOTTOM REFLECTED SHOCK WAVE

As in the case of the direct wave, an effort was made to characterize the bottom-reflected shock wave near the water surface. Once again because of the sparseness of measurements this effort was not confined, except in aim, to the region near the water surface.

An intrinsic difficulty in treating sea bottom reflections arises from the fact that the reflected wave cannot strictly be described as the incident wave multiplied by a numerical factor, i.e., the bottom reflection coefficient; the pressure history of the reflected wave may well be distinctly different from that of the incident wave, and the degree of difference will depend upon the reflection angle. Nevertheless, it appears sufficient for present purposes to introduce the term "bottom reflection coefficient" in the sense of the ratio of the pressure jump, corresponding to the arrival of the first specular reflection ray, to that of the peak pressure to be expected if the incident ray had been totally reflected. Certainly, the ideal way to measure such reflection coefficients is to measure the pressure history just before and after the incident ray impinges upon the bottom, i.e., measurements close to the bottom itself. The measurements secured in Shot Wahoo were not ideal; they were secured from deep gages only in the cases of the DD-593 and EC-2, and insight into the variation of the reflection coefficient with reflection angle could be gained only by utilizing additional measurements made at shallow depths (less than or equal to 100 feet) at other ranges.

All available experimental results concerning specular reflection wave peak pressures are listed in Table A.3. Short duration spikes were ignored in establishing a peak pressure in all cases where an actual pressure history was available for study. In some cases, it was felt that the meaning of peak pressure was ambiguous; because this ambiguity could well be associated with effects other than the bottom reflection process itself, a corresponding pressure range is noted in the table. At each of the gage locations at which readings were secured, reflected-wave peak pressures were computed assuming a reflection coefficient equal to unity, and the resulting values are also noted in Table A.3. These computations were carried out by machine, utilizing ray path refraction theory in the manner described previously. The experimentally determined bottom reflection coefficients, i.e., the ratio of the experimental to the computed peak pressures, are plotted as a function of bottom reflection angle in Figure A.13; the bottom reflection angle was derived for each gage location from appropriate bottom contour charts but can be estimated also from Figure A.8. The smooth curve shown in Figure A.13 was faired through the experimental points so as to define the reflection coefficient as used in the present report, throughout the range of interest. Also shown in Figure A.13, as a matter of general interest, is the theoretical bottom reflection coefficient derived from plane wave harmonic acoustic theory applied to an impervious bottom in accordance with the governing equation indicated; a bottom sound speed of 8,000 ft/sec was used and a bottom density chosen to match the experimental curve at normal incidence. Although the difference between the experimental and theoretical curve is, of course, striking, there is a limited region of agreement within about 15° of normal incidence ($\beta = 0$). To the extent that this region

of agreement is physically meaningful, the construction in Figure A.13 implies that the specific density of bottom material is about 1.05. However, it is rather hard to attach any physical significance to such a value of density; in fact, it is clear that the assumption that the bottom is impervious is not a good one.

Experimental values of reflected wave surface cutoff times at the EC-2 were plotted as a function of depth and are shown in Figure A.14. Cutoff times were also computed, again assuming that the effective water surface was 5 feet below the average surface, and the resulting curve is shown in Figure A.14. The comparison between computed and measured cutoff times is not very good; the causes of this are unknown. However, the validity of the experimental measurements is considered to be inadequately established in this case; no suitable recordings were available at the DD-593 position to shed any further light on this question. Therefore, the computed values are considered to be the best estimate of cutoff times and the concept was used in the main text (Figure 48).

A.4 BULK CAVITATION

Observations on bulk cavitation following the direct shock wave were made from a motion-picture camera mounted on an RB-50 aircraft 22,000 feet above surface zero. The treatment of these observations is described below; the results have been incorporated in Section 4.1 of the main text.

The best of the films for observing bulk cavitation was film 51393, recorded at a nominal speed of 100 frames/sec. When the film is projected at normal speed, a dark circle can be seen spreading out from surface zero, visible out to about 4,000 feet. Within this dark circle a central portion shows a white aspect, at first out to about a range of 1,300 feet from surface zero. Shortly thereafter an irregular whitish ring can be observed to run inward, from a radius about equal to the EC-2 range, to join the central white disk. Because this seemed to be associated with the bulk cavitation phenomenon closer investigation was undertaken.

The film unfortunately lacked timing marks and therefore the first step required was to calibrate it. This was done by assuming that the dark circle was the slick created by the direct shock wave; arrival times of the shock-wave front at the water surface had already been computed (Table A.1), and a distance scale was available based on the derived standoff of the midposition of the EC-2.

It was now attempted to measure, on the film, the time at which the white ring was observed as a function of horizontal distance from surface zero. Unfortunately, when the film was examined frame by frame, rather than run on a projector, it proved difficult to make precise measurements of the inward-running whitish ring. However, it was established that between Frames 55 and 67 the radius of the white inner area could no longer be distinguished from the diffuse white area left by the inward-running whitish ring commencing at about 2,300 feet. This was shown in Figure 4.9 as an area delineating the phenomenon. Closer examination of the film revealed a local white spot lying about 300 feet to the inside of the EC-2 position, which could be traced from frame to frame as it moved inward. Since it seemed possible that this local white spot was also connected with the bulk cavitation phenomenon a plot of its movement was also shown in Figure 4.9.

TABLE A.1 COMPUTED DIRECT SHOCK WAVE ARRIVAL TIMES

Horizontal Distance from Surface Zero	Shock Wave Arrival Time
feet	msec
0	82.3
500	122
2,000	388
4,000	780
9,000	1,774
15,000	2,960

TABLE A.2 REFLECTED WAVE ARRIVAL TIME (SPECULAR REFLECTION)

Array Line	Horizontal Distance from Surface Zero	Experimental Arrival Time at Midships (with respect to direct shock wave arrival time)	Experimental Arrival Time at Midships (with respect to detonation time)	Computed Arrival Time with Respect to Detonation Time
degrees	feet	msec	msec	msec
29	2,360 (EC-2)		1,072	1,056
	3,410 (YC-1)	455 *	1,115	1,113
120	18,450 (SSK-3)	300 †	3,960	3,920
155	15,150 (DD-728)	410 †	3,450	3,450
248	9,180 (DD-593)	–	2,345	2,344

* Project 1.1. † Project 3.3.

TABLE A.3 SPECULARLY REFLECTED WAVE PEAK PRESSURES

Array Time	Horizontal Distance from Surface Zero	Gage Depth	Experimental Peak Pressure	Computed Peak Pressure Assuming Reflection Coefficient Equal to Unity
degrees	feet	feet	psi	psi
29	2,300	22	125 *	732
		22	145 *	732
		47	200 *	732
		300	188 †	756
		825	226 †	855
		1,000	220 †	894
		1,875	337 †	1,138
	3,400	90	185 †	647
155	15,000	50	75 to 102 †	212
		100	71 to 95 †	212
248	9,080	400	60 to 118 ‡	308
		500	111 ‡	306
		600	70 ‡	304
		700	105 ‡	302
		800	120 ‡	299
		900	60 ‡	299
		1,000	105 ‡	302

* Project 3.4. † Project 1.1. ‡ Project 1.5.

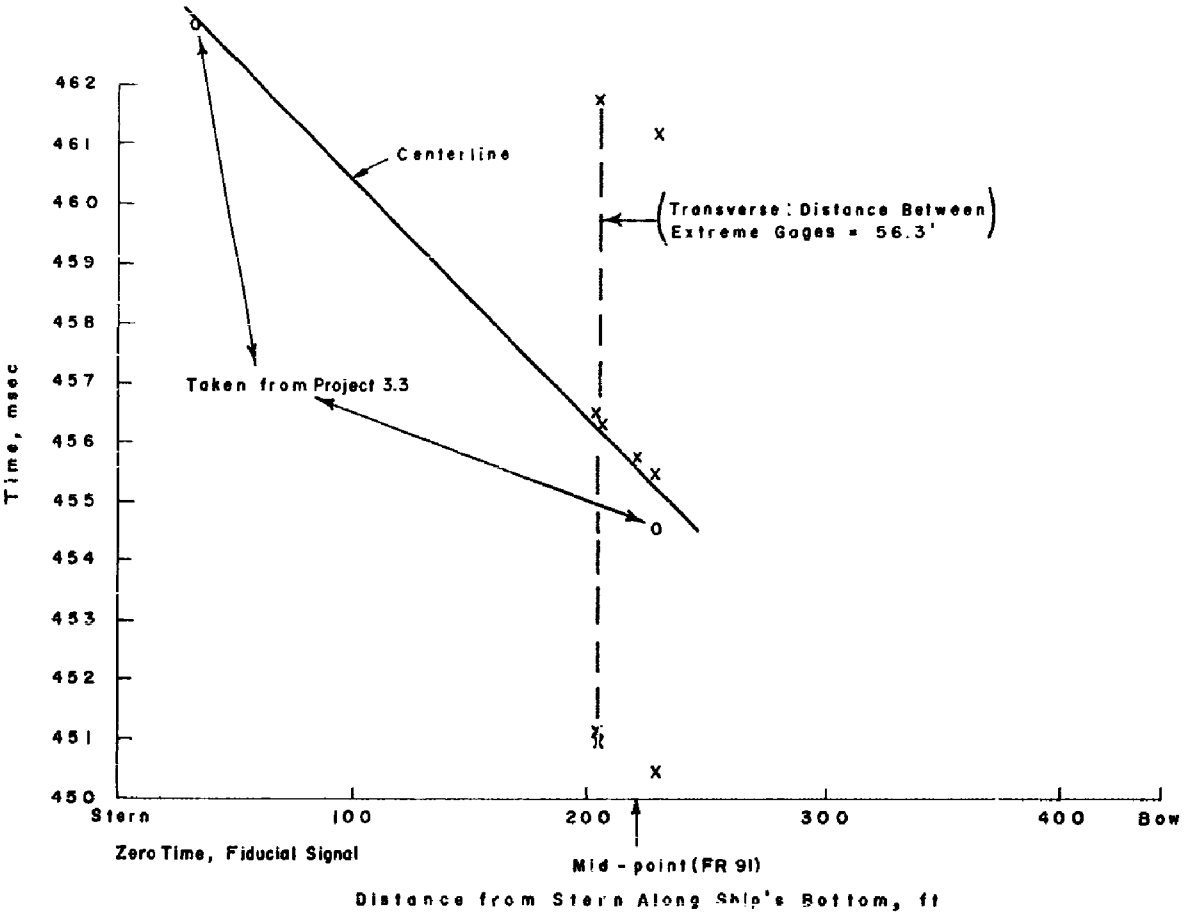

Figure A.1 Experimental shock wave arrival times at EC-2 bottom, Shot Wahoo.

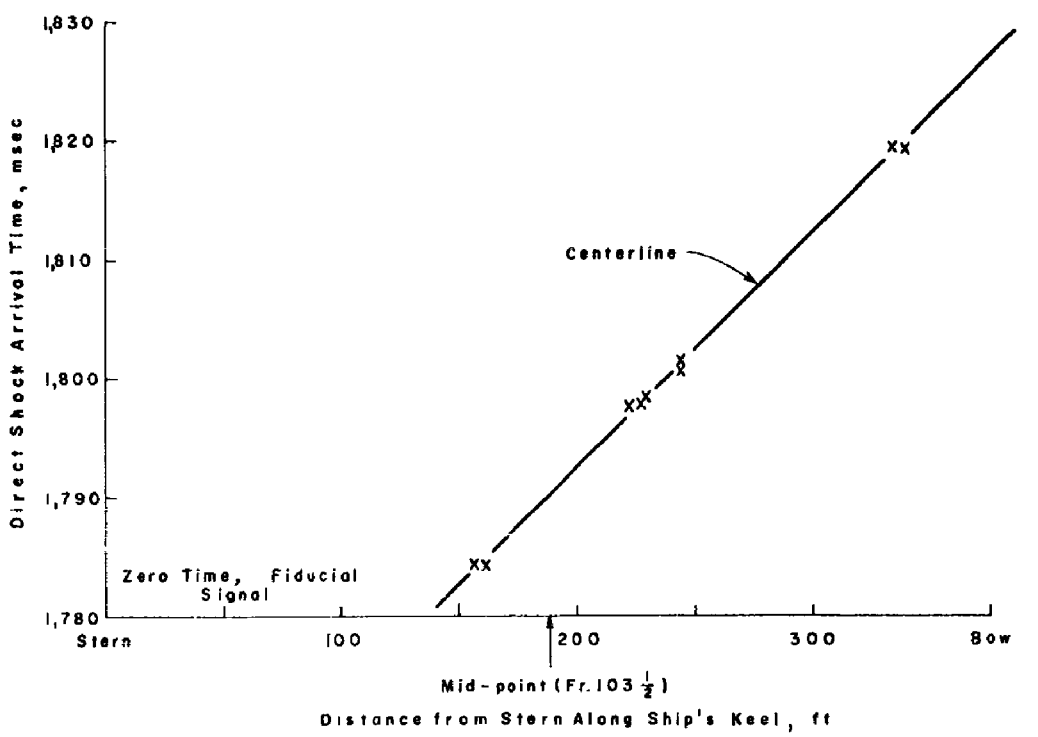

Figure A.2 Experimental shock wave arrival times at DD-593 bottom, Shot Wahoo.

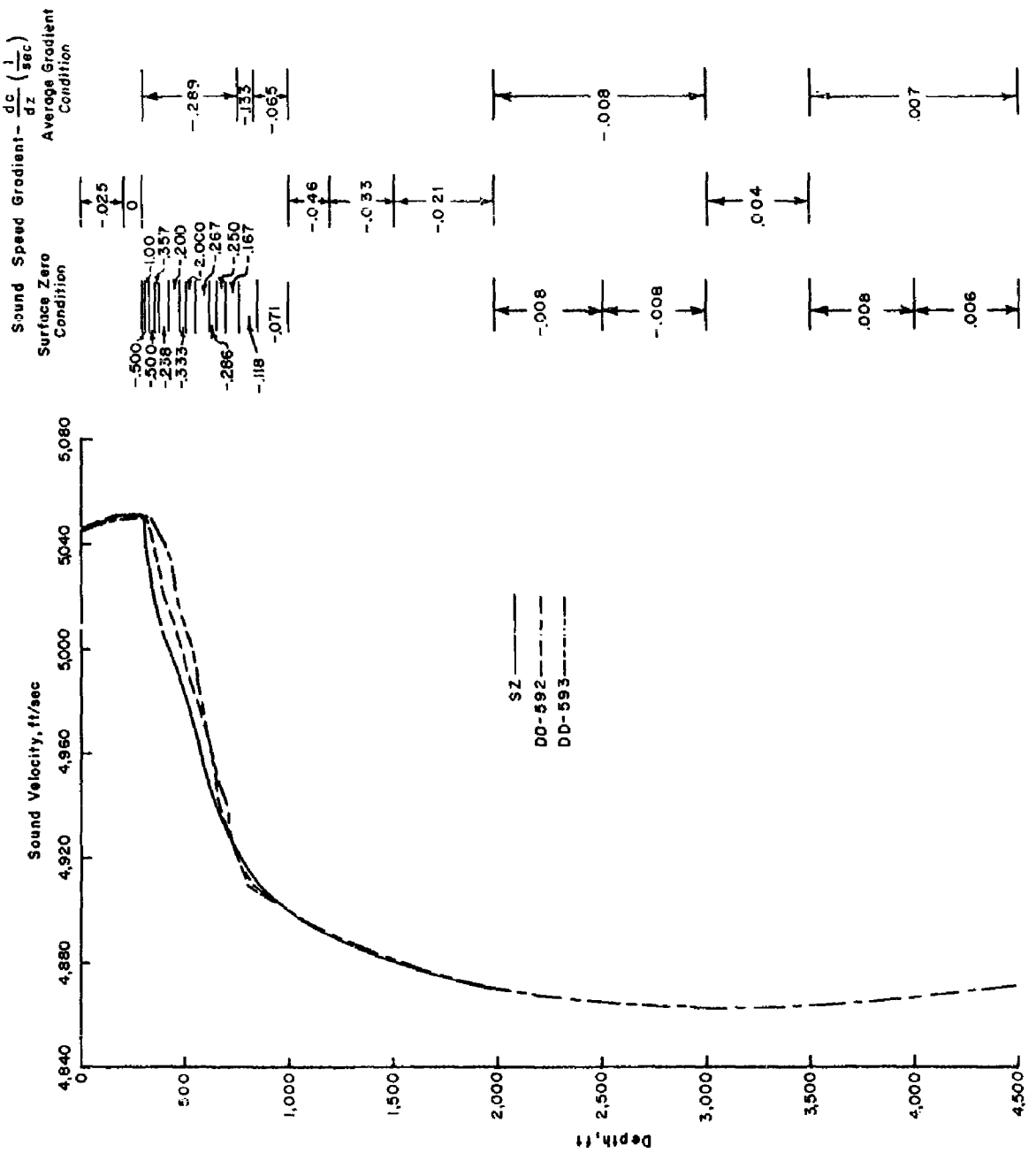

Figure A.3 Variation of sound velocity with depth at key locations and velocity gradients, Shot Wahoo.

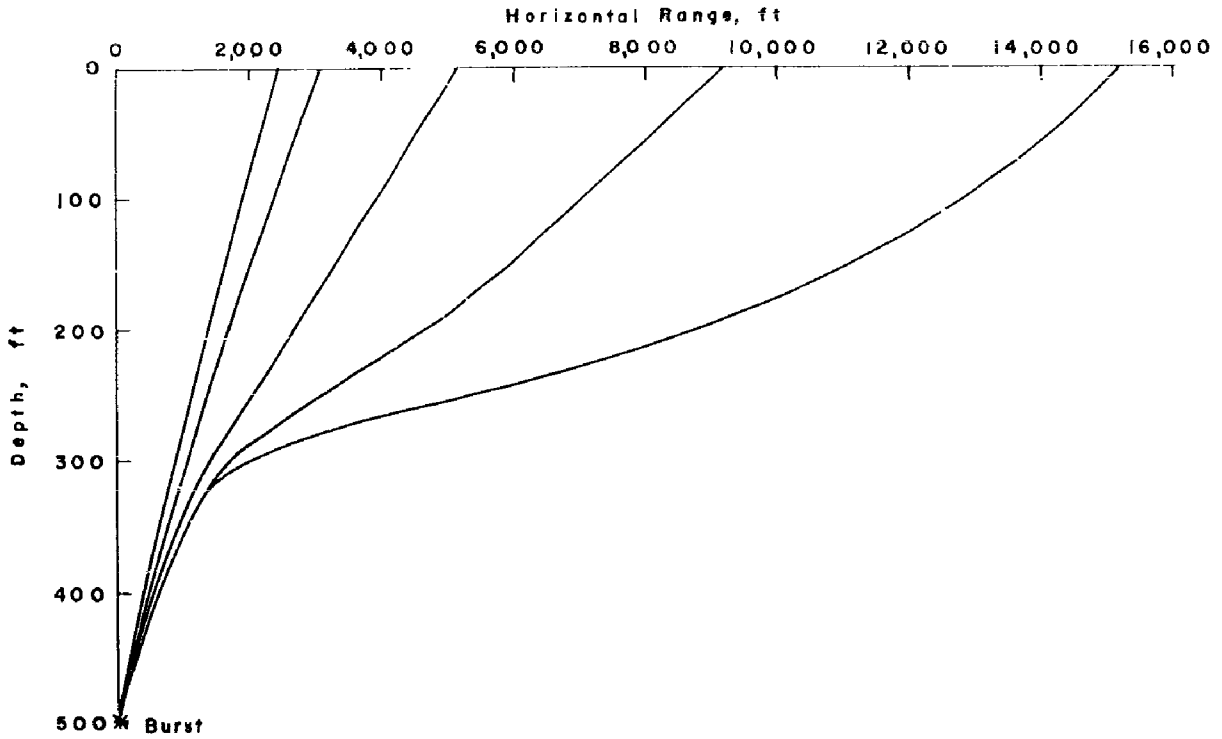

Figure A.4 Refraction ray paths computed for the surface zero sound velocity structure, Shot Wahoo.

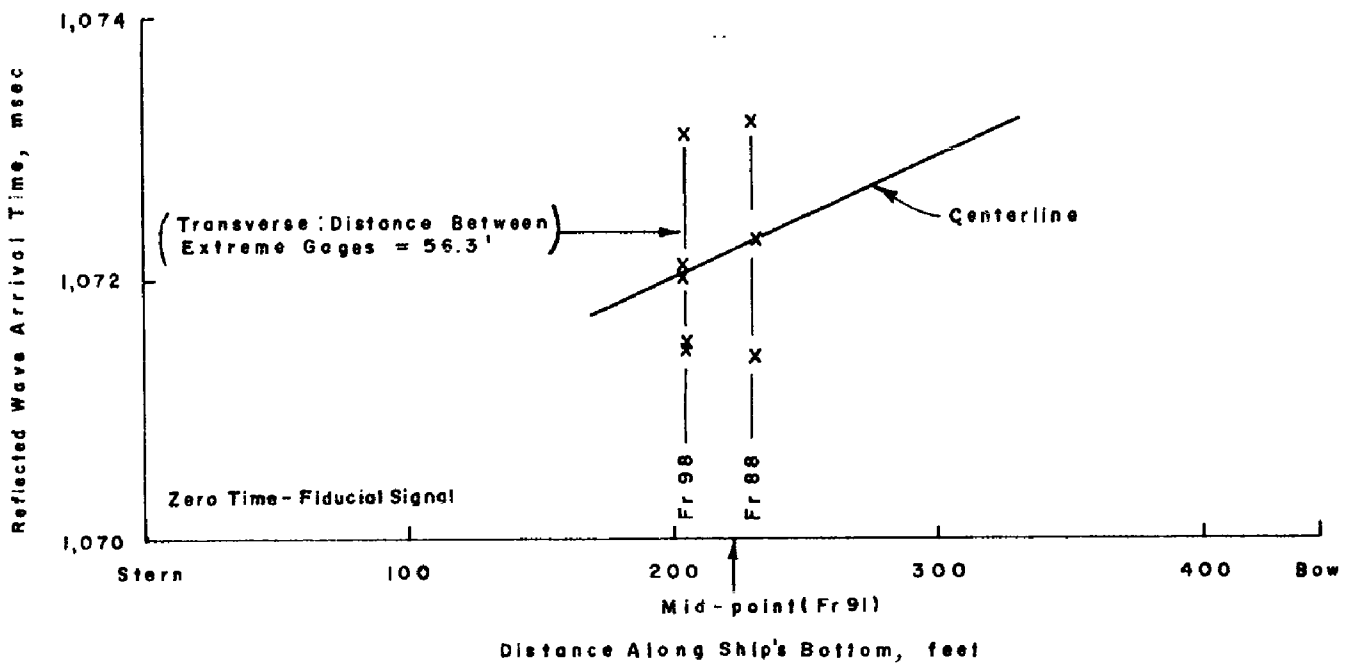

Figure A.5 Experimental bottom reflected wave arrival times at EC-2 bottom, Shot Wahoo.

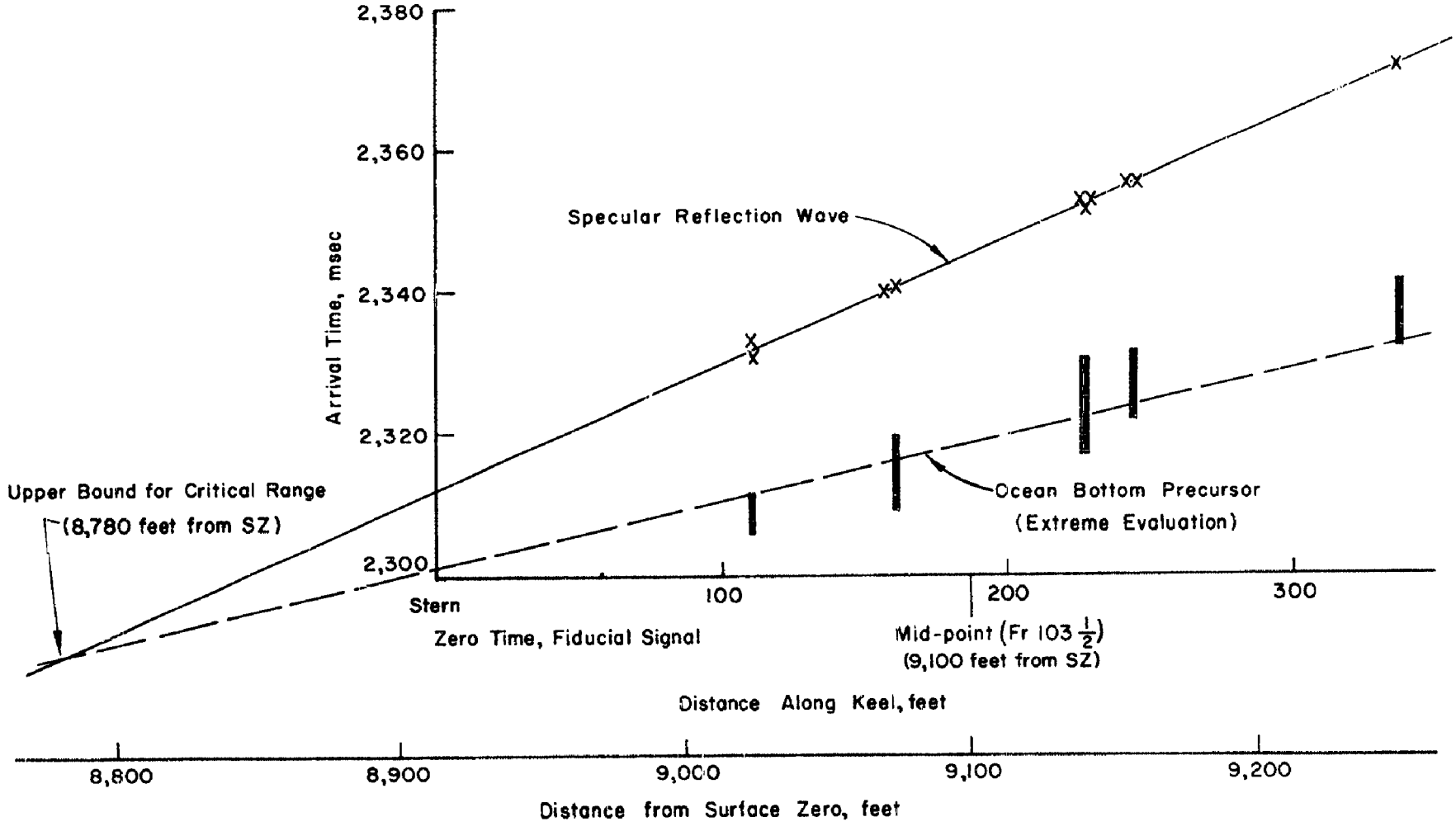

Figure A.6 Bottom reflected wave versus distance along keel, DD-593, Shot Wahoo.

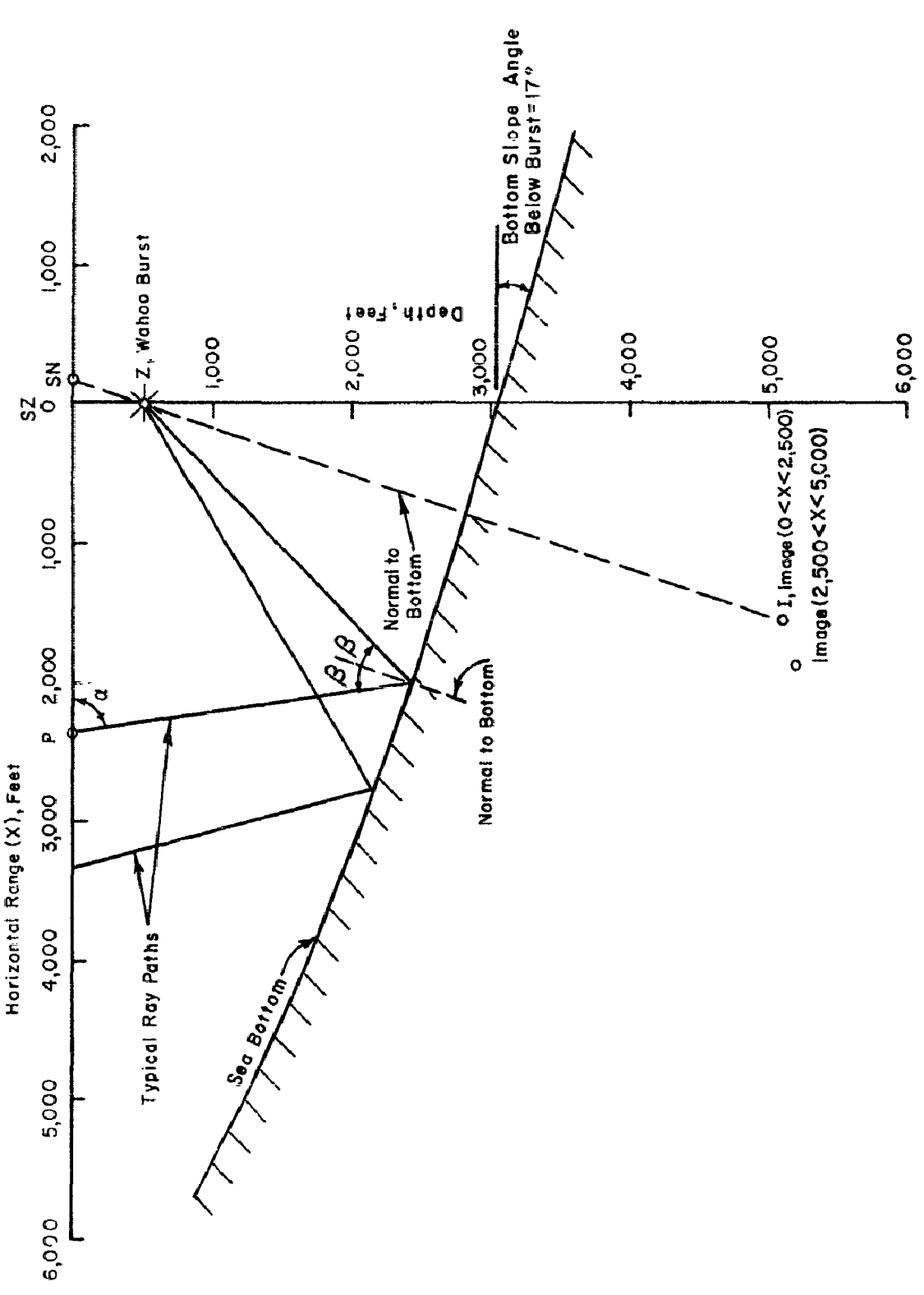

Figure A.7 Bottom contour along slope gradient, 29° array, Shot Wahoo.

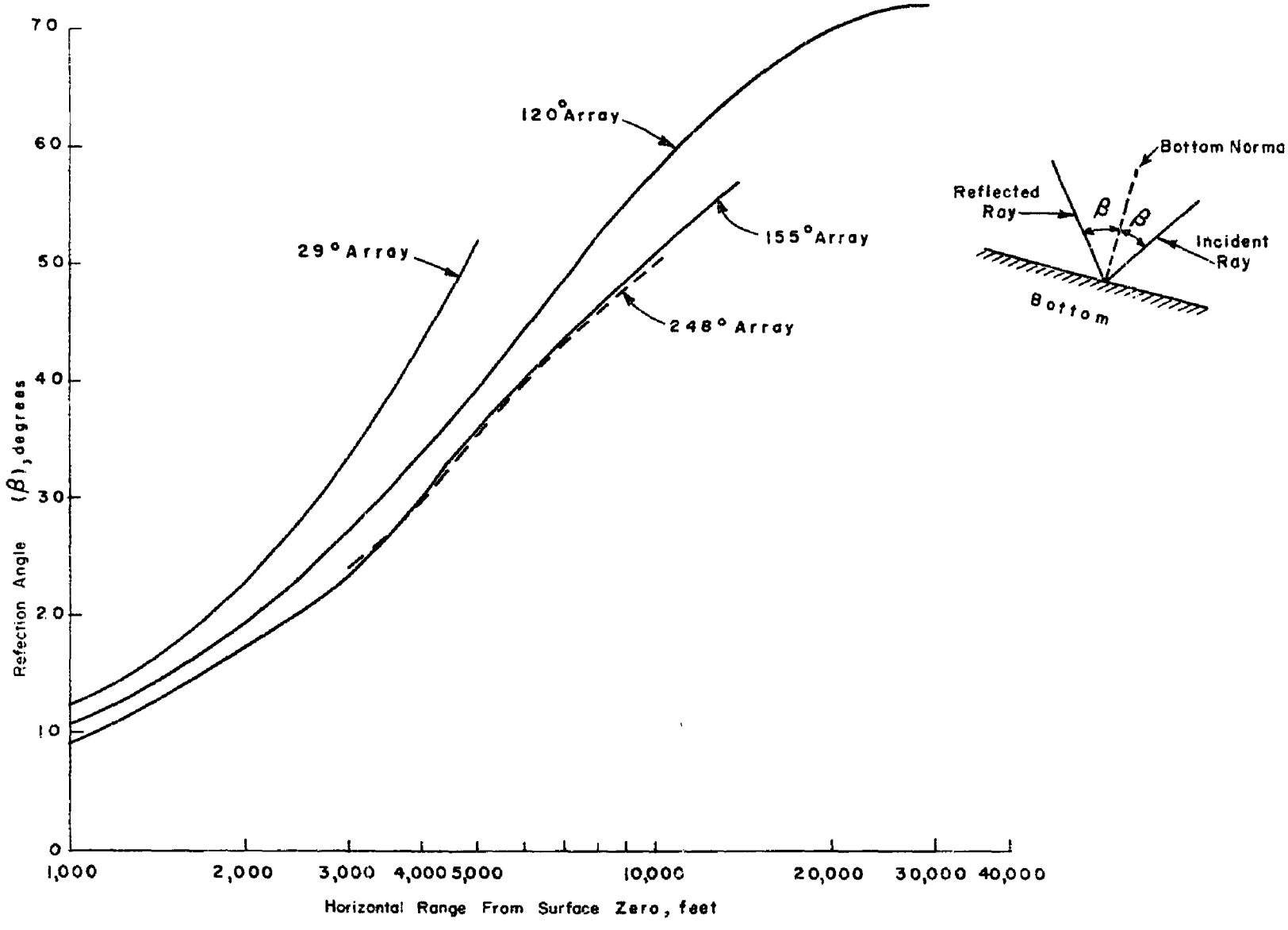

Figure A.8 Variation of angle between specularly reflected wave and bottom normal with horizontal range from surface zero, Shot Wahoo.

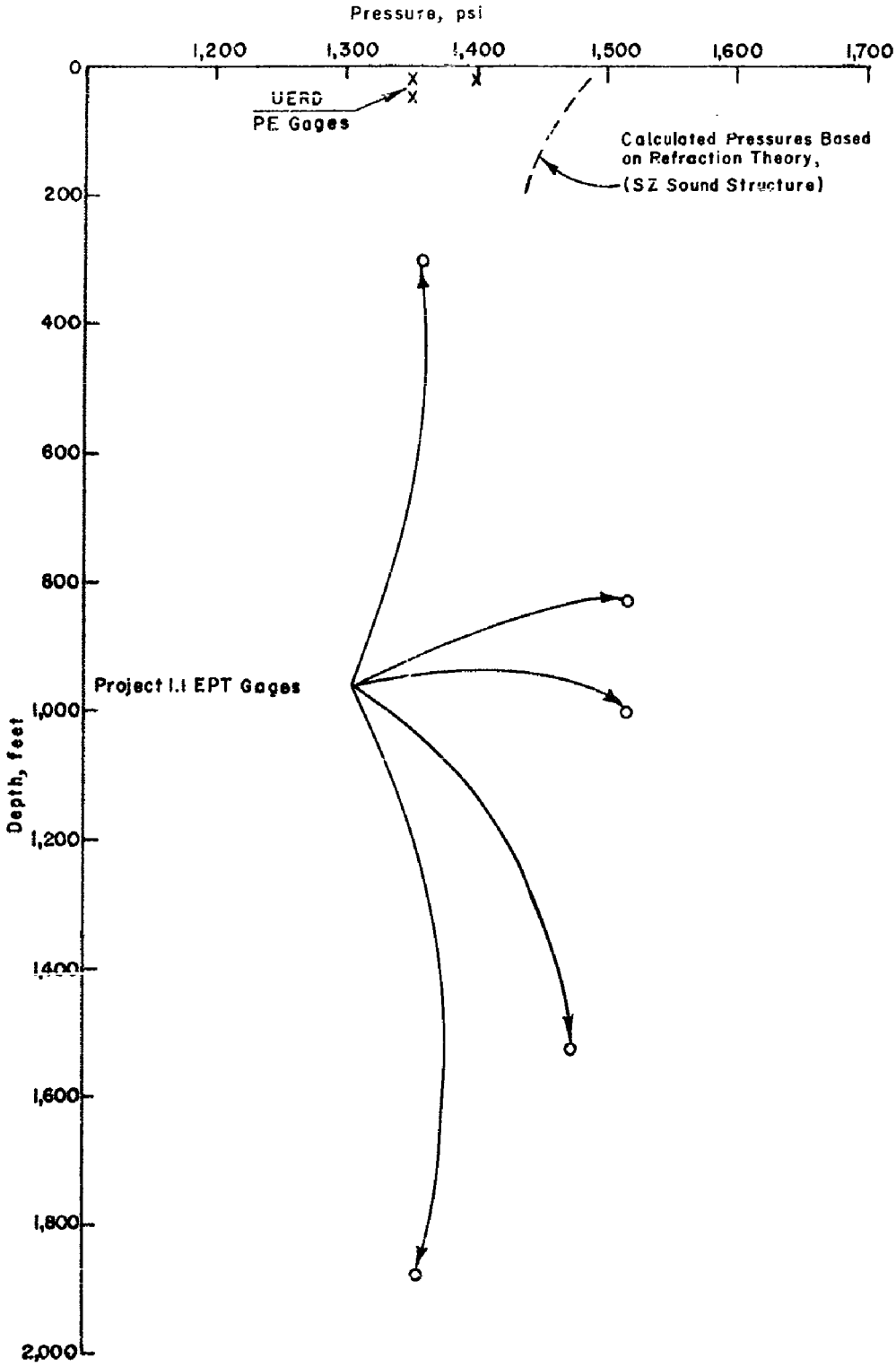

Figure A.9 Experimental and computed peak shock wave pressures at EC-2 location, Shot Wahoo.

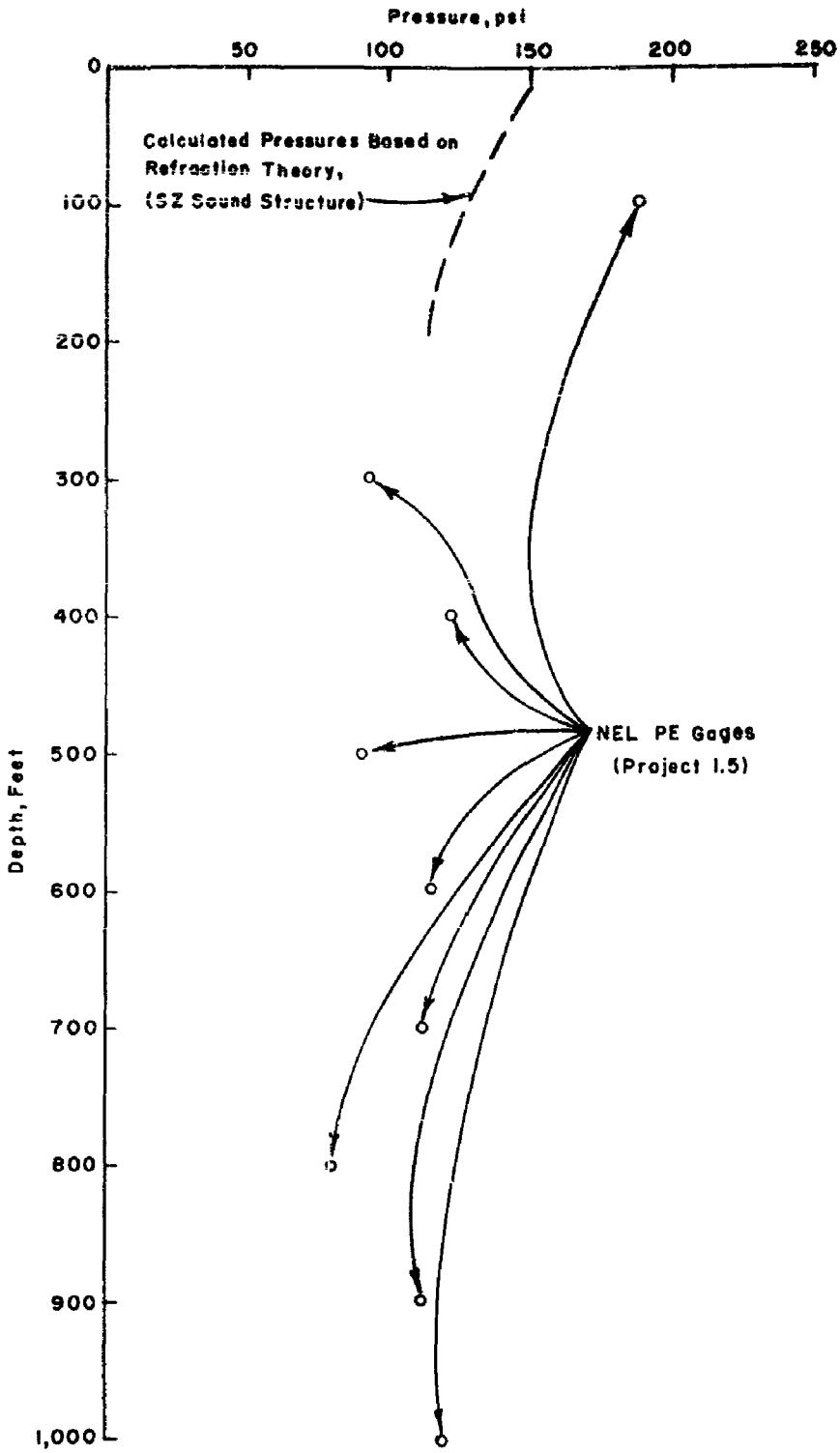

Figure A.10 Experimental and computed peak shock wave pressures at DD-593 location, Shot Wahoo.

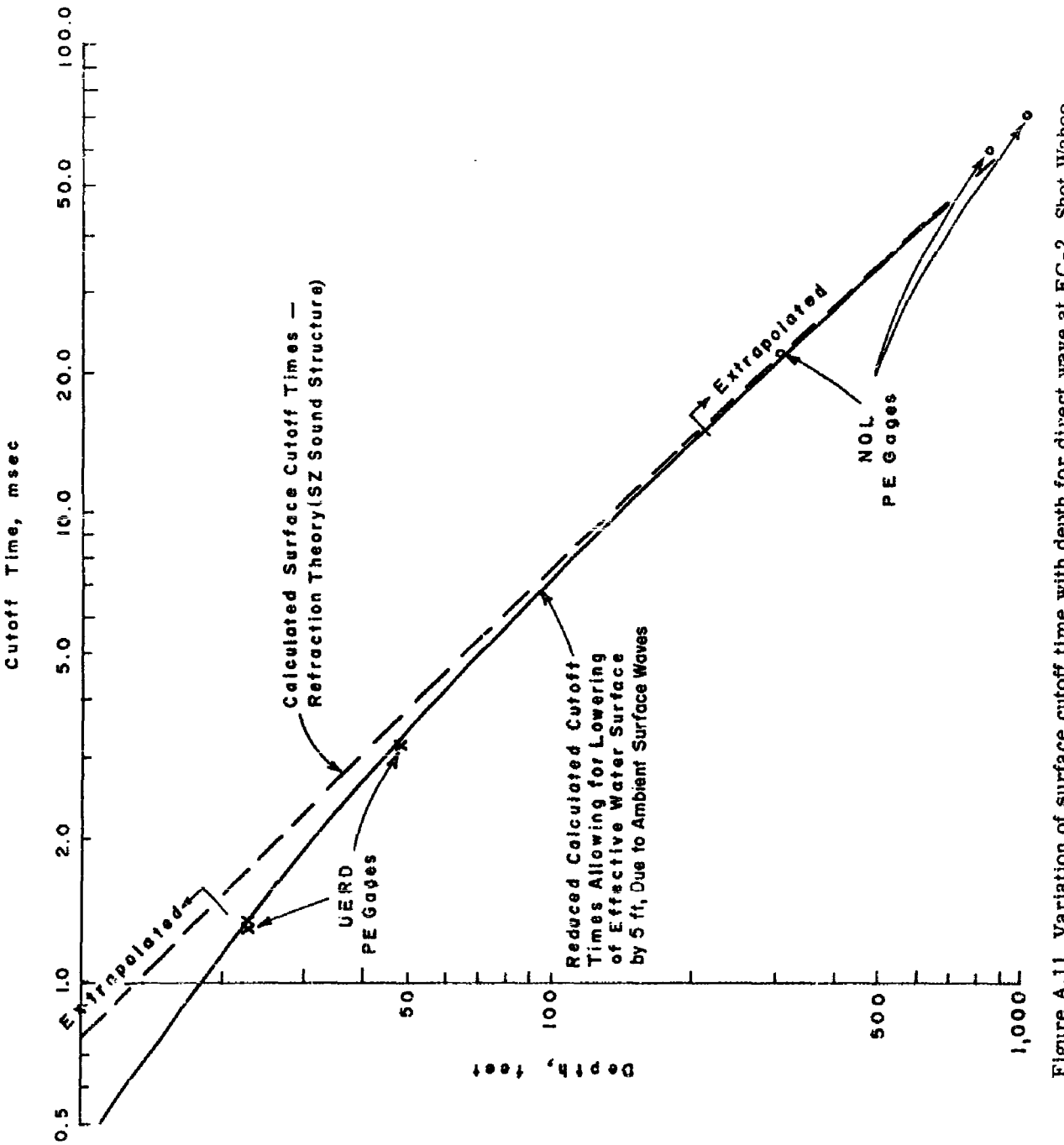

Figure A.11 Variation of surface cutoff time with depth for direct wave at EC-2, Shot Wahoo.

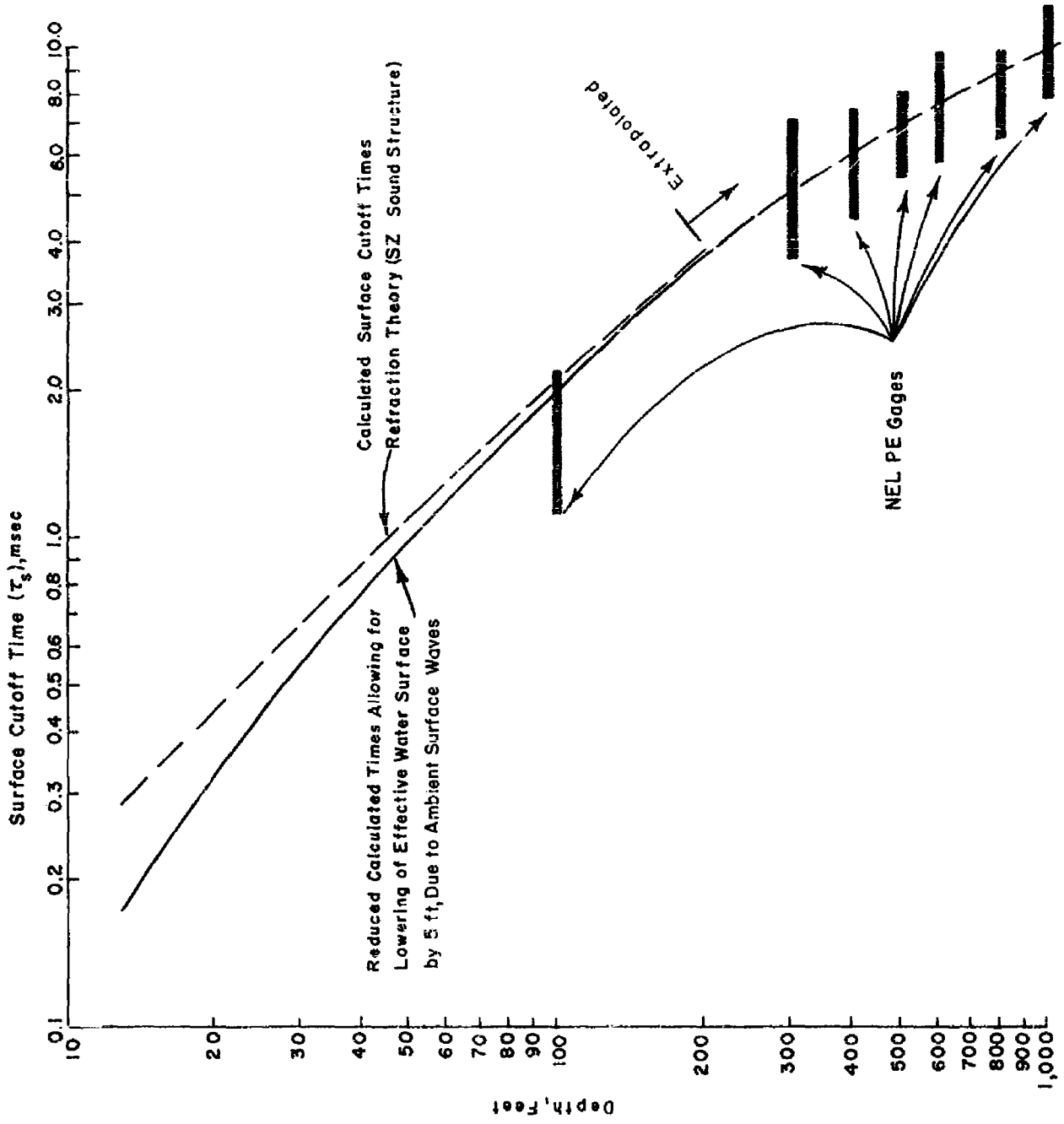

Figure A.12 Variation of surface cutoff time with depth for direct wave at DD-593, Shot Wahoo.

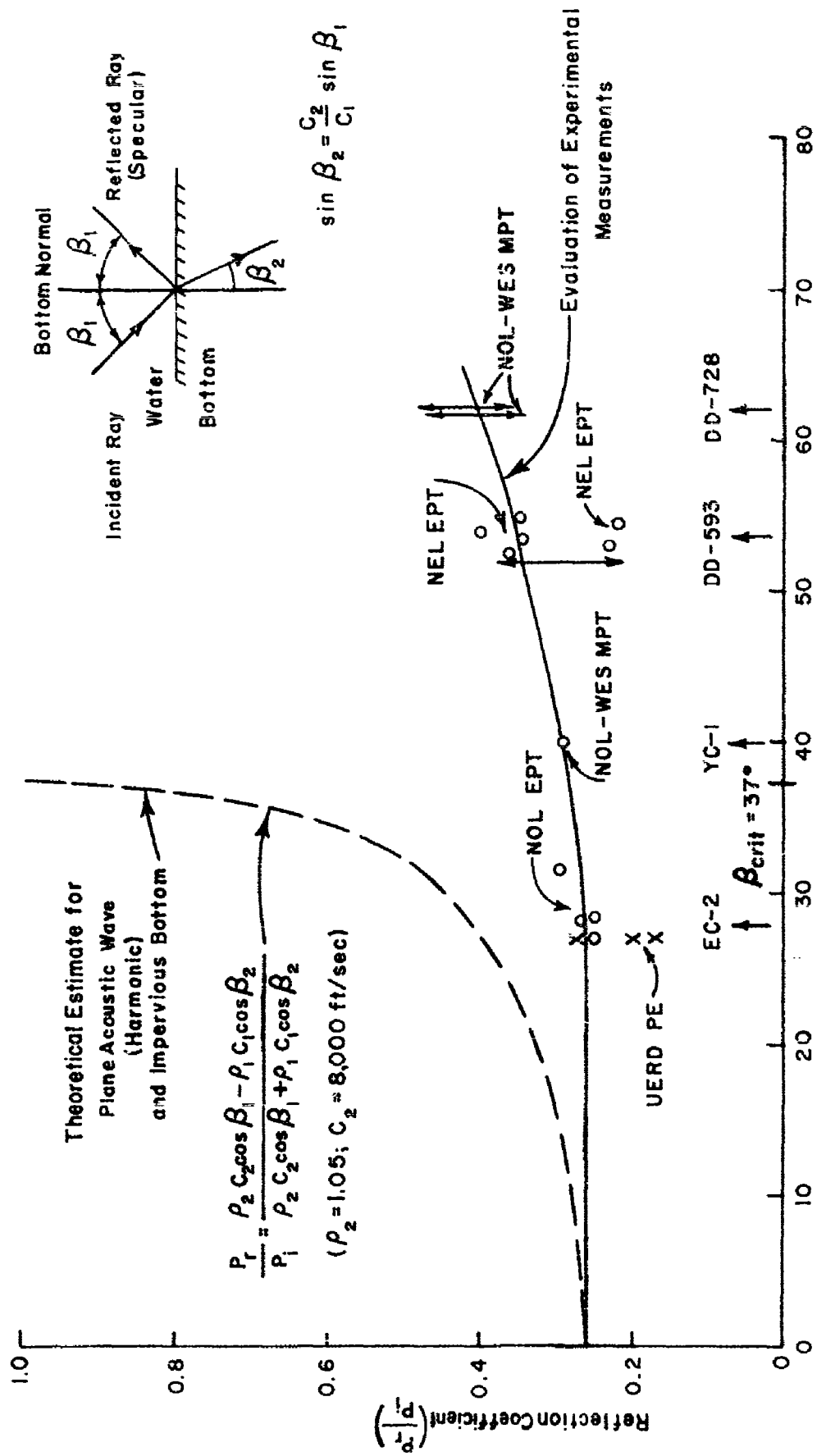

Figure A.13 Bottom reflection coefficient (specular reflection).

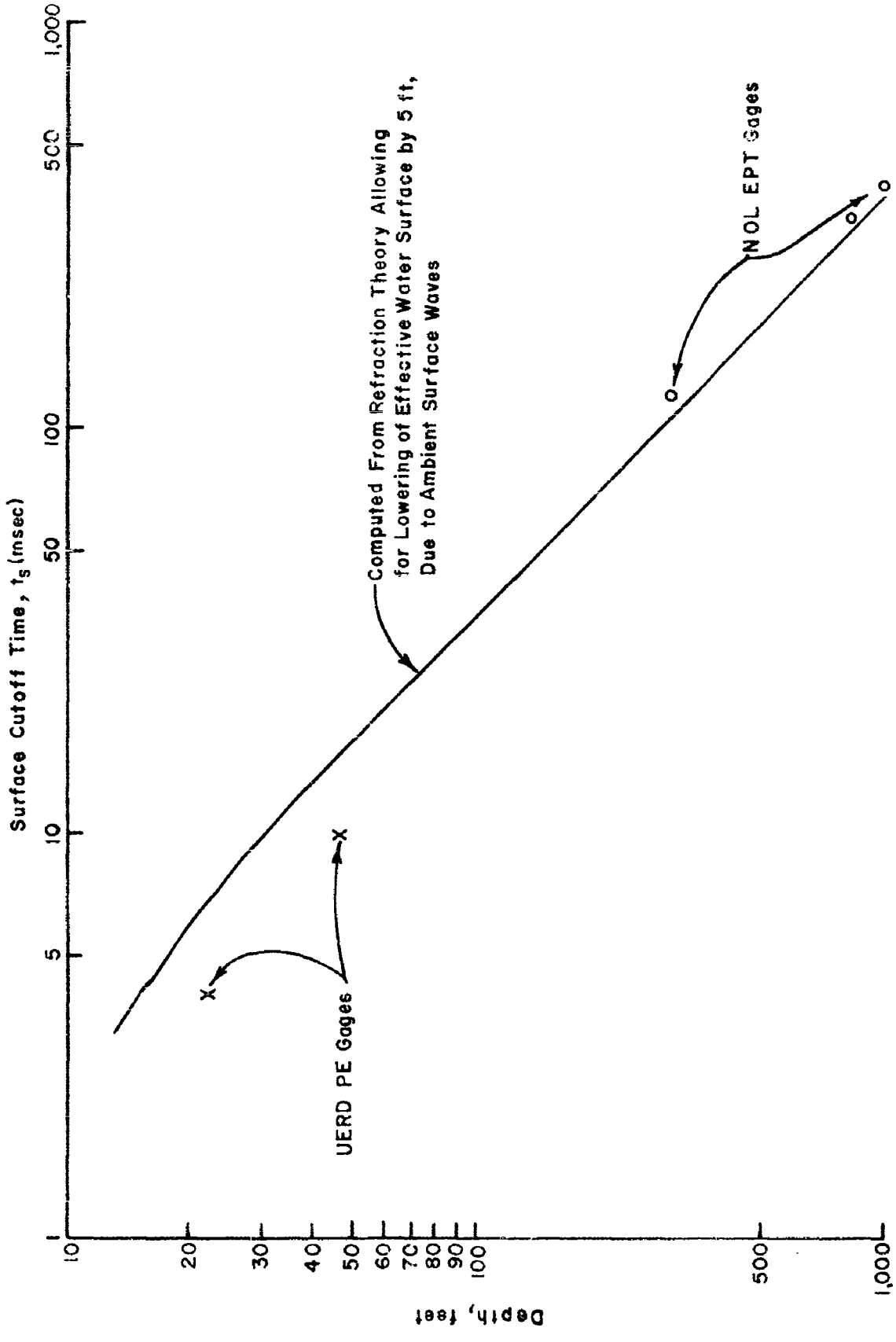

Figure A.14 Surface cutoff time versus depth for reflected wave at EC-2 position, Shot Wahoo.

Appendix B

DETAILED EVALUATION OF UNDERWATER PRESSURE PHENOMENA, SHOT UMBRELLA

An evaluation of available information concerning test conditions and underwater pressure phenomena was carried out to establish a suitable framework for analysis of surface-ship response. Data was made available to UERD by Project 1.1 prior to publication of its own analysis. The UERD conclusions have been summarized in the main text; detailed justifications are presented below in those cases where this was felt necessary.

B.1 TEST CONCLUSIONS

Estimates of the ranges of the target ships were made based on measurements and calculations or shock wave arrival times.

Direct shock wave arrival times measured by bottom gages (pressure gages and velocity meters attached to the hull) along the EC-2, DD-474, and DD-592 centerlines are plotted as a function of distance from the stern of each ship in Figures B.1 through B.3. The experimental points are connected by straight lines denoted "centerline" so that arrival times can be derived at the midship locations (Frame 91 for the EC-2 and Frame 103½ for the DD's).

The arrival time of the direct shock wave front at various ranges along the water surface was computed by estimating the correction to sound-signal arrival times in order to allow for the finite amplitude of the shock wave; to employ this type of correction, experimental peak pressures (Section 6.1) were employed in to a range of 500 feet. Since the experimental pressures appeared to approach values to be expected from a burst of identical yield in free-water conditions, this assumption was utilized to extrapolate the experimental pressures in to closer ranges. At each of a series of ranges the instantaneous shock front velocity was estimated, and arrival times were computed by numerically integrating these instantaneous shock front speeds. The shock wave arrival times thus computed are presented as a function of horizontal range from surface zero in Table B.1. These computational results, together with Figures B.1 to B.3, allow the midship positions of the key target ships to be located as shown in Table 6.1. Differences between these results and those derived from the aerial photographic survey are considered slight.

The orientation, or heading, of the ships was also derived both from arrival-time measurements and from the aerial-photographic survey. In the cases of ships attached side-on (EC-2 and DD-592) arrival-time estimates were considered the more reliable and were used in Table 6.1 of the main text; in other cases the aerial photographic survey was used.

Measurements of the lagoon bottom precursor arrival times at the target ship locations were compiled and are presented in Figure B.4; that these measurements are relatively more inaccurate than those for the shock front is indicated by the use of short lines rather than points. To orient the reader, shock wave arrival times are also included, as a dashed line, in Figure B.4. Similar measurements of precursor arrival times as a function of range were made by Project 1.1 (Reference 16); these are shown as a solid line in Figure B.4. The degree of agreement between the two types of measurements is considered reasonably good, considering the inherent inaccuracies.

An extremely crude interpretation of Figure B.4 can be made on the basis of assuming that sound speed in the bottom material is constant; this would suggest that sound speed in the bottom material is 9,300 ft/sec (Reference 16). Such an estimate of sound speed is considerably higher than the corresponding estimate made in Shot Wahoo, although no reason exists to suppose that sound speed in the upper layers of the bottom materials in the two sites are indeed so much different (Reference 26). No doubt, as suggested in Reference 16, the above crude interpretation is overly simplified for Shot Umbrella, and lower substrata of higher sound speed are contributing to produce the higher average sound speed suggested by the measurements.

B.2 BULK CAVITATION

Observations on bulk cavitation were made from a motion-picture camera mounted on an RB-50 aircraft 25,000 feet above surface zero. The treatment of these observations is described below; the results have been incorporated in Section 6.1 of the main text.

The best of the films for observing bulk cavitation was Film 52254 recorded at a nominal speed of 100 frames/sec. When the film is projected at normal speed, a dark circle can be seen spreading out from surface zero, visible out to about 3,000 feet. Within this dark circle a central portion shows a white aspect, at first out to a range of about 900 feet from surface zero. Shortly thereafter an irregular whitish ring, originating about 1,700 feet from surface zero, runs inward and appears to join the central white disk. Because this seemed clearly associated with the bulk cavitation phenomena, closer investigation was undertaken.

The film, unfortunately, lacked timing marks and therefore the first step required was to calibrate it. This was done by assuming that the dark circle was the slick created by the direct shock wave. Utilizing the arrival times already computed for the shock wave front at the water surface and using a distance scale based on the derived standoff of the midposition of the EC-2, the film was essentially calibrated; an extrapolation had to be employed to complete the task. An effort was now made to use the film to measure the bulk cavitation absolute reloading time as a function of horizontal distance from surface zero. Again, as in Shot Wahoo, when the movie film was examined frame by frame, rather than run on a projector, it proved difficult to make precise measurements of the inward-running whitish ring. However, a rough estimate was derived, and this served to provide the information incorporated in Figure 6.7 of the main text.

TABLE B.1 COMPUTED SHOCK WAVE ARRIVAL TIMES

Horizontal Range	Arrival Time
feet	msec
0	18.0
38	18.8
222	39.3
494	86.1
743	132.3
1,090	199.1
1,679	313.6
1,747	327.2
1,905	358.2
2,047	386.0
2,420	459.4
2,965	566.2
5,707	1,108.9
7,900	1,543.1

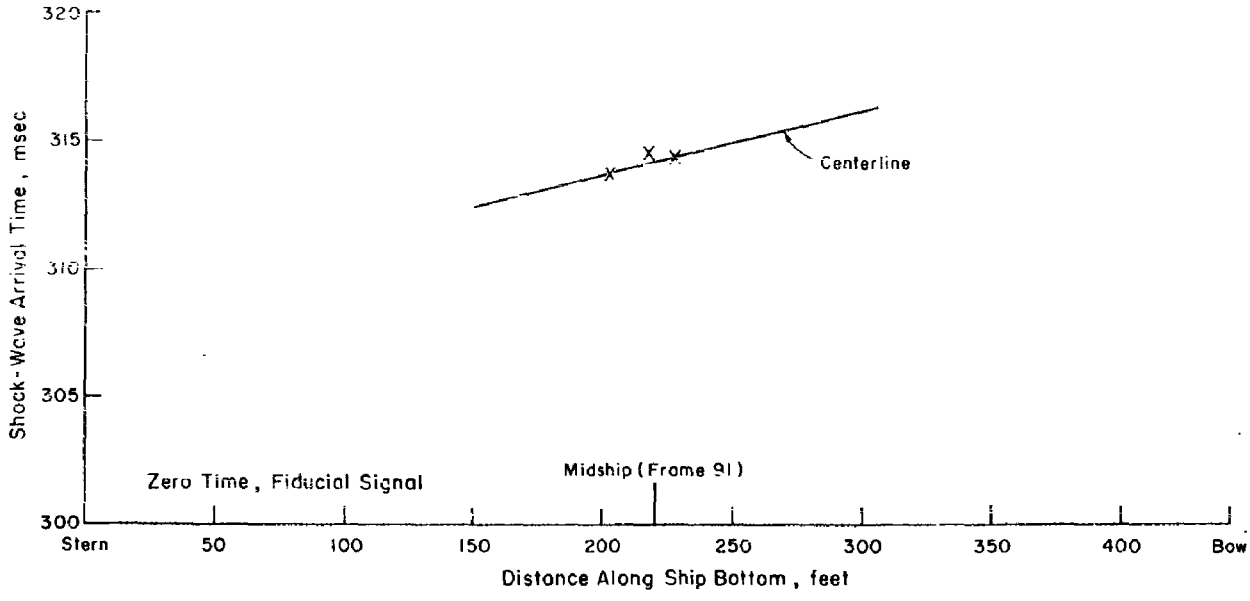

Figure B.1 Experimental shock wave arrival times at keel, EC-2, Shot Umbrella.

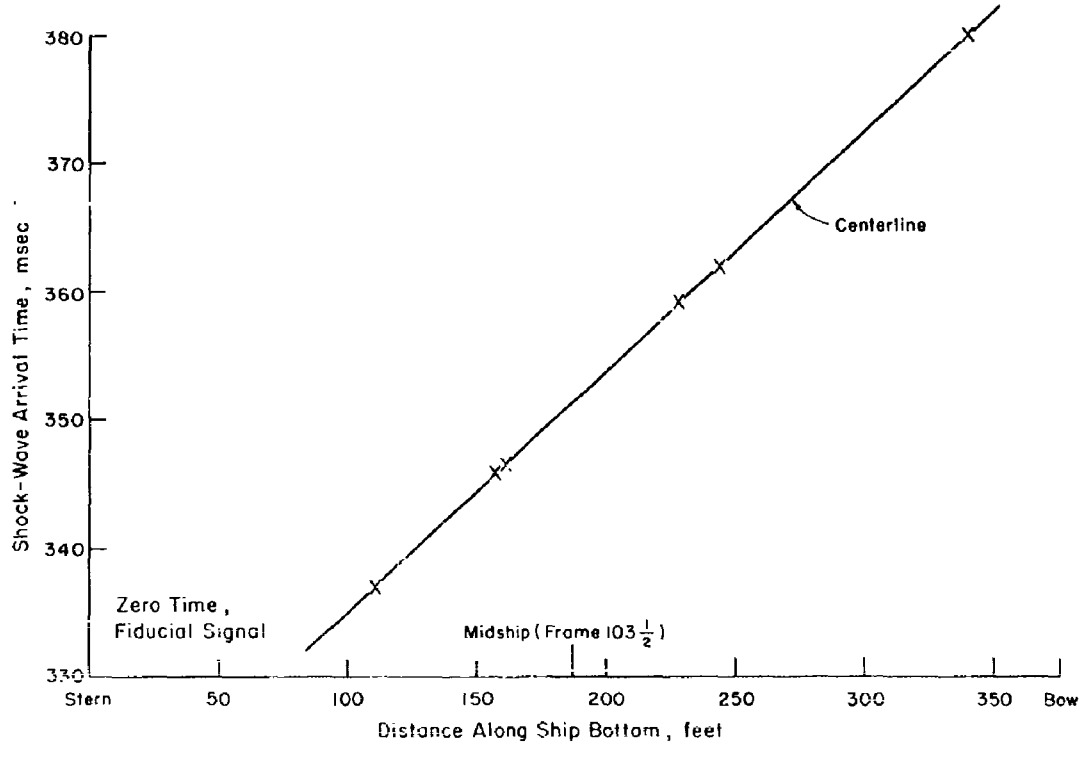

Figure B.2 Experimental shock wave arrival times at keel, DD-474, Shot Umbrella.

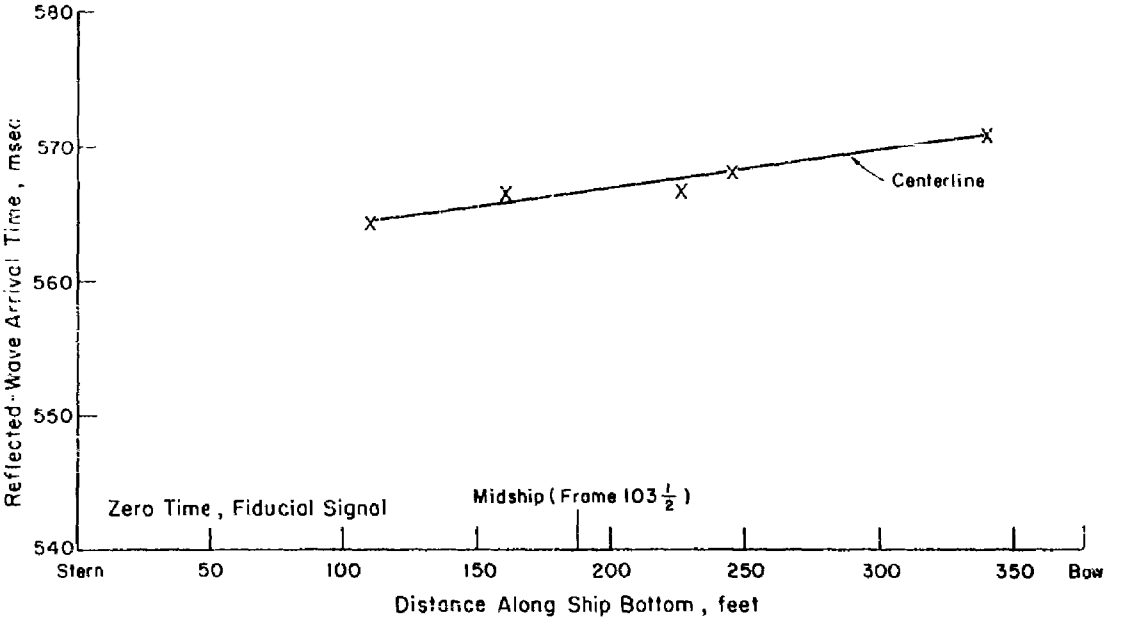

Figure B.3 Experimental shock wave arrival times at keel, DD-592, Shot Umbrella.

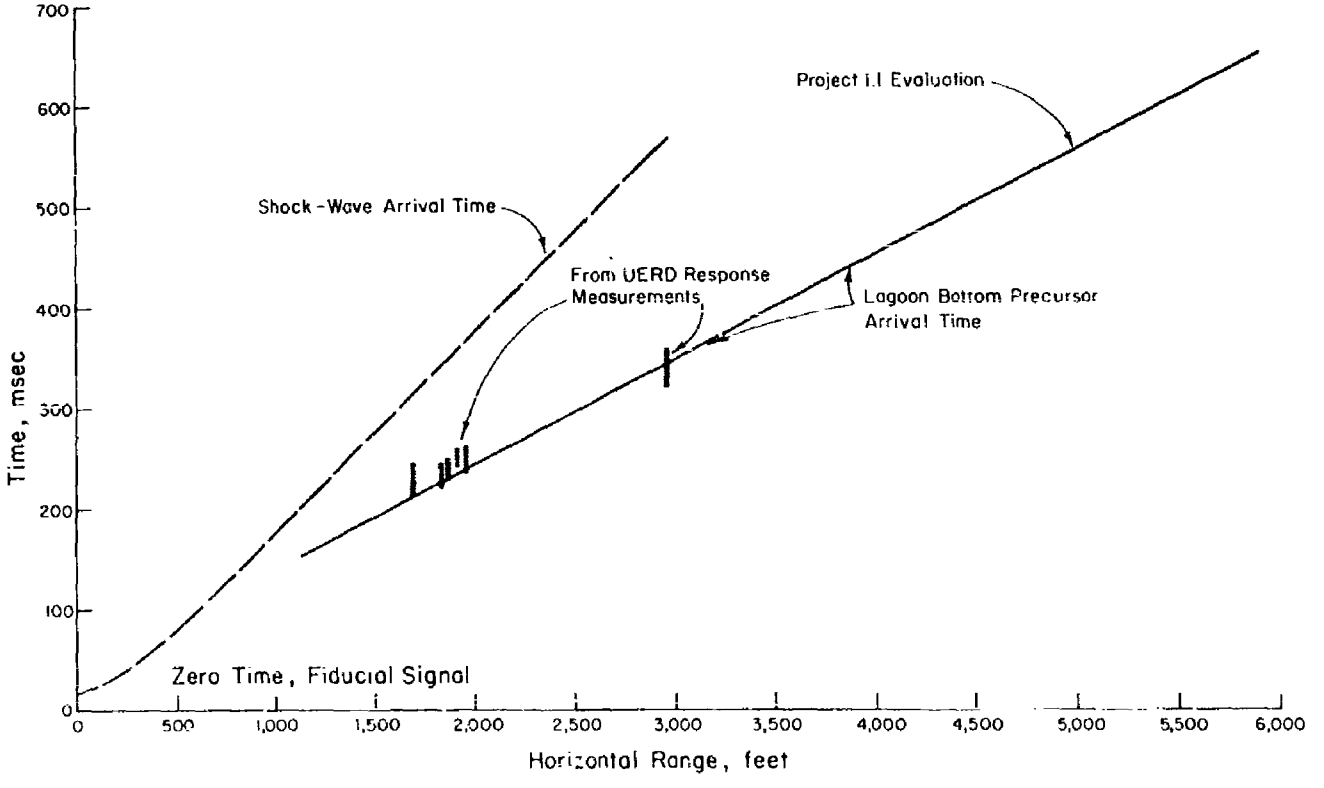

Figure B.4 Lagoon bottom precursor arrival times, Shot Umbrella.

REFERENCES

1. A. H. Keil; "Introduction to Underwater Explosion Research"; UERD Report 19-56, December 1956; Underwater Explosions Research Division, Norfolk Naval Shipyard, Portsmouth, Va.; Confidential.

2. J. H. Rosenbaum and H. G. Snay; "On The Oblique Reflection of Underwater Shock Waves from a Free Surface I"; NAVORD Report 2710, 1953; Bureau of Naval Ordnance, Washington 25, D.C.; Confidential.

3. D. H. Towne and K. G. Wilson; "Refraction and Diffraction of Explosive Pressure Pulses by Gradients in the Propagation Velocity II Status of Application of Mathematical Analysis to the Problem of Calculation of Pulse Shapes"; Report 57-45 (unpublished manuscript); Woods Hole Oceanographic Institution, Woods Hole, Mass.

4. A. H. Keil and others; "Project Papoose"; UERD Report 18-54 (AFSWP-256), 1954; Underwater Explosions Research Division, Norfolk Naval Shipyard, Portsmouth, Va.; Confidential Formerly Restricted Data.

5. H. L. Rich and others; "Hull Response and Shock Motion—Background, Instrumentation, and Test Results"; Project 3.2 (Part I), Operation Wigwam, WT-1023, May 1955; David Taylor Model Basin, Washington 7, D. C.; Confidential Formerly Restricted Data.

6. W. W. Murray; "Model Studies on Effects of Underwater Atomic Explosions on Ships, Part III, Analysis of Cargo Ship Model Tests"; UERD Report 2-57, AFSWP-1068, October 1957; Underwater Explosions Research Division, Norfolk Naval Shipyard, Portsmouth, Va.; Confidential.

7. R. M. Santamaria; "Model Studies on Effects of Underwater Atomic Explosions on Ships, Part IV, Tests of Cruiser Model"; UERD-Report 1-58, AFSWP-1085, April 1958; Underwater Explosions Research Division, Norfolk Naval Shipyard, Portsmouth, Va.; Confidential.

8. W. W. Murray and R. M. Santamaria; "Model Studies on Effects of Underwater Atomic Explosions on Cargo Ships, Effect of Orientation and Draft of Target"; UERD Report 5-59; Underwater Explosions Research Division, Norfolk Naval Shipyard, Portsmouth, Va.; Confidential.

9. W. W. Murray; "Tapered Charge Tests Against $\frac{1}{35}$-Scale Surface Ship Models"; UERD Report 18-56, November 1956; Underwater Explosions Research Division, Norfolk Naval Shipyard, Portsmouth, Va.; Confidential.

10. H. M. Schauer; "Instruments Employed by the UERD of the Norfolk Naval Shipyard"; UERD Report 3-50, July 1950; Underwater Explosions Research Division, Norfolk Naval Shipyard, Portsmouth, Va.

11. C. J. Aronson and others; "Underwater Free-Field Pressures to Just Beyond Target Locations"; Project 1.2, Operation Wigwam, Report WT-1005, May 1955; Explosives Research Department, Naval Ordnance Laboratory, White Oak, Silver Spring, Md., Confidential Formerly Restricted Data.

12. J. W. Winchester and others; "Characteristics of Ocean and Bottom for Shots Wahoo and Umbrella, Including Umbrella Crater"; Project 1.13, Operation Hardtack, WT-1618; U. S. Navy Hydrographic Office, Washington 25, D. C.; Confidential Formerly Restricted Data.

13. E. Swift and others; "Surface Phenomena from Underwater Bursts"; Project 1.3, Operation Hardtack, WT-1608; U. S. Naval Ordnance Laboratory, White Oak, Silver Spring, Md.; Confidential Formerly Restricted Data.

14. L. W. Kidd and W. S. Montgomery; "Water Waves Produced by Underwater Bursts"; Project 1.6, Operation Hardtack, WT-1611; Scripps Institution of Oceanography, University of California, La Jolla, California; Confidential Formerly Restricted Data.

15. J. J. Kearns and others; "Assessment of Ship Damage and Target Preparation for Shots Wahoo and Umbrella"; Project 3.8, Operation Hardtack, WT-1632; Bureau of Ships, Washington 25, D. C.; Confidential Formerly Restricted Data.

16. E. Swift and others; "Underwater Pressures from Underwater Bursts"; Project 1.1, Operation Hardtack, WT-1606; Waterways Experiment Station, Vicksburg, Mississippi; Confidential Formerly Restricted Data.

17. C. J. Burbank and others; "Refraction of Shock Waves from a Deep-Water Burst"; Project 1.5, Operation Hardtack, WT-1610; U. S. Navy Electronics Laboratory, San Diego 52, California; Confidential Formerly Restricted Data.

18. A. H. Keil; "Boundary of Disturbance for Nonlinear Reflection of Underwater Shock Waves at a Free Surface"; UERD Report 3-58, AFSWP-1103, September 1958; Underwater Explosions Research Division, Norfolk Naval Shipyard, Portsmouth, Va.; Confidential.

19. E. H. Kennard; "Underwater Explosions, A Summary of Results"; DTMB Report C-334, February 1951; David Taylor Model Basin, Washington, D. C.; Confidential.

20. W. W. Murray; "Tapered-Charge Testing of the DD-592—Loading and Basic Target Response"; Project 3.4, Operation Hardtack, Part III of WT-1605 (Project 3.1); Underwater Explosions Research Division, Norfolk Naval Shipyard, Portsmouth, Va.; Confidential Formerly Restricted Data.

21. H. L. Rich and others; "Shock Loading in Ships from Underwater Bursts and Response of Shipboard Equipment"; Project 3.3, Operation Hardtack, WT-1627; David Taylor Model Basin, Washington 7, D.C.; Confidential Formerly Restricted Data.

22. W. G. Penny; "The Physical Effects of Atomic Bombs—Part I. Damage to Ships by Underwater Explosions of Atomic Bombs—January 1948"; USAEC FWE-180, September 1958; United Kingdom Atomic Energy Authority, Atomic Weapons Research Establishment, Aldermaston, Berks., England; Secret Restricted Data.

23. W. W. Murray; "Model Studies on Effects of Underwater Atomic Explosions on Ships, Part V, Results of Panel Tests"; UERD Report 3-58, AFSWP-1103, September 1958; Underwater Explosions Research Division, Norfolk Naval Shipyard, Portsmouth, Va.; Confidential.

24. J. H. Haywood; "The Effect of Refraction on the Pressure Pulse from Underwater Atomic Explosions"; NCRE Report R406, November 1958; Naval Construction Research Establishment, St. Leonard's Hill, Dunfermline, Fife, England; Confidential Discreet.

25. C. Hartdegen and G. R. Hamilton; "Results of the Oceanographic Survey at Eniwetok, September - October 1957"; Technical Report No. 4, CU-57-1-N ONR 266-37-GEOL,

February 1958; Lamont Geological Observatory (Columbia University), Palisades, New York.

26. R. W. Raitt; "Seismic-Refraction Studies of Eniwetok Atoll"; Geological Survey Professional Paper 260-S, U. S. Government Printing Office, Washington, D. C., 1957.

DISTRIBUTION

Military Distribution Categories 16 and 36

ARMY ACTIVITIES

1 Deputy Chief of Staff for Military Operations, D/A, Washington 25, D.C. ATTN: Dir. of SW&R
2 Chief of Research and Development, D/A, Washington 25, D.C. ATTN: Atomic Div.
3 Assistant Chief of Staff, Intelligence, D/A, Washington 25, D.C.
4 Chief of Engineers, D/A, Washington 25, D.C. ATTN: ENGNB
5 Chief of Engineers, D/A, Washington 25, D.C. ATTN: ENGEB
6 Chief of Engineers, D/A, Washington 25, D.C. ATTN: ENGTB
7 Chief of Transportation, D/A, Office of Planning and Int., Washington 25, D.C.
8- 10 Commanding General, U.S. Continental Army Command, Ft. Monroe, Va.
11 Director of Special Weapons Development Office, Headquarters CONARC, Ft. Bliss, Tex. ATTN: Capt. Chester I. Peterson
12 President, U.S. Army Artillery Board, Ft. Sill, Okla.
13 President, U.S. Army Air Defense Board, Ft. Bliss, Tex.
14 Commandant, U.S. Army Command & General Staff College, Ft. Leavenworth, Kansas. ATTN: ARCHIVES
15 Commanding General, Chemical Corps Training Comd., Ft. McClellan, Ala.
16 Commanding General, The Engineer Center, Ft. Belvoir, Va. ATTN: Asst. Cmdt, Engr. School
17 Director, Armed Forces Institute of Pathology, Walter Reed Army Med. Center, 625 16th St., NW, Washington 25, D.C.
18 Commanding Officer, U.S. Army Research Lab., Ft. Knox, Ky.
19 Commandant, Walter Reed Army Inst. of Res., Walter Reed Army Medical Center, Washington 25, D.C.
20- 21 Commanding Officer, Chemical Warfare Lab., Army Chemical Center, Md. ATTN: Tech. Library
22 Commanding General, Engineer Research and Dev. Lab., Ft. Belvoir, Va. ATTN: Chief, Tech. Support Branch
23 Director, Waterways Experiment Station, P.O. Box 631, Vicksburg, Miss. ATTN: Library
24- 25 Commanding General, Aberdeen Proving Grounds, Md. ATTN: Director, Ballistics Research Laboratory
26 Commanding General, U.S. Army Electronic Proving Ground, Ft. Huachuca, Ariz. ATTN: Tech. Library
27 Commanding Officer, USA Transportation Combat Development Group, Ft. Eustis, Va.
28 Director, Operations Research Office, Johns Hopkins University, 6935 Arlington Rd., Bethesda 14, Md.
29 President, Beach Erosion Board, Corps of Engineers, U.S. Army, 5201 Little Falls Rd., N.W., Washington 16, D.C.
30 Commander-in-Chief, U.S. Army Pacific, APO 958, San Francisco, Calif. ATTN: Ordnance Officer

NAVY ACTIVITIES

31- 32 Chief of Naval Operations, D/N, Washington 25, D.C. ATTN: OP-03EG
33 Chief of Naval Operations, D/N, Washington 25, D.C. ATTN: OP-31
34 Chief of Naval Operations, D/N, Washington 25, D.C. ATTN: OP-75
35 Chief of Naval Operations, D/N, Washington 25, D.C. ATTN: OP-91
36 Chief of Naval Operations, D/N, Washington 25, D.C. ATTN: OP-922G1
37 Chief of Naval Operations, D/N, Washington 25, D.C. ATTN: OP-922G2
38- 39 Chief of Naval Research, D/N, Washington 25, D.C. ATTN: Code 811
40- 42 Chief, Bureau of Naval Weapons, D/N, Washington 25, D.C. ATTN: DLI-3
43 Chief, Bureau of Ordnance, D/N, Washington 25, D.C.
44- 47 Chief, Bureau of Ships, D/N, Washington 25, D.C. ATTN: Code 423
48 Chief, Bureau of Supplies and Accounts, D/N, Washington 25, D.C.
49 Chief, Bureau of Yards and Docks, D/N, Washington 25, D.C. ATTN: D-440
50 Director, U.S. Naval Research Laboratory, Washington 25, D.C. ATTN: Mrs. Katherine H. Cass
51- 52 Commander, U.S. Naval Ordnance Laboratory, White Oak, Silver Spring 19, Md.
53 Commanding Officer and Director, Navy Electronics Laboratory, San Diego 52, Calif.
54 Commanding Officer, U.S. Naval Mine Defense Lab., Panama City, Fla.
55- 56 Commanding Officer, U.S. Naval Radiological Defense Laboratory, San Francisco, Calif. ATTN: Tech. Info. Div.
57- 58 Commanding Officer and Director, U.S. Naval Civil Engineering Laboratory, Port Hueneme, Calif. ATTN: Code L31
59 Commanding Officer, U.S. Naval Schools Command, U.S. Naval Station, Treasure Island, San Francisco, Calif.
60 Superintendent, U.S. Naval Postgraduate School, Monterey, Calif.
61 Commanding Officer, U.S. Fleet Sonar School, U.S. Naval Base, Key West, Fla.
62 Commanding Officer, U.S. Fleet Sonar School, San Diego 47, Calif.
63 Officer-in-Charge, U.S. Naval School, CEC Officers, U.S. Naval Construction Bn. Center, Port Hueneme, Calif.
64 Commanding Officer, Nuclear Weapons Training Center, Atlantic, U.S. Naval Base, Norfolk 11, Va. ATTN: Nuclear Warfare Dept.
65 Commanding Officer, Nuclear Weapons Training Center, Pacific, Naval Station, San Diego, Calif.
66 Commanding Officer, U.S. Naval Damage Control Trng. Center, Naval Base, Philadelphia 12, Pa. ATTN: ABC Defense Course
67 Commanding Officer, Naval Air Material Center, Philadelphia 12, Pa. ATTN: Technical Data Br.
68 Commanding Officer, U.S. Naval Medical Research Institute, National Naval Medical Center, Bethesda, Md.
69- 70 Commanding Officer and Director, David W. Taylor Model Basin, Washington 7, D.C. ATTN: Library
71 Commanding Officer and Director, U.S. Naval Engineering Experiment Station, Annapolis, Md.
72 Commander, Norfolk Naval Shipyard, Portsmouth, Va. ATTN: Underwater Explosions Research Division
73 Commandant, U.S. Marine Corps, Washington 25, D.C. ATTN: Code AO3H
74 Director, Marine Corps Landing Force, Development Center, MCS, Quantico, Va.
75 Commanding Officer, U.S. Naval CIC School, U.S. Naval Air Station, Glynco, Brunswick, Ga.
76 Chief of Naval Operations, Department of the Navy, Washington 25, D.C. ATTN: OP-09B5
77- 79 Chief, Bureau of Naval Weapons, Navy Department, Washington 25, D.C. ATTN: RR12

AIR FORCE ACTIVITIES

80 Air Force Technical Application Center, HQ. USAF, Washington 25, D.C.
81 HQ. USAF, ATTN: Operations Analysis Office, Office, Vice Chief of Staff, Washington 25, D. C.

86 HQ. USAF, Washington 25, D.C. ATTN: AFCIN-3D1
87 Director of Research and Development, DCS/D, HQ. USAF, Washington 25, D.C. ATTN: Guidance and Weapons Div.
88 The Surgeon General, HQ. USAF, Washington 25, D.C. ATTN: Bio.-Def. Pre. Med. Division
89 Commander, Tactical Air Command, Langley AFB, Va. ATTN: Doc. Security Branch
90 Commander, Hq. Air Research and Development Command, Andrews AFB, Washington 25, D.C. ATTN: RDRWA
91 Commander, Air Force Ballistic Missile Div. HQ. ARDC, Air Force Unit Post Office, Los Angeles 45, Calif. ATTN: WDSOT
92-93 Commander, AF Cambridge Research Center, L. G. Hanscom Field, Bedford, Mass. ATTN: CRQST-2
94-98 Commander, Air Force Special Weapons Center, Kirtland AFB, Albuquerque, N. Mex. ATTN: Tech. Info. & Intel. Div.
99-100 Director, Air University Library, Maxwell AFB, Ala.
101 Commander, Lowry Technical Training Center (TW), Lowry AFB, Denver, Colorado.
102-104 Commander, Wright Air Development Center, Wright-Patterson AFB, Dayton, Ohio. ATTN: WCACT (For WCOSI)
105-106 Director, USAF Project RAND, VIA: USAF Liaison Office, The RAND Corp., 1700 Main St., Santa Monica, Calif.
107 Commander, Air Technical Intelligence Center, USAF, Wright-Patterson AFB, Ohio. ATTN: AFCIN-4Bla, Library
108 Assistant Chief of Staff, Intelligence, HQ. USAFE, APO 633, New York, N.Y. ATTN: Directorate of Air Targets
109 Commander-in-Chief, Pacific Air Forces, APO 953, San Francisco, Calif. ATTN: PFCIE-MB, Base Recovery

OTHER DEPARTMENT OF DEFENSE ACTIVITIES

110 Director of Defense Research and Engineering, Washington 25, D.C. ATTN: Tech. Library
111 Chairman, Armed Services Explosives Safety Board, DCD, Building T-7, Gravelly Point, Washington 25, D.C.
112 Director, Weapons Systems Evaluation Group, Room 1E880, The Pentagon, Washington 25, D.C.
113-115 Chief, Defense Atomic Support Agency, Washington 25, D.C. ATTN: Document Library
117 Commander, Field Command, DASA, Sandia Base, Albuquerque, N. Mex.
118 Commander, Field Command, DASA, Sandia Base, Albuquerque, N. Mex. ATTN: FCTG
119-120 Commander, Field Command, DASA, Sandia Base, Albuquerque, N. Mex. ATTN: FCWT
121 Commander-in-Chief, Strategic Air Command, Offutt AFB, Neb. ATTN: OAWS
122 Commandant, US Coast Guard, 1300 E. St., N.W., Washington 25, D.C. ATTN: Cdr B. E. Kolkhorst
123 U.S. Documents Officer, Office of the United States National Military Representative - SHAPE, APO 55, New York, N.Y.

ATOMIC ENERGY COMMISSION ACTIVITIES

124-126 U.S. Atomic Energy Commission, Technical Library, Washington 25, D.C. ATTN: For DMA
127-128 Los Alamos Scientific Laboratory, Report Library, P.O. Box 1663, Los Alamos, N. Mex. ATTN: Helen Redman
129-133 Sandia Corporation, Classified Document Division, Sandia Base, Albuquerque, N. Mex. ATTN: H. J. Smyth, Jr.
134-143 University of California Lawrence Radiation Laboratory, P.O. Box 808, Livermore, Calif. ATTN: Clovis G. Craig
144 Division of Technical Information Extension, Oak Ridge, Tenn. (Master)
145-175 Division of Technical Information Extension, Oak Ridge, Tenn. (Surplus)

Defense Threat Reduction Agency
8725 John J Kingman Road MS 6201
Ft Belvoir, VA 22060-6201

TDANP/TRC

March 2, 2001

MEMORANDUM TO THE DEFENSE TECHNICAL INFORMATION CENTER
ATTN: OCQ

SUBJECT: DOCUMENT UPDATES

The Defense Threat Reduction Agency Security Office has performed a classification/distribution statement review of the following documents. The documents should be changed to read as follows:

WT-1628, AD-357954, OPERATION HARDTACK, PROJECT 3.4, LOADING AND RESPONSE OF SURFACE-SHIP HULL STRUCTURES FROM UNDERWATER BURSTS, UNCLASSIFIED, DISTRIUBTION STATEMENT A.

WT-1301, AD-341065, OPERATION REDWING, PROJECT 1.1, GROUND SURFACE AIR BLAST PRESSURE VERSUS DISTANCE, UNCLASSIFIED, DISTRIBUTION STATEMENT A.

WT-748, OPERATION UPSHOT KNOTHOLE, PROJECT 5.1, ATOMIC WEAPON EFFECTS ON AD TYPE AIRCRAFT IN FLIGHT. UNCLASSIFIED, DISTRIBUTION STATEMENT A. FORWARD TO YOU FOR YOUR COLLECTION

WT-9001-SAN, GENERAL REPORT ON WEAPONS TESTS, UNCLASSIFIED, DISTRIBUTION STATEMENT A. FORWARD TO YOU FOR YOUR COLLECTION.

POR-2260-SAN, OPERATION SUN BEAM, SHOTS LITTLE FELLER 1 AND 2, PROJECT 1.1, AIRBLAST PHENOMENA FROM SMALL YIELD DEVICES, SANITIZED VERSION. UNCLASSIFIED, DISTRIBUTION STATEMENT A. FORWARD TO YOU FOR YOUR COLLECTION.

If you have any questions, please call me at 703-325-1034.

Ardith Jarrett

ARDITH JARRETT
Chief, Technical Resource Center